DIMETHYLGERMYLENE AND TETRAMETHYLDIGERMENE IN SOLUTION

The direct detection and kinetic studies of dimethylgermylene and tetramethyldigermene in solution by nanosecond laser flash photolysis

By

FARAHNAZ BEGUM LOLLMAHOMED, B. Sc.

A Thesis
Submitted to the School of Graduate Studies
In Partial Fulfilment of the Requirements
for the Degree
Doctor of Philosophy

McMaster University

Abstract

Dimethylgermylene ($GeMe_2$) has been generated by laser flash photolysis of 1,1-dimethyl-3-phenylgermacyclopent-3-ene (**23**) and 1,1,3-trimethyl-4-phenylgermacyclopent-3-ene (**24**) in hexanes at 25°C and its absorption maximum (λ_{max}) has been unambiguously established to be 470 nm. $GeMe_2$ decays with second-order kinetics under these conditions ($2k/\varepsilon = (10 \pm 2) \times 10^7$ cm s^{-1}) to give Ge_2Me_4 ($\lambda_{max} = 370$ nm). Kinetic studies of the reactions of $GeMe_2$ and Ge_2Me_4 with typical germylene/digermene scavengers such as 1,3-dienes, olefins, alkynes, alkyl halides, group 14 metal hydrides, carboxylic acids, and amines have been carried out.

$GeMe_2$ reacts reversibly with MeOH, t-BuOH and THF to form Lewis acid-base complexes which exhibit relatively strong absorption bands that are blue-shifted with respect to $GeMe_2$ ($\lambda_{max} \sim 295$-310 nm). The decay of the Me_2Ge-MeOH complex is accelerated in the presence of a Brønsted acid (acetic acid or methanesulfonic acid) or base (MeONa). The reactions of the Me_2Ge-THF complex with sodium methoxide, methanesulfonic acid, 4,4-dimethyl-1-pentene, 2,3-dimethyl-1-butadiene, acetic acid and CCl_4 have also been studied in THF.

The photochemistry of two well-known precursors to $GeMe_2$, namely dodecamethylcyclohexagermane (**14**) and dimethylphenyl(trimethylsilyl)germane (**18**) was reinvestigated. Laser flash photolysis of **14** in hexanes led to the formation of two

transients, one with λ_{max} = 490 nm ($\tau \leq 10$ ns) and the second with λ_{max} = 470 nm. The latter decays with second-order kinetics with concomitant formation of a new transient with λ_{max} = 370 nm. The transient at 470 nm is assigned to $GeMe_2$ and that at 370 nm to Ge_2Me_4, based on comparisons to the results obtained from laser flash photolysis of **23** and **24**. Laser flash photolysis of **18** in hexane gives rise to two absorption bands centered at λ_{max} = 300 nm and λ_{max} = 430 nm, which are assigned to the dimethylphenylgermyl radical and the conjugated germene derivative **38**, respectively. $GeMe_2$ cannot be detected in laser flash photolysis experiments with this compound.

Acknowledgements

First and foremost, I express my deepest gratitude to my supervisor, Professor William Leigh for his invaluable support, motivation and guidance throughout my Ph.D. studies. Willie's undiminished enthusiasm and engagement provided a stimulating environment for my intellectual development. I am also very grateful to my supervisory committee members, Dr Vargas-Baca, Dr Alfredo Capretta, and Dr David J. H. Emslie, who have greatly contributed to this work through their suggestions and insightful remarks.

I thank the chemistry staff for their help during the course of my studies. Special thanks go to Dr Donald Hughes and Dr Green Kirk of the NMR and mass spectroscopy facilities, respectively, for being always ready to help.

I am also grateful to the current and past members of my group. I especially thank Drs. Cameron Harrington and Thomas Owens for their guidance and technical help when I just started. I also thank Dr. Andrey Moiseev, Ileana Dumbrava, Lawrence Huck, Svetlana Kostina and Adroha Bhattacharya for their time and friendship.

To all the friends who spent priceless times with me during my graduate studies. Special acknowledgements go to Joshua Fraser, Mher Paboudjian, Dr. Kevin Moonoosamy, Trish Laurie, Renya Benjamen, Dr. Rahima Benhabbour and Jade Greg for their special support during writing this thesis.

Finally, I would like to express my eternal gratitude to my parents, Issoop and Rooksana Lollmahomed and close relatives for their encouragement in pursuing my goal even though it involved geographical separation. To my sister Jameelah and brother Abdus Samad who made sure I keep in touch. Particular thanks go to Sarah Peerbocus for her constant boost. To my deceased grandfather, Yousouf Peerbocus, who has constantly encouraged me in my studies and would have been very proud of this thesis. Thank you all, you have been the backbone of each and every achievement in my life.

LIST OF FIGURES xi

LIST OF TABLES xxii

LIST OF SCHEMES xxiv

CHAPTER 1 **Introduction**

1.1 Group 14 reactive intermediates 1

1.2 Divalent group 14 compounds and their dimers 1

1.2.1 Electronic structure of divalent group 14 compounds 4

1.2.2 Divalent State Stabilization Energy 7

1.3 Techniques used for the study of group 14 reactive intermediates 9

1.4 Germylenes 11

1.4.1 Sources of germylenes 12

1.4.2 Reactions of transient germylenes in solution 15

1.5 Digermenes 18

1.5.1 The structural properties of and bonding in digermenes 19

1.5.2 Sources of digermenes 21

1.5.3 Reactions of digermenes 22

1.6 The direct detection and kinetic studies of $GeMe_2$, the simplest dialkylgermylene 25

1.7 Thesis objectives 37

References 42

CHAPTER 2 **The direct detection and kinetic studies of dimethylgermylene in solution**

2.1 Introduction 56

2.2 Synthesis of 1,1-dimethyl-3-phenylgermacyclopent-3-ene derivatives 58

2.3 Steady state photolysis of **26** and **27** 64

2.4 Quantum yield determination for the formation of $GeMe_2$ from **26** 71

2.5 **Direct detection of $GeMe_2$ and Ge_2Me_4 in solution by laser flash photolysis** 74

- **2.5.1** Laser flash photolysis of **26** 74
- **2.5.2** Laser flash photolysis of **27** 80

2.6 **Determination of the molar extinction coefficient of $GeMe_2$ at 480 nm** 82

2.7 **Absolute rate constant for dimerization of $GeMe_2$ in solution** 85

2.8 **Kinetic studies of reactions of $GeMe_2$ in solution** 86

- **2.8.1** Reaction with acetic acid 100
- **2.8.2** Reactions with group 14 metal hydrides 103
- **2.8.3** Reactions of $GeMe_2$ with alkene, alkyne and diene 107
- **2.8.4** Reaction with amines 115
- **2.8.5** Reaction with carbon tetrachloride 118
- **2.8.6** Reaction with oxygen 120

2.9 **Summary and Conclusions** 121

References 124

CHAPTER 3 Reinvestigation of some dimethylgermylene precursors in solution by laser flash photolysis

3.1 **Introduction** 128

3.2 **Laser flash photolysis studies of dodecamethylcyclohexagermane (18)** 136

- **3.2.1** Synthesis of **18** 136

3.2.2 Laser flash photolysis of **18** in hexane solution 137

3.2.3 Laser flash photolysis of **18** in the presence of THF 138

3.2.4 Further identification of the 470 nm transient 140

3.2.5 Reaction with oxygen 142

3.3 **Laser flash photolysis studies of dimethylphenyl(trimethylsilyl)germane (22)** 145

3.3.1 Synthesis of dimethylphenyl(trimethylsilyl)germane (**22**) 145

3.3.2 Laser flash photolysis of **22** in deoxygenated hexane 146

3.3.3 Kinetic studies of precursor **22** in hexane 147

3.3.3.1 *Reaction with oxygen* 149

3.3.3.2 *Reactions with other reagents* 153

3.3.4 Laser flash photolysis of **22** in THF 158

3.4 **Summary and Conclusions** 163

References 165

CHAPTER 4 **Reactions of $GeMe_2$ with THF and alcohols in hexane**

4.1 **Introduction** 167

4.2 **The reaction of $GeMe_2$ with THF** 170

4.3 **The reaction of $GeMe_2$ with methanol** 177

4.4 **The reaction of $GeMe_2$ with t-butanol** 183

4.5 **A comparison of the reactivities of GeR_2 with alcohols and THF in hexane** 186

4.6 **Conclusions** 190

References 192

CHAPTER 5 The reactivities of the Me_2Ge-MeOH and Me_2Ge-THF complexes in neat O-donors as solvents

5.1 Introduction 195

5.2 Direct detection and kinetic studies of the Me_2Ge-MeOH complex in methanol 200

5.2.1 Direct detection of the Me_2Ge-MeOH complex in methanol 200

5.2.2 Reactions of the Me_2Ge-MeOH complex with acids in MeOH solution 203

5.2.3 Reactivity of the Me_2Ge-THF complex in THF 205

5.2.4 Mechanistic study of acid- or base-catalyzed decomposition of R_2Ge-MeOH complexes in neat MeOH 206

5.3 Reactivity of the Me_2Ge-THF complex in THF 210

5.3.1 Steady state photolysis of 1,1-dimethyl-3-phenylgermacyclopent-3-ene in THF-$_{d8}$ in the presence of AcOH and $MeSO_3H$ 210

5.3.2 Direct detection and kinetic studies of Me_2Ge-THF complex in THF 217

5.3.3 Reactions of the Me_2Ge-THF complex with acids in THF 219

5.3.4 Reaction of the Me_2Ge-THF complex with MeONa 222

5.3.5 Reactions of the Me_2Ge-THF complex with other scavengers 224

5.4 Summary and Conclusions 229

References 231

CHAPTER 6 The kinetic studies of some reactions of tetramethyldigermene in hexane

6.1 Introduction 233

6.2. Reaction with acetic acid 237

6.3 Reactions with n-$BuNH_2$ and alcohols 238

6.4 Reactions with group 14 metal hydrides 241

6.5 **Reaction with carbon tetrachloride** 242

6.6 **Reaction with oxygen** 245

6.7 **Reactions with alkenes, alkynes and dienes** 247

6.8 **Summary and Conclusions** 250

References 252

CHAPTER 7 **Conclusions and Future Work**

7.1 **Summary and conclusions** 256

7.2 **Future Work** 259

References 262

CHAPTER 8 **Experimental**

8.1 **General** 263

8.2 **Laser flash photolysis** 265

8.3 **Synthesis and characterization of compounds** 266

8.4 **Steady state photolysis experiments** 276

References 280

List of Figures

Figure 1.1	Common nomenclature for divalent group 14 compounds and their dimers.	2
Figure 1.2	Examples of stable singlet divalent group 14 compounds.	3
Figure 1.3	Singlet and triplet electronic structure of divalent group 14 compounds.	4
Figure 1.4	Experimentally generated triplet silylenes.	7
Figure 1.5	Electronic transition from singlet ground state (S_0) to singlet excited state (S_1) in a germylene.	12
Figure 1.6	Some characteristic reactions of germylenes.	17
Figure 1.7	Bonding in digermene.	20
Figure 1.8	(a) Transient absorption spectra from laser flash photolysis of **7** in deoxygenated hexane recorded 50-300 ns (○), 8.2-8.9 μs (□) after the laser pulse. The inset shows transient decay/growth profiles recorded at 480 nm and 370 nm. Reproduced with permission from Ref 52. Copyright 2004, American Chemical Society; (b) Transient absorption spectra recorded by laser photolysis (193 nm) of **5** (△) and **21** (o) in the gas phase. Adapted with permission from Ref 51. Copyright 1996, Elsevier Science B.V.	31
Figure 2.1	UV-Vis absorption spectrum of (a) **23** and (b) **24** in hexanes.	63
Figure 2.2	Concentration versus time plots for 254 nm irradiation of a deoxygenated solution of **23** (0.05 M) in C_6D_{12} containing AcOH (0.25 M). The solid lines represent the linear least-squares fits of the data. The slopes (x 10^2) are: (□; 2.14 ± 0.08) for **34**; (○; 2.31 ± 0.07) for **28**; (•; -2.3 ± 0.2) for **23**.	65
Figure 2.3	^{1}H NMR spectra (200 MHz) of the crude reaction mixture from photolysis (254 nm) of a solution of **23** (0.05 M) in the presence of AcOH (0.25 M) in deoxygenated cyclohexane-d_{12} at (a) t = 0 min and (b) after ca. 60 % conversion of **23**.	66

Figure 2.4 ^{1}H NMR spectra (600 MHz) of the crude reaction mixture from photolysis (254 nm) of a solution of **23** (0.04 M) in the presence of MeOH (0.24 M) in deoxygenated cyclohexane-d_{12} at (a) t = 0 min and (b) after *ca.* 20 % conversion of **23**. 67

Figure 2.5 Plots of relative area ($A_x/A_{dodecane}$) of the precursor **23**, and products **7** and **28** (A_x) to dodecane (internal standard) versus photolysis time of a mixture of **23** (0.03 M) and DMB (0.05 M) in deoxygenated hexanes. The solid lines are the linear least-squares fits of the data and the slopes are: (○; -0.23 ± 0.03) for **23**; (□; 0.12 ± 0.02) for **7**; (△; 0.14 ± 0.02) for **28**. 69

Figure 2.6 ^{1}H NMR spectra (200 MHz) of the crude reaction mixture from photolysis (254 nm) of a solution of **22** (0.05 M) in the presence of AcOH (0.26 M) in deoxygenated cyclohexane-d_{12} at (a) t = 0 min and (b) after *ca.* 30 % conversion of **22**. Hexamethyldisilane was used as an integration standard. 70

Figure 2.7 Concentration versus time plots for 254 nm irradiation of a deoxygenated solution of **24** (0.05 M) in C_6D_{12} containing AcOH (0.25 M). Hexamethyldisilane was used as an integration standard (0.0028 M). The solid lines are the linear least-squares fits of the data and the slopes (x 10^4) are: (○; -9.9 ± 0.7) for **24**; (●; 9.0 ± 0.3) for **34**; (□; 9.8 ± 0.2) for **31**. 71

Figure 2.8 Plots of concentration ([X]/M) versus time for precursors: **23** (•) and **36** (♦) and products: **37** (○) and **35** (□) from the photolysis of **23** (0.041 M) and **36** (0.037 M) in deoxygenated C_6D_{12} in the presence of 0.24 M MeOH. The slopes (x 10^3) are: (○; 1.4 ± 0.2) for **37**; (□; 0.54 ± 0.03) for **35**; (♦; -0.67 ± 0.02) for **36**; (•; -1.4 ± 0.2) for **23**. 73

Figure 2.9 (a) Transient absorption spectra recorded by laser flash photolysis (248 nm) of **23** (ca. 7 x 10^{-5} M) in argon-saturated anhydrous hexanes at 25 °C, 51-70 ns (○), 0.12-0.19 μs (◊) and 2.96-3.07 μs (□) after the laser pulse. The inset shows typical transient profiles at 290 nm, 370 nm and 470 nm. The solid line superimposed on the 470 nm decay trace is the non-linear least-squares fit of the data to eq (2.3); (b) The residuals obtained after the fit of the 470 nm transient decay trace to eq (2.3). 76

Figure 2.10 (a) Transient absorption spectra recorded by laser flash photolysis of **23** in deoxygenated hexanes 0-12.8 μs (○) and 1.82-1.85 ms (□) after the laser pulse. The inset shows transient decay profiles recorded at 290 nm and 370 nm; (b) Transient absorption spectra recorded by laser flash photolysis of **23** in deoxygenated hexanes containing 3 mM AcOH, 0-12.8 μs (○) and 416-422 μs (□) after the laser pulse. The solid line represents the non-linear least-squares fit to eq (2.8). 79

Figure 2.11 (a) Transient absorption spectra recorded by laser flash photolysis of **24** (ca. 1.5 x 10^{-4} M) in deoxygenated hexanes recorded 32-58 ns (○), 0.70-0.72 μs (◊) and 3.10-3.12 μs (□) after the laser pulse. The inset shows transient decay/growth profiles monitored at 470 nm and 370 nm; (b) Transient absorption spectra recorded 0.11-0.13 μs (○), 5.47-6.06 μs (□) after the laser pulse. The inset shows transient decay/growth profiles recorded at 470 nm and 370 nm. The solid line represents the non-linear least-squares fit of the data to eq (2.3) ($k_{\mathrm{dim}}/\varepsilon$ = 5.75 x 10^7 cm s^{-1}). 82

Figure 2.12 Determination of the molar absorptivity of $GeMe_2$ at 480 nm using benzophenone triplet at 525 nm (ε_{525} = 6250 ± 1250) in deoxygenated dry hexanes as actinometer. Effects of laser dose on transient decay profiles recorded by laser flash photolysis of (a) BP monitored at 525 nm and (b) **23** monitored at 480 nm in deoxygenated hexanes; (c) Plots of ΔA_{max} versus laser dose (% of 86 mJ) for the optically matched deoxygenated solutions of BP and **23** in dry hexanes at 25 °C; (d) Expanded plot of ΔA_{max} versus laser dose (% of 86 mJ) for **23**. Errors in the slopes of the plots are listed as twice the standard error from linear least squares analysis. Slope of $^3BP^*$ = (8.93 ± 0.38) x 10^{-4}; Slope of $GeMe_2$ = (5.69 ± 0.42) x 10^{-5}; $\mathrm{Slope}_{\mathrm{GeMe2}}/\mathrm{Slope}_{\mathrm{3BP*}}$ = 0.064 ± 0.003. 84

Figure 2.13 Simulation of germylene (GeR_2) decay profiles for its reaction with scavenger (Q), with bimolecular rate constant k_Q = 9 x 10^9 $M^{-1}s^{-1}$ and K_{eq} (a) 100 M^{-1}, (b) 5000 M^{-1}, (c) 20 000 M^{-1}, and (d) 100 000 M^{-1} in hydrocarbon solvents. The first 20 ns portion of the decay profiles in (a) has been grayed to illustrate the area that cannot be resolved. 92

Figure 2.14 (a) Absorption versus time plot of GeR_2 for a hypothetical reversible reaction of GeR_2 with Q, illustrating the parameters used to determine the K_{eq} for the reaction, according to eq (2.12) when (a) the residual absorptions are non-decaying and when (b) residual absorptions are decaying. 94

Figure 2.15 Effects of added acetic acid on the: (a) transient decay profiles of $GeMe_2$, monitored at 480 nm; (b) transient growth/decay profiles of Ge_2Me_4, monitored at 370 nm. 100

Figure 2.16 (a) Plots of pseudo-first-order decay rate constant of $GeMe_2$ (k_{decay}) versus nominal [AcOH] (□) and the plot of $(\Delta A_{370})_{max,0}/(\Delta A_{370})_{max,Q}$ versus [Q] (○). The solid lines represent the linear least-squares fit of the data to eqns (2.17) and (2.16), respectively; (b) Plots of pseudo-first-order decay rate constant of $GeMe_2$ (k_{decay}) versus $[AcOH]_{monomer}$. The solid line represents the best linear least-squares fit to eq (2.17). 102

Figure 2.17 Effects of added (a) $n\text{-}Bu_3SnH$, (b) Et_3GeH and (c) Et_3SiH on (i) the pseudo-first-order rate constant (k_{decay}) of $GeMe_2$, monitored at 480 nm (□; eq 2.17), and (ii) the maximum transient absorbance of Ge_2Me_4 monitored at 370 nm (○; eq 2.16). The inset in (a) shows an expanded Stern-Volmer plot according to eq (2.16) for $n\text{-}Bu_3SnH$. 105

Figure 2.18 (a) Effects of added DMB on (a) transient decay profiles recorded at 480 nm by laser flash photolysis of **23** in deoxygenated hexanes; (b) Plots of pseudo-first-order rate constant (k_{decay}) of $GeMe_2$, monitored at 480 nm (□) and $(\Delta A_{370})_{max,0}/(\Delta A_{370})_{max,Q}$ (○) versus [DMB], showing linear least-squares fits of data to eqs (2.17) and (2.16), respectively. 108

Figure 2.19 Effects of added DMB on the transient growth/decay profiles recorded at 370 nm by laser flash photolysis of **23** in deoxygenated hexanes (a) on shorter time scale and (b) on longer time scale. 109

Figure 2.20 (a) Effects of added DMP on the transient decay profiles recorded at 480 nm by laser flash photolysis of **23**; (b) Plots of pseudo-first-order rate constant (k_{decay}) of $GeMe_2$, monitored at 480 nm (□) and $(\Delta A_{370})_{max,0}/(\Delta A_{370})_{max,Q}$ (○) versus [DMP], showing linear least-squares fits of data to eqs (2.17) and (2.16), respectively. 110

Figure 2.21 Effects of added TBE on the (a) transient decay profiles monitored at 480 nm and (b) transient growth/decay profiles monitored at 370 nm, and (c) plots of pseudo-first-order rate constant (k_{decay}) of $GeMe_2$, monitored at 480 nm (□) and $(\Delta A_{370})_{max,0}/(\Delta A_{370})_{max,Q}$ (○) versus [TBE], showing linear least-squares fits of data to eqs (2.17) and (2.16), respectively. 113

Figure 2.22 Effects of added n-$BuNH_2$ on the (a) transient decay profiles of $GeMe_2$ at 480 nm and (b) transient growth/decay profiles of Ge_2Me_4 at 370 nm, and (c) plots of the pseudo-first-order decay rate constant (k_{decay}) of $GeMe_2$, monitored at 480 nm (□) and $(\Delta A_{370})_{max,0}/(\Delta A_{370})_{max,Q}$ (○) versus [n-$BuNH_2$], showing linear least-squares fits of data to eqs (2.17) and (2.16), respectively. 117

Figure 2.23 Effects of added CCl_4 on the pseudo-first-order decay rate constants of $GeMe_2$ (□), monitored at 480 nm, and on the maximum signal intensity (○) of Ge_2Me_4, monitored at 370 nm. The solid lines are the linear least-squares fits to eq (2.17) and eq (2.16), respectively. 119

Figure 3.1 Transient absorption spectra recorded by laser flash photolysis of: (a) cyclo-Ge_6Me_{12} (**14**) in cyclohexane at 293 K, recorded (○) 0.2 μs, (◉) 1 μs and (●) 2 μs after the laser pulse. Reproduced with permission from Ref. 3 Copyright 1991, Elsevier Sequoia S.A. (b) cyclo-Ge_5Me_{10} (**15**) in cyclohexane at 293 K recorded (●) 0.2 μs, (□) 0.5 μs and (■) 2 μs after the laser pulse. Reproduced with permission from Ref. 6. Copyright 1992, The Chemical Society of Japan. 132

Figure 3.2 Transient absorption spectrum recorded by laser flash photolysis of **18** in degassed cyclohexane recorded 0-5 μs after the laser pulse. Reproduced with permission from ref. 7. Copyright 1991, American Chemical Society. 134

Figure 3.3 (a) Transient absorption spectra recorded by laser flash photolysis of deoxygenated solution of **14** (ca. 4 x 10^{-4} M) in hexane (○) 16 ns, 80-112 ns (□) and (◊) 2.08-2.13 μs after the laser pulse. The inset shows transient decay/growth profiles recorded at 470 nm and 370 nm. The solid line represents the non-linear least-squares fit to eq (2.3); (b) Transient decay profile recorded at 490 nm. The solid line represents the nonlinear least-squares fit of the data to eq (2.4). 138

Figure 3.4 Transient absorption spectra recorded by laser flash photolysis of **14** in deoxygenated hexane containing 15 mM THF 16-32 ns (△), 48-80 ns (○) and 7.76-7.82 μs (□) after the laser pulse. The sharp drop in the ΔA signals at < 320 nm is due to fluorescence from the sample. The inset shows transient growth/decay profiles recorded at 310 nm, 370 nm and 470 nm from the same experiment. 139

Figure 3.5 (a) Effects of added AcOH on the transient decay profiles recorded at 470 nm by laser flash photolysis of **14** in deoxygenated hexane at 25 °C; (b) Identical decay profiles as in (a) but on a magnified scale; (c) Effects of added AcOH on the transient growth/decay profiles recorded at 370 nm; (d) Plots of k_{decay} versus [AcOH]. 141

Figure 3.6 Effects of laser dose (% of 108 mJ) on the initial transient absorbance values of the 470 nm and 490 nm transient, from laser flash photolysis of **14** in anhydrous hexane. 144

Figure 3.7 Transient absorption spectra recorded by laser flash photolysis of a deoxygenated solution of **18** (ca. 6 x 10^{-4} M) in hexane at 25 °C, 50-210 ns (○) and 2.14-2.26 μs (□) after the laser pulse. The inset shows transient profiles recorded at 300 nm, 370 nm, 430 nm and 480 nm during the same experiment. 147

Figure 3.8 Transient absorption spectra recorded by laser flash photolysis of **18** in deoxygenated hexane containing 3 mM AcOH, recorded 96-128 ns (○) and 8.34-8.46 μs (□) after the laser pulse. The inset shows transient decay profiles recorded at 300 nm and 430 nm during the same experiment. 149

Figure 3.9 Transient absorption spectra recorded by laser flash photolysis of **18** in oxygen-saturated hexane at 25 °C, 0.07-0.10 μs (○) and 0.42-0.46 μs (□) after the laser pulse. The inset shows transient decay profiles recorded at 300 nm and 430 nm during the same experiment. 150

Figure 3.10 (a) Effects of oxygen concentration on transient decay profiles recorded at 430 nm by laser flash photolysis of a solution of **18** (6 x 10^{-4} M) in hexane. The solid lines represent the non-linear least-squares fit to first-order kinetics, according to eq (2.4); (b) Plots of k_{decay} versus [O_2] for the 430 nm transient. The solid line represents the linear least-squares fit to eq (2.17). 152

Figure 3.11 Dependence of the pseudo-first-order decay rate constant (k_{decay}) of the 430 nm transient on [Q] in anhydrous hexane for reactions with (a) DMB, (b) CCl_4 and (c) acetone. The solid lines are the linear least-squares fit to eq (2.17). 153

Figure 3.12 Transient absorption spectra recorded by laser flash photolysis of **18** in deoxygenated THF at 25 °C, 0.03-0.10 μs (○) and 7.87-7.94 μs (□) after the laser pulse. The inset shows transient decay profiles recorded at 300 nm, 430 nm and 480 nm during the same experiment. 159

Figure 3.13 Transient absorption spectra recorded by laser flash photolysis of a solution of **18** (ca. 6 x 10^{-4} M) in oxygen-saturated THF solution 16-48 ns (□) and 0.88-0.94 μs (○) after the laser pulse. The inset shows transient decay profiles recorded at 300 nm and 430 nm during the same experiment. 160

Figure 3.14 Transient decay profiles recorded by laser flash photolysis of **18** in argon-saturated THF and oxygen-saturated THF showing the bimodal decay at 310 nm on (a) long time scale and (b) initial decay component on shorter time scale. The solid lines represent the non-linear least-squares fit to two-phase exponential decay, according to eq (3.7). 161

Figure 3.15 Transient decay profiles recorded at 430 nm by laser flash photolysis of **18** in (a) argon-saturated THF; the solid line represents the non-linear least-squares fit to eq (3.7), and (b) oxygen-saturated THF; the solid line represents the non-linear least-squares fit to eq (2.4). 162

Figure 4.1 Effects of added THF on the transient decay profiles recorded at 480 nm by laser flash photolysis of **23** in deoxygenated hexane. 171

Figure 4.2 Effects of added THF on the transient decay/growth profiles monitored at 370 nm by laser flash photolysis of **23** in deoxygenated hexane. 172

Figure 4.3 Transient absorption spectra from laser flash photolysis of **23** (ca. 7 x 10^{-5} M) in 0.015 M THF recorded 0.02 - 0.22 μs (□) and 7.90 - 9.62 μs (○) after the laser pulse. The transient absorption spectrum of **23** recorded in deoxygenated hexane at 0.13 - 0.18 μs (◊) after the laser pulse is also shown for comparison. The inset shows the transient growth/decay profiles recorded at 310 nm, 370 nm and 480 nm. 173

Figure 4.4 (a) Determination of K_{eq} for the reaction of $GeMe_2$ with THF in hexane at 25 °C. Plots of $\Delta A_{0,480nm}$ / $\Delta A_{res,480nm}$ for $GeMe_2$, monitored at 480 nm versus [THF]; (b) Plot of k_{decay} at 480 nm versus [THF]. 175

Figure 4.5 Effects of added methanol on the transient decay profiles of $GeMe_2$ recorded at 480 nm by laser flash photolysis of **23** in deoxygenated anhydrous hexane at 25 °C. 179

Figure 4.6 (a) Transient decay profile of $GeMe_2$, monitored at 480 nm in deoxygenated hexane containing 4.30 mM methanol. The broken line illustrates the extrapolation used to estimate the residual absorption intensity ($\Delta A_{res,480nm}$) at 480 ml; (b) Plot of ($\Delta A_{0,480nm}$ / $\Delta A_{res,480nm}$) versus [MeOH]. 180

Figure 4.7 (a) Effects of added MeOH on the transient decay profiles recorded at 370 nm by laser flash photolysis of **23** in deoxygenated hexane; (b) Plot of ratio of the absorption maximum $[(\Delta A_{370})_{0,max}$ / $\Delta A_{370})_{Q,max}]$ versus [MeOH]. 181

Figure 4.8 Transient absorption spectra recorded by laser photolysis of **23** (7 x 10^{-5} M) at 25 °C in deoxygenated hexane containing 54 mM MeOH (a) 0.14-0.21 μs (○), 9.46-9.97 μs (△) and 136-142 μs (•) after the laser pulse. The inset shows the transient decay profiles recorded at 295 nm, 370 nm and 430 nm in the presence of 54 mM MeOH; (b) The transient decay profile recorded at 295 nm. 183

Figure 4.9 Effects of added t-BuOH on the: (a) transient decay profiles recorded at 480 nm; (b) Transient growth profiles recorded at 370 nm; (c) Ratio $\Delta A_{0,max}/\Delta A_{Q,max}$ of the transient profiles recorded at 480 nm; (d) Ratio of the maximum absorption, $(\Delta A_{370})_{0,max}/(\Delta A_{370})_{Q,max}$, at 370 nm recorded in the absence and presence of t-BuOH. 185

Figure 4.10 Transient absorption spectra recorded by laser flash photolysis of **23** in 8.2 mM t-BuOH in deoxygenated hexane at 0.14-0.21 μs (○) and 8.42-8.53 μs (△) after the laser pulse. Also shown the transient absorption spectrum of **23** recorded in deoxygenated hexane at 0.13-0.18 μs (◊) after the laser pulse. The inset shows growth/decay transient profiles monitored at 300 nm, 370 nm and 480 nm. 186

Figure 5.1 Transient absorption spectra recorded by laser flash photolysis of **23** in deoxygenated methanol, 0.19-0.32 μs (○) and 4.51-5.44 μs (□) after the laser pulse. The transient absorption spectrum recorded for **23** in deoxygenated hexane containing 54 mM MeOH (0.16-0.22 μs (△) after the laser pulse) is also shown for comparison. The inset shows transient decay profile recorded at 300 nm. The solid line represents the non-linear least-squares fit of the data to a single-exponential decay, according to eq (2.4) (k_{decay} = (2.60 ± 0.08) x 10^6 s^{-1}; R^2 = 0.9781). 202

Figure 5.2 Effects of added (a) $MeSO_3H$ and (b) AcOH on the pseudo-first-order decay rate constants of the Me_2Ge-MeOH complex, monitored at 295 nm, in deoxygenated methanol at 25 °C. The solid lines are the best linear least-squares fit of the data to eq (2.17). 204

Figure 5.3 (a) Effects of added MeONa on the transient decay profiles of Me_2Ge-MeOH monitored at 295 nm by laser flash photolysis of **23** in deoxygenated methanol at 25 °C; (b) Plots of k_{decay} vs. [MeONa] for the Me_2Ge-MeOH complex monitored at 295 nm. The solid line represents the linear least-squares fit to eq (2.17). 206

Figure 5.4 ^1H NMR spectra (600 MHz) of the crude photolysis mixture of **23** (0.025 M) and AcOH (0.04 M) in deoxygenated THF-d_8: (a) before photolysis, and (b) after 40 % conversion of **23**. The insets are expansions of the Ge-$\underline{H}$ and Ge(C$\underline{H}_3$)$_2$ peaks due to the major product **34**. 212

Figure 5.5 Concentration vs. time plots for $GeMe_2$ precursor **23**, diene **28** and insertion product **34** as a function of photolysis time, from irradiation of a mixture of **23** (0.025 M) and AcOH (0.04 M) in THF-d_8. Hexamethyldisilane was used as integration standard. The slopes (x 10^3) are: (□; -2.08 ± 0.04) for **23**; (◊; 1.83 ± 0.03) for **34** and (●; 2.07 ± 0.03) for **28**. 213

Figure 5.6 (a) ^{1}H NMR (600 MHz) spectrum of crude photolysis mixture recorded after 60 % conversion of irradiation of **23** in the presence of $MeSO_3H$, and (b) ^{1}H NMR (600 MHz) spectrum of starting mixture (0.035 M of **23**, and 0.09 M $MeSO_3H$ in THF-d_8) at t = 0 min. Hexamethyldisilane was used as an integration standard. 215

Figure 5.7 Expanded ^{1}H NMR spectra (600 MHz) of photolysis mixture of **23** (0.035 M) and $MeSO_3H$ (0.09 M) in THF-d_8 before irradiation and after 60 % conversion. 216

Figure 5.8 Plot of concentration for $GeMe_2$ precursor **23** (○), diene **28** (◊) and insertion product **44** (•, △) as a function of photolysis time of a mixture of **23** (0.035 M) and $MeSO_3H$ (0.09 M) in deoxygenated THF-d_8. Slopes (x 10^3) are: (**23**; -2.20 ± 0.01); (**28**; +2.27 ± 0.05); (**44**; +0.96 ± 0.03). 217

Figure 5.9 Transient absorption spectra recorded by laser flash photolysis of **23** (ca. 70 μM) in THF at 0.16 – 0.29 μs (□) and 2.75 – 2.98 μs (○) after the laser pulse. The inset shows transient decay/growth profiles at monitoring wavelengths 310 nm and 370 nm. 218

Figure 5.10 (a) Effects of added $MeSO_3H$ on the transient decay profiles recorded at 310 nm by laser flash photolysis of **23** in deoxygenated THF; (b) Plots of k_{decay} vs. [$MeSO_3H$]. The solid line represents the linear least-squares fit of the data to eq (2.17). 219

Figure 5.11 Plots of k_{decay} vs. [AcOL] for quenching of the Me_2Ge-THF complex by AcOH (○) and AcOD (□) in THF at 25 °C. The solid lines are the linear least squares fits of the data to eq (2.17). The slopes are: $k_{AcOH} = (1.3 \pm 0.1) \times 10^7\ M^{-1}s^{-1}$ and $k_{AcOD} = (4.6 \pm 0.4) \times 10^6\ M^{-1}s^{-1}$. 221

Figure 5.12 Effects of added MeONa (as a 0.1 M solution in MeOH) on the transient decay profiles recorded at 310 nm, from laser flash photolysis of **23** in deoxygenated THF at 310 nm; (b) Plots of k_{decay} versus [MeONa]; the solid line represents the linear least-squares fit of the data to eq (2.17). 224

Figure 5.13 (a) Effects of added CCl_4 on the transient decay profiles recorded at 310 nm; (b) Plots of k_{decay} versus [CCl_4] for the reactions of Me_2Ge-THF complex with CCl_4 in THF. 225

Figure 5.14 Effects of oxygen on the transient decay profiles recorded at 310 nm by laser flash photolysis of **23** in THF. The solid line represents the non-linear best fit line to eq (2.4), affording $k_{decay} = (1.56 \pm 0.04) \times 10^5\ s^{-1}$ ($R^2 = 0.9857$). 226

Figure 6.1 (a) Effects of added AcOH on the decay profiles of Ge_2Me_4, monitored at 370 nm. The solid lines represent the non-linear least-squares fits of the data to a single-phase exponential decay, according to eq (2.4). $k_{decay} = k_0 + k_Q[Ge_2Me_4]$; (b) Plot of k_{decay} versus [AcOH]. The solid line is the linear least-squares fit to eq (2.17). 238

Figure 6.2 (a) Effects of added n-$BuNH_2$ on transient decay profiles recorded at 370 nm, by laser flash photolysis of **23** in deoxygenated anhydrous hexane. The solid lines represent the non-linear least-squares fits of the data to single-phase exponential decays, according to eq (2.4); (b) Plot of k_{decay} versus [n-$BuNH_2$], according to eq (2.17). 239

Figure 6.3 (a) Effects of added CCl_4 on the growth/decay profiles recorded at 370 nm; (b) Plots of k_{decay} versus [CCl_4], monitored at 370 nm. The solid line represents the linear least-squares fit of the data to eq (2.17). 243

Figure 6.4 Plots of k_{decay} vs. [O_2], monitored at 370 nm. The solid line represents the linear least-squares fit to eq (2.17). 246

Figure 6.5 Transient decay profiles recorded at 370 nm by laser flash photolysis of 26 in deoxygenated hexane containing (a) 0.52 mM DMB; (b) 0.49 mM TBE; (c) 1.30 mM isoprene and (d) 1.73 mM DMP. The solid lines represent the non-linear least-squares fits of the data to a single-phase exponential decay, according to eq (2.4). The inserts shows the residuals obtained after fitting the data. 248

List of Tables

Table 1.1	Successive bond dissociation energies (BDE / kcal mol^{-1}) in MH_4 (M = C, Si, and Ge) compounds and Divalent State Stabilization Energies (DSSE / kcal mol^{-1}) of MH_2 species.	8
Table 1.2	A list of the photochemical precursors employed and absorption maxima (λ_{max}) assigned to "$GeMe_2$" in low temperature matrixes, solution and gas phase.	28
Table 1.3	Comparison of some reported bimolecular rate constants (k_Q / $M^{-1}s^{-1}$) for the reactions of $SiMe_2$ and "$GeMe_2$" in the gas phase and in solution.	33
Table 2.1	Absolute rate constants (k_Q), Stern-Volmer "constants" (K_{sv}) and the ratios of K_{sv}/k_Q for the reactions of $GeMe_2$ with various scavengers in deoxygenated hexanes at 25° ± 2 C.^{a,b}	99
Table 2.2	The BDE (kcal / mol) for selected group 14 hydrides and a comparison of the absolute rate constants (k_Q / 10^6 $M^{-1}s^{-1}$) of their reactions with GeR_2 and $SiMe_2$ in hexanes.	104
Table 2.3	A comparison of the transient intermediates formed from the reactions of $GePh_2$^{a} and GeMePh^b with isoprene, DMP and TBE in hexanes.	111
Table 2.4	Comparison of bimolecular rate constants, k_Q (10^9 $M^{-1}s^{-1}$) and equilibrium constants, K_{eq} (M^{-1}) for the reactions of $GeMe_2$, $GePh_2$ and $SiMe_2$ with alkene, diene and alkyne in hexanes at 23-25 °C.	115
Table 2.5	Rate constants for the reactions of $GeMe_2$ in deoxygenated hexanes and the gas phase at 298 K.^{a}	122
Table 3.1	Comparison of absorption maximum and bimolecular rate constants (k_Q / 10^9 $M^{-1}s^{-1}$) for the reactions of the transients assigned to $GeMe_2$ in hexane.	145
Table 3.2	Pseudo-first-order decay rate constants for the reactions of oxygen with the 430 nm transient species produced by laser flash photolysis of **18** in hexane at 25 °C.	150

Table 3.3	A comparison of the rate constants (k_Q / 10^8 $M^{-1}s^{-1}$) for the reactions of 1,3,5-(1-metalla)hexatriene derivatives **40-42** in hydrocarbon solvents with the transient (λ_{max} = 425-430 nm) formed by laser flash photolysis of **18**.	157
Table 4.1	A comparison of the absolute rate constant (k_Q) and equilibrium constant (K_{eq}) for the reactions of $GeMe_2$, $GePh_2$ and $GeMes_2$ with methanol, t-butanol and THF.	188
Table 5.1	Absolute rate constants for the reactions of the Me_2Ge-MeOH complex with Brønsted acids in deoxygenated methanol at 25 °C, and the pK_a values of the acids in methanol.	204
Table 5.2	Rate constants for the reactions of the Me_2Ge-THF complex in deoxygenated THF and free $GeMe_2$ in deoxygenated hexane at 25 °C.[a]	227
Table 6.1	Bimolecular rate constants (k_Q / 10^6 $M^{-1}s^{-1}$) for the reactions of Ge_2R_4 in hexane at 25 °C.	240
Table 6.2	Absolute rate constants (k_Q / 10^6 M^{-1} s^{-1}) for the reactions of Ge_2Me_4 and Ge_2Ph_4 with group 14 metal hydrides in hexane at 23-25 °C.	241
Table 6.3	Bimolecular rate constants for the reactions of digermenes and Si_2Me_4 with CCl_4 in hexane at 25 °C.	244
Table 6.4	Absolute rate constants for the reaction of digermenes with oxygen in hexane at 25 °C.	246
Table 6.5	Rate constants (k_Q / 10^6 $M^{-1}s^{-1}$) for the reaction of Ge_2Me_4, Ge_2Ph_4 and Si_2Me_4 with alkene, alkyne and diene in deoxygenated hexane.	250

List of Schemes

Scheme 1.1	Photochemical or thermal generation of germylenes from 1-metallacyclopent-3-enes.	15
Scheme 1.2	Typical reactions of digermenes.	24
Scheme 1.3	Some common precursors used to generate $GeMe_2$ in matrixes and/or in solution.	26
Scheme 1.4	Photochemical precursors for the generation of $GeMe_2$ by 193 nm laser flash photolysis in the gas phase.	30
Scheme 2.1	Photolysis of **25** in methylcyclohexane in the presence of DMB and trimethylsilane.	57
Scheme 2.2	Synthesis of 2-phenyl-1,3-butadiene **28**.	59
Scheme 2.3	Synthesis of 2-methyl-3-phenyl-1,3-butadiene **31**.[a]	59
Scheme 2.4	Synthesis of germacyclopent-3-enes **23** and **24**.	60
Scheme 2.5	Steady state photolysis of **23** (0.04-0.05 M) in the presence of MeOH (0.24 M) and AcOH (0.25 M) in cyclohexane-d_{12}.	65
Scheme 2.6	Steady state photolysis of **23** in the presence of DMB in cyclohexane-d_{12}.	68
Scheme 2.7	Steady state photolysis of **24** in the presence of AcOH in C_6D_{12}.	70
Scheme 2.8	Steady state photolysis of **36** in the presence of methanol.	73
Scheme 2.9	Generation of $GeMe_2$ by laser flash photolysis of **23** in deoxygenated hexanes and its reaction in the absence of a scavenger.	80
Scheme 2.10	Photochemical decomposition of **24** in deoxygenated hexanes.	81
Scheme 2.11	Reactions of $GeMe_2$ in solution in the presence of scavenger Q.	88
Scheme 2.12	Reaction of GeR_2 with scavenger (Q).	90
Scheme 2.13	Postulated mechanism for the reaction of GeR_2 with AcOH.	103

Scheme 2.14	Postulated mechanism for the reaction of MR_2 with R'_3M'-H.	106
Scheme 2.15	Postulated mechanism for the reaction of GeR_2 with a primary or secondary amine; for e.g. n-$BuNH_2$.	116
Scheme 2.16	Postulated mechanism for the reaction of $GeMe_2$ with CCl_4.	120
Scheme 3.1	Photolysis of **18** in the presence of DMB.[7]	133
Scheme 3.2	Photolysis of **18** in the presence of CCl_4, MeOH and DMB.[8]	135
Scheme 3.3	Photolysis of **18** in hexane.	156
Scheme 4.1	Reactions of $GeMe_2$ in deoxygenated hexane containing THF.	177
Scheme 4.2	Postulated reaction pathways for the reactions of GeR_2 in the presence of alcohols.	189
Scheme 5.1	Reaction pathways of $GeMe_2$ and Me_2Ge-THF complex in the presence of Q in neat THF.	199
Scheme 5.2	Proposed mechanism for the solvent-catalyzed decay of the Me_2Ge-methanol complex in methanol.	202
Scheme 5.3	Reactions of R_2Ge-MeOH complex in the presence of a Brønsted acid in neat MeOH.	208
Scheme 5.4	Proposed mechanisms for the reactions of germylene-MeOH complexes with MeONa in MeOH.	210
Scheme 5.5	Reactions of GeR_2 and the R_2Ge-THF complex in THF	218
Scheme 5.6	Postulated mechanism for the reaction of the Me_2Ge-THF complex with AcOH in THF.	222
Scheme 5.7	Postulated mechanism for the reaction of the Me_2Ge-THF complex with MeONa in THF.	224
Scheme 6.1	Reaction pathways of $GeMe_2$ and Ge_2Me_4 in the presence of a scavenger (Q) when (a) the reaction of $GeMe_2$ with Q is *irreversible*, and (b) the reaction of $GeMe_2$ with Q is *reversible.*	235
Scheme 6.2	Trapping of $GePh_2$ and Ge_2Ph_4 by methanol in a laser-drop experiment.	236

Scheme 6.3	Addition of digermenes to AcOH.	237
Scheme 6.4	Postulated reaction mechanism of Ge_2Me_4 with carbon tetrachloride.	243
Scheme 6.5	Reaction of digermenes with oxygen.	245
Scheme 6.6	Reactions of digermene with diene and alkyne.	249
Scheme 7.1	Photochemical generation of $GeMe_2$.	257

CHAPTER 1

1.1 Group 14 reactive intermediates

The study of reactive intermediates of group 14 elements (MR_2: M = C, Si, Ge, Sn), for example radicals ($R_3M\bullet$), cations (R_3M^+), anions (R_3M^-), divalent compounds ($R_2M\colon$), etc. is of central importance to contemporary mechanistic, synthetic and theoretical chemistry. Organic reactive intermediates have been extensively explored because of their major roles in organic chemical reactions. To date, several fascinating trends have been established for reactive intermediates of group 14 elements, and some of the reactivities once considered specific to organic reactive intermediates are also exhibited by members down the group. In the past years, advancements in synthetic methodologies, spectroscopic tools and computational methods have significantly increased our understanding of the chemistry of group 14 reactive intermediate chemistry and new developments continue to emerge.

1.2 Divalent group 14 compounds and their dimers

Divalent group 14 compounds include carbenes, silylenes, germylenes, stannylenes and plumbylenes. They are neutral species in which the di-coordinate atom possesses only six valence electrons. Unless kinetically or thermodynamically stabilized by the substituents on the central atom, these divalent compounds readily dimerize to form the corresponding M=M doubly-bonded dimers.[1] While alkenes adopt a planar geometry around the carbon atom, the heavier analogues typically have a trans-bent geometry.[2]

The common nomenclature of the divalent group 14 compounds and their dimers is shown in Figure 1.1.

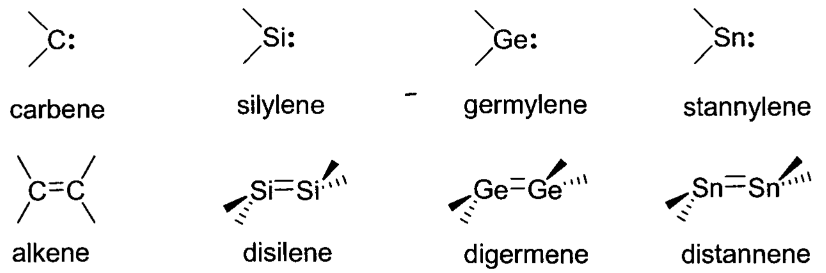

Figure 1.1. Common nomenclature for divalent group 14 compounds and their dimers.

Their study has been significantly furthered by the use of experimental methods such as time-resolved UV-Vis and IR spectroscopy, Electron Paramagnetic Resonance (EPR) spectroscopy, Chemically Induced Dynamic Nuclear Polarization (CIDNP), X-Ray crystallography, etc., which has helped shed new light on the understanding of their structural, electronic and chemical properties. Moreover, powerful computational methods have been used to predict several features of these reactive intermediates such as their energies, UV-Vis spectra, and the mechanisms of their reactions.

The chemistry of the divalent group 14 compounds and their dimers has experienced a profound revolution with the development of a number of stable derivatives.[1,3-7] They are greatly stabilized by the presence of bulky and/or σ- or π-donor substituents. A few examples of stable singlet carbenes, silylenes and germylenes are given in Figure 1.2.

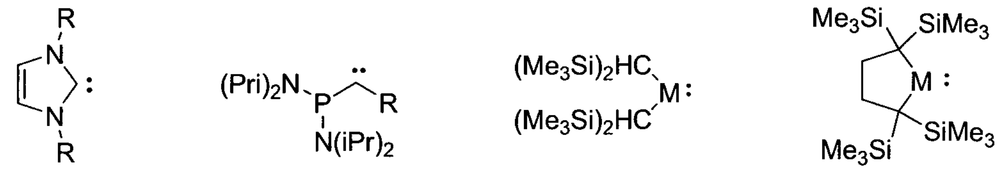

R = alkyl, aryl (Arduengo)[8]

R = $SiMe_3$, CF_3, aryl (Bertrand)[3]

M = Si or Ge (Lappert)[9]

M = Si or Ge (Kira)[10,11]

Figure 1.2. Examples of stable singlet divalent group 14 compounds.

The growing knowledge about the chemistry of divalent group 14 reactive intermediates has raised interest in their potential industrial applications. For example, currently, carbenes are being used as catalysts for the polymerization of alkenes or as ligands in transition metal complexes catalysts.[12,13] The intermediacy of silylene (SiH_2) and germylene (GeH_2) has been invoked in the low or high temperature chemical vapor deposition (CVD) of silicon and germanium hydrides in semiconductor manufacturing processes.[14,15] Digermenes, like alkenes, serve as excellent starting materials for the synthesis of more elaborate organogermanium compounds.[4,16,17] In recent years, there has been a growing interest in understanding the chemistry of molecular disilenes and digermenes, as models for the bonding on Si and Ge semiconductor surfaces.[18-20] It has been found that the Si=Si or Ge=Ge dimers on the Si(100) or Ge(100) – 2x1 dimer surfaces are highly prone to cycloaddition reactions with unsaturated organic molecules, and this feature has been exploited for the manufacture of ordered organic monolayers on these surfaces.[21] It is clear that an understanding of the physical and chemical properties of these divalent compounds and their dimers is of fundamental importance in order to further exploit, improve and expand their applications.

1.2.1 Electronic structure of divalent group 14 compounds

The central atom in a divalent group 14 compound is connected to two substituents by covalent bonds and possesses a pair of non-bonding electrons. The divalent compound can thus exist in either a closed shell singlet or open shell triplet ground state configuration (Figure 1.3).[22] The singlet state adopts a bent geometry, and has a vacant p orbital and a doubly occupied σ-orbital. The triplet state is still bent but has a wider R-M-R angle, and contains unpaired electrons with parallel spins (one electron in a sp^2-orbital and one in a p-orbital). The triplet state is generally considered as a biradical. The ground state multiplicity of divalent group 14 compounds is governed by the energy difference between the σ (HOMO) and p_π (LUMO) orbitals on the central atom. The singlet state is favored by a large energy difference between these two orbitals.

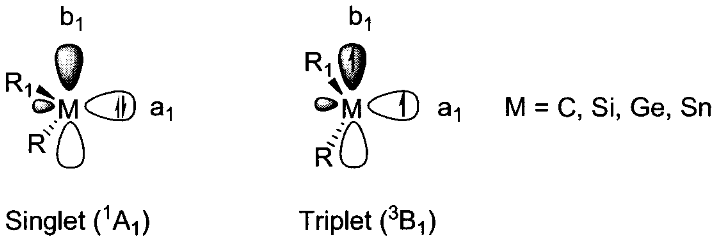

Figure 1.3. Singlet and triplet electronic structure of divalent group 14 compounds.

The energy difference between the lowest energy singlet and triplet states (the singlet-triplet energy gap) is denoted by $\Delta E_{S\text{-}T}$, and is given by eq (1.1). A positive $\Delta E_{S\text{-}T}$ indicates that the singlet state is lower in energy than the triplet state, and is roughly equal to the electron-electron repulsion in the σ-orbital minus the energy required to promote an electron to the p-orbital.

$$\Delta E_{ST} = E_{triplet} - E_{singlet} \qquad \textbf{(1.1)}$$

Theoretical calculations have predicted that the magnitude of $\Delta E_{S\text{-}T}$ is influenced by both the electronic nature and the steric bulk of the substituents on the central atom.[23,24] The singlet ground state is favored by substituents that are strong σ-acceptors or π-donors; σ-acceptors inductively stabilize the nonbonding σ-orbital by increasing its s character, leaving the p-orbital unaffected, while π-donors stabilize the singlet state by donating electrons into the formally vacant p-orbital.[25,26] In contrast, the triplet state is favored by substituents that are strong σ-donors (electropositive) or π-acceptors, which cause a decrease in the magnitude of ΔE_{ST} by elevating the HOMO and lowering the LUMO orbital levels. Bulky substituents tend to cause a widening of the R-M-R_1 angle (α), favoring the triplet state. As α increases, the singlet state is destabilized relative to the triplet state due to a loss in s-character of the σ-orbital. Eventually the singlet and triplet state potential energy curves cross; for SiH_2 the angle at which the singlet and triplet states are degenerate is ~ 129°.[27]

Both experimental data and theoretical calculations show that methylene (CH_2) possesses a triplet ground state, with the singlet state lying higher in energy by only ca. 9 kcal/mol.[28-30] Because the two spin states of methylene are so close in energy, their relative ordering is extremely sensitive to the nature of the substituents on the central carbon in substituted carbenes. For example, most aryl- and alkylcarbenes are ground state triplets, whereas carbenes bearing lone-pair-containing substituents (CX_2; X = halogen, OR, NR) are generally ground state singlets.[31,32] Because the magnitude of the singlet-triplet energy gap ($\Delta E_{S\text{-}T}$) increases as one progresses down group 14, the singlet states of silylenes and germylenes are much more stable than their triplet states, and thus derivatives with a triplet ground state are relatively rare.[33] Examples of $\Delta E_{S\text{-}T}$, 18-21 kcal mol^{-1} (experimental)[34] and 19-23 kcal mol^{-1} (calculated)[35-37] for SiH_2; 23 kcal mol^{-1} (calculated)[38] for GeH_2; 23-26 kcal mol^{-1} (calculated)[39,40] for $Si(CH_3)_2$; 27 kcal mol^{-1} (calculated)[41] for $Ge(CH_3)_2$. Thus, the singlet is the lower energy state in the great majority of silylene and germylene derivatives.

For years researchers have been working on ways for generating silylenes or germylenes that possess a triplet ground state and a number of experimental attempts and theoretical studies have been reported.[24,42-44] However, this remains a tremendous challenge. Strong electropositive and/or sterically bulky substituents on the central atom have been commonly employed in an attempt to achieve this goal. To date, only four cases of silylenes with triplet ground states have been reported. Jiang and Gaspar reported that $(^tBu_3Si)(^iPr_3Si)Si$ reacts from its triplet state based on its reactivity: it was found to undergo both intramolecular and intermolecular C-H insertion reactions, which is atypical for singlet silylenes.[43,45,46] Sekiguchi *et al.* have successfully generated the ground state triplet silylenes **1-3** and characterized them by EPR spectroscopy: the triplet state of **1** is stabilized by both electronic and steric effects, while that of **2** and **3** are stabilized mainly by electronic effects (Figure 1.4).[45,46]

1

2 M = Li
3 M = K

Figure 1.4. Experimentally generated triplet silylenes.

1.2.2 Divalent State Stabilization Energy

Walsh investigated the successive bond dissociation energies (BDE) of a series of tetravalent silicon-containing compounds (SiX_4; X = H or Cl or F), as defined by eq (1.2), and in all cases, found that the second BDE is significantly lower than the first BDE.[47] This indicates some extra stability associated with the divalent Si species, compared to the situation with carbon, where second BDEs are generally higher. Walsh introduced the term Divalent State Stabilization Energy (DSSE), which is defined as the difference between the first and the second M-X BDE in MX_4 compounds (M = C, Si, Ge, Pb; eq. 1.3).[47] The term DSSE has been commonly used as an index of reactivity for divalent group 14 compounds.

$$MX_4 \xrightarrow[-X]{\text{BDE }(X_3M\text{-}X)} \cdot MX_3 \xrightarrow[-X]{\text{BDE }(X_2\dot{M}\text{-}X)} :MX_2 \qquad \textbf{(1.2)}$$

$$\text{DSSE }(MX_2) = \text{BDE }(X_3M\text{-}X) - \text{BDE }(X_2M\text{-}X) \qquad \textbf{(1.3)}$$

The trends in the first and second BDEs of methane, silane and germane and the resulting DSSE values are illustrated in Table 1.1. It is observed that the DSSE increases with increasing atomic number of the central atom as we proceed down group 14. Walsh speculated that this is due to a decrease in the energy of the HOMO and an increase in its s character as we descend the group.[47] Methylene does not experience such stabilization and possesses a triplet ground state. Walsh also found that DSSE correlates linearly with the electronegativity of the substituents on the Si, and suggested that this is due to a deshielding effect. Electronegative substituents pull electron density away from the Si nucleus, thereby increasing its attraction toward the nonbonding electrons.[48]

Table 1.1. Successive bond dissociation energies (BDE / kcal mol^{-1}) in MH_4 (M = C, Si, and Ge) compounds and Divalent State Stabilization Energies (DSSE / kcal mol^{-1}) of MH_2 species.

Bond	**BDE**[a]	**Bond**	**BDE**[a]	**Bond**	**BDE**[b]
CH_3-H	104.8	SiH_3-H	90	GeH_3-H	84
CH_2-H	111.0	SiH_2-H	64	GeH_2-H	57
CH-H	100.4	SiH-H	84	GeH-H	-
C-H	81	Si-H	70	Ge-H	-
DSSE	-6.2	DSSE	26	DSSE	27

(a) Ref. 47; (b) Ref. 49.

1.3 Techniques used for the study of group 14 reactive intermediates

Product studies

In product study experiments, the reactive intermediate is generated *in situ* by the thermal or photochemical decomposition of a suitable precursor in solution or in the gas phase. Usually, it is generated in the presence of a reagent that reacts with it to form stable product(s). The latter are then isolated and characterized by spectroscopic techniques such as NMR and IR spectroscopy. In these types of experiments, conclusions about the properties of the reactive intermediate are drawn based on the nature of the products.

Competitive trapping experiments can be carried out to obtain the relative rates of reactions. These experiments involve generating the reactive intermediate (RI) in the presence of known concentrations of two substrates (Q_1 and Q_2). The relative rates are obtained by determining the relative yields of the products formed from the reaction with each added reagent, and correcting for the relative concentrations of the competing substrates (see eq 1.4). In these experiments, it is important that the reagents react with the reactive intermediates irreversibly to give products that are stable within the experimental time-frame. It is preferable that each reagent reacts with the reactive intermediate to form a single stable product. In addition, it is important to ensure that the products are formed from the reaction of the reagents with the reactive intermediate and not from a different pathway.

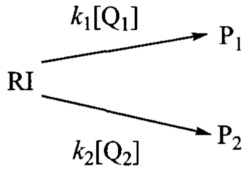

$$\frac{P_1}{P_2} = \frac{k_1[Q_1]}{k_2[Q_2]} \qquad \textbf{(1.4)}$$

UV-Vis absorption spectroscopy

The direct spectroscopic characterization of group 14 reactive intermediates has been commonly achieved by the use of matrix isolation spectroscopy or time-resolved spectroscopy. One version of the matrix isolation technique involves the generation of the reactive intermediate by the photochemical decomposition of a suitable precursor in frozen solvents (commonly referred to as organic glasses) or rare gas (nitrogen, argon, neon or krypton) matrixes at very low temperatures (77 K or below).[50] Under these conditions, the reactive intermediate is immobilized; diffusion is inhibited and its bimolecular reactions are therefore suppressed. Moreover, there is usually not enough thermal energy to overcome activation barriers associated with unimolecular reactions. The reactive intermediate can thus be studied by a variety of spectroscopic techniques (eg. UV-Vis, IR, EPR or fluorescence spectroscopy), from which information about its electronic and structural properties can be obtained. Often inert matrixes are doped with a reactive material to form reactive matrixes. When a reactive intermediate is generated in this type of matrix, annealing of the matrix leads to the formation of characteristic products, and these are used as evidence for the identity of the reactive intermediate.

Time-resolved UV-Vis absorption spectroscopy allows the study of the reactive intermediate in real time such that quantitative information about its reactivity in the absence and presence of a scavenger can be obtained.[51] In a laser flash photolysis experiment, a solution of a photochemical precursor is irradiated with a pulsed UV laser. This allows a rapid generation of the reactive intermediate. A variety of types of pulsed UV lasers are available for use in such systems, such as, excimer, Nd-YAG, and nitrogen lasers. These typically have pulse widths of 5-25 ns, and provide monochromatic excitation pulses ranging from 193-351 nm.

1.4 Germylenes

Germylenes (GeR_2) bearing simple alkyl and aryl substituents are highly reactive intermediates whose direct study, in all known examples, requires the use of matrix isolation or time-resolved spectroscopic techniques. The kinetic behavior of these species is significantly under-explored as compared to that of singlet carbenes. Germylenes are conveniently studied by UV-Vis absorption spectroscopy. The lowest energy electronic transition occurs between the HOMO (σ-type orbital) to the LUMO (p-type), as shown in Figure 1.5. The UV-Vis spectroscopic properties and kinetic behavior of a number of transient germylenes have been studied in the gas phase (e.g. GeH_2, $GeMe_2$, GeHMe),[52-54] in solution (e.g. $GeMe_2$, GeMePh, $GePh_2$ and $GeMes_2$)[55-59] and in low-temperature matrixes (e.g. $GeMe_2$, $GePh_2$ and $GeMes_2$).[60]

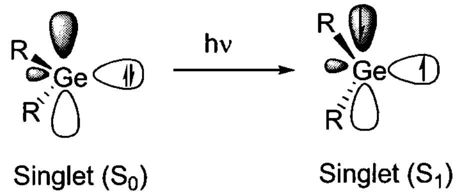

Figure 1.5. Electronic transition from singlet ground state (S_0) to singlet excited state (S_1) in a germylene.

Transient germylenes are produced by the thermal or photochemical decomposition of a large number of germanium-containing compounds. Stable germylenes can be synthesized by a variety of synthetic methods. Germylenes are known to react with a number of classes of functional groups in an analogous way to singlet carbenes and silylenes. Elaboration on the most common sources and reactions of germylenes will follow in the sub-sections below.

1.4.1 Sources of germylenes

Advances in organometallic chemistry have enabled the preparation of a wide variety of precursors that have been used to generate germylenes under various conditions. Synthetic methods used for the preparation of silylenes can often be adapted to prepare germylenes in solution. The α-elimination of halogenated- or hydridoalkoxy-silicon and germanium derivatives give silylenes and germylenes in solution (eq 1.5).[61-63] Dichlorogermylene is conveniently prepared by the reduction of germanium tetrachloride in 1,4-dioxane and the resultant dichlorogermylene-dioxane complex is stable at room temperature under argon (eq 1.6).

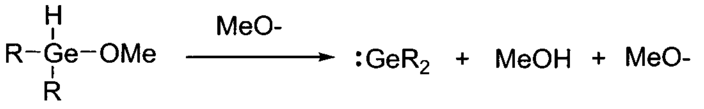

(1.5)

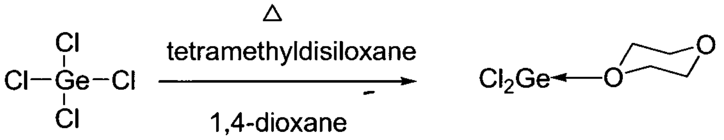

(1.6)

A number of classes of compounds that have been used to generate carbenes and silylenes can be employed to generate germylenes. For instance, the decomposition of 7-norbornadiene derivatives under mild thermal conditions (70 - 150 °C) or photochemical conditions is an important source of carbenes and their heavier analogues (eq 1.7).[64-67] The co-product tetraphenylnaphthalene is unreactive toward the generated reactive intermediates.

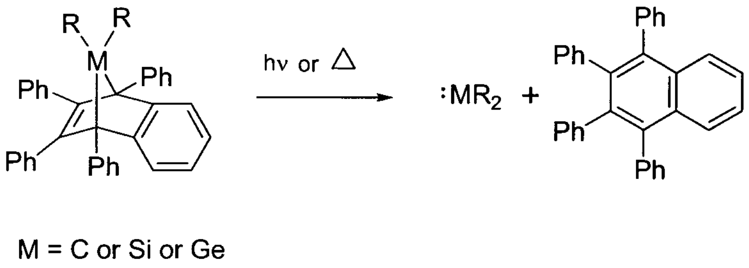

(1.7)

Germylenes can be obtained by the photochemical decomposition of silylgermanes, disilylgermanes and certain digermanes (with formula $[R_2Ge]_n$ (n = 2-6)).[68-73] Examples are given in eq (1.8-1.12).[68-70]

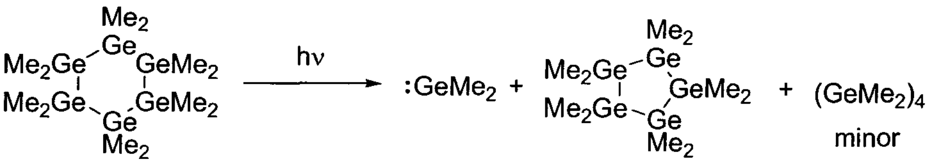

(1.8)

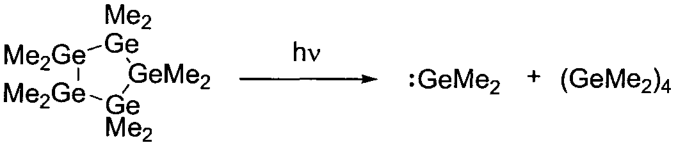

(1.9)

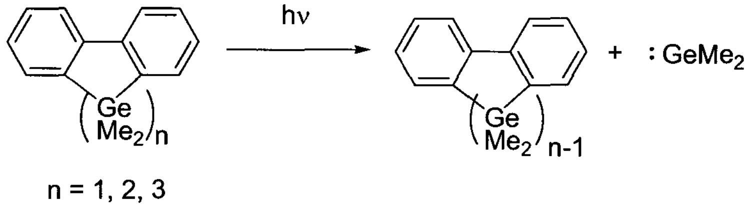

(1.10)

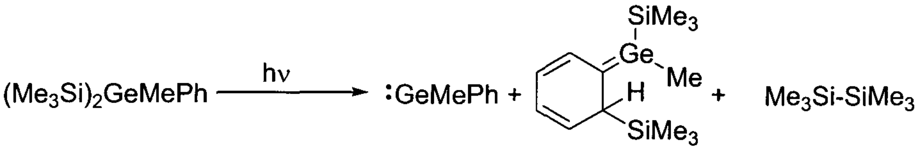

(1.11)

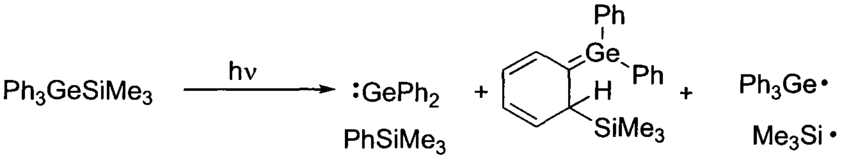

(1.12)

Germylenes are also formed by the thermolysis or photolysis of 1-germacyclopent-3-ene derivatives in solution or gas phase (Scheme 1.1).[43,52,54,55,57] These precursors can be synthesized by relatively straightforward synthetic routes, and are insensitive to air and moisture.

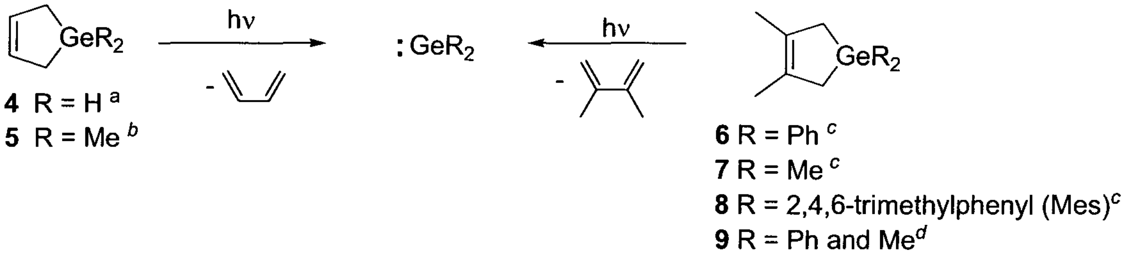

Scheme 1.1 Photochemical or thermal generation of germylenes from 1-metallacyclopent-3-enes. (a) Ref. 52; (b) Ref. 54; (c) Ref. 55; (d) Ref. 57.

1.4.2 Reactions of transient germylenes in solution

As mentioned earlier, germylenes exist in the singlet ground state and are sp^2 hybridized with a lone pair of electrons and an empty p-orbital. This type of electronic structure makes them potentially ambiphilic in nature, i.e. they can act as *electrophiles* by accepting a pair of electrons from electron-pair donors or they can act as *nucleophiles* by donating their lone pair of electrons to electron-pair acceptors. Characteristic reactions of transient germylenes include dimerization, addition to multiple bonds, insertion into polarized sigma bonds, reaction with oxygen, and complexation with Lewis bases.[58] A summary of the characteristic reactions of germylenes is given in Figure 1.6.

One of the best known reactions of germylenes is their insertion into σ-bonds. The σ-bond usually involves at least one atom that bears a lone pair of electrons, e.g. X-H (X = S, O, N, Cl),[53,74-76] and C-X (X = halogen)[77,78] bonds. Germylenes also insert into M-H (M = Si, Ge, Sn)[79] and M-M (M = Si, Ge and Sn) bonds.[80] To date, mechanistic studies suggest that most reactions involving germylenes are stepwise, and proceed by an initial electrophilic interaction to form intermediate complexes with the substrates.[81]

Analogous to singlet carbenes, germylenes add to the carbon-carbon multiple bonds of alkenes,[82,83] alkynes[84,85] and 1,3-dienes[82] by (2+1)-cycloaddition to form the corresponding germirane or germirene derivatives. In contrast to cyclopropanes and cyclopropenes, the germanium analogues are typically thermally unstable due largely to ring strain and the higher divalent state stabilization energy (DSSE) of germylenes compared to analogous carbenes.[86] The reactions with 1,3-dienes are more well-known than those with alkenes because they ultimately give germacyclopent-3-ene derivatives which are typically stable. In early work, Köcher, Neumann, Gaspar and others have debated whether the formation of 1-germacyclopent-3-enes from the reaction of germylenes with 1,3-dienes occurs by direct by (4+1)-cycloaddition or via the intermediacy of a vinylgermirane formed by (2+1)-cycloaddition.[87-90] In subsequent years, both experimental and theoretical results that strongly support the intermediacy of a vinylgermirane in these reactions emerged.[56,82,91] Recent theoretical and experimental work support that the germacyclopent-3-ene derivative is formed from the direct (1+4)-cycloaddition reaction.[92,93] It is postulated that the reaction proceeds reversibly to form the corresponding vinylgermirane. The 1,3-sigmatropic rearrangement of the vinylgermirane to form the germacyclopent-3-ene derivative is not energetically favored and is slow. Instead, the vinylgermirane dissociates to form the germylene which then undergoes a concerted (1+4)-cycloaddition reaction with the 1,3-diene to give the germacyclopent-3-ene derivative (thermodynamic product).

Germylenes, like carbenes and silylenes, are known to form complexes with Lewis bases such as ethers, amines, and phosphines.[60] Spectroscopic evidence for the formation of aryl-substituted germylene complexes with ethers, amines, sulfides, phosphines and alkyl halides in hydrocarbon matrixes at 77 K have been reported.[60,94] These complexes exhibit distinct absorption bands at shorter wavelengths as compared to the free germylene. Moreover, to date, several germylenes stabilized by intermolecular or intramolecular coordination with electron-pair donors have been reported.[1]

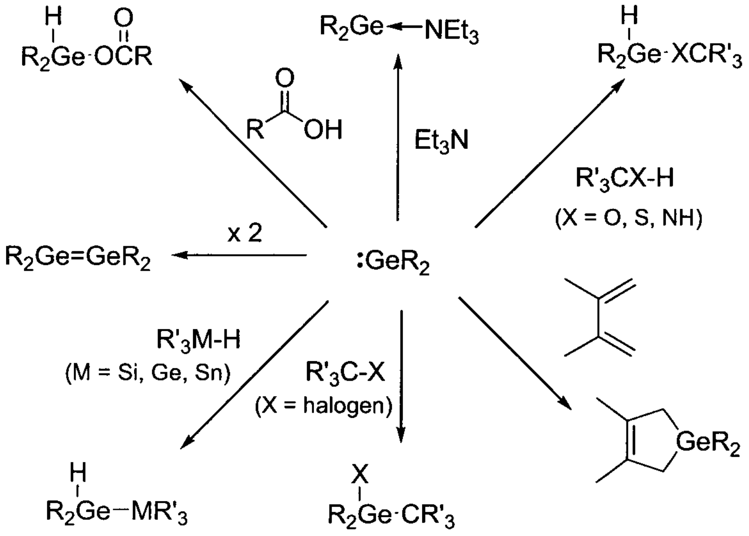

Figure 1.6. Some characteristic reactions of germylenes.

1.5 Digermenes

Compounds containing doubly-bonded heavy group 14 elements (M=M; M = Si, Ge, Sn) have gained considerable attention in the past years owing to their fascinating structural features and their rich chemistry.[16,95] The chemistry of these compounds has attracted a mounting interest since the isolation of the first stable disilene by West and Fink in 1981.[96] Digermenes ($R_2Ge{=}GeR_2$) are homonuclear doubly-bonded Ge compounds and are the heavier analogues of alkenes and disilenes ($R_2M{=}MR_2$, where M = C or Si). They are typically too reactive to be isolated unless they are stabilized by bulky substituents. Digermenes are often used as starting materials or have been invoked as intermediates in several organogermanium reactions.[4,5,17,97,98] In 1982, the first UV-Vis spectrum of a digermene, tetrakis(2,6-dimethylphenyl)digermene was reported in solution by Masamune *et al.*[99] Two years later, Hitchcock *et al.* reported the X-ray structure of the first stable crystalline digermene **10**,[100] and about the same time, Snow *et al.* reported the synthesis of another stable digermene **11**.[101]

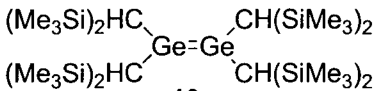
$[(Me_3Si)_2HC]_2Ge{=}Ge[CH(SiMe_3)_2]_2$

10

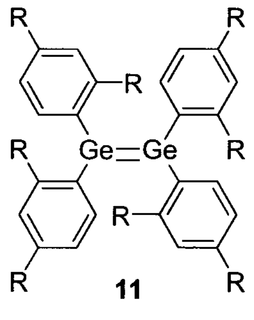

11

R = ethyl

The formation of the simplest tetraalkyl-substituted digermene, namely tetramethyldigermene (Ge_2Me_4), was first evidenced by trapping experiments by Sakurai *et al.* in 1982 and was characterized in low temperature matrixes by IR spectroscopy in 1984.[102,103] There are only a few UV-Vis spectroscopic and kinetic studies reported on the reactions of transient digermenes in solution. Typically, in hydrocarbon solutions, transient phenylated digermenes exhibit π-π^* transitions in the 400-440 nm UV range and alkyl substituted digermenes in the 360-380 nm range. For example, Leigh *et al.* has reported that Ge_2Ph_4 exhibits an absorption maximum at λ_{max} = 440 nm[55] while $Ge_2Me_2Ph_2$ exhibits an absorption maximum at λ_{max} = 420 nm;[57] Mochida *et al.* reported that Ge_2Me_4 and Ge_2Et_4 exhibit absorption maxima at λ_{max} = 370-380 nm[55,68,69,104] and 380 nm, respectively.[104]

1.5.1 Bonding and structural properties of digermenes

X-ray structural analysis of several crystalline digermenes has revealed that, unlike alkenes which adopt planar geometries around their C=C bonds, the Ge=Ge double bond in digermenes adopts a trans-bent geometry with pyramidalization at the germanium center.[100,105-107] These findings confirmed the early theoretical predictions of Trinquier *et al*,[108] who in addition, suggested that the double bond in digermenes can be best described as two donor-acceptor bent bonds between two singlet germylenes, with delocalization of the lone pair on one Ge into the empty p orbital of the other and vice versa, as shown in Figure 1.7.[108]

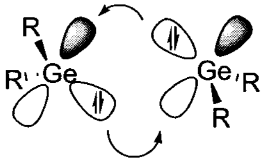

Figure 1.7. Bonding in digermene.

The trans-bending phenomena in digermenes has been explained on the basis of π-σ*-orbital mixing: as one descends group 14 from C to Pb, the energy difference between the π and σ* orbitals associated with the M=M bond decreases, thereby, allowing more orbital mixing.[109,110] This leads to a lowering in the energy of the trans-bent structure as compared to the planar structure.[109] The degree of mixing is affected by two factors: the intrinsic π-σ* gap of the double bond (stronger double bonds have larger π-σ* gaps) and the electronic nature of the substituents.[110] Theoretical calculations predict that the presence of electronegative substituents or π-donating substituents on the germanium atom enhances trans-bending while electropositive substituents favor planarity.[110-112] Indeed, Kira *et al.* reported that X-ray structural analysis of a series of tetrakis(trialkylsilyl)digermenes ($(R_3Si)_2Ge{=}Ge(SiR_3)_2$, R = *i*-$Pr_2Me$ or *t*-$BuMe_2$ or *i*-Pr_3) showed that they possess nearly a planar geometry around the Ge=Ge bonds, consistent with theoretical predictions.[113]

1.5.2 Sources of digermenes

The most common routes for the generation of transient digermenes are the thermal or photochemical cycloreversions of strained cyclic compounds.[16,103,104,114-117] For example, the photolysis of 7,8-digermabicylo[2.2.2]octadiene derivatives in solution gives the corresponding digermene and 1,4-diphenylnaphthalene as the major products, along with minor amounts of the photochemical rearrangement product, 1,4-diphenyl-2,3-benzo-6,6,7,7-tetraalkyl-6,7-digermatricyclo[3.3.0.0]-octane (eq 1.13).[104] Cyclotrigermanes decompose thermally or photochemically to give the corresponding digermenes and germylenes (eq 1.14).[99,105,118] Digermenes can also be generated by dimerization of germylenes (eq 1.15).[5,118]

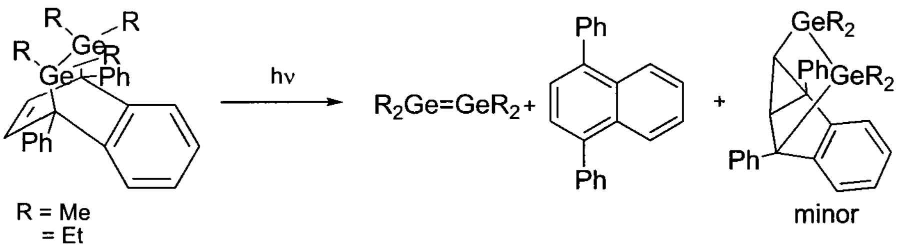

(1.13)

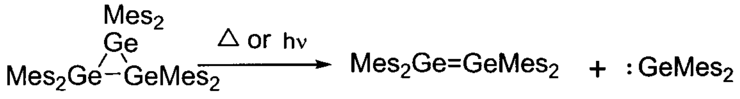

(1.14)

$$:\mathrm{GeMes_2} \xrightarrow{\mathrm{x}\,2} \mathrm{Mes_2Ge{=}GeMes_2}$$ **(1.15)**

Stable digermenes can be synthesized by reductive elimination reactions, for example, from the reaction of dichlorogermane derivatives with sodium in toluene or lithium naphthalenide in THF (eq 1.16).[107] They can also be prepared by the reaction of dichlorogermylene-dioxane complex with a Grignard reagent (eq 1.17) or by the reaction of a stable diaminogermylene with an organolithium reagent (eq 1.18).[101,119]

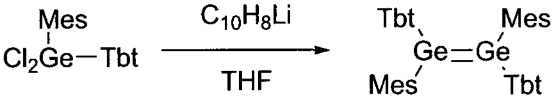

(1.16)

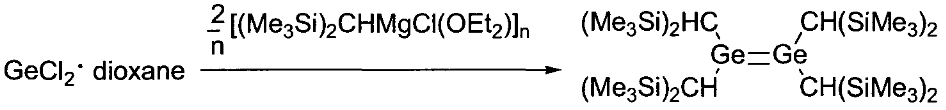

(1.17)

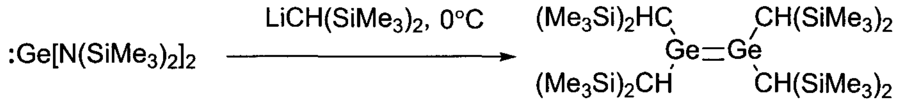

(1.18)

1.5.3 Reactions of digermenes

Transient digermenes are unstable with respect to di-, oligo- or polymerization reactions. Their kinetic stability is highly influenced by the bulkiness of the substituents on the germanium atoms. Several stable digermenes bearing moderately bulky substituents on the Ge=Ge bond have been isolated and characterized.[4,5] On the other hand, highly bulky substituents on the Ge=Ge bond induces dissociation of the digermene to the free germylenes (eq 1.19).[120]

(1.19)

The reactions of digermenes are similar to those of disilenes. Some of their characteristic reactions involve dimerization, nucleophilic addition, cycloadditions and oxidation reactions (Scheme 1.2).[121] Digermenes react with halogens, chloroform, hydrogen halides and alcohols to give 1,2-addition products.[55,105,122,123] The 1,2-addition reactions are stepwise and occur either by a zwitterionic or radical pathway. It has been suggested that digermenes react with nucleophiles such as alcohols and amines, by a stepwise mechanism involving initial nucleophilic attack.[5,55,105] It is postulated that digermenes react with haloalkanes or group 14 metal hydrides in a stepwise via a radical pathway, analogous to disilenes.[123,124] Digermenes undergo [2+2] or [2+4]-cycloaddition reactions with a variety of unsaturated compounds such as alkynes, alkenes, dienes, aldehydes and ketones to give the corresponding cycloadducts.[117,125-127] However, it is generally observed that stable and relatively stable digermenes are unreactive toward dienes.[128,129] Digermenes react with singlet oxygen to form 1,2-digermadioxetanes, which undergo thermal rearrangement to form 1,3-digermadioxetanes.[130,131]

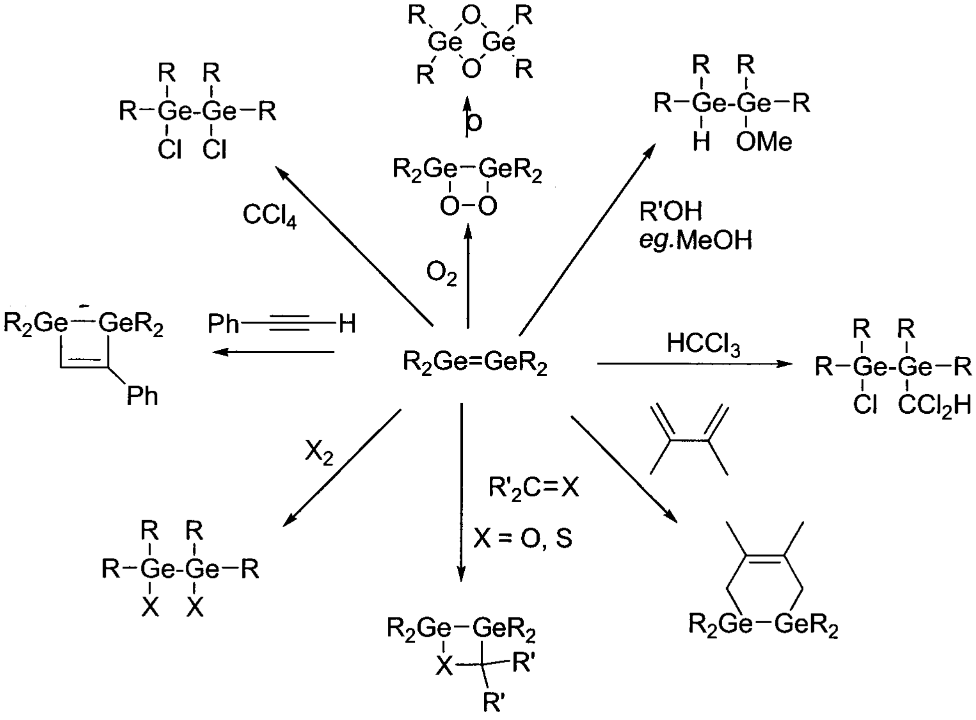

Scheme 1.2 Typical reactions of digermenes.

1.6 The direct detection and kinetic studies of $GeMe_2$, the simplest dialkylgermylene

In the past years, a large number of attempts has been made to prove the existence of dimethylgermylene ($GeMe_2$), and characterize its spectral and kinetic properties. A few reviews of this work are available.[58,59,132] UV-Vis absorption spectroscopy in low temperature matrixes or time-resolved transient absorption spectroscopy in solution and gas phase has been commonly used in attempts to detect and/or follow the kinetics of reactions of $GeMe_2$. Product studies have also been carried out to prove the formation of $GeMe_2$-trapping products.

The UV–Vis absorption spectrum of "$GeMe_2$" was reported for the first time in 1984 by Sakurai *et al.* by the photolysis of the dibenzotrigermacycloheptane derivative **17** in 3-methylpentane at 77 K.[70] They observed a transient absorption band at 430 nm, which they assigned to $GeMe_2$ based on comparison to the spectrum reported for $SiMe_2$ (450 nm).[133] In the following several years, "$GeMe_2$" has been generated by the photolysis of various other precursors in rigid 3-methylpentane at 77 K and in solution. Some of the precursors that have been used for the generation of $GeMe_2$ by photolysis in matrixes and/or in solution are shown in Scheme 1.3.

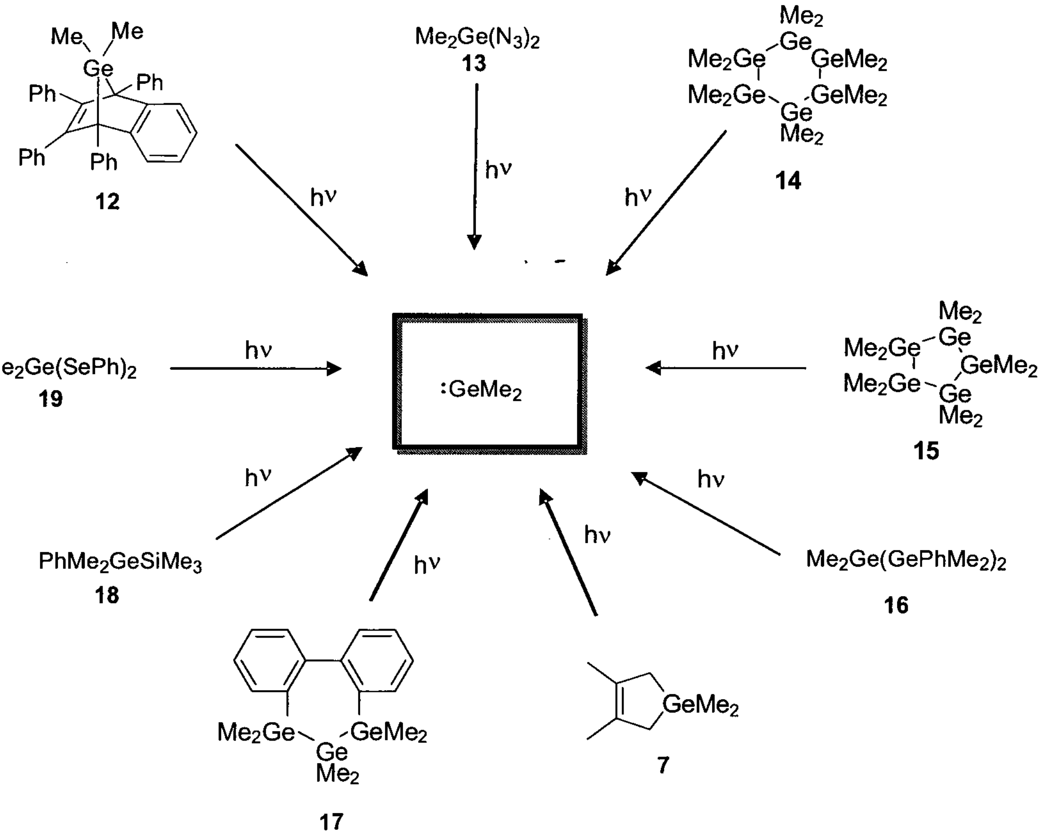

Scheme 1.3 Some common precursors used to generate $GeMe_2$ in matrixes and/or in solution

A survey of the literature on the direct detection of $GeMe_2$ prior to the work published in our group in 2004,[55] reveals there to be little consistency in the UV-Vis spectroscopic and kinetic data assigned to this transient germylene.[59] The absorption maximum (λ_{max}) assigned to "$GeMe_2$" in hydrocarbon matrixes or Ar matrixes (at 77 K or below) varies between 400-506 nm, while a larger scatter is observed in solution (λ_{max} = 380-490 nm).[59] It is difficult to determine which, if any, of the transient species assigned to $GeMe_2$ in the early studies is in fact the species in question. The photochemical precursors employed for the generation of $GeMe_2$ in these studies and assignments made in low temperature matrixes, in solution and in the gas phase are listed in Table 1.2. The data seem to depend primarily on the types of precursors used. Nevertheless, for the same precursor, a small variation is still observed in the absorption maximum reported from independent studies, indicating that other factors also affect the results.

Similar absorption spectra for "$GeMe_2$" are obtained when compounds $PhMe_2GeSiMe_3$ (λ_{max} = 418 nm and 425 nm), $Me_2Ge(SePh)_2$ (λ_{max} = 420 nm) and $Me_2Ge(GePhMe_2)_2$ (λ_{max} = 422 nm and 420 nm) are photolyzed in low-temperature matrixes and in solution (see Table 1.2). In addition, the photolysis of $PhMe_2GeGeMe_3$ (λ_{max} = 430 nm) in solution give a transient species that absorbs in the similar spectral region. In most cases, the assignments of the transient species to "$GeMe_2$" in solution were made on the basis of comparisons with the absorption maximum observed in low-temperature matrixes from the same precursor.

Table 1.2 A list of the photochemical precursors employed and absorption maxima (λ_{max}) assigned to "GeMe$_2$" in low temperature matrixes, solution and gas phase.

Precursor	**Photolysis conditions**	λ_{max}
17	3-MP at 77 K	430[70]
12	3-MP at 77 K	416[134]
12	3-MP at 77 K	420[60,115]
12	3-MP/IP (3:7) at 77 K	420[94]
$Me_2Ge(SePh)_2$	3-MP at 77 K or Ar matrix at 21 K	420[135]
$Me_2Ge(N_3)_2$	Ar matrix, 12-18 K	405[136]
cyclo-$(GeMe_2)_6$	3-MP at 77 K	430[68,134]
cyclo-$(GeMe_2)_5$	3-MP at 77 K	506[69]
$(PhMe_2Ge)_2GeMe_2$	3-MP at 77 K	422[72]
$Me(Me_2Ge)_5Me$	3-MP at 77 K	436[134]
$Me(Me_2Ge)_5Me$	3-MP at 77 K	437[137]
$PhMe_2GeSiMe_3$	"matrix"	418[88]
$PhMe_2GeGeMe_2Ph$	THF, rt	440[84]
cyclo-$(GeMe_2)_6$	Cyclohexane	450[68]
cyclo-$(GeMe_2)_5$	Cyclohexane	490[69]
12	Heptane	380[138]
12	Heptane	370[139]
$Me_2Ge(SePh)_2$	Cyclohexane	420[135]
$PhMe_2GeSiMe_3$	Cyclohexane	425[88]
$PhMe_2GeSiMe_3$	Cyclohexane	430[140]
$PhMe_2GeGeMe_3$	Cyclohexane	430[140]
$(PhMe_2Ge)_2GeMe_2$	Cyclohexane	420[141]
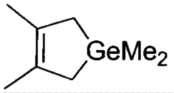	Hexane, 23 °C	480[55]
$Me_3GeGeMe_2H$	Gas phase	480[54]
	Gas phase	480[54]
$HGeMe_2GeMe_2H$	Gas phase	480[76]

Numerous kinetic studies have been carried out in the gas phase in an interest to understand the reactivities of germylenes and the mechanisms of their reactions in solution.[52] The parent germylene (GeH_2), $GeMe_2$ and GeMeH are the only germylenes that have been studied by laser flash photolysis (193 nm) in the gas phase.[52-54] Gas phase reactions have the advantage of being free from interfering factors such as solvent effects; in this way the intrinsic properties of the reactive intermediate can be known. Hence, the absorption maximum and kinetic data obtained for $GeMe_2$ in solution can be reliably compared with the ones observed in the gas phase. However, kinetic studies performed in the gas phase are restricted to substrates and precursors of low molecular weight in order for them to be sufficiently volatile; many of these analogous studies in solution are difficult because of their volatility and because of the necessity of using 193 nm laser excitation.

Becerra *et al.* reported that 193 nm laser flash photolysis of 1,1-dimethyl-1-germacyclopent-3-ene **5**, pentamethyldigermane **20** and 1,1,2,2-tetramethyldigermane **21** in the gas phase gave rise to a common transient species exhibiting λ_{max} = 480 nm (Scheme 1.4).[54,76] The kinetic behavior of the transient species was similar in all three cases. The formation of 1,1-dimethylgermacyclopentene as the major product from the irradiation of precursor **20** in the presence of 1,3-butadiene indicated that extrusion of $GeMe_2$ is the major photochemical process. In addition, photolysis of **5** yielded 1,3-butadiene as major product, suggesting extrusion of $GeMe_2$. On the basis of these results, the transient species observed in these studies was assigned to $GeMe_2$. However, it was observed that the rate constants determined for its reactions were higher than those that had been reported for "$GeMe_2$" in solution (*vide supra*), for structurally similar substrates.

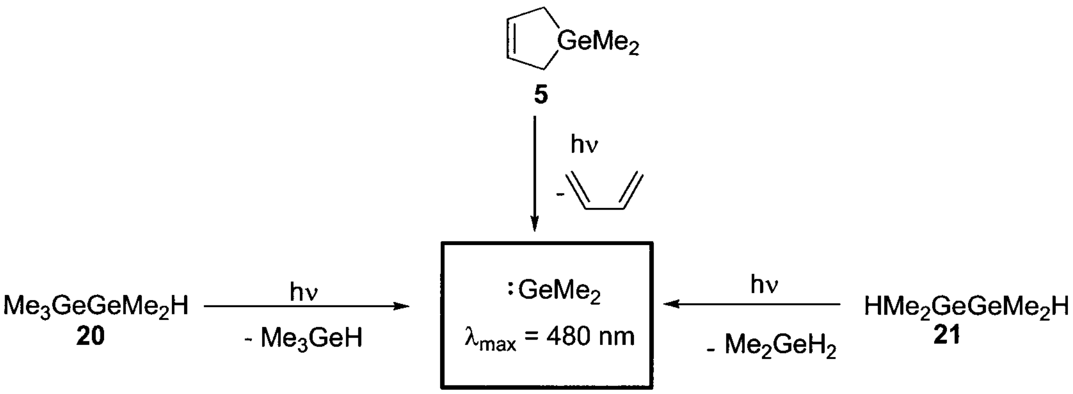

Scheme 1.4 Photochemical precursors for the generation of $GeMe_2$ by 193 nm laser flash photolysis in the gas phase.

Laser flash photolysis (193 nm) of a solution of **7** (ca. 5 x 10^{-5} M) in dry, deoxygenated hexane, gave rise to a transient species which exhibits the same absorption maximum (λ_{max} = 480 nm) as the one observed in the gas phase by Becerra *et al.*[55] The transient absorption spectra obtained after photolysis of **7** in hexane and of compounds **5** and **20** in the gas phase are shown in Figure 1.8. This represents the first report in solution that is consistent with gas phase data. Moreover, there is a good agreement with the calculated absorption spectrum (λ_{max} = 463 nm) derived from time-dependent DFT calculations.[55] In addition, it was observed that in hexane, the primary transient product decays with second-order kinetics to afford a second transient with absorption spectrum centered at λ_{max} = 370 nm; the spectrum and kinetic behavior of this species are consistent with those assigned to Ge_2Me_4 by Mochida *et al.* using 7,8-digermabicyclo[2.2.2]octadiene derivative **22** as precursor to the digermene.[68,104] This too is consistent with the assignment of the 480 nm transient to $GeMe_2$ (eq 1.20).

Unfortunately, the necessity of using 193 nm excitation made it impossible to carry out kinetic studies of the reactions of the 480 nm species with added substrates.

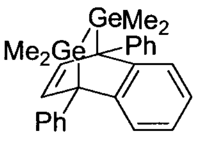

22

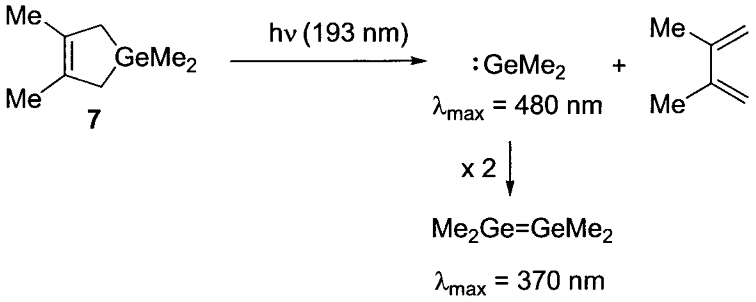

(1.20)

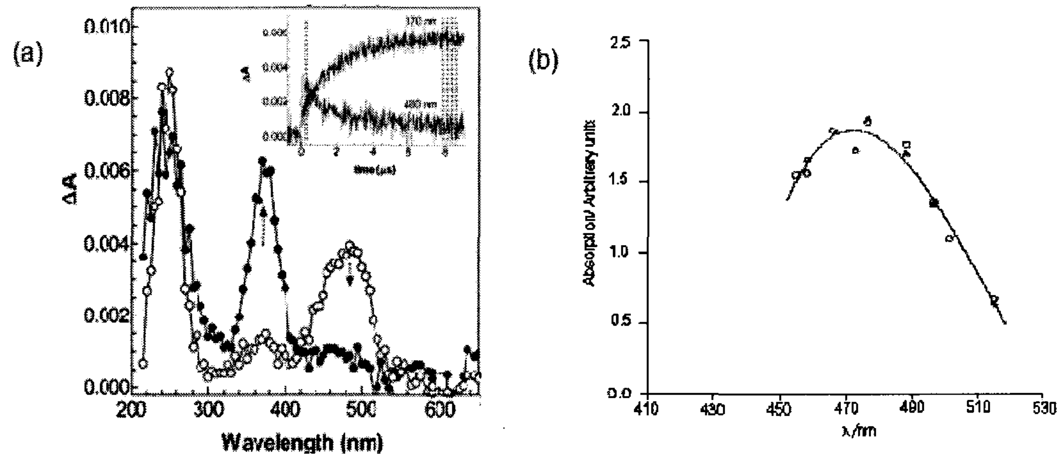

Figure 1.8. (a) Transient absorption spectra from laser flash photolysis of **7** in deoxygenated hexane recorded 50-300 ns (○), 8.2-8.9 μs (□) after the laser pulse. The inset shows transient decay/growth profiles recorded at 480 nm and 370 nm. Reproduced with permission from Ref 55. Copyright 2004, American Chemical Society; (b) Transient absorption spectra recorded by laser photolysis (193 nm) of **5** (△) and **21** (o) in the gas phase. Adapted with permission from Ref 54. Copyright 1996, Elsevier Science B.V.

Kinetic data reported for some common reactions of "$GeMe_2$" and $SiMe_2$ in solution and the gas phase are collected in Table 1.3. The gas phase rate constants, which were originally reported in units of cm^3 molecule s^{-1} have been converted to molar units ($M^{-1}s^{-1}$) to enable easier comparison with the rate constants in solution. A large scatter is observed in the rate constants for the reactions of "$GeMe_2$" in solution, strongly suggesting that different transient species were being observed in each case. The kinetic data for the reactions of $SiMe_2$ in the gas phase correlate closely with those reported in solution for a set of similar scavengers. The gas phase results suggest that both $SiMe_2$ and $GeMe_2$ react at close to the collision-controlled rate with most of the scavengers studied, with $SiMe_2$ reacting slightly faster than $GeMe_2$. On the other hand, the studies performed in solution suggest that $GeMe_2$ is much less reactive than $SiMe_2$. If we assume that the rate constants for the reactions of $GeMe_2$ in hydrocarbon solvents should be similar to the gas phase values, it becomes clear that the rate constants reported in solution are inconsistent with "$GeMe_2$", particularly those for the reactions of alkynes and 2,3-dimethyl-1,3-butadiene. On the basis of the varying results, we conclude that $GeMe_2$ has not yet been correctly characterized in solution except (perhaps) for the study using **7** as precursor.

Table 1.3. Comparison of some reported bimolecular rate constants (k_Q / $M^{-1}s^{-1}$) for the reactions of $SiMe_2$ and "$GeMe_2$" in the gas phase and in solution

	Gas Phase		Hydrocarbon Solution	
Reagent	**$SiMe_2$** (λ_{max} = 465 nm)	**$GeMe_2$**[b] (λ_{max} = 480 nm)	**$SiMe_2$** (λ_{max} = 465 nm)	**"$GeMe_2$"** (λ_{max} = 380-490 nm)
$R-\equiv-H$	2.77 x 10^{10} (R = H)[a]	7.83 x 10^{9} (R = H)	8.0 x 10^{9} (R = Me_3Si)[f]	<10^{5} (R =CH_3)[j]
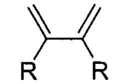	4.52 x 10^{10} (R = H)[a]	6.62 x 10^{9} (R = H)	1.59 x 10^{10} (R = Me) [c]	(1.1-4.1) x 10^{7} (R = Me)[d]
O_2	1.51 x 10^{8} [e]	2.7 x 10^{7}	2.2 x 10^{9} [f]	0.2-21 x 10^{8} [g]
R_3Si-H	2.71 x 10^{9} (R = Me)[h]	< 3.61 x 10^{6} (R = Me)	2.9 x 10^{9} (R= Et)[f] 3.6 x 10^{9} (R = n-C_3H_6)[c]	<10^{4} (R = Et)[g] 4.2 x 10^{6} (R = Et)[i]
Alkene	2.23 x 10^{10} ($CH_3CH=CH_2$)[a]	7.83 x 10^{9} ($Me_3CCH=CH_2$)	7.3 x 10^{9} (1-hexene)[f]	< 10^{5}(1-butene)[j] < 10^{4} (1-hexene)[j]

Photochemical precursors for $GeMe_2$ or $SiMe_2$ are given in parentheses after each of the following references. (a) Ref. 142 (**12**); (b) Ref. 54 (**5** and **20**); (c) Ref. 143 (*cyclo*-Si_6Me_{12}); (d) Refs. 68 (*cyclo*-Ge_6Me_{12}), 69 (*cyclo*-Ge_5Me_{10}), 72 (($PhMe_2Ge)_2GeMe_2$), 88 (**18**), 140 ($PhMe_2GeGeMe_3$; **18**), 141 (($PhMe_2Ge)_2GeMe_2$) (e) Ref. 144 (Me_5HSi_2; $Me_3SiSiMe_2SiMe_3$); (f) Ref. 145 (Si_6Me_{12}); (g) Refs. 140 ($PhMe_2GeGeMe_3$; **18**), 88 (**18**), 68 (*cyclo*-Ge_6Me_{12}), 69 (*cyclo*-Ge_5Me_{10}); (h) Ref. 146 (Me_5HSi_2; $Me_3SiSiMe_2SiMe_3$); (i) Ref. 72 (($PhMe_2Ge)_2GeMe_2$); (j) Ref. 88 (**18**) The rate constants for the gas phase have been converted to molar units for easier comparison. The rate constants for $SiMe_2$ are the high-pressure limiting values while those for $GeMe_2$ were determined at 100 Torr (SF_6).

One of the most important difficulties encountered in the direct UV-Vis spectroscopic studies of "$GeMe_2$" in solution has been the lack of clean photochemical precursors. Most of the precursors employed are known to generate other reactive intermediates along with $GeMe_2$ (for example, see eq 1.21). Although in many cases product studies confirmed that $GeMe_2$ is formed as the major product, the formation of other transient intermediates that exhibit UV-Vis spectra in the 400-500 nm range, make transient assignments difficult. For example, the photolysis of phenylated digermanes and silylgermanes yields conjugated germenes which absorb in the 400-480 nm spectral range (see eq 1.22-1.24).[73,147] The extinction coefficient of $GeMe_2$ is unknown; however, it can be expected to be $\varepsilon < 1000\ dm^3\ mol^{-1}cm^{-1}$ based on the extinction coefficients determined or estimated for $GePh_2$ ($\varepsilon = 1850 \pm 400\ dm^3\ mol^{-1}cm^{-1}$)[55] and $GeMes_2$ ($\sim 800\ dm^3\ mol^{-1}cm^{-1}$).[147] Mochida *et al.* attributed the difference in the rate constants obtained when $GeMe_2$ is generated from phenylated precursors, such as dibenzotrigermacycloheptane derivative **17** and 7-germanorbornadiene derivative **12**, to the formation of π-complexes between $GeMe_2$ and the aromatic rings of the precursors.[134]

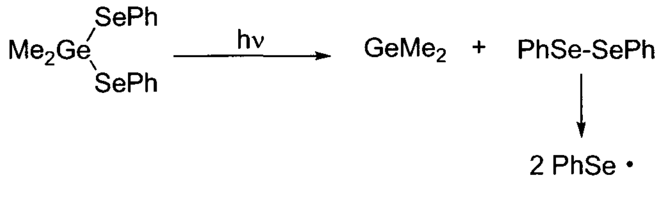

(1.21)

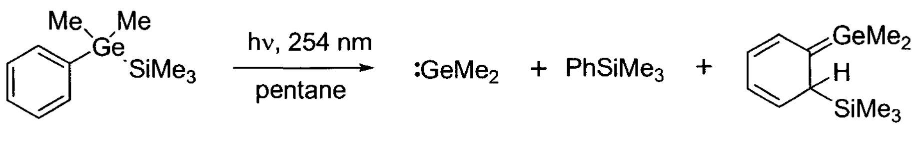

(1.22)

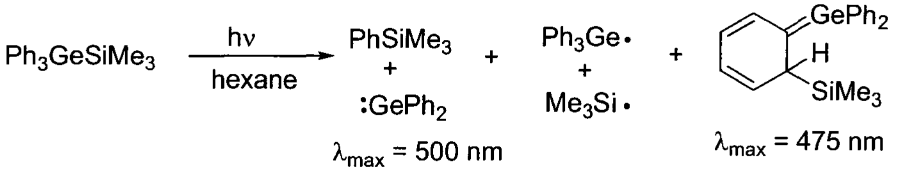

(1.23)

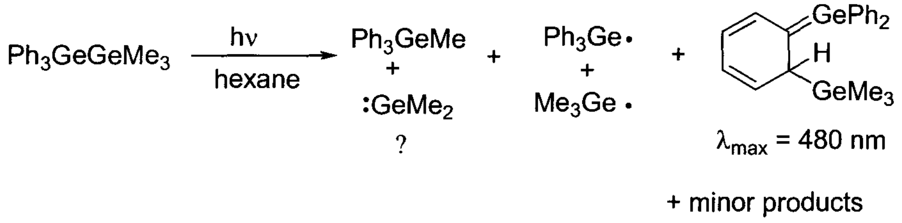

(1.24)

The experience our group had in the first studies of transient arylgermylenes was that rigorous standards of purity and anhydrous reaction conditions are essential for the spectroscopic and kinetic studies of transient germylenes in solution to be successful.[55-57] To this end, solvents and glassware need to be meticulously dried, and the precursors and substrates to be investigated need to be of high purity. As pointed out by other authors the presence of small quantities of reactive impurities in a substrate can cause great alterations in the measured rate constants, especially for those with relatively unreactive scavengers.[148]

The dimerization of transient germylenes such as $GePh_2$ in solution occurs at close to the diffusion-controlled rate ($k_{dim} = (1.2 \pm 0.2) \times 10^{10}$ $M^{-1}s^{-1}$) in hexane at 25 °C.[55] The digermenes formed, in turn, react to ultimately form oligogermanes. In general, compounds containing Ge-Ge bonds are photolabile and absorb strongly in the UV-Vis region, generating conjugated germene derivatives and germanium-centered radicals upon photolysis.[137,149] In this regard, a flow system that continuously removes the photolysate and replenishes the sample cell with fresh solution is necessary to avoid accumulation of products derived from the initially produced reactive intermediates. In addition, replenishing the solution in the sample cell avoids depletion of the precursor and ensures a constant concentration of precursor throughout the experiment.

In summary, we suggest that the discrepancies in the early reported spectral and kinetic data for "$GeMe_2$" in solution are most likely due to the formation of other transient species with absorption spectra that overlap with that of $GeMe_2$, reactions of the germylene to form complexes, or unsuitable experimental conditions. The successful detection and kinetic studies of $GeMe_2$ requires that these problems be eliminated.

1.7 Thesis objectives

Significant progress has been made in the last couple of decades toward understanding the chemistry of transient germylenes and transient digermenes under various conditions. However, it is evident that there are insufficient kinetic data available in solution to allow a sound understanding of the electronic and steric factors influencing their reactivities. Consequently, the mechanisms of many of their reactions are still not well understood. The trends in the kinetics of the reactions of MR_2 (M = C, Si, Ge, Sn) and their dimers also remain to be fully established. We hope that the kinetic studies of $GeMe_2$ in solution will provide quantitative data that will contribute a great deal to enriching our knowledge of the chemistry of the so-far-poorly understood transient germylene. We think that $GeMe_2$ is a prime candidate to study because it has been the most studied germylene in solution by UV-Vis absorption spectroscopy, product studies and computational methods. However, the literature is rife with inconsistencies, which underscores the need for more research in this field. Being the simplest dialkyl-substituted germylene, its reactivity should have the least influence from steric and electronic factors from the substituents.

As discussed in the previous section, a large number of studies on the direct detection and reaction kinetics of $GeMe_2$ in solution by flash photolysis techniques have been reported. The absorption maxima and kinetic data reported vary depending on the precursor, solvent and reaction conditions used. In some cases, it seems that reports were based on mere speculation and erroneous transient assignments. Moreover, most $GeMe_2$

assignments in solution were made on the basis of comparison of UV-Vis spectra to those recorded in low temperature matrixes.

One of the main hurdles in the UV-Vis absorption spectroscopic and kinetic studies of $GeMe_2$ has been the lack of efficient photochemical precursors. Most of the $GeMe_2$ precursors that have been used undergo competing photochemical reactions that produce other reactive intermediates which absorb in the same UV-Vis range as $GeMe_2$. This problem has rendered spectral assignments and kinetic studies ambiguous. Therefore, there is a need for the development of more suitable precursors. We believe that all of the kinetic studies performed in solution prior to the beginning of our efforts are incorrect. We place greater confidence in the gas phase studies conducted by Becerra *et al.* in 1996 because of the consistencies of their spectral and kinetic data for $GeMe_2$, $SiMe_2$, GeH_2 and SiH_2. We considered their work to be the benchmark against which to base an assignment in the solution phase. The gas phase results indicate that the absorption maximum for $GeMe_2$ should be around 480 nm in solution, which is consistent with the results obtained from flash photolysis of 1,1,3,4-tetramethyl-1-germacyclopent-3-ene.

The primary aim of this thesis is to establish the spectral characteristics of $GeMe_2$ in solution and provide a comprehensive study of the kinetics of its reactions with a large variety of known germylene scavengers in solution. We wanted to directly compare the reactivity of $GeMe_2$ with those of $GePh_2$ and GeMePh, in order to understand the effects of alkyl and phenyl substituents on the reactivities of simple transient diorganogermylenes. We also wanted to compare the reactivities of $SiMe_2$ with $GeMe_2$.

Another motivation for this thesis work was to try to understand and hopefully clarify the cause of some of the prevailing inconsistencies in the literature. The first step was to develop a new photochemical precursor for $GeMe_2$. We needed a precursor whose photodecomposition does not yield other reactive intermediates or products that absorb in the same UV-Vis range as $GeMe_2$, or react with the germylene once it is produced. The precursors so far reported to yield $GeMe_2$ cleanly in solution, based on product studies, are: dodecamethylcyclohexagermane **14**, decamethylcyclopentagermane **15**, the 7,7-dimethyl-7-germanornadiene derivative **12** and 1,1-dimethylgermacyclopent-3-ene **7**; only **7** has been shown to afford results consistent with those of Becerra *et al.* in the gas phase in laser flash photolysis experiments in solution. In the present work, we thus decided to develop a precursor based on the germacyclopent-3-ene system for the generation of $GeMe_2$ by 248 nm laser flash photolysis. Therefore, 1,1-dimethyl-3-phenylgermacyclopent-3-ene **23** and 1,1,4-trimethyl-3-phenylgermacyclopent-3-ene **24** were suggested; their photochemistry was anticipated to occur as shown in eq (1.25). Chapter 2 gives details of the synthesis of these precursors and the results of initial studies of their photochemistry by steady state photolysis and laser flash photolysis methods. Kinetic studies of the reactions of $GeMe_2$ in hexanes with a variety of scavengers are also presented.

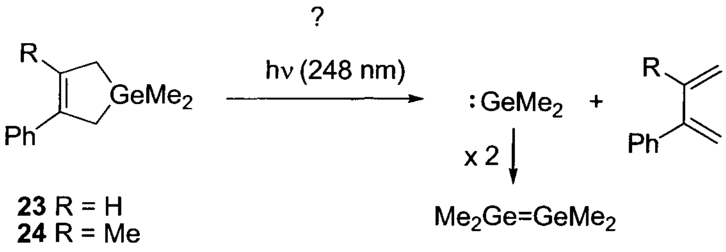

(1.25)

In Chapter 3, we describe the results of a reinvestigation of the photochemistry of dodecamethylcyclohexagermane **14** and dimethylphenyl(trimethylsilyl)germane **18** in solution, and characterize the transients that are formed. Overall, this work addresses the most important discrepancies in the existing literature on the spectral assignments of the transients formed from the photolysis of these compounds. We also reassigned the transient species formed from the photolysis of **18**. The results from these experiments also verify the kinetic and spectroscopic data collected in Chapter 2.

In Chapter 4, we present and discuss the results of a study of the reactions of $GeMe_2$ with methanol, t-butanol and THF in hexane. Although it has been proposed in the literature that germylenes react with alcohols and ethers by initial complex formation and evidence for this has been reported in the gas phase for GeH_2 and in matrixes for aryl germylenes, no reports exist on the direct detection of Me_2Ge-alcohol or Me_2Ge-THF complexes in solution. In this work, we investigated whether Me_2Ge-alcohol (MeOH and t-BuOH) and Me_2Ge-THF complexes could be detected in solution and tried to elucidate the mechanism of the O-H insertion reaction of transient $GeMe_2$ with alcohols in dilute solution.

Chapter 5 provides details of our kinetic and mechanistic investigations of the reactions of Me_2Ge-MeOH and Me_2Ge-THF complexes in methanol and THF, respectively. We have explored the role of acid and base catalysis in the decomposition of the Me_2Ge-MeOH complex with methanesulfonic acid, acetic acid (AcOH) and sodium methoxide. Moreover, the reactivity of the Me_2Ge-THF complex was probed with a variety of scavengers, specifically AcOH, carbon tetrachloride (CCl_4), oxygen, isoprene, 4,4-dimethyl-1-pentene, methanesulfonic acid and sodium methoxide in the interest of comparing its reactivity with that of free $GeMe_2$ in hexane.

In Chapter 6, the kinetics of some of the reactions of Ge_2Me_4 in solution are discussed. In our experiments, Ge_2Me_4 is formed as a secondary product from the dimerization of $GeMe_2$ in solution. Absolute rate constants for the reactions of Ge_2Me_4 with numerous scavengers have been successfully determined, and a comparison of the rates of these reactions with those for Ge_2Ph_4 and $Ge_2Me_2Ph_2$ are made.

References

1. Barrau, J. and Rima, G. *Coord. Chem. Rev.* **1998**, *178-180*, 593.
2. Grev, R. S. *Adv. Organomet. Chem.* **1991**, *33*, 125.
3. Bourissou, D.; Guerret, O.; Gabbaï, F. P.; Bertrand, G. *Chem. Rev.* **2000**, *100*, 39.
4. Barrau, J.; Escudié, J.; Satgé, J. *Chem. Rev.* **1990**, *90*, 283.
5. Baines, K. M. and Stibbs, W. G. *Adv. Organomet. Chem.* **1996**, *39*, 275.
6. Okazaki, R. and West, R. *Adv. Organomet. Chem.* **1996**, *39*, 231.
7. Kira, M. *J. Organomet. Chem.* **2004**, *689*, 4475.
8. Arduengo, A. J.; Dias, H. V. R.; Harlow, R. L.; Kline, M. *J. Am. Chem. Soc.* **1992**, *114*, 5530.
9. Goldberg, D. E.; Harris, D. H.; Lappert, M. F.; Thomas, K. M. *J. Chem. Soc., Chem. Commun.* **1976**, *120*, 261.
10. Kira, M.; Ishida, S.; Iwamoto, T.; Ichinohe, M.; Kabuto, C.; Ignatovich, L.; Sakurai, H. *Chem. Lett.* **1999**, 263.
11. Kira, M.; Ishida, S.; Iwamoto, T.; Kabuto, C. *J. Am. Chem. Soc.* **1999**, *121*, 9722.

12. Kühl, O. *Coord. Chem. Rev.* **2004**, *248*, 411.
13. Górski, M.; Kochel, A.; Szymanska-Buzar, T. *J. Organomet. Chem.* **2006**, *691*, 3708.
14. Jasinki, J. M. and Gates, S. M. *Acc. Chem. Res.* **1991**, *24*, 9.
15. Veprek, S.; Prokop, J.; Glatz, F.; Merica, R.; Klingan, F. R.; Herrmann, W. A. *Chem. Mater.* **1996**, *8*, 825.
16. Tsumuraya, T.; Batcheller, S. A.; Masamune, S. *Angew. Chem. Int. Ed.* **1991**, *30*, 902.
17. Escudie, J.; Couret, C.; Ranaivonjatovo, H.; Satge, J. *Coord. Chem. Rev.* **1994**, *130*, 427.
18. Hamers, R. J.; Coulter, S. K.; Ellison, M. D.; Hovis, J. S.; Padowitz, D. F.; Schwartz, M. P.; Greenlief, C. M.; Russell, J. N. *Acc. Chem. Res.* **2000**, *33*, 617.
19. Buriak, J. M. *Chem. Rev.* **2002**, *102*, 1271.
20. Kachian, J. S. and Bent, S. F. *J. Am. Chem. Soc.* **2009**, *131*, 7005.
21. Hamers, R. J. *Annu. Rev. Anal. Chem.* **2008**, *1*, 707.

22. Jones M., Jr.; Moss, R. A. In *Reactive intermediate chemistry*; Moss. R. A.; Platz, M. S.; Jones M. ,Jr., Eds.; John Wiley & Sons, Inc.: New Jersey, 2004; Chapter 7, pp. 273-321.

23. Holthausen, M. C.; Koch, W.; Apeloig, Y. *J. Am. Chem. Soc.* **1999**, *121*, 2623.

24. Yoshida, H. and Tamaoki, N. *Organometallics* **2002**, *21*, 2587.

25. Barthelat, J. C.; Roch, B. S.; Trinquier, G.; Satgé, J. *J. Am. Chem. Soc.* **1980**, *102*, 4080.

26. Su, M.-D. and Chu, S.-Y. *J. Am. Chem. Soc.* **1999**, *121*, 4229.

27. Gordon, M. S. *Chem. Phys. Lett.* **1985**, *114*, 348.

28. Leopold, D. G.; Murray, K. K.; Miller, A. E. S.; Lineberger, W. C. *J. Chem. Phys.* **1985**, *83*, 4849.

29. McKellar, A. R. W.; Bunker, P. R.; Sears, T. J.; Evenson, K. M.; Saykally, R. J.; Langhoff, S. R. *J. Chem. Phys.* **1983**, *79*, 5251.

30. Kalemos, A.; Dunning, Jr. T. H.; Mavridis, A.; Harrison, J. F. *Can. J. Chem.* **2004**, *82*, 684.

31. Mueller, P. H.; Rondan, N. G.; Houk, K. N.; Harrison, J. F.; Hooper, D.; Willen, B. H.; Liebman, J. F. *J. Am. Chem. Soc.* **1981**, *103*, 5049.

32. Scuseria, G. E.; Duran, M.; Maclagan, R. G. A. R.; Schaefer, H. F. *J. Am. Chem. Soc.* **1986**, *108*, 3248.
33. Selmani, A. and Salahub, D. R. *J. Chem. Phys.* **1988**, *89*, 1529.
34. Berkowitz, J.; Greene, J. P.; Cho, H.; RusCic, B. *J. Chem. Phys.* **1987**, *86*, 1235.
35. Balasubramanian, K. and McLean, A. D. *J. Chem. Phys.* **1986**, *85*, 5117.
36. Bauschlicher, J.; Langhoff, S. R.; Taylor, P. R. *J. Chem. Phys.* **1987**, *87*, 387.
37. Grev, R. S. and Schaefer III, H. F. *J. Chem. Phys.* **1992**, *97*, 8389.
38. Selmani, A. and Salahub, D. R. *J. Chem. Phys.* **1988**, *89*, 1529.
39. Grev, R. S. and Schaefer, H. F. *J. Am. Chem. Soc.* **1986**, *108*, 5804.
40. Krogh-Jespersen, K. *J. Am. Chem. Soc.* **1985**, *107*, 537.
41. Su, M.-D. *Chem. Eur. J.* **2004**, *10*, 6073.
42. Grev, R. S.; Schaefer III, H. F.; Gaspar, P. P. *J. Am. Chem. Soc.* **1991**, *113*, 5638.
43. Jiang, P. and Gaspar, P. P. *J. Am. Chem. Soc.* **2001**, *123*, 8622.
44. Apeloig, Y.; Pauncz, R.; Karni, M.; West, R.; Steiner, W.; Chapman, D. *Organometallics* **2003**, *22*, 3250.

45. Sekiguchi, A.; Tanaka, H.; Ichinohe, M.; Akiyama, K.; Tero-Kubota, S. *J. Am. Chem. Soc.* **2003**, *125*, 4962.
46. Sekiguchi, A.; Tanaka, T.; Ichinohe, M.; Akiyama, K.; Gaspar, P. P. *J. Am. Chem. Soc.* **2008**, *130*, 426.
47. Walsh, R. *Acc. Chem. Res.* **1981**, *14*, 246.
48. Walsh, R. *Organometallics* **1989**, *8*, 1973.
49. Grev, R. S.; Schaefer, H. F.; Baines, K. M. *J. Am. Chem. Soc.* **1990**, *112*, 9458.
50. Bally T. In *Reactive Intermediate Chemistry*; John Wiley & Sons, Inc.: New Jersey, 2004; Chapter 17, pp. 797-838.
51. Moss, R. A.; Platz, M. S.; Jones, M., Jr. *Reactive intermediate chemistry*, John Wiley & Sons, Inc.: New Jersey, 2004.
52. Becerra, R.; Boganov, S. E.; Egorov, M. P.; Nefedov, O. M.; Walsh, R. *Chem. Phys. Lett.* **1996**, *260*, 433.
53. Becerra, R.; Harrington, C. R.; Leigh, W. J.; Kefala, L. A.; Walsh, R. *Organometallics* **2006**, *25*, 4439.
54. Becerra, R.; Boganov, S. E.; Egorov, M. P.; Lee, V.; Nefedov, O. M.; Walsh, R. *Chem. Phys. Lett.* **1996**, *250*, 111.

55. Leigh, W. J.; Harrington, C. R.; Vargas-Baca, I. *J. Am. Chem. Soc.* **2004**, *126*, 16105.
56. Leigh, W. J. and Harrington, C. R. *J. Am. Chem. Soc.* **2005**, *127*, 5084.
57. Leigh, W. J.; Dumbrava, I.; Lollmahomed F.B. *Can. J. Chem.* **2006**, *84*, 934.
58. Neumann, W. P. *Chem. Rev.* **1991**, *91*, 311.
59. Boganov S. E.; Egorov, M. G.; Faustov, V. I.; Nefedov, O. M. In *The chemistry of organic germanium, tin, and lead compounds*; John Wiley & Sons, Ltd. New York.: 2002; Chapter 12, pp. 749-841.
60. Ando, W.; Itoh, H.; Tsumuraya, T. *Organometallics* **1989**, *8*, 2759.
61. Atwell, W. H. and Weyenberg, D. R. *Angew. Chem. Int. Ed. Engl.* **1969**, *8*, 469.
62. Satge, J.; Massol, M.; Riviere, P. *J. Organomet. Chem.* **1973**, *56*, 1.
63. Satgé, J. and Dousse, G. *J. Organomet. Chem.* **1973**, *61*, C26-C32.
64. Hoffmann, R. W. *Angew. Chem. Int. Ed.* **1971**, *10*, 529.
65. Gilman, H.; Cottis, S. G.; Atwell, W. H. *J. Am. Chem. Soc.* **1964**, *86*, 1596.
66. Schriewer, M. and Neumann, B. *Angew. Chem. Int. Ed. Engl.* **1981**, *20*, 1019.
67. Neumann, W. P. and Schriewer, M. *Tetrahedron Lett.* **1980**, *21*, 3273.

68. Mochida, K.; Kanno, N.; Kato, R.; Kotani, M.; Yamauchi, S.; Wakasa, M.; Hayashi, H. *J. Organomet. Chem.* **1991**, *415*, 191.

69. Mochida, K. and Tokura, S. *Bull. Chem. Soc. Jpn.* **1992**, *65*, 1642.

70. Sakurai, H.; Sakamoto, K.; Kira, M. *Chem. Lett.* **1984**, 1379.

71. Konieczny, S.; Jacobs, S. J.; Braddock-Wilking, J. K.; Gaspar, P. P. *J. Organomet. Chem.* **1988**, *341*, C17-C22.

72. Mochida, K.; Yoneda, I.; Wakasa, M. *J. Organomet. Chem.* **1990**, *399*, 53.

73. Harrington, C. R.; Leigh, W. J.; Chan, B. K.; Gaspar, P. P.; Zhou, D. *Can. J. Chem.* **2005**, *83*, 1324.

74. Klein, B.; Neumann, W. P.; Weisbeck, M. P.; Weinken, S. *J. Organomet. Chem.* **1993**, *446*, 149.

75. Becerra, R.; Boganov, S. E.; Egorov, M. G.; Faustov, V. I.; Nefedov, O. M.; Walsh, R. *J. Am. Chem. Soc.* **1998**, *120*, 12657.

76. Becerra, R.; Egorov, M. P.; Krylova, I. V.; Nefedov, O. M.; Walsh, R. *Chem. Phys. Lett.* **2002**, *351*, 47.

77. Köcher, J. and Lehnig, M. *Organometallics* **1984**, *3*, 937.

78. Köcher, J.; Lehnig, M.; Neumann, W. P. *Organometallics* **1988**, *7*, 1201.

79. Mochida, K. and Hasegawa, A. *Chem. Lett.* **1989**, 1087.

80. Castel, A.; Escudie, J.; Riviere, P.; Satge, J.; Bochkarev, M. N.; Maiorova, L. P.; Razuvaev, G. A. *J. Organomet. Chem.* **1981**, *210*, 37.

81. Becerra, R. and Walsh, R. *Phys. Chem. Chem. Phys.* **2007**, *9*, 2817.

82. Ando, W.; Ohgaki, H.; Kabe, Y. *Angew. Chem. Int. Ed.* **1994**, *33*, 659.

83. Becerra, R. and Walsh, R. *J. Organomet. Chem.* **2001**, *636*, 49.

84. Billeb, G.; Brauer, H.; Neumann, W. P.; Welsbeck, M. *Organometallics* **1992**, *11*, 2069.

85. Egorov, M. P.; Ezhova, M. B.; Kolesnikov, S. P.; Nefedov, O. M.; Taraban, M. B.; Kruppa, A. I.; Leshina, T. V. *Mendeleev Commun.* **1991**, 143.

86. Horner, D. A.; Grev, R. S.; Schaefer, H. F. *J. Am. Chem. Soc.* **1992**, *114*, 2093.

87. Neumann, W. P.; Michels, E.; Köcher; J. *Tetrahedron Lett.* **1987**, *28*, 3783.

88. Bobbitt, K. L.; Maloney, V. M.; Gaspar, P. P. *Organometallics* **1991**, *10*, 2772.

89. Schriewer, M. and Neumann, W. P. *J. Am. Chem. Soc.* **1983**, *105*, 897.

90. Köcher, J. and Neumann, W. P. *J. Am. Chem. Soc.* **1984**, *106*, 3861.

91. Su, M.-D. and Chu, S.-Y. *J. Am. Chem. Soc.* **1999**, *121*, 11478.

92. Nag, M. and Gaspar, P. P. *Organometallics* **2009**, *28*, 5612.

93. Huck, L. A. and Leigh, W. J. *in press* **2009**.

94. Ando, W.; Itoh, H.; Tsumuraya, T.; Yoshida, H. *Organometallics* **1988**, *7*, 1880.

95. Power, P. P. *J. Chem. Soc., Dalton Trans.* **1998**, 2939.

96. West, R. and Fink, M. J. *Science* **1981**, *214*, 1343.

97. Gusel'nikov, L. E. and Nametkin, N. S. *Chem. Rev.* **1979**, *79*, 529.

98. Nagase, S.; Kudo, T.; Ito, K. *Appl. Quantum Chem.* **1986**, 249.

99. Masamune, S.; Hanzawa, Y.; Williams, D. J. *J. Am. Chem. Soc.* **1982**, *104*, 6136.

100. Hitchcock, P. B.; Lappert, M. F.; Miles, S. J.; Thorne, A. J. *J. Chem. Soc., Chem. Commun.* **1984**, 480.

101. Snow, J. T.; Murakami, S.; Masamune, S.; Williams, D. J. *Tetrahedron Lett.* **1984**, *25*, 4191.

102. Sakurai, H.; Nakadaira, Y.; Tobita, H. *Chem. Lett.* **1982**, 1855.

103. Bleckmann, P.; Minkwitz, R.; Neumann, W. P.; Schriewer, M.; Thibud, M.; Watta, B. *Tetrahedron Lett.* **1984**, *25*, 2467.

104. Mochida, K.; Kayamori, T.; Wakasa, M.; Hayashi, H.; Egorov, M. P. *Organometallics* **2000**, *19*, 3379.

105. Snow, J. T.; Murakami, S.; Masamune, S.; Williams, D. J. *Tetrahedron Lett.* **1984**, *25*, 4191.

106. Batcheller, S. A.; Tsumuraya, T.; Tempkin, O.; Davis, W. M.; Masamune, S. *J. Am. Chem. Soc.* **1990**, *112*, 9394.

107. Tokitoh, N.; Kishikawa, K.; Okazaki, R.; Sasamori, T.; Nakata, N.; Takeda, N. *Polyhedron* **2002**, *21*, 563.

108. Trinquier, G.; Malrieu, J.; Rivière, P. *J. Am. Chem. Soc.* **1982**, *104*, 4529.

109. Goldberg, D. E.; Hitchcock, P. B.; Lappert, M. F.; Thomas, K. M.; Thorne, A. J.; Fjeldberg, T.; Haaland, A.; Schilling, B. E. R. *J. Chem. Soc., Dalton Trans.* **1986**, 2387.

110. Liang, C. and Allen, L. C. *J. Am. Chem. Soc.* **1990**, *112*, 1039.

111. Karni, M. and Apeloig, Y. *J. Am. Chem. Soc.* **1990**, *112*, 8589.

112. Chen, W. C.; Su, M. D.; Chu, S. Y. *Organometallics* **2001**, *20*, 564.

113. Kira, M.; Iwamoto, T.; Maruyama, T.; Kabuto, C.; Sakurai, H. *Organometallics* **1996**, *20*, 1820.

114. Taraban, M. B.; Volkova, O. S.; Plyusnin, V. F.; Ivanov, Y. V.; Leshina, T. V.; Egorov, M. P.; Nefedov, O. M.; Kayamori, T.; Mochida, K. *J. Organomet. Chem.* **2000**, *601*, 324.

115. Ando, W.; Tsumuraya, T.; Sekiguchi, A. *Chem. Lett.* **1987**, 317.

116. Marchand, A.; Gerval, P.; Duboudin, F.; Joanny, M.; Mazerolles, P. *J. Organomet. Chem.* **1984**, *267*, 93.

117. Apeloig, Y.; Bravo-Zhivotovskii, D.; Zharov, I.; Panov, V.; Leigh, W. J.; Sluggett, G. W. *J. Am. Chem. Soc.* **1998**, *120*, 1398.

118. Toltl, N. P.; Leigh, W. J.; Kollegger, G. M.; Stibbs, W. G.; Baines, K. M. *Organometallics* **1996**, *15*, 3732.

119. Fjeldberg, T.; Haaland, A.; Schilling, B. E. R.; Lappert, M. F.; Thorne, A. J. *J. Chem. Soc., Dalton Trans.* **1986**, 1551.

120. Kishikawa, K.; Tokitoh, N.; Okazaki, R. *Chem. Lett.* **1998**, 239.

121. Escudie, J. and Ranaivonjatovo, H. *Adv. Organomet. Chem.* **1999**, *44*, 113.

122. Fink, M. J.; DeYoung, D. J.; West, R.; Michl, J. *J. Am. Chem. Soc.* **1983**, *105*, 1070.

123. Samuel, M. S.; Jennings, M. C.; Baines, K. M. *Organometallics* **2001**, *20*, 590.

124. De Young, D. J.; Fink, M. J.; West, R.; Michl, J. *Main Group Met. Chem.* **1987**, *10*, 19.

125. Batcheller, S. A. and Masamune, S. *Tetrahedron Lett.* **1988**, *29*, 3383.

126. Dixon, C. E.; Cooke, J. A.; Baines, K. M. *Organometallics* **1997**, *16*, 5437.

127. Nefedov, O. M.; Egorov, M. P.; Gal'minas, A. M.; Kolesnikov, S. P. *J. Organomet. Chem.* **1986**, *301*, C21-C22.

128. Baines, K. M.; Cooke, J. A.; Dixon, C. E.; Liu, H. W.; Netherton, M. R. *Organometallics* **1994**, *13*, 631.

129. Tsumuraya, T.; Kabe, Y.; Ando, W. *J. Organomet. Chem.* **1994**, *482*, 131.

130. Masamune, S.; Batcheller, S. A.; Park, J.; Davis, W. M.; Yamashita, O.; Ohta, Y.; Kabe, Y. *J. Am. Chem. Soc.* **1989**, *111*, 1888.

131. Samuel, M. S.; Jennings, M. C.; Baines, K. M. *J. Organomet. Chem.* **2001**, *636*, 130.

132. Boganov, S. E.; Egorov, M. P.; Faustov, V. I.; Krylova, I. V.; Nefedov, O. M.; Becerra, R.; Walsh, R. *Russ. Chem. Bull., Int. Ed.* **2005**, *54*, 483.

133. Drahnak, T. J.; Michl, J.; West, R. *J. Am. Chem. Soc.* **1979**, *101*, 5427.

134. Mochida, K.; Tokura, S.; Murata, S. *J. Chem. Soc., Chem. Commun.* **1992**, 250.

135. Tomoda, S.; Shimoda, M.; Takeuchi, Y.; Kajii, Y.; Obi, K.; Tanaka, I.; Honda, K. *J. Chem. Soc., Chem. Commun.* **1988**, 910.

136. Barrau, J.; Bean, D. L.; Welsh, K. M.; West, R.; Michl.J. *Organometallics* **1989**, *8*, 2606.

137. Mochida, K.; Chiba, H.; Okano, M. *Chem. Lett.* **1991**, 109.

138. Kolesnikov, S. P.; Egorov, M. P.; Dvornikov, A. S.; Kuz'min, V. A. *Metalloorg. Khim.* **1989**, *2*, 799.

139. Egorov, M. G.; Dvornikov, A. S.; Kolesnikov, S. P.; Kuz'min, V. A.; Nefedov, O. M. *Izv. Akad. Nauk. SSSR, Ser. Khim.* **1987**, 1200.

140. Mochida, K.; Kikkawa, H.; Nakadaira, Y. *J. Organomet. Chem.* **1991**, *412*, 9.

141. Wakasa, M.; Yoneda, I.; Mochida, K. *J. Organomet. Chem.* **1989**, *366*, C1-C5.

142. Baggott, J. E.; Blitz, M. A.; Frey, H. M.; Lightfoot, P. D.; Walsh, R. W. *J. Chem. Soc. , Faraday Trans.* **1988**, *84*, 515.

143. Moiseev, A. G. and Leigh, W. J. *Organometallics* **2007**, *26*, 6277.

144. Baggott, J. E.; Blitz, M. A.; Frey, H. M.; Lightfoot, P. D.; Walsh, R. *Int. J. Chem. Kinet.* **1992**, *24*, 127.

145. Levin, G.; Das, P. K.; Lee, C. L. *Organometallics* **1988**, *7*, 1231.

146. Baggott, J. E.; Blitz, M. A.; Frey, H. M.; Walsh, R. *J. Am. Chem. Soc.* **1990**, *112*, 8337.

147. Leigh, W. J.; Toltl, N. P.; Apodaca, P.; Castruiti, M.; Pannell, K. H. *Organometallics* **2000**, *19*, 3232.

148. Becerra, R.; Boganov, S. E.; Egorov, M. P.; Faustov, V. I.; Krylova, I. V.; Nefedov, O. M.; Promyslov, V. M.; Walsh, R. *Phys. Chem. Chem. Phys.* **2007**, *9*, 4395.

149. Mochida, K.; Kikkawa, H.; Nakadaira, Y. *Chem. Lett.* **1988**, 1089.

CHAPTER 2

The direct detection and kinetic studies of dimethylgermylene in solution

2.1 Introduction

In Chapter 1, we mentioned that 1,1-disubstituted-3,4-dimethyl-1-germacyclopent-3-enes (e.g. **4-9**) are highly efficient photochemical precursors for germylenes in solution.[1,2] Of particular interest is that 193 nm laser photolysis of 1,1,3,4-tetramethyl-1-germacyclopent-3-ene **7** in deoxygenated anhydrous hexanes produced a transient absorption spectrum that is in excellent agreement with the one reported by Becerra *et al.* in the gas phase for $GeMe_2$, which they obtained by 193 nm laser photolysis of three different precursors.[1,3] A transient absorption band with λ_{max} = 480 nm was assigned to $GeMe_2$ in both reports. The main thrust of the present work is to fully characterize $GeMe_2$ in solution by laser flash photolysis. It is not possible to carry out kinetic studies in solution using 193 nm laser excitation because most substrates that are of interest absorb significantly at this wavelength. Therefore, in order to determine rate constants for the reactions of $GeMe_2$ with a wide variety of scavengers and explore its reactions in various solvents, we need a precursor that absorbs at a more convenient laser wavelength.

In our laboratory, we study divalent group 14 reactive intermediates mainly by the laser flash photolysis technique, using pulses from an excimer laser filled with F_2/Kr/Ne mixtures (248 nm; ~20 ns; 100 ± 5 mJ). We anticipated that the incorporation of a chromophore such as a phenyl ring on the germacyclopent-3-ene ring will cause a red-shift in the static absorbance of the precursor, enabling us to generate $GeMe_2$ and study the kinetics of its reactions using 248 nm laser flash photolysis techniques. Jiang *et al.* reported that the photolysis of 1-tri-*tert*-butylsilyl-1-triisopropylsilyl-3-phenyl-1-silacyclopent-3-ene **25** in methylcyclohexane in the presence of 2,3-dimethylbutadiene (DMB) and trimethylsilane as trapping agents gave products that are consistent with reaction of tri-*tert*-butylsilyl(triisopropylsilyl)silylene (Scheme 2.1).[4] On the basis of these results, we anticipated that the photolysis of analogous 3-phenylgermacyclopent-3-ene systems would likely lead to the extrusion of the corresponding germylenes.

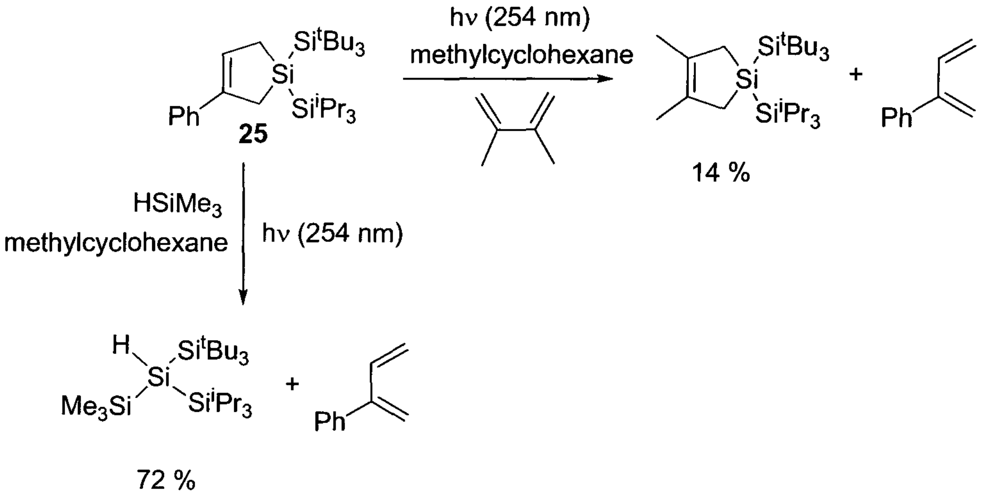

Scheme 2.1 Photolysis of **25** in methylcyclohexane in the presence of DMB and trimethylsilane.

We have thus developed two new photochemical precursors for $GeMe_2$ in solution, namely, 1,1-dimethyl-3-phenylgermacyclopent-3-ene **23** and 1,1,3-trimethyl-4-phenylgermacyclopent-3-ene **24**. In this Chapter, we will discuss the results of steady state and laser flash photolysis studies on these two compounds, and the results of kinetic studies on the transients that are formed.

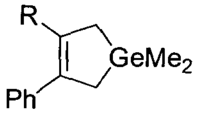

23 R = H
24 R = Me

2.2 Synthesis of 1,1-dimethyl-3-phenylgermacyclopent-3-ene derivatives

The germacyclopent-3-ene precursors **23** and **24** were synthesized by a modification of the synthetic procedure reported by Mazerolles and Manuel.[1,5] 2-Phenyl-1,3-butadiene **28** and 2-methyl-3-phenyl-1,3-butadiene **31** were first synthesized by a modification of the synthetic procedures described by Brown *et al.*[6] The synthetic routes are shown in Schemes 2.2-2.3.

Benzoyl chloride and acetyl chloride were reacted with chloromethyltrimethylsilylmagnesium chloride in the presence of CuI to form 1-phenyl-2-(trimethylsilyl)ethanone **26** and 1-trimethylsilyl-2-propanone **29**, respectively. Ketone **26** was then treated with vinylmagnesium bromide to form 2-phenyl-1-(trimethylsilyl)but-3-en-2-ol **27**, while ketone **29** was treated with (1-phenylvinyl)magnesium bromide to form 2-methyl-3-phenyl-1-(trimethylsilyl)-1-buten-3-ol **30**. Finally, Peterson elimination in the presence of a mixture of AcOH and sodium acetate afforded the target dienes **28** and **31**. The chemical yields obtained for each step are given in Schemes 2.2 and 2.3. Diene **28** was purified by column chromatography while diene **31** was purified by vacuum distillation.

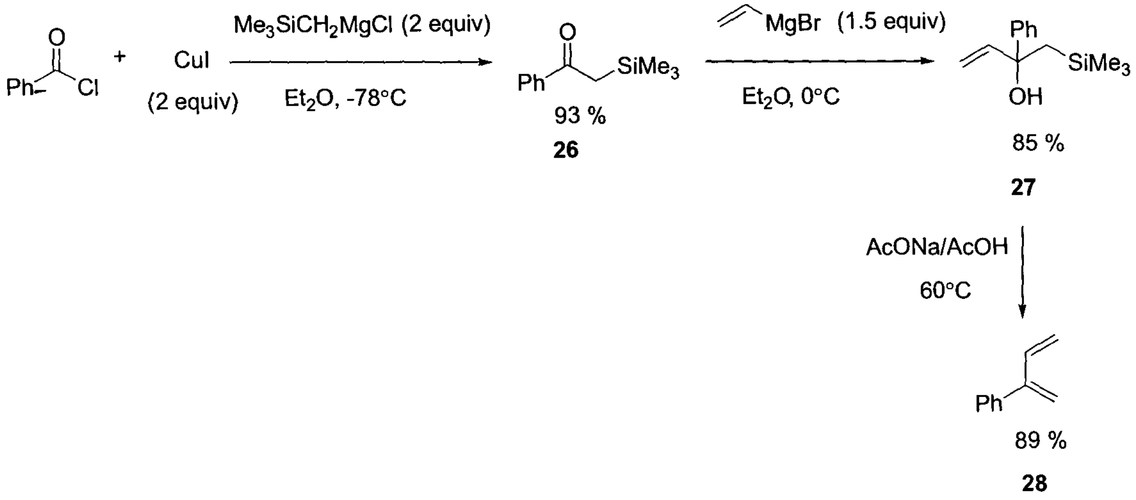

Scheme 2.2 Synthesis of 2-phenyl-1,3-butadiene (**28**).

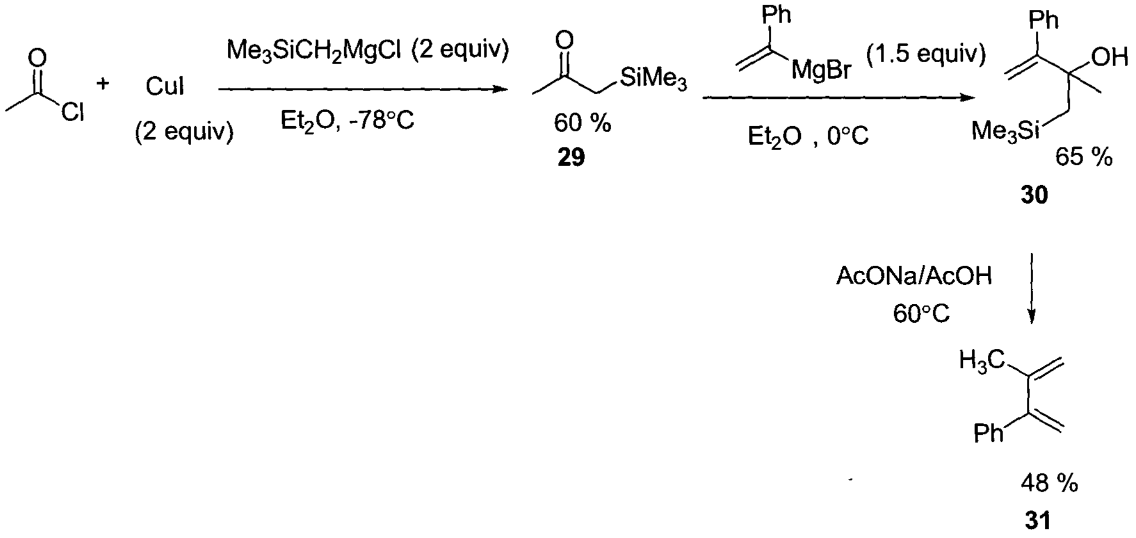

Scheme 2.3 Synthesis of 2-methyl-3-phenyl-1,3-butadiene (**31**).[a]

[a] *Katie Beleznay is acknowledged for the synthesis of diene* **31**.

Germanium dichloride-1,4-dioxane and the 1,1-dichlorogermacyclopent-3-ene derivatives **32** and **33** were prepared by adaptations of the synthetic procedures previously described by Leigh *et al* (Scheme 2.4).[1] Germanium tetrachloride and 1,1,3,3-tetramethyldisiloxane were refluxed in 1,4-dioxane at 85 °C for one hour, affording germanium dichloride-1,4-dioxane as colorless needle-like crystals in 85 % yield. The reaction of germanium dichloride-1,4-dioxane with the dienes **28** and **31** afforded the corresponding 1,1-dichlorogermacyclopent-3-ene derivatives **32** and **33**, respectively. These were then treated with two molar equivalents of methylmagnesium bromide to yield the crude products, which were in both cases distilled under vacuum to afford colorless oils. These oils were further purified by column chromatography to afford **23** and **24** in 89 % and 76 % yield respectively, and in purities > 98 %, as determined by GC-MS.

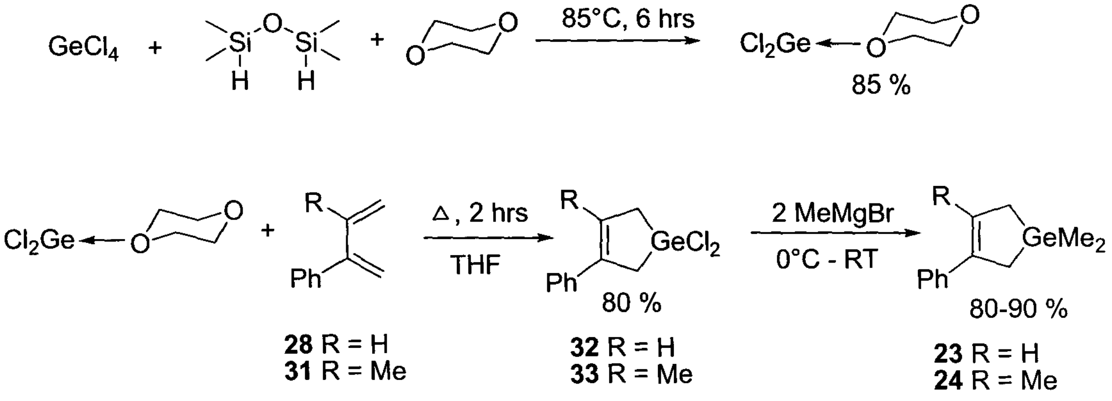

Scheme 2.4 Synthesis of germacyclopent-3-enes **23** and **24**.

Compounds **23** and **24** were identified by ^{1}H and ^{13}C NMR spectroscopy and high resolution mass spectrometry. The ^{1}H NMR spectrum of **23** (700 MHz, C_6D_6) showed a 6H singlet at δ 0.24 ppm assignable to the $Ge(C\underline{H}_3)_2$ protons. A triplet at δ 7.12 ppm and δ 7.23 ppm, and a doublet at δ 7.54 ppm were consistent with a monosubstituted aromatic ring. A multiplet at δ 6.46 ppm (1H) was attributed to the vinylic proton (H-4), and exhibited allylic coupling interaction with H-2 ($^4J_{2,4}$ = 2.0 Hz) and with H-5 ($^3J_{4,5}$ = 3.5 Hz). Protons H-2 appeared as a multiplet at 1.76 ppm (2H) and in turn exhibited allylic coupling with H-4 ($^4J_{2,4}$ = 2.0 Hz) and homoallylic interactions with H-5 ($^5J_{2,5}$ = 2.0 Hz). A multiplet at δ 1.64 ppm was assigned to protons H-5 ($^3J_{4,5}$ = 3.5 Hz and $^5J_{2,5}$ = 2.0 Hz). A NOE experiment, in which the vinylic proton H-4 was irradiated, showed strong enhancements of the signals due to the ortho aromatic protons and H-5. A spin decoupling experiment showed that irradiation of H-4 leads to decoupling of the signals due to H-2 and H-5, confirming coupling interactions between H-4 and these protons. In this experiment, the signals of H-2 and H-5 appeared as triplets due to their homoallylic coupling. In addition, a COSY experiment confirmed the long-range coupling interactions between the H-2 and H-5 protons. The ^{13}C NMR spectrum (700 MHz, C_6D_6) of **23** showed a peak at δ -2.16 ppm assignable to the carbon (C-1) of the methyl groups on Ge. Peaks at δ 20.83 and 20.90 ppm were assigned to C-5 and C-2, respectively, while peaks at δ 126.38, 126.96, 128.35, 128.48 ppm were assigned to the aromatic carbons. Signals at δ 141.65 and δ 142.90 (CH=*C*Ph) ppm were assigned to the vinylic carbons C-3 and C-4 on the germacyclopentene ring. The EI mass spectrum of **23** shows major peaks with m/z (I) = 234.04 (30, M^+), 219 (100, M^+-CH_3), while HR/MS gave an exact mass of 234.0442 for the molecular ion (calculated for $C_{12}H_{16}{}^{74}Ge$: 234.0464).

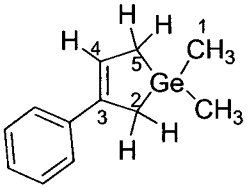

23

The ^1H NMR spectrum of **24** (600 MHz, C_6D_6) displays a singlet at δ 0.28 (6 H, $Ge(CH_3)_2$), multiplets at δ 1.67 (2H, $^5J_{2,5}$ = 2.0 Hz) and δ 1.97 (2H, $^5J_{2,5}$ = 2.0 Hz) corresponding to H-5 and H-2, respectively, a 3H singlet at δ 1.80 attributable to H-6 and multiplets at δ 7.09 (4H) and δ 7.24 (1H) corresponding to the aromatic protons. The ^{13}C NMR spectrum (150 MHz, C_6D_6) showed a peak at δ -2.4 that can be assigned to the methyl carbons attached to Ge. Other peaks at δ 27.4 and δ 27.6 can be assigned to C-2 and C-5, respectively. The aromatic carbons appeared at δ 126.2, 127.8, 128.2, 128.6 and 134.7. A signal at δ 21.1 ppm was assigned to the C-6 methyl group attached to C-4 of the germacyclopentene ring, while signals at δ 137.0 and δ 144.3 were assigned to C-4 and C-3, respectively. The mass spectrum showed major peaks with m/z (I) = 248 (M^+, 58), 233 (48, M^+-CH_3), 104 (50, $(Ge(CH_3)_2)^+$), 89 (100, $(GeCH_3)^+$), 77 (28, $C_6H_5{}^+$), and HRMS analysis of the molecular ion gave an exact mass of 248.0613 (calculated for $C_{13}H_{18}{}^{74}Ge$, 248.0620).

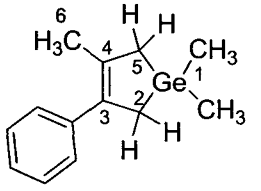

24

Both **23** ($\varepsilon_{248\text{nm}}$ = 6960 dm^3 mol^{-1} cm^{-1}) and **24** ($\varepsilon_{248\text{nm}}$ = 4913 $\text{dm}^{3-}\text{mol}^{-1}$ cm^{-1}) exhibit sufficiently strong UV absorptions at 248 nm to make them suitable for laser flash photolysis studies at 248 nm. The plots of molar absorptivity (ε) versus wavelength in hexanes for the two precursors are shown in Figure 2.1.

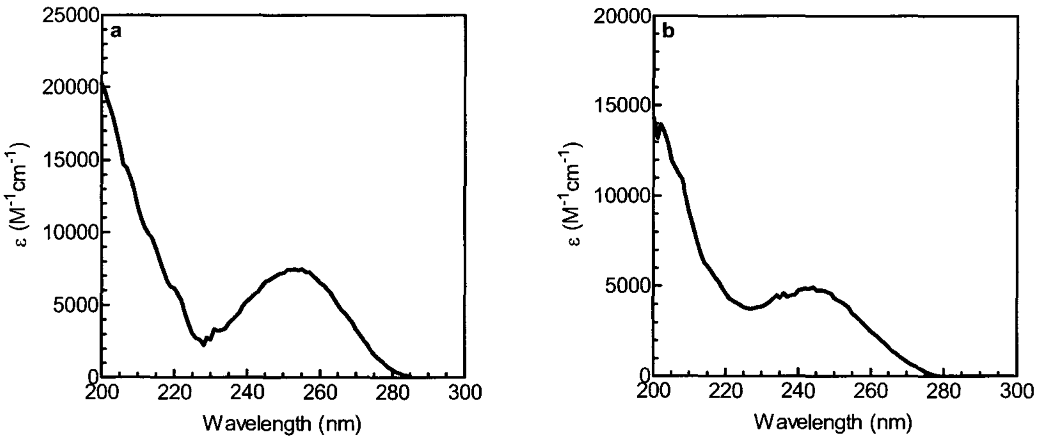

Figure 2.1. UV-Vis absorption spectrum of (a) **23** and (b) **24** in hexanes.

2.3 Steady state photolysis of 23 and 24

Steady state photolysis (254 nm, 6 low-pressure mercury lamps) of argon-saturated solutions of **23** (0.04 - 0.05 M) in cyclohexane-d_{12} containing AcOH (0.25 M) or MeOH (0.24 M) and hexamethyldisilane (< 0.003 M) was performed in 5 mm quartz NMR tubes at 25 °C using a merry-go-round apparatus. The photolysis mixtures were monitored periodically by ^{1}H NMR spectroscopy. The concentrations of the products and the precursor were calculated from the integrals of the peaks relative to that of the internal standard (Si_2Me_6). In both cases, the plots of concentration versus photolysis time were linear at low conversions, as shown in Figures 2.2 and 2.8. The chemical yields of the products were determined from the ratios of the slopes of the lines corresponding to the products and the precursor (eq 2.1). Scheme 2.5 shows the products and their chemical yields from the two reactions. The errors in the chemical yields are ca. 3-8 %, as defined by the standard errors in the slopes of the product and precursor concentration versus time plots.

$$\% \text{ Yield of product} = (\text{Slope}_{(\text{product})} / |\text{Slope}_{(\text{precursor})}|) \times 100\ \% \qquad \textbf{(2.1)}$$

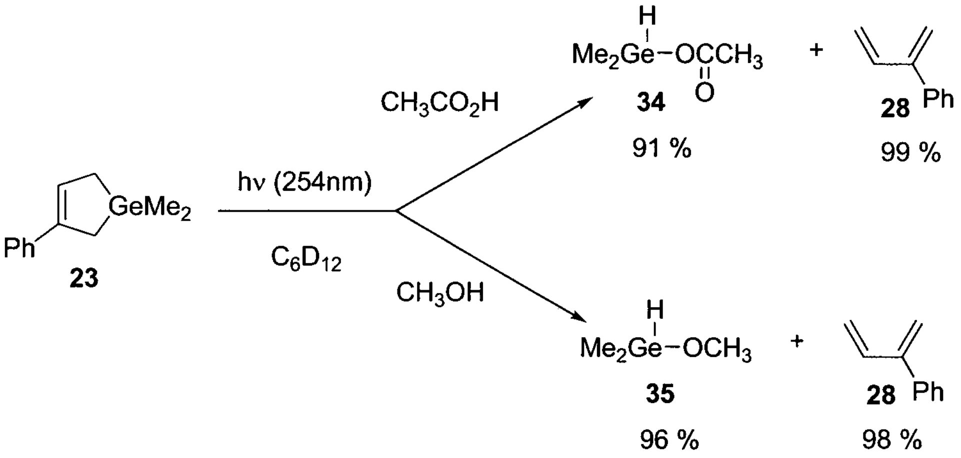

Scheme 2.5 Steady state photolysis of **23** (0.04-0.05 M) in the presence of MeOH (0.24 M) and AcOH (0.25 M) in cyclohexane-d_{12}.

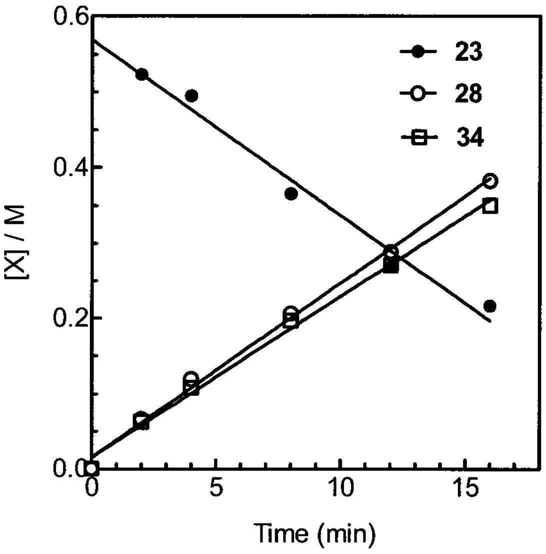

Figure 2.2. Concentration versus time plots for 254 nm irradiation of a deoxygenated solution of **23** (0.05 M) in C_6D_{12} containing AcOH (0.25 M). The solid lines represent the linear least-squares fits of the data. The slopes (x 10^2) are: (□; 2.14 ± 0.08) for **34**; (○; 2.31 ± 0.07) for **28**; (•; -2.3 ± 0.2) for **23**.

^{1}H NMR spectra (200 MHz) recorded before and after photolysis to ca. 60 % conversion of **23** in the presence of AcOH are shown in Figure 2.3. New peaks at δ 6.46 - 6.51 (dd, 1H, C*H*=CH$_2$, ^3J = 11.2 and ^3J = 17.0 Hz) and δ 5.0 - 5.30 (m, 4H), are due to diene **28**.[6] The doublet at δ 0.56 (6H, ^3J = 2.4 Hz) and septet at δ 5.63 (1H, ^3J = 2.4 Hz), respectively are assigned to acetoxydimethylgermane **34**-based on comparisons to its reported ^{1}H NMR spectrum.[7] The methyl protons of the acetyl group (-C(O)C*H*$_3$) cannot be observed as they coincide with those of AcOH. The ^{1}H NMR spectrum of the photolysate suggests that the reaction is "clean" at 60 % conversion; i.e. no other products could be detected in > ca. 5 % yield of **34**.

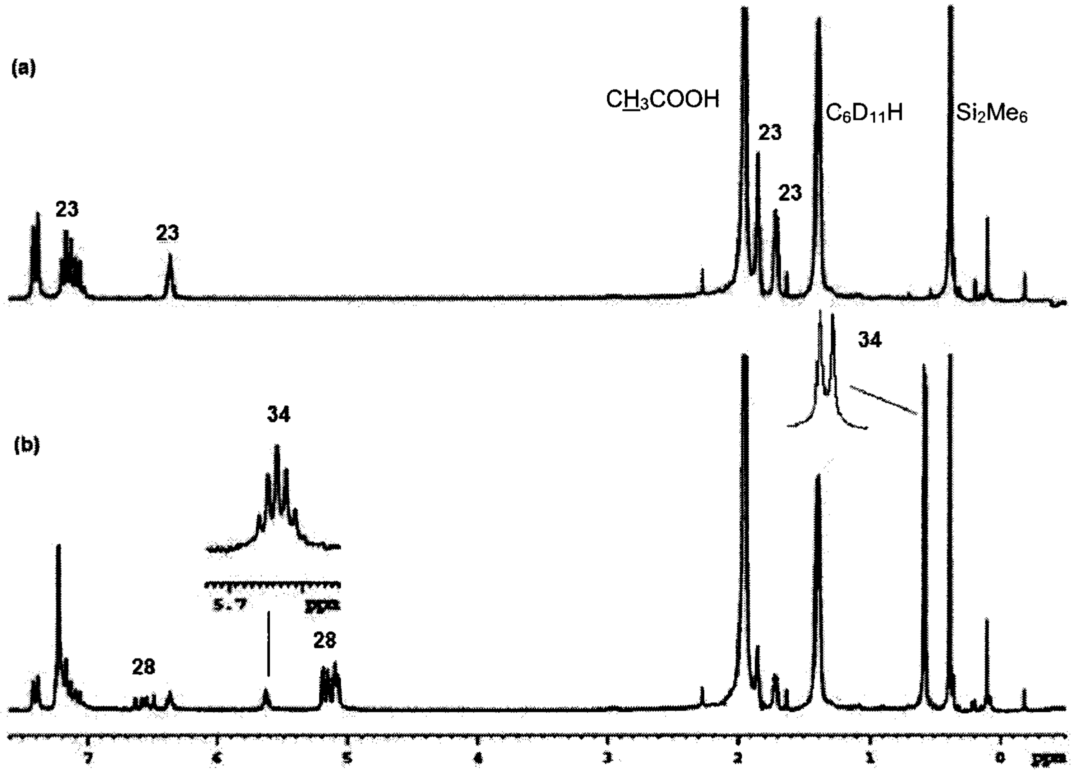

Figure 2.3. ^{1}H NMR spectra (200 MHz) of the crude reaction mixture from photolysis (254 nm) of a solution of **23** (0.05 M) in the presence of AcOH (0.25 M) in deoxygenated cyclohexane-d_{12} at (a) t = 0 min and (b) after ca. 60 % conversion of **23**.

Representative ^{1}H NMR spectra (600 MHz) of **23** (0.04 M) in the presence of MeOH (0.24 M) recorded before and after photolysis (to 20 % conversion) are shown in Figure 2.4. The latter spectrum shows the formation of diene **28** and one product which was identified as methoxydimethylgermane **35** (δ 5.2 (sept, 1H, $^{3}J = 2.5$ Hz), δ 3.5 (s, 3H) and δ 0.4 (d, 6H, $^{3}J = 2.5$ Hz) ppm).[8] The chemical yields of **28** and **35** were determined to be 98 % and 96 %, respectively, from concentration versus time plots constructed over 0-20 % conversion range in **23** (see Figure 2.4).

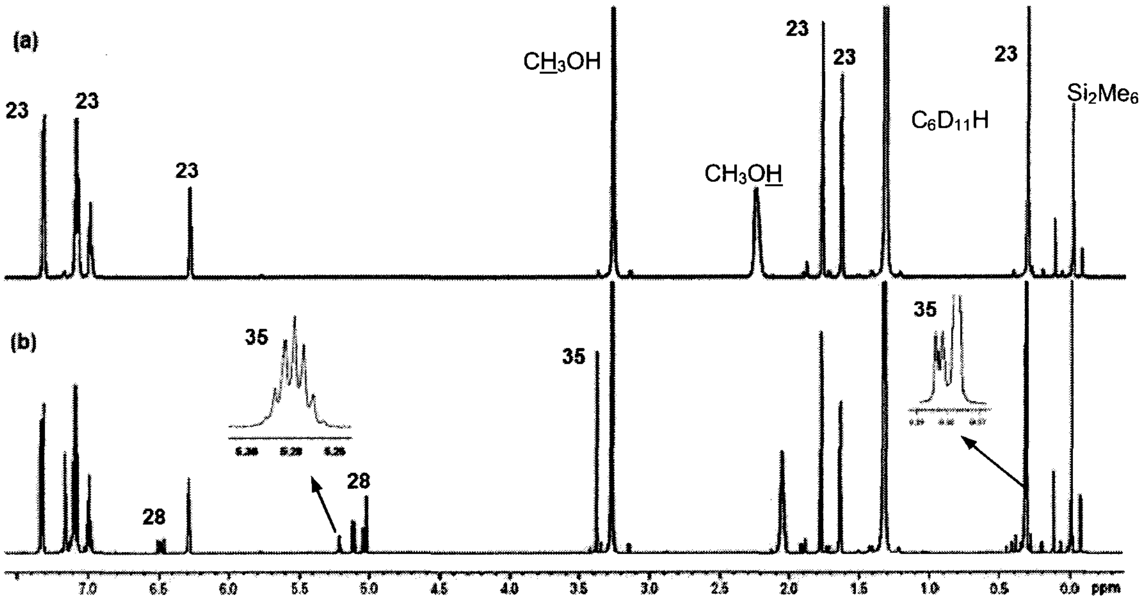

Figure 2.4. ^{1}H NMR spectra (600 MHz) of the crude reaction mixture from photolysis (254 nm) of a solution of **23** (0.04 M) in the presence of MeOH (0.24 M) in deoxygenated cyclohexane-d_{12} at (a) t = 0 min and (b) after *ca.* 20 % conversion of **23**.

An argon-saturated hexanes solution of **23** (0.03 M) in the presence of DMB (0.05 M) and n-dodecane as standard was irradiated (254 nm, 6 low-pressure mercury lamps) in 5 mm quartz NMR tubes for a total of 12 minutes. The reaction was monitored periodically by gas chromatography. The formation of two new peaks was observed; these were identified as diene **28** and 1,1,3,4-tetramethylgermacyclopent-3-ene **7** (Scheme 2.6) by spiking the photolysate with authentic samples of **7** and **28**. Two other minor products were also formed in 3-5 % of the yield of **7** but were not identified. The plots of relative peak areas for **23**, **28** and **7** with respect to dodecane are shown in Figure 2.5.

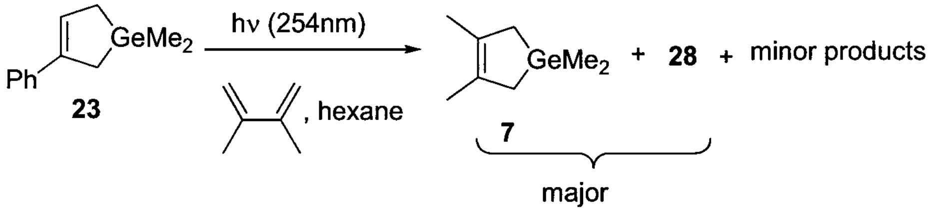

Scheme 2.6 Steady state photolysis of **23** in the presence of DMB in cyclohexane-d_{12}.

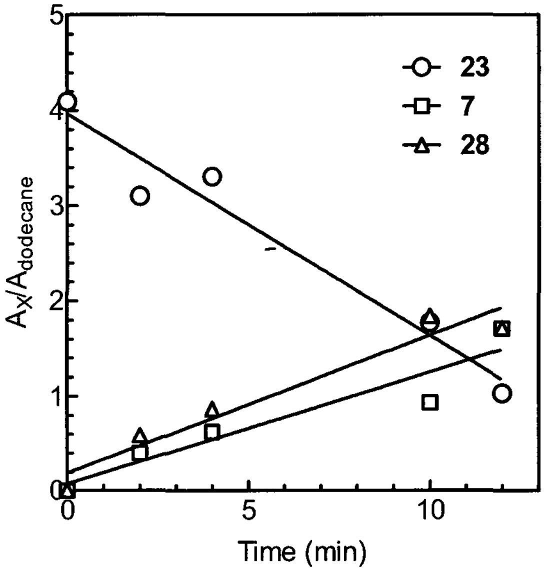

Figure 2.5. Plots of relative area ($A_x/A_{dodecane}$) of the precursor **23**, and products **7** and **28** (A_x) to dodecane (internal standard) versus photolysis time of a mixture of **23** (0.03 M) and DMB (0.05 M) in deoxygenated hexanes. The solid lines are the linear least-squares fits of the data and the slopes are: (○; -0.23 ± 0.03) for **23**; (□; 0.12 ± 0.02) for **7**; (△; 0.14 ± 0.02) for **28**.

Irradiation (254 nm, 6 low-pressure mercury lamps) of an argon-saturated solution of **24** (0.05 M) in cyclohexane-d_{12} containing AcOH (0.26 M) and hexamethyldisilane (0.02 M) as an internal standard, yielded diene **31** and acetoxygermane **34** in 99 % and 98 % yields, respectively, over the 0-30 % conversion range (Scheme 2.7). Figure 2.6 shows the ^{1}H NMR spectra (600 MHz) of the photolysis mixture recorded before and after 30 % photochemical conversion of **24**. The product yields were calculated in a similar way as described for the photolysis of precursor **23**; the concentration versus time plots for **24**, **35** and **31** are shown in Figure 2.7.

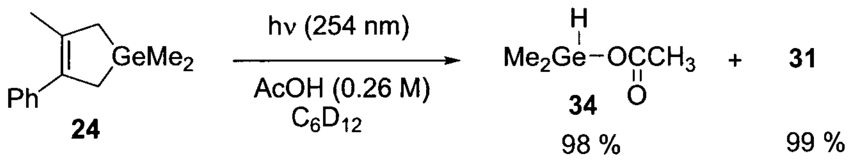

Scheme 2.7 Steady state photolysis of **24** in the presence of AcOH in C_6D_{12}.

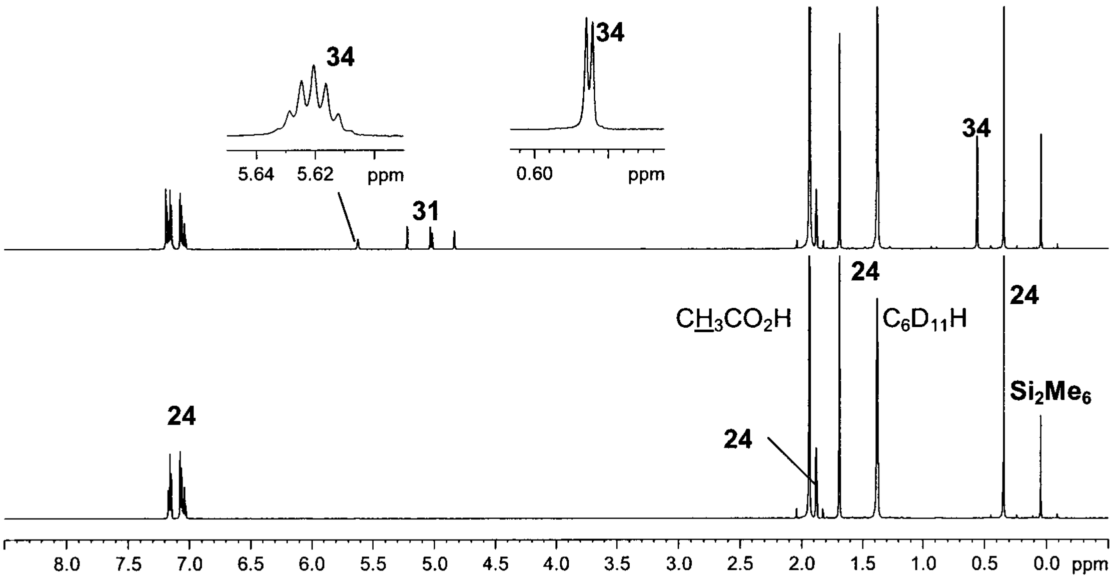

Figure 2.6. ^1H NMR spectra (200 MHz) of the crude reaction mixture from photolysis (254 nm) of a solution of **24** (0.05 M) in the presence of AcOH (0.26 M) in deoxygenated cyclohexane-d_{12} at (a) t = 0 min and (b) after *ca.* 30 % conversion of **24**. Hexamethyldisilane was used as an integration standard.

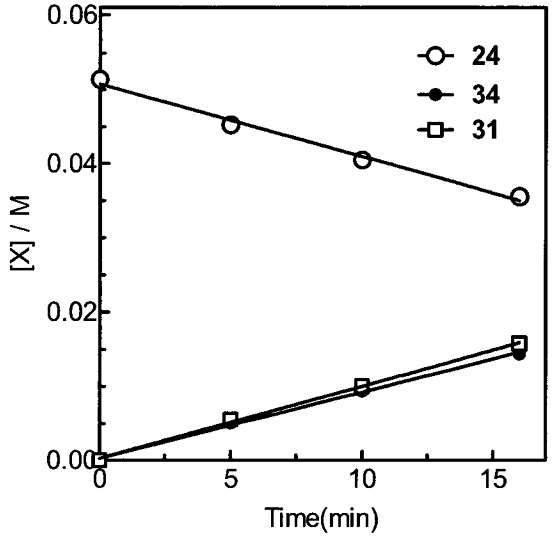

Figure 2.7. Concentration versus time plots for 254 nm irradiation of a deoxygenated solution of **24** (0.05 M) in C_6D_{12} containing AcOH (0.25 M). Hexamethyldisilane was used as an integration standard (0.0028 M). The solid lines are the linear least-squares fits of the data and the slopes (x 10^4) are: (○; -9.9 ± 0.7) for **24**; (●; 9.0 ± 0.3) for **34**; (□; 9.8 ± 0.2) for **31**.

These steady state experiments show that compounds **23** and **24** undergo clean photochemical decomposition to afford the dienes **28** and **31**, respectively, and $GeMe_2$-trapping products as the exclusive products in close to quantitative yields.

2.4 Quantum yield determination for the formation of $GeMe_2$ from 23

The quantum yield (Φ) for the formation of $GeMe_2$ from the photochemical decomposition of **23** was determined by an experiment in which an optically dense deoxygenated solution of 1,1-diphenylsilacyclobutane (**36**) was simultaneously photolysed. Toltl *et al.* have previously reported that photolysis of **36** in C_6D_{12} containing MeOH yields ethene and methoxymethylsilane (**37**) (1,1-diphenylsilene trapping product)

(Scheme 2.8); a quantum yield of $\Phi = 0.21 \pm 0.02$ was determined for the formation of **37**.[9]

Solutions of **23** (0.041 M) and **36** (0.037 M) containing MeOH (0.24 M) in cyclohexane-d_{12} were placed in two different quartz NMR tubes and were deoxygenated with argon. Hexamethyldisilane (0.0017 M) was used as an internal integration standard in both solutions. The two NMR tubes were irradiated simultaneously using 6 low-pressure mercury lamps (254 nm) in a merry-go-round apparatus, which ensured that both reaction mixtures received equal light exposure. The progress of the photolyses was determined at various time intervals by 600 MHz ^{1}H NMR spectroscopy. The quantum yield (Φ_{GeMe2}) for the formation of **35** from **23** was determined from the relative slopes of the concentration vs. time plots (see Figure 2.8) using eq (2.2) and was found to be 0.55 ± 0.09, assuming quantitative trapping of $GeMe_2$ to form **35**. The results show that the precursor **23** extrudes $GeMe_2$ with comparable efficiency to 3,4-dimethyl-1,1-diphenylgermacyclopent-3-ene ($\Phi_{GePh2} = 0.55 \pm 0.07$), used by our group as a precursor to $GePh_2$.[1]

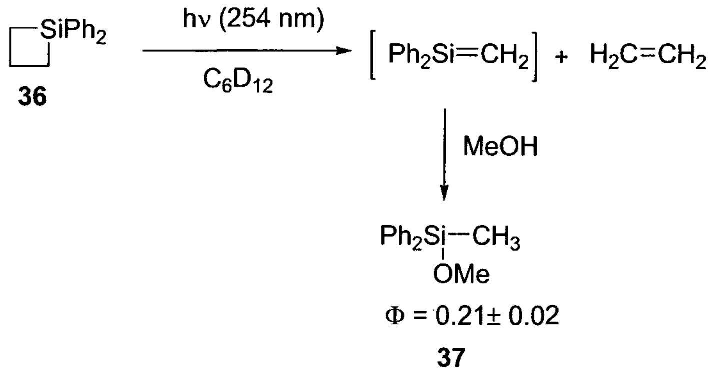

Scheme 2.8 Steady state photolysis of **36** in the presence of methanol.

$$\Phi_{26} = \frac{slope_{26}}{slope_{38}} \text{ X } \Phi_{38} \qquad \textbf{(2.2)}$$

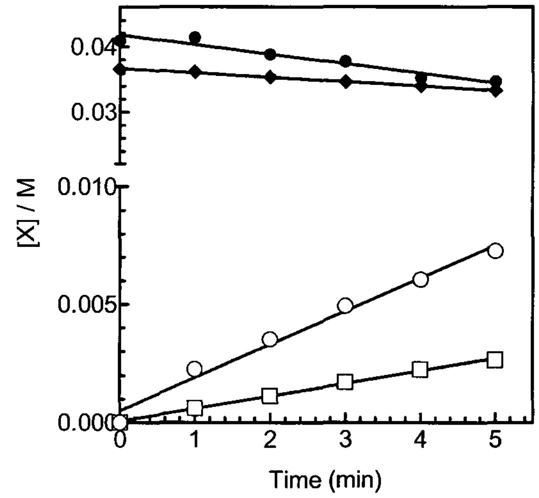

Figure 2.8. Plots of concentration ([X]/M) versus time for precursors: **23** (•) and **36** (♦) and products: **37** (○) and **35** (□) from the photolysis of **23** (0.041 M) and **36** (0.037 M) in deoxygenated C_6D_{12} in the presence of 0.24 M MeOH. The slopes (x 10^3) are: (○; 1.4 ± 0.2) for **37**; (□; 0.54 ± 0.03) for **35**; (♦; -0.67 ± 0.02) for **36**; (•; -1.4 ± 0.2) for **23**.

2.5 Direct detection of $GeMe_2$ and Ge_2Me_4 in solution by laser flash photolysis

For all the laser flash photolysis experiments conducted, meticulously dried hexanes (dried over activated alumina) and glassware were used. In these experiments, it is crucial to work under anhydrous conditions as it was found that the maximum *intensity* of the signal due to $GeMe_2$ at 470 nm is highly sensitive to traces of water or (presumably) other hydroxylic impurities (this will be discussed in Chapter 4). In a typical flash photolysis experiment, solutions of the photochemical precursors were prepared at concentrations that gave a static absorbance of *ca.* 0.8 at the excitation wavelength (248 nm). During the experiment, the solutions were continuously pumped from a calibrated 100 mL or 250 mL reservoir through a vacuum oven-dried thermostatted 7 x 7 mm Suprasil flow cell, using a peristaltic pump fitted with Teflon tubing to pull the solution through the sample cell at ca. 3 mL/min. The reservoirs were fit with a glass frit that allows bubbling of argon gas through the solution for ca. 30 minutes prior to the experiment and throughout the experiment. Solution temperatures were measured with a Teflon-coated copper/constantan thermocouple attached to the sample compartment, and are considered accurate to ± 2 °C.

2.5.1 Laser flash photolysis of 23

Laser flash photolysis of a continuously flowing deoxygenated solution of **23** (ca. 7 x 10^{-5} M) in deoxygenated anhydrous hexanes with the pulses from a KrF excimer laser (248 nm, ca. 20 ns, 100 ± 5 mJ) gave rise to a relatively weak, but easily detectable transient species that was formed with the laser pulse. Figure 2.9a shows transient absorption spectra recorded at three different time intervals after the laser pulse in a typical experiment. The first-formed transient species exhibits an absorption maximum of 470 nm, and decays with second-order kinetics over ~ 2 μs with the concomitant formation of a second transient species exhibiting an absorption maximum of 370 nm (see inset in Figure 2.9). The transient spectrum recorded 51-70 ns after the laser pulse is distorted because of fluorescence below ca. 320 nm. The fit of the 470 nm signal to eq (2.3) afforded an average value of $k_{dim}/\varepsilon = (5.3 \pm 1.2) \times 10^7$ cm s^{-1}. The dimerization rate constant could then be obtained after determination of the extinction coefficient of $GeMe_2$ at its maximum absorption (see Section 2.6). The 370 nm transient species decays over a much longer time scale (~ 100 μs) with mixed-order kinetics (see inset in Figure 2.10).

$$\Delta A_{\lambda,t} = \Delta A_{\lambda,0} / [1 + (2k_{dim}\Delta A_{\lambda,0} / l\ \varepsilon_{\lambda})t] \qquad \textbf{(2.3)}$$

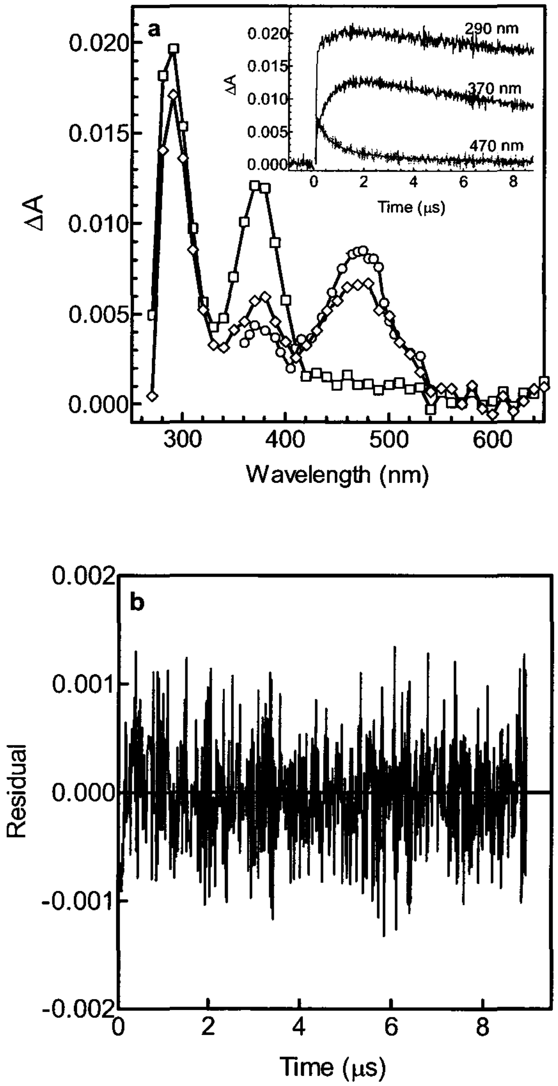

Figure 2.9. (a) Transient absorption spectra recorded by laser flash photolysis (248 nm) of **23** (ca. 7 x 10^{-5} M) in argon-saturated anhydrous hexanes at 25 °C, 51-70 ns (○), 0.12-0.19 μs (◊) and 2.96-3.07 μs (□) after the laser pulse. The inset shows typical transient profiles at 290 nm, 370 nm and 470 nm. The solid line superimposed on the 470 nm decay profile is the non-linear least-squares fit of the data to eq (2.3); (b) The residuals obtained from the fit of the 470 nm transient decay trace to eq (2.3).

These results are consistent with the absorption maximum reported for $GeMe_2$, generated by the photolysis of 1,1-dimethylgermacyclopent-3-ene (**5**), 1,1,1,2,2-pentamethyldigermane (**20**) and 1,1,2,2-tetramethyldigermane (**21**) in the gas phase by Becerra *et al.* and with that reported by Leigh *et al.* from 193 nm laser flash photolysis of 1,1,3,4-tetramethylgermacyclopent-3-ene (**7**) in dry deoxygenated hexanes.[1,3,10] In addition, the absorption maximum observed is in accordance with that predicted for $GeMe_2$ by time-dependent density functional theory calculation (TD-DFT), λ_{max} = 463 nm.[1] On the basis of these comparisons, we assign the transient species with absorption maximum at 470 nm to $GeMe_2$. The 370 nm transient species is consistent with the previously reported spectral characteristics of Ge_2Me_4 by Leigh *et al.* from photolysis of 1,1-dimethyl-1-germacyclopent-3-ene[1] and by Mochida *et al.* from their laser flash photolysis studies of the 7,8-digermabicylo[2.2.2]-octadiene derivative **22** in cyclohexane at room temperature.[11]

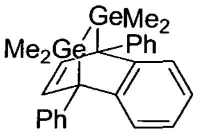

22

A long-lived absorption band with higher intensity (λ_{max} ~ 290 nm) was also formed, and decays with mixed-order kinetics over a much longer time scale than Ge_2Me_4 (see inset in Figure 2.10a). Transient absorption spectra recorded by laser flash photolysis of **23** over the 0-1.9 ms timescale are shown in Figure 2.10a. The weak band at ~ 355 nm is due to Ge_2Me_4, shifted to the blue because of overlap with the stronger band at 290 nm. Transient absorption spectra recorded by laser flash photolysis of **23** in deoxygenated hexanes containing 3 mM AcOH revealed that the transient absorption band at 290 nm is still present, but under these conditions exhibits reduced initial signal intensities. $GeMe_2$ reacts irreversibly with AcOH with a bimolecular rate constant, $k_Q = 7.5 \times 10^9$ $M^{-1}s^{-1}$ (*vide infra*). Therefore, in the presence of 3 mM AcOH, $GeMe_2$ is quenched. The fact that a weak absorption band at 300 nm is present indicates that it is associated with neither $GeMe_2$ nor Ge_2Me_4. Under these conditions, the transient profile recorded at 300 nm shows a very short-lived decay followed by a longer-lived decaying component. The lifetime of the longer-lived transient species is $\tau \sim 400$ μs and corresponds to a bimolecular rate constant of $k_Q = 2.5 \times 10^3$ $M^{-1}s^{-1}$ for its reaction with acetic acid (inset of Figure 2.10b). We did not try to study this transient species further as its absorption intensity is very weak, and it did not affect our kinetic study of $GeMe_2$ and Ge_2Me_4. A summary of the photochemistry of the precursor **23** is depicted in Scheme 2.9.

$$\Delta A_t = \Delta A_0 e^{-k_{decay}t} \qquad \textbf{(2.4)}$$

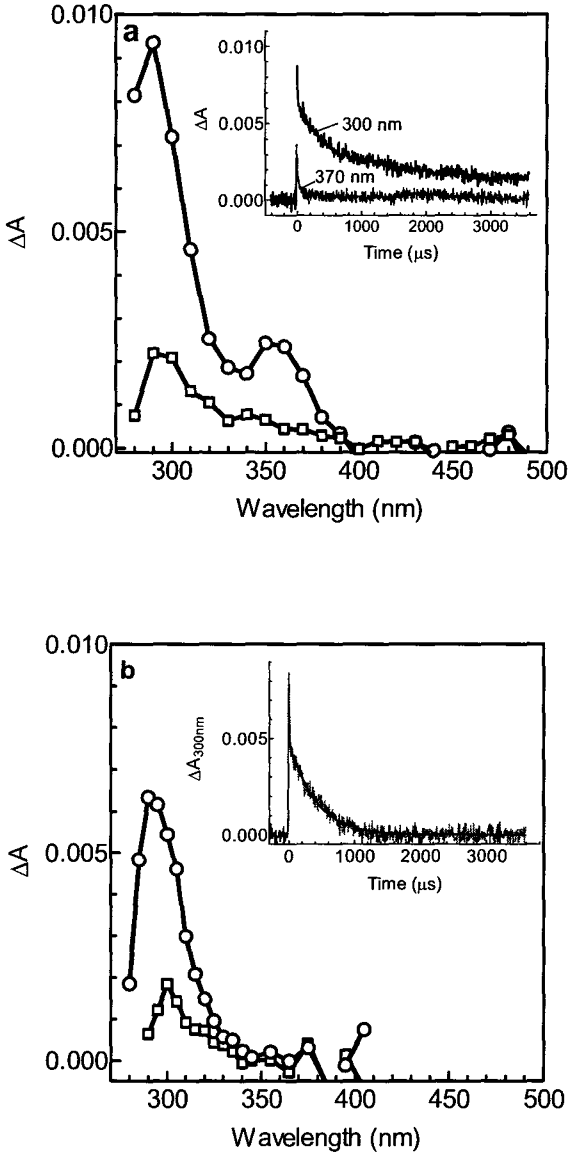

Figure 2.10. (a) Transient absorption spectra recorded by laser flash photolysis of **23** in deoxygenated hexanes 0-12.8 μs (○) and 1.82-1.85 ms (□) after the laser pulse. The inset shows transient decay profiles recorded at 300 nm and 370 nm; (b) Transient absorption spectra recorded by laser flash photolysis of **23** in deoxygenated hexanes containing 3 mM AcOH, 0-12.8 μs (○) and 416-422 μs (□) after the laser pulse. The inset shows the transient decay profile recorded at 300 nm. The solid line represents the non-linear least-squares fit to eq (2.4).

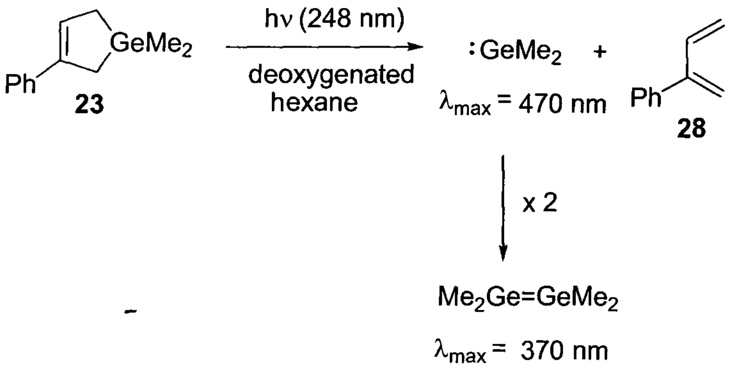

Scheme 2.9 Generation of $GeMe_2$ by laser flash photolysis of **23** in deoxygenated hexanes and its reaction in the absence of a scavenger.

2.5.2 Laser flash photolysis of 24

Laser flash photolysis of **24** (ca. 7 x 10^{-5} M) in deoxygenated anhydrous hexanes at 25 °C also led to the formation of a transient absorption band centered at λ_{max} = 470 nm, which decayed with second-order kinetics on the microsecond time-scale to form a second transient band centered at λ_{max} = 370 nm. These results are in agreement with those from photolysis of **23**, and thus support the assignment of the transient at 470 nm to $GeMe_2$ and that at 370 nm to Ge_2Me_4. Figures 2.11a and 2.11b show transient absorption spectra recorded in different experiments. The initial intensities of $GeMe_2$ varied from experiment to experiment, presumably due to the variation in the amount of water present. For example, in Figure 2.11a, the initial signal intensity of the transient at 470 nm is higher than in Figure 2.11b. This can be attributed to a better control over the amount of adventitious water present in the solvent in this experiment. Figure 2.11a shows the transient absorption spectra recorded over 350-600 nm spectral range; points were collected at 5 nm intervals in order to better resolve the absorption maximum of the longer wavelength band. Figure 2.11b shows transient absorption spectra recorded over the 270-650 nm wavelength range, revealing the band at shorter wavelength ~ 290 nm. It can also be observed that the 470 nm transient decays over a slightly longer time scale compared to the one recorded from photolysis of precursor **23**. This is because $GeMe_2$ decays in a second-order process to form its dimer; thus, the decay rate (k_{obs}) of the signal appears to proceed on a longer time scale when the initial concentration is lower. For the same reason, a slower apparent rate of growth is observed for the formation of Ge_2Me_4. Laser flash photolysis of **24** and **23** gave similar results under similar experimental conditions, indicating that both germacyclopent-3-ene derivatives give rise to the same transient species (Scheme 2.10). The rate coefficient for the decay of $GeMe_2$ (k_{dim}/ε = (5.8 ± 1.2) x 10^7 $cm^{-1}s^{-1}$) is in excellent agreement with the value determined using **23** as precursor.

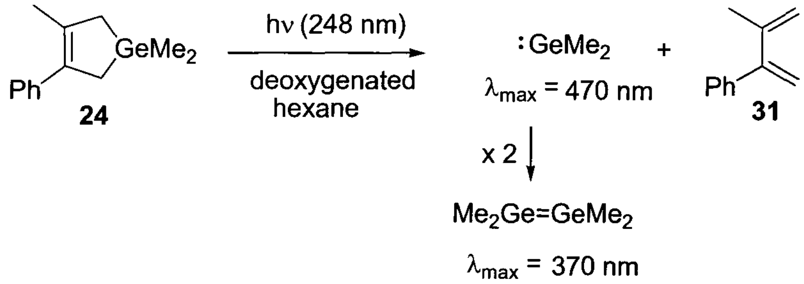

Scheme 2.10 Photochemical decomposition of **24** in deoxygenated hexanes.

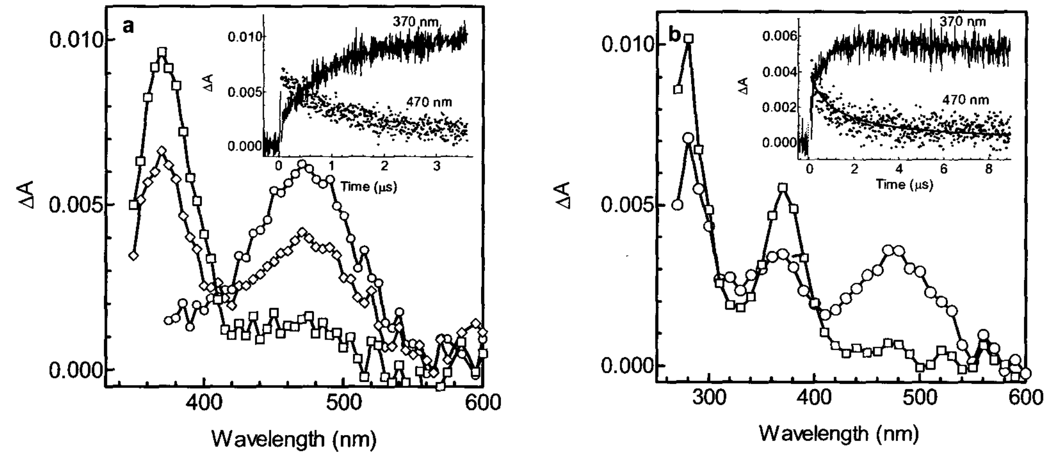

Figure 2.11. (a) Transient absorption spectra recorded by laser flash photolysis of **24** (ca. 7 x 10^{-5} M) in deoxygenated hexanes recorded 32-58 ns (○), 0.70-0.72 μs (◊) and 3.10-3.12 μs (□) after the laser pulse. The inset shows transient decay/growth profiles monitored at 470 nm and 370 nm; (b) Transient absorption spectra recorded by laser flash photolysis of **24** (ca. 7 x 10^{-5} M) 0.11-0.13 μs (○), 5.47-6.06 μs (□) after the laser pulse. The inset shows transient decay/growth profiles recorded at 470 nm and 370 nm. The solid line represents the non-linear least-squares fit of the data to eq (2.3) ($k_{\text{dim}}/\varepsilon$ = 5.75 x 10^7 cm s^{-1}).

2.6 Determination of the molar extinction coefficient of $GeMe_2$ at 480 nm

The molar extinction coefficient (ε) of $GeMe_2$ at 480 nm was determined by the intensity variation method using benzophenone (BP) as actinometer.[12] Laser photolysis of BP yields the BP triplet state (^{3}BP*) with a quantum yield (Φ_{3BP*}) of unity.[13] ^{3}BP* exhibits a long-wavelength absorption band centered at λ_{max} = 525 nm and an extinction coefficient of $\varepsilon_{525\ nm}$ = 6250 ± 1250 M^{-1} cm^{-1}.[14] Solutions of **23** and BP in dry deoxygenated hexanes were optically matched at the laser wavelength (248 nm) to ensure equal light absorption. The two solutions were subjected to laser flash photolysis under similar conditions, using the flow system described earlier. Figures 2.12a and 2.12b show the effects of laser dose on the initial signal intensities of $^3BP^*$ (λ_{max} = 525 nm) and $GeMe_2$ (λ_{max} = 480 nm), respectively. The change in the maximum initial absorbance $(\Delta A)_{0,max}$ of the solutions of **23** and $^3BP^*$ as a function of varying laser intensity was measured. A set of calibrated neutral density filters made of fine wire mesh screens was used to control the laser intensity. The $(\Delta A)_{0,max}$ at each laser intensity was measured several times and averaged in order to minimize random fluctuations. At 100 % laser intensity, the energy delivered at 248 nm was 86 mJ/pulse. The plots of $(\Delta A)_{0,max}$ at 480 nm or 525 nm versus laser intensity for $GeMe_2$ or $^3BP^*$ were both linear, according to eq (2.5), where l is 0.5 cm and ε is the extinction coefficient ($M^{-1}cm^{-1}$) of $^3BP^*$ or $GeMe_2$, Φ is the quantum yield of $^3BP^*$ or $GeMe_2$, and I_a is the laser dose absorbed (Figure 2.12c-d).

$$(\Delta A)_{0,max} = \Phi \varepsilon l I_a \qquad \textbf{(2.5)}$$

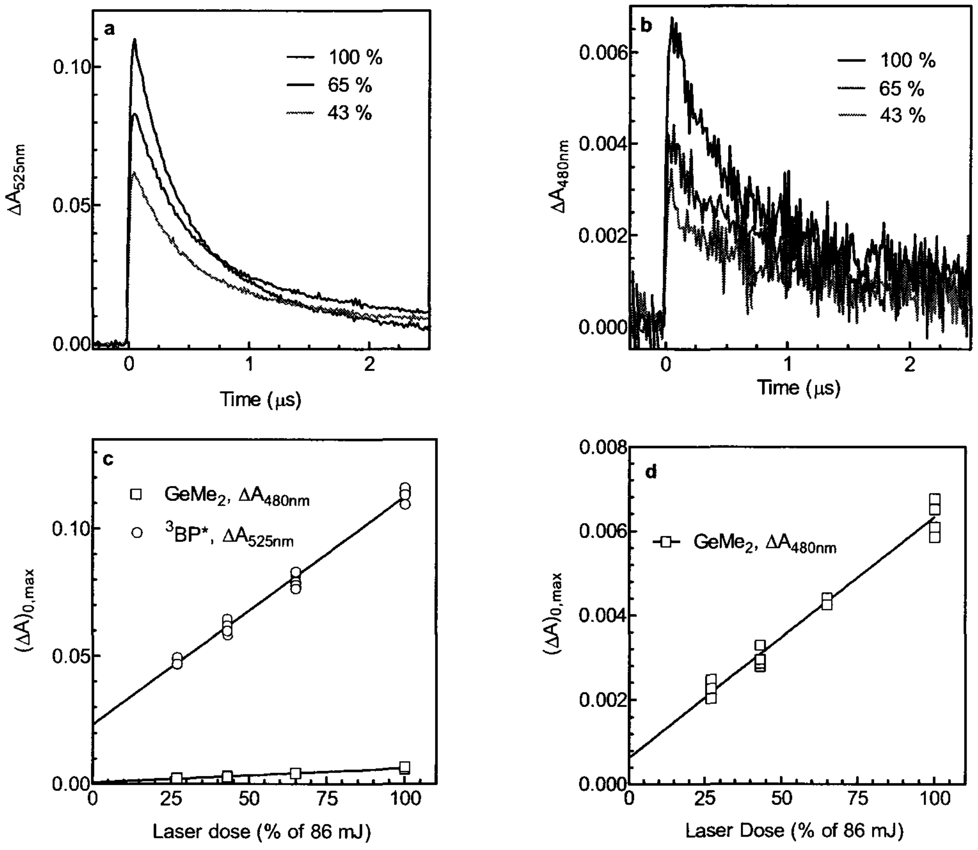

Figure 2.12. Determination of the molar absorptivity of $GeMe_2$ at 480 nm using the benzophenone triplet at 525 nm ($\varepsilon_{525} = 6250 \pm 1250$) in deoxygenated dry hexanes as actinometer. Effects of laser dose on the transient decay profiles recorded by laser flash photolysis of (a) BP monitored at 525 nm and (b) **23** monitored at 480 nm in deoxygenated hexanes; (c) Plots of ΔA_{max} versus laser dose (% of 86 mJ) for the optically matched deoxygenated solutions of BP and **23** in dry hexanes at 25 °C; (d) Expanded plot of ΔA_{max} versus laser dose (% of 86 mJ) for **23**. Errors in the slopes of the plots are listed as twice the standard error from linear least squares analysis. Slope of $^3BP^* = (8.93 \pm 0.38) \times 10^{-4}$; Slope of $GeMe_2 = (5.69 \pm 0.42) \times 10^{-5}$; $Slope_{GeMe2}/Slope_{3BP^*} = 0.064 \pm 0.003$.

The extinction coefficient (ε_{480nm}) for $GeMe_2$ was determined from the relative slopes of the plots, the quantum yield ($\Phi_{GeMe2} = 0.55 \pm 0.09$) for the formation of $GeMe_2$

and the extinction coefficient of ^{3}BP* (ε_{525nm} = 6250 ± 1250 M^{-1} cm^{-1}), according to eq (2.6). The value obtained is ε_{480nm} = 730 ± 300 dm^3 mol^{-1} cm^{-1}.

$$\Phi_{GeMe_2}\,\varepsilon_{GeMe_2} = \frac{S_{GeMe_2}}{S_{^3BP*}}\,\varepsilon_{^3BP*}\,\Phi_{^3BP*} \qquad \textbf{(2.6)}$$

(where S_{GeMe_2} = slope of the plot for $GeMe_2$ and $S_{^3BP*}$ = slope of the plot for ^{3}BP* and $\Phi_{^3BP*}$ = 1)

2.7 Absolute rate constant for dimerization of $GeMe_2$ in solution

In the absence of a scavenger, transient germylenes dimerize at close to the diffusion-controlled rate in hydrocarbon solvents to form the corresponding dimer, Ge_2R_4; for example, k_{dim} values for $GePh_2$ and $GeMes_2$ were determined to be k_{dim} = (1.1 ± 0.2) x 10^{10} $M^{-1}s^{-1}$ and k_{dim} = (5.4 ± 1.5) x 10^9 $M^{-1}s^{-1}$, respectively, in hexanes at 23 °C.[1] In this work, transient decay profiles of $GeMe_2$ recorded in deoxygenated hexanes fit reasonably well to second-order kinetics (eq 2.3), and k_{dim}/ε = (5 ± 1) x 10^7 cm s^{-1} was obtained by averaging the results from second-order fits of the plots of decay profiles collected in ten different experiments. The dimerization rate constant for $GeMe_2$ can thus be calculated using the extinction coefficient (ε_{GeMe2} = 730 ± 300 dm^3 mol^{-1} cm^{-1}), based on eq 2.7 where l is the path length of the irradiated sample (0.5 cm). The k_{dim} for $GeMe_2$ is (3.6 ± 1.8) x 10^{10} M^{-1} s^{-1} and is in reasonable agreement with the diffusion-controlled rate constant (k_{diff} = 2.2 x 10^{10} $M^{-1}s^{-1}$) in hexanes at 25 °C. The latter can be calculated from the standard Debye equation (eq 2.8);[15] η is the viscosity of hexane ($\eta_{\mathrm{hexane}} = 2.942 \times 10^{-2}$ Pa s at 25 °C)[16], T is the temperature in Kelvin and R is the gas constant (8.314 J K^{-1} mol^{-1}).

$$\frac{2k_{\dim}\Delta A_{\mathrm{GeMe_2},0}}{l\varepsilon} = k_{decay}$$

$$k_{\dim} = k_{decay}\frac{l\varepsilon}{2\Delta A_{\mathrm{GeMe_2},0}} \qquad \textbf{(2.7)}$$

$$k_{\mathrm{diff}} = 8\ \mathrm{RT} / 3000\eta \qquad \textbf{(2.8)}$$

2.8 Kinetic studies of reactions of GeMe$_2$ in solution

In Chapter 1, we reviewed the numerous early reports regarding the kinetics of the reactions of "GeMe$_2$" in solution and the gas phase, emphasizing the lack of consistency in the UV-Vis absorption spectra and kinetic behavior assigned to this species from different precursors. We believe that this lack of consistency is the result of erroneous transient assignments, caused by the competing formation of other reactive intermediates which exhibit absorption bands in a similar spectral range as GeMe$_2$, inappropriate reaction conditions, and at the time, a simple lack of knowledge of the spectra and reactivities of transient germylenes, germenes and silenes in solution. However, in recent years the reactivities of conjugated germenes and silenes in solution have been well established in solution, largely through the efforts of our group.[17-21] The latter reactive intermediates are one of the common co-products formed upon photolysis of phenylated germylene precursors such as digermanes and silylgermanes. In addition, in 2005 a systematic study of the reactions of $GePh_2$ in solution by Cameron Harrington of our group shed new light on the reactivities of transient germylenes in solution.[2] This work provided many important insights and points of comparison for my work with $GeMe_2$.[22]

In the present study, in order to gain a better understanding of the kinetic behavior of $GeMe_2$ in solution, we studied the kinetics of its reactions with a wide variety of common germylene scavengers, including alkenes, dienes, group 14 metal hydrides, carboxylic acids, halocarbons and amines. We particularly chose substrates that were previously used in Harrington's studies of $GePh_2$, so as to be able to make direct comparisons of the reactivities of these two transient germylenes under similar conditions. The absorption spectrum observed for $GeMe_2$ in the gas phase by Becerra *et al.* is the only one reported that is consistent with the present work, and with previous work using 1,1,3,4-tetramethylgermacyclopent-3-ene as precursor.[1,3] Therefore, we compared our kinetic results to those of Becerra *et al.*, who determined bimolecular rate constants for reaction of the species with structurally related but not identical scavengers of a particular class in the gas phase.

In the absence of a scavenger, the decay of $GeMe_2$ is dominated by the dimerization reaction and follows second-order kinetics. We determined that dimerization of $GeMe_2$ to give Ge_2Me_4 is diffusion-controlled ($k_{dim} = (3.6 \pm 1.8) \times 10^{10}$ M^{-1} s^{-1}) in hexanes at 25 °C (*vide supra*). In order to explore the kinetics of the reactions of $GeMe_2$ with added scavengers (Q) under the conditions of our experiments, the rate of the reaction under study needs to exceed that of the dimerization reaction. When Q is added to the solution, we have two competing processes as shown in Scheme 2.11, assuming the absence of any unintentional reactive impurities such as water or oxygen. As previously mentioned, anhydrous and deoxygenated solvents, as well as scrupulously dried glassware, were used in all of our kinetic experiments in order to minimize complications from water and oxygen.

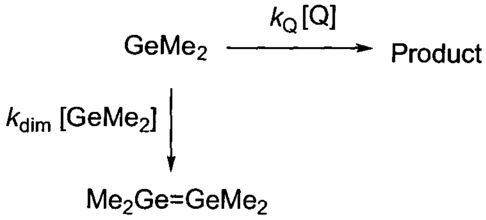

Scheme 2.11 Reactions of $GeMe_2$ in solution in the presence of scavenger Q.

In principal, addition of increasing amounts of a scavenger is expected to cause an enhancement in the decay rates of $GeMe_2$. In a situation where the reaction is first-order with respect to $GeMe_2$, a gradual change in its kinetic behavior from second-order to mixed first- and second-order kinetics should be observed. Once a sufficient amount of Q is present such that the decay of the germylene is due predominantly to its reaction with Q, its decay should follow pseudo-first-order kinetics according to eq (2.4), where $k_{decay} = k_Q[Q]$. Experimentally, we have observed that $GeMe_2$ decays with first-order kinetics at scavenger concentrations which cause a *ca.* 50 % or more reduction decrease in the initial yield of the digermene, which is directly proportional to the maximum intensity of its signals (*vide infra*). We thus employed the Ge_2Me_4 signal at 370 nm to gauge when the necessary minimum scavenger concentration is reached to ensure the validity of fitting the germylene signal to first-order decay kinetics. We took this precaution because the transient absorptions due to $GeMe_2$ are quite weak, and generally fit "acceptably" to first-order kinetics even when dimerization is clearly the dominant decay channel based on the characteristics of the digermene signal.

Based on Harrington's results for $GePh_2$,[1,2] we anticipated the kinetic behavior of $GeMe_2$ to vary in complexity with various substrates chosen for study, depending on the magnitude of the equilibrium constant that defines the reaction in question. Thus, before presenting our actual results, it is appropriate to illustrate the various behaviors that are possible using kinetic simulations. The transient decay profiles of a germylene (such as $GeMe_2$) were simulated based on Scheme 2.12. As mentioned earlier, in the absence of an added scavenger, $GeMe_2$ dimerizes at the diffusion-controlled rate to form Ge_2Me_4, but this diminishes in importance as the scavenger concentration increases. The competing dimerization reaction was *not* considered in the simulations, described below.

The simulation assumes that the only reaction occurring is that of the germylene with added Q, occurring with a forward bimolecular rate constant $k_1 = 9 \times 10^9$ $M^{-1}s^{-1}$ and equilibrium constants of K_{eq} = 100 M^{-1}, 5000 M^{-1}, 20 000 M^{-1} or 100 000 M^{-1}. Thus, overall the simulation is for a very simplistic case but serves to illustrate the expected behavior under the different conditions. The expression for K_{eq} is given by eq (2.9). The value of the bimolecular rate constant (k_1) was chosen based on the experimental observation that most reactions of $GeMe_2$ in solution are close to diffusion-controlled (*vide infra*). The K_{eq} values represent situations of low, intermediate and high equilibrium constants. The initial absorption intensity of the germylene was taken as 0.01 arbitary units, which is roughly the intensity observed in our experiments.

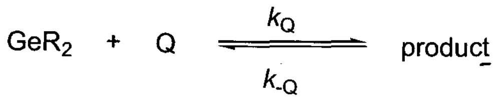

$$GeR_2 + Q \underset{k_{-Q}}{\overset{k_Q}{\rightleftharpoons}} \text{product}$$

Scheme 2.12 Reaction of GeR_2 with scavenger (Q).

$$K_{eq} = k_Q/k_{-Q} = \frac{[\text{Product}]_{eqm}}{[GeR_2]_{eqm}[Q]} \qquad [Q] >> [GeR_2]_0 \qquad \textbf{(2.9)}$$

$$\Delta A_t = (\Delta A_0 - \Delta A_{eqm})\, e^{-(k_Q[Q]+k_{-Q})} + \Delta A_{eqm} \qquad \textbf{(2.10)}$$

Figure 2.13a displays the simulated transient profiles for GeR_2 for the case where $K_{eq} = 100\ M^{-1}$. The decay profile of the germylene exhibits an initial fast decay due to the approach to equilibrium, followed by a non-decaying residual absorption (plateau). The plateau represents the amount of free germylene present at equilibrium. Experimentally, since the germylene is unstable and dimerizes to form the digermene, decaying residual absorptions can be expected to be observed; because it arises from a second-order reaction, the apparent decay rate of the residual absorption (due to GeR_2 at equilibrium) will decrease as the average residual absorption value decreases. In this situation, the actual value of k_Q cannot be determined, but analysis of the residual absorption levels according to eq (2.10) allows determination of K_{eq}. Note that when K_{eq} is as small as ~ 100 M-1, the approach to equilibrium is too fast to be measured given the time resolution of our instrument.

From Figure 2.13a, it is evident that for reactions with $k_Q \geq 10^9$ $M^{-1}s^{-1}$ and $K_{eq} \leq 100$ M^{-1}, the initial approach to equilibrium is too fast to be resolved from the laser pulse. Consequently, only a decreasing initial absorbance intensity and a second-order decay are observed with increasing concentration of Q. An example of this behavior is given in Chapter 4, for the reaction of $GeMe_2$ with t-BuOH. We believe that this situation also pertains when Q = water, which explains the dependence of $GeMe_2$ signal strengths on the degree to which the solvent and glassware are dried prior to the beginning of an experiment.

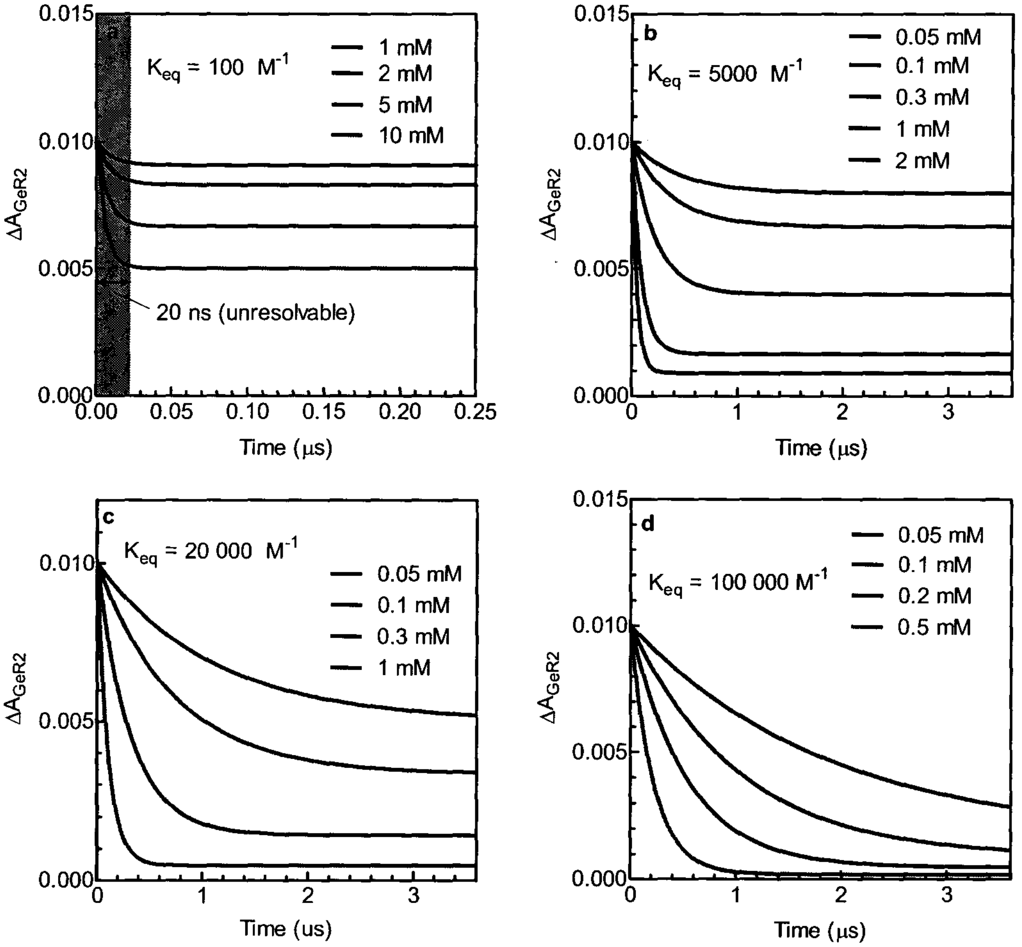

Figure 2.13. Simulation of germylene (GeR_2) decay profiles for its reaction with scavenger (Q), with bimolecular rate constant $k_Q = 9 \times 10^9$ M^{-1}s^{-1} and K_{eq} (a) 100 M^{-1}, (b) 5000 M^{-1}, (c) 20 000 M^{-1}, and (d) 100 000 M^{-1} in hydrocarbon solvents. The first 20 ns portion of the decay profiles in (a) has been grayed to illustrate the area that cannot be resolved.

At the opposite extreme (K_{eq} = 100 000 M^{-1}), it is evident that the plateau is indistinguishable from the baseline (ΔA = 0), given the noise inherent in our data (Figure 2.13d); when the amount of residual germylene becomes negligible, the reaction is "essentially" *irreversible*. In such situations, k_Q can be determined experimentally, but K_{eq} cannot be.

Figures 2.13b and 2.13c represent intermediate situations, and in both cases the initial fast decay and plateau are discernible. When K_{eq} for the reaction of GeR_2 with Q falls into the intermediate category, we can thus determine both k_Q and K_{eq} from the experimental data: k_Q from plots of k_{decay} versus [Q] (eq 2.11), and K_{eq} from plots of (ΔA_0 - ΔA_{res} / ΔA_{res}) versus [Q], according to eq (2.12). As illustrated in Figure 2.14a, the plateau (ΔA_{res}) is proportional to the concentration of the free GeR_2 at equilibrium and the span (ΔA_0 - ΔA_{res}) is proportional to the equilibrium concentration of the primary product formed. Experimentally, if we observed decaying residual absorptions instead of a plateau, we estimated the $\Delta A_{res,}$ as illustrated in Figure 2.14b. The decaying residual absorptions are due to dimerization of free germylene after equilibrium has been established.

$$k_{decay} = k_{-Q} + k_Q[Q] \qquad \textbf{(2.11)}$$

$$K_{eq}\,[Q] = [\text{Product}]/[GeR_2]_{eq}$$

$$\therefore\ K_{eq}\,[Q] = (\Delta A_0 - \Delta A_{res} / \Delta A_{res}) \qquad \textbf{(2.12)}$$

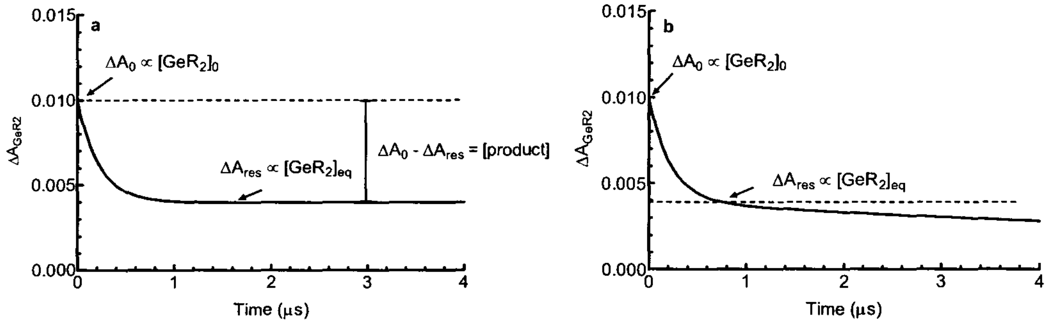

Figure 2.14. (a) Absorption versus time plot of GeR_2 for a hypothetical reversible reaction of GeR_2 with Q, illustrating the parameters used to determine the K_{eq} for the reaction, according to eq (2.12) when (a) the residual absorptions are non-decaying and when (b) residual absorptions are decaying.

In addition, the variation in the magnitude of K_{eq} has distinct effects on the growth/decay profile due to the dimerization product, Ge_2R_4. For reactions with low equilibrium constant, $K_{eq} < 25\ 000\ M^{-1}$, a lengthening in the growth time of Ge_2Me_4 is generally observed with increasing addition of the scavenger, and the formation of digermene persisted at concentrations of Q beyond which the germylene could no longer be detected (*vide infra*). However, it should be noted that the kinetic behavior of the digermene varies depending on whether or not it also reacts with the added scavenger. If the digermene reacts with the added Q, the lengthening in the growth time will not be observed, and a greater decrease in its signal intensities will be observed. In contrast, for reactions with $K_{eq} > 25\ 000\ M^{-1}$, increasing addition of scavenger continuously caused a decrease in the yield of the digermene. In this thesis, we will employ the term "irreversible" for any reaction for which $K_{eq} > 25\ 000\ M^{-1}$ and the efficiency with which Ge_2Me_4 formation is quenched is high. The digermene signals were thus employed as a qualitative method of gauging the efficiency of the reaction of Q with $GeMe_2$ (i.e. the magnitude of K_{eq}).

The quantum yield of Ge_2R_4 in the *absence* of Q is given by eq (2.13), where [i] is the concentration of any reactive impurities present. Assuming the concentration of impurities is negligible, in the presence of added Q (low concentrations), the decay of GeR_2 is dominated by dimerization to form Ge_2R_4, and the bimolecular reaction with Q to form products, with rate constants k_{dim} and k_Q, respectively. Under these conditions, the quantum yield of Ge_2R_4 ($\Phi_{Ge_2R_4}$) is given by eq (2.14). Hence, the ratio of quantum yields for Ge_2R_4 in the absence and presence of added Q is given by eq 2.15, which is a modified version of the Stern-Volmer equation.

$$\Phi_{Ge_2R_4,0} = \frac{k_{dim}[GeR_2]_0^2}{k_{dim}[GeR_2]_0^2 + k_i[GeR_2]_0[i]} \frac{\Phi_{GeMe2}}{2} \qquad \textbf{(2.13)}$$

$$\Phi_{Ge_2R_4,Q} = \frac{k_{dim}[GeR_2]_0^2}{k_{dim}[GeR_2]_0^2 + k_Q[GeR_2]_0[Q]} \frac{\Phi_{GeMe2}}{2} \qquad \textbf{(2.14)}$$

assuming [i] in our experiments is 0

$$\therefore \frac{\Phi_{Ge_2R_4,Q}}{\Phi_{Ge_2R_4,0}} = 1 + \frac{k_Q}{k_{dim}[GeR_2]_0}[Q] \qquad \textbf{(2.15)}$$

where the Stern-Volmer constant, $K_{sv} = \frac{k_Q}{k_{dim}[GeR_2]_0}$

The yield of the digermene is proportional to its maximum absorption intensity, thus, eq (2.16) is obtained. The maximum signal intensity due to Ge_2Me_4 is denoted by $(\Delta A_{370})_{max,0}$ in the absence of Q, and $(\Delta A_{370})_{max,Q}$ in the presence of Q. A plot of the ratio of absorption intensities versus [Q], according to eq. (2.16) is expected to be linear. The slope is the Stern-Volmer constant (K_{sv}) and is the product of the bimolecular rate constant (k_Q) for the reaction of $GeMe_2$ with Q and the second-order lifetime ($\tau = 1/k_{dim}[GeR_2]_0$) of $GeMe_2$ in the absence of Q.

$$(\Delta A_{370})_{max,0}/(\Delta A_{370})_{max,Q} = 1 + K_{sv}[Q] \qquad \textbf{(2.16)}$$

The Stern-Volmer "constants" obtained in our experiments should be interpreted with caution, because they depend on the initial concentration of $GeMe_2$ (see eq 2.15). The latter in turn depends on the concentration of the precursor and especially on the laser intensity. In our experiments, these two parameters were kept constant as far as possible: a static UV-Vis absorbance of the precursor solution ranging between 0.8-9 and a laser dose of 100-112 mJ were used throughout. Moreover, the maximum intensities of the signals due to Ge_2Me_4 in the presence of a scavenger vary depending on its reactivity with Q. Strictly speaking, eq (2.16) holds when Ge_2R_4 is *unreactive* toward Q. If this is not the case, artificially high K_{sv} values will be obtained. Experimentally, we found that Ge_2Me_4 is reactive toward most of the scavengers used, though the rate constants for their reactions are generally much lower than those of $GeMe_2$. Only in a few cases was it clear that the rate constant for reaction of the digermene with the scavenger approaches that of the germylene (*vide infra*).

The ratio of K_{sv}/k_Q (listed in Table 2.1) provides a better qualitative indication of the scavenging efficiency of the reaction of $GeMe_2$ with Q than K_{sv} itself, because K_{sv} depends on k_Q. In general, it is observed that reversible reactions exhibit lower K_{sv}/k_Q values than "irreversible" reactions. For example, $GeMe_2$ reacts with similar rate constants with Et_3N and AcOH; however, the K_{sv}/k_Q for triethylamine (Et_3N) is ca. 4 times smaller than that for AcOH. In other situations, for example with AcOH and CCl_4, both reactions are "irreversible" with $GeMe_2$. The reaction of $GeMe_2$ with AcOH is two orders of magnitude higher than that of CCl_4, but the K_{sv}/k_Q for the latter reaction is higher. This is because Ge_2Me_4 is more reactive toward CCl_4 than AcOH.

Typical irreversible behavior was observed when $GeMe_2$ was scavenged with AcOH, carbon tetrachloride (CCl_4), oxygen, triethylgermane (Et_3GeH), triethylsilane (Et_3SiH) and tributylstannane (Bu_3SnH), while the reactions with isoprene, Et_3N and n-butylamine (n-$BuNH_2$) showed evidence of reversibility, but with $K_{eq} > 20\ 000\ M^{-1}$. The bimolecular rate constants (k_Q), K_{sv} and K_{sv}/k_Q values determined for the reactions of $GeMe_2$ are collected in Table 2.1. In general a low K_{sv}/k_Q ratio (< 0.5) was considered as an indication of reversibility. Each reaction will be discussed individually in the sections that follow.

Values of the pseudo-first-order decay rate constant (k_{decay}) at increasing scavenger concentrations were obtained from single-phase exponential fits of the decay profiles, using eq (2.4). For irreversible reactions the plots of k_{decay} monitored at 480 nm versus [scavenger] were linear and were analyzed according to eq (2.17), where the slope, k_Q, is the bimolecular rate constant for the reaction of $GeMe_2$ and k_0 is the hypothetical pseudo-first-order rate constant for decay of $GeMe_2$ in the absence of a scavenger.

$$k_{decay} = k_0 + k_Q\,[Q] \qquad \textbf{(2.17)}$$

Table 2.1. Absolute rate constants (k_Q), Stern-Volmer "constants" (K_{sv}) and the ratios of K_{sv}/k_Q for the reactions of $GeMe_2$ with various scavengers in deoxygenated hexanes at 25° ± 2 C.[a,b]

Reagent	**$GeMe_2$ k_Q / 10^9 M^{-1} s^{-1}**	**K_{sv} / M^{-1}**	**(K_{sv}/k_Q)/μs**
AcOH	7.5 ± 0.4 (11.3 ± 2.4)	7600 ± 1300 (8300 ± 950)	1.01 (0.73)
CCl_4	0.08 ± 0.02	130 ± 20	1.63
$H_2C{=}CHCH_2CMe_3$ (DMP)	9.6 ± 1.2	1700 ± 250	0.18
Isoprene	11 ± 3	2500 ± 800	0.23
2,3-dimethyl-1,3-butadiene (DMB)	13 ± 6 (8.1 ± 0.2)	2800 ± 340 (5100 ± 1400)	0.22 (0.63)
$HC{\equiv}CCMe_3$ (TBE)	13 ± 3 (9.2 ± 1.9)	5300 ± 600 (5000 ± 600)	0.41 (0.54)
Bu_3SnH	14 ± 2	9600 ± 1400	0.70
Et_3SiH	0.0006 ± 0.0002	1.4 ± 0.2	2.55
Et_3GeH	0.05 ± 0.02	31 ± 1	0.69
Et_3N	8.7 ± 0.7	2030 ± 200	0.23
$BuNH_2$	12 ± 3	3610 ± 110	0.30
O_2	0.09 ± 0.01	150 ± 80	1.67

[a] Errors are listed as ± 2σ from the linear least-squares analysis of k_{decay} versus [Q] (see eq 2.17). The rate constants recorded from scavenging experiments using **23** as $GeMe_2$ precursor are shown in parentheses.

2.8.1 Reaction with acetic acid

Addition of AcOH resulted in a shortening in the lifetimes of $GeMe_2$ a change in its kinetic behavior from second-order to clean pseudo-first-order in the presence of [AcOH] ≥ 0.5 mM was observed. This indicates that at those concentrations the decay of $GeMe_2$ is dominated by its reaction with AcOH and that dimerization is negligible. Typical transient decay/growth traces for $GeMe_2$ and Ge_2Me_4 recorded at 0 mM, 0.05 mM and 0.54 mM of AcOH are shown in Figures 2.15a and 2.15b. $GeMe_2$ decays with excellent fits to first-order kinetics over a concentration range of 0.5-2 mM AcOH.

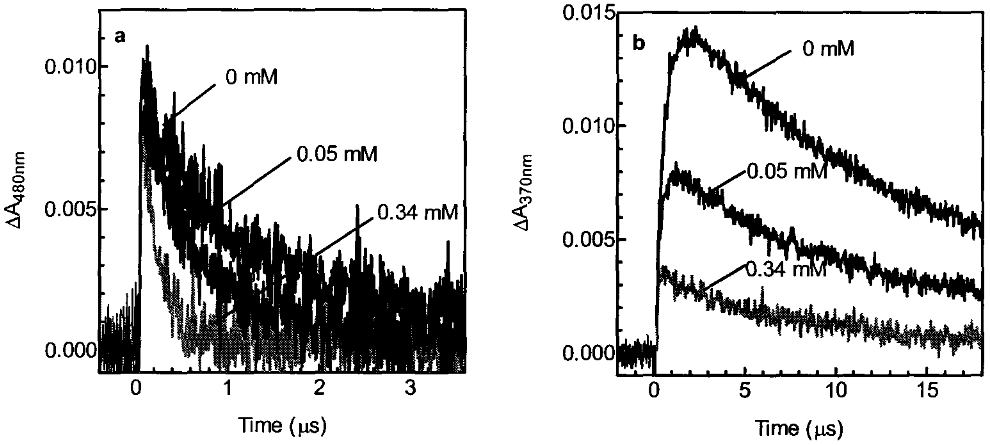

Figure 2.15. Effects of added AcOH on the: (a) transient decay profiles of $GeMe_2$, monitored at 480 nm; (b) transient growth/decay profiles of Ge_2Me_4, monitored at 370 nm.

A plot of the pseudo-first-order decay rate constants versus nominal [AcOH] is linear, consistent with eq (2.17), and indicates that the reaction is first-order with respect to AcOH within the concentration range studied as shown in Figure 2.16. A bimolecular rate constant, $k_Q = 7.5 \times 10^9\ M^{-1}s^{-1}$ was obtained from this plot. It is known that AcOH monomers form hydrogen-bonded dimers (cyclic and linear forms) with an equilibrium constant, $K_{eq} = 3200 \pm 500\ M^{-1}$ in hexanes at 25 °C.[23] The plot of k_{decay} versus the concentration of AcOH monomer (Figure 2.16b) afforded a bimolecular rate constant, $k_Q = (2.9 \pm 0.4) \times 10^{10}\ M^{-1}s^{-1}$, indicating that the reaction is diffusion-controlled. It is to be noted that the intercept is slightly negative (-1.223 ± 1.005), but is acceptable taking into account the errors associated with the determination of the AcOH monomer concentration. Overall, the linearity of the plot obtained with the nominal AcOH concentration shows that within this concentration range, both the AcOH monomer and dimer react unselectively with $GeMe_2$.

The yield of Ge_2Me_4 is directly proportional to the maximum intensity of the transient growth/decay profile recorded at 370 nm. It is observed that addition of increasing concentrations of AcOH resulted in a reduction in the maximum intensities at 370 nm and a gradual shift of the maxima to shorter times (Figure 2.15b). This behavior is an indication that the reaction of AcOH with $GeMe_2$ is irreversible (i.e. $K_{eq} >> 25\ 000\ M^{-1}$).

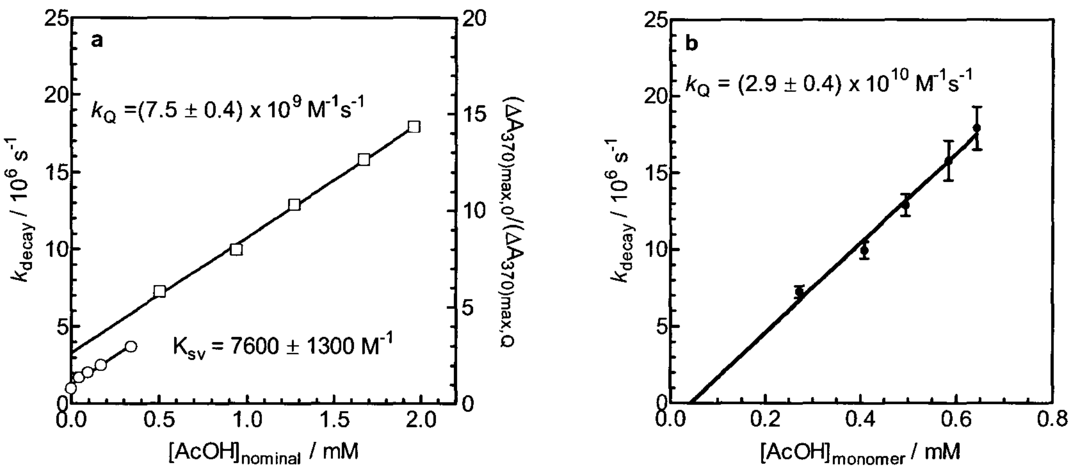

Figure 2.16. (a) Plots of pseudo-first-order decay rate constant of $GeMe_2$ (k_{decay}) versus nominal [AcOH] (□) and the plot of $(\Delta A_{370})_{max,0}/(\Delta A_{370})_{max,Q}$ versus [Q] (○). The solid lines represent the linear least-squares fit of the data to eqns (2.17) and (2.16), respectively; (b) Plots of pseudo-first-order decay rate constant of $GeMe_2$ (k_{decay}) versus $[AcOH]_{monomer}$. The solid line represents the best linear least-squares fit to eq (2.17).

The transient behavior observed at 480 nm is consistent with "irreversible" scavenging of the germylene. As discussed earlier, the germylene decays with first-order kinetics completely to baseline. A qualitative indication of irreversibility is also obtained from the digermene transient behavior. The growth/decay profiles recorded for Ge_2Me_4 are similar to what was previously observed for $GePh_2$ in the presence of AcOH in hexanes.[2] A plot of the relative maximum absorption intensities ($[(\Delta A_{370})_{max}]_0$ / $[(\Delta A_{370})_{max}]_{[Q]}$) of Ge_2Me_4 versus [AcOH] was linear, consistent with eq (2.16).

Huck and Leigh explored the effects of electron-donating and electron-withdrawing substituents on the rates of the reactions of a series of aryl-substituted germylenes with AcOH in hexanes.[24] Their study revealed excellent linear correlations of the rate constants with Hammett ρ-values, leading to $\rho = +0.19 \pm 0.01$. This indicates that the rate-determining step of these reactions involves development of a negative charge at the germanium center. On the basis of these results, it was postulated that the reaction with AcOH occurs by initial, rate-determining nucleophilic attack of the lone pair on the oxygen of the acid into the vacant p-orbital of the germylene. No new transient intermediate that could be assigned to a donor-acceptor complex between the germylene and the acid was detected. These results are consistent with a rapid proton transfer in the second step of the reaction to afford the final product (Scheme 2.13).

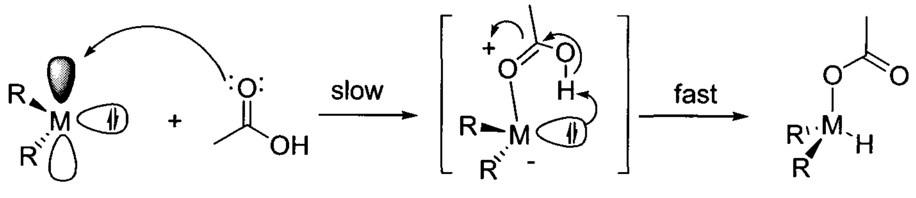

Scheme 2.13 Postulated mechanism for the reaction of GeR_2 with AcOH.

2.8.2 Reactions with group 14 metal hydrides

Addition of Et_3SiH, Et_3GeH and Bu_3SnH results in an enhancement in the decay rates of $GeMe_2$ and a decrease in the intensity of the signals due to Ge_2Me_4 in proportion to the concentration of the scavenger added. The kinetic behaviors of $GeMe_2$ and Ge_2Me_4 were similar to those observed in the presence of AcOH, consistent with "irreversible" reaction of $GeMe_2$ with the scavenger. Plots of the pseudo-first-order decay rate constants for $GeMe_2$ versus [scavenger] and Stern-Volmer plots, according to eqs (2.16) and (2.17), respectively were linear in all cases, and are shown in Figure 2.17.

It is observed that the rate constants for the reaction with $GeMe_2$ increase in the order Et_3SiH < Et_3GeH < n-Bu_3SnH; i.e. with decreasing M-H bond dissociation energy (BDE) (Table 2.2). The kinetic data reported for the reactions of GeMePh and $GePh_2$ with the same set of group 14 hydrides follow similar trends.[2,25] The rate constant for the reaction of $GeMe_2$ with Et_3SiH and Et_3GeH are similar to that of $GePh_2$, while that of n-Bu_3SnH is approximately four times larger.

Table 2.2. The BDE (kcal / mol) for selected group 14 hydrides and a comparison of the absolute rate constants (k_Q / 10^6 $M^{-1}s^{-1}$) of their reactions with GeR_2 and $SiMe_2$ in hexanes.

Scavenger	**BDE (kcal/mol)**	**$GeMe_2$**	**GeMePh[a]**	**$GePh_2$[b]**	**$SiMe_2$[c]**
Et_3Si-H	90.1[d]	0.6 ± 0.2	≤ 0.44	0.56 ± 0.09	3600 ± 300
Et_3Ge-H	82.3[e]	50 ± 20	nd	30 ± 2	2500 ± 200
n-Bu_3Sn-H	73.7[f]	13800 ± 1800	3700 ± 400	3490 ± 90	18900 ± 1400

nd – not determined. (a) Ref. 25; (b) Ref. 2; (c) Ref. 26; (d) Ref. 27; (e) Ref. 28; (f) Ref. 29.

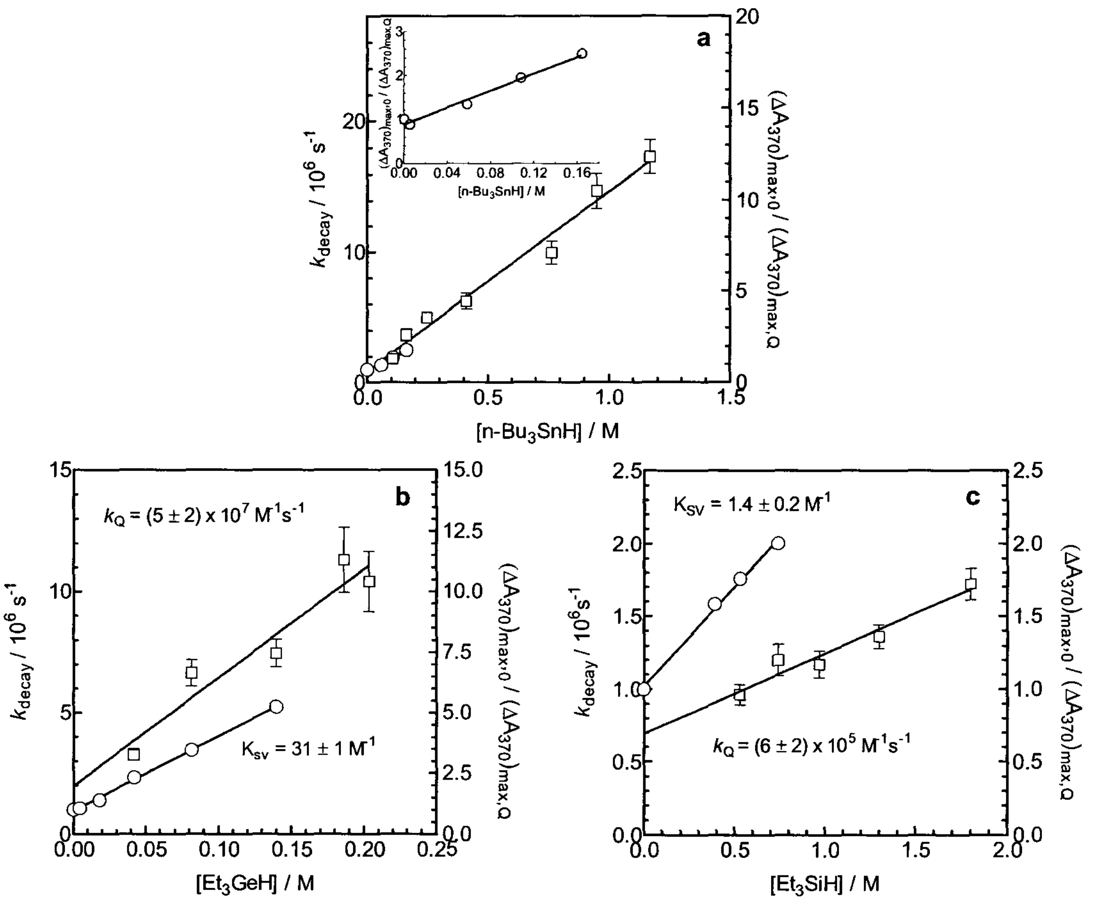

Figure 2.17. Effects of added (a) n-Bu$_3$SnH, (b) Et$_3$GeH and (c) Et$_3$SiH on (i) the pseudo-first-order rate constant (k_{decay}) of GeMe$_2$, monitored at 480 nm (□; eq 2.17), and (ii) the maximum transient absorbance of Ge$_2$Me$_4$ monitored at 370 nm (○; eq 2.16). The inset in (a) shows an expanded Stern-Volmer plot according to eq (2.16) for n-Bu$_3$SnH.

The rate constant for the reaction of GeMe$_2$ with Et$_3$SiH (k = 5.5 ± 1.5) x 10^5 $M^{-1}s^{-1}$ is at least an order of magnitude higher than the upper limit ($k < 10^4$ $M^{-1}s^{-1}$) reported by Bobbitt *et al.* for the transient they assigned (incorrectly) to GeMe$_2$.[30] On the other hand, Becerra *et al.* have reported an upper limit of $k < 6 \times 10^{-15}$ cm^3 molecule^{-1} s^{-1}

(corresponding to *ca.* < 3.6 x 10^6 M^{-1} s^{-1} in molar units) for the reaction of trimethylsilane with $GeMe_2$ in the gas phase.[3] This value is consistent with the rate constant obtained in the present work.

Although we did not perform any product studies for these reactions there are a few studies that showed the formation of the net insertion products from the reactions of silylenes with group 14 M-H bonds. For examples: Sefcik *et al.* have reported the formation of silylgermanes from the reaction of SiH_2 with methylgermanes.[31,32] Sakurai *et al.* reported that SiMePh inserts into Ge-H bond of Et_3GeH to form the insertion product, $MePh(H)SiGeEt_3$;[33] Moiseev and Leigh reported that $SiPh_2$ inserts into Et_3Ge-H and Bu_3Sn-H to give the corresponding Ge-H and Sn-H insertions products.[26] Studies of the temperature dependence of the reactions of $SiMe_2$ with $MeSiH_3$, Me_2SiH_2 and Me_3SiH or GeH_2 with Et_3GeH in the gas phase revealed that all these reactions exhibit negative activation energies.[34,35] The two-step mechanism shown in Scheme 2.14 has been proposed to account for these results and is supported by theoretical calculations.[36-39] The reaction involves the initial formation of a weakly-bound H-bridged complex between the silylene (or germylene) and the metal hydride, followed by a slow rearrangement to give the final insertion product.

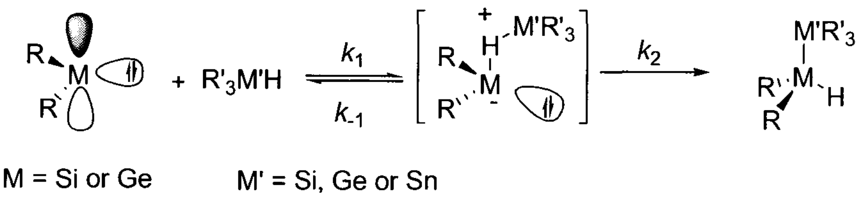

Scheme 2.14 Postulated mechanism for the reaction of MR_2 with R'_3M'-H.

$GeMe_2$ is markedly less reactive than $SiMe_2$ toward Et_3Si-H and Et_3Ge-H bonds, while they both react with n-Bu_3SnH at close to the diffusion limit in hexanes. Unexpectedly, $SiMe_2$ does not show a similar trend in reactivity as $GeMe_2$ toward these substrates. It is observed that the rate of reaction with Et_3Ge-H is slightly slower than that of Et_3SiH, and that with Bu_3SnH is only ca. 5 times faster.[26] A similar trend has also been reported for the reactions of $SiMe_2$ with Me_2GeH_2 and Me_2SiH_2 in the gas phase.[40] Quantum chemical calculations by Becerra *et al.* predicted that the lower reactivity of $SiMe_2$ with Ge-H bond as compared to Si-H is due to a higher activation energy barrier for the rearrangement of the initially formed complex (step 2) in the case of the Ge-H insertion reaction.[41,42]

2.8.3 Reactions of $GeMe_2$ with alkene, alkyne and diene

Addition of increasing amounts of DMB, isoprene and DMP resulted in an enhancement in the decay rates of $GeMe_2$ at 480 nm in all three cases. Figure 2.18a shows representative transient decay profiles recorded at 480 nm in the absence and presence of 0.12 mM DMB. It was reported that $GePh_2$ decays with bimodal kinetics, consisting of an initial fast decay, followed by a residual decay to a plateau in the presence of 0.2-3 mM of DMP and isoprene.[1] This type of transient behavior is indicative of a reversible reaction of the germylene (*vide infra*). Analogous behavior could not be detected for $GeMe_2$, mainly because of the larger equilibrium constant for the reaction with the scavenger and faster dimerization rate of $GeMe_2$. In all three cases, the residual absorptions were low enough such that the decays fit to simple first-order kinetics at all concentrations studied. The plots of k_{decay} versus [Q] were linear. Figure 2.18b shows representative plots for k_Q and K_{sv} determination for the reactions of $GeMe_2$ with DMB in hexanes.

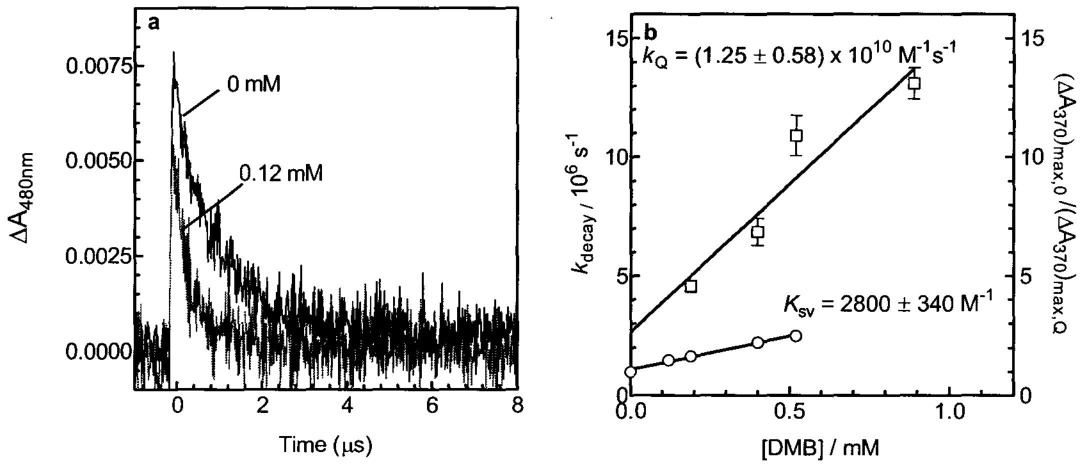

Figure 2.18. (a) Effects of added DMB on (a) transient decay profiles recorded at 480 nm by laser flash photolysis of **23** in deoxygenated hexanes; (b) Plots of pseudo-first-order rate constant (k_{decay}) of $GeMe_2$, monitored at 480 nm (□) and $(\Delta A_{370})_{max,0}/(\Delta A_{370})_{max,Q}$ (○) versus [DMB], showing linear least-squares fits of data to eqs (2.17) and (2.16), respectively.

Figure 2.19 shows some of the growth/decay profiles recorded at 370 nm on short and long time-scales in the presence of increasing DMB concentrations. A lengthening in the growth time of Ge_2Me_4 is observed with increasing concentrations of DMB. This transient behavior of the digermene is similar to that observed for Ge_2Ph_4 in the presence of isoprene and DMP under similar conditions, and is consistent with reversible scavenging of the germylene.[2] The K_{sv}/k_Q values obtained for these reactions are lower than those exhibited by "irreversible" reactions such as that with AcOH (see Table 2.1).

Ge_2Me_4 is formed on a longer time scale because it continues to be formed after equilibrium has been established. In spite of the fact that similar K_{sv}/k_Q values were observed for DMP and isoprene, no such lengthening in the growth time was observed in these two cases.

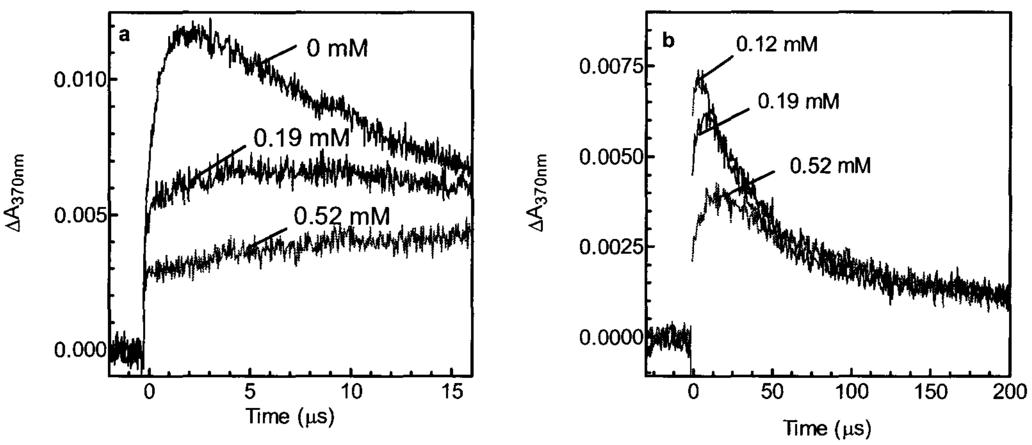

Figure 2.19. Effects of added DMB on the transient growth/decay profiles recorded at 370 nm by laser flash photolysis of **23** in deoxygenated hexanes (a) on shorter time scale and (b) on longer time scale.

K_{eq} values could not be determined for the reactions of $GeMe_2$ with isoprene, DMB and DMP; however, upper limits were estimated (based on eq (2.18)) by using the ΔA_0 and ΔA_{res} from decay profiles of $GeMe_2$ at the highest concentration where a hint of a plateau could be discerned.

$$K_{eq} = \frac{1}{[Q]}\left[\frac{\Delta A_0}{\Delta A_{res}} - 1\right] \qquad \textbf{(2.18)}$$

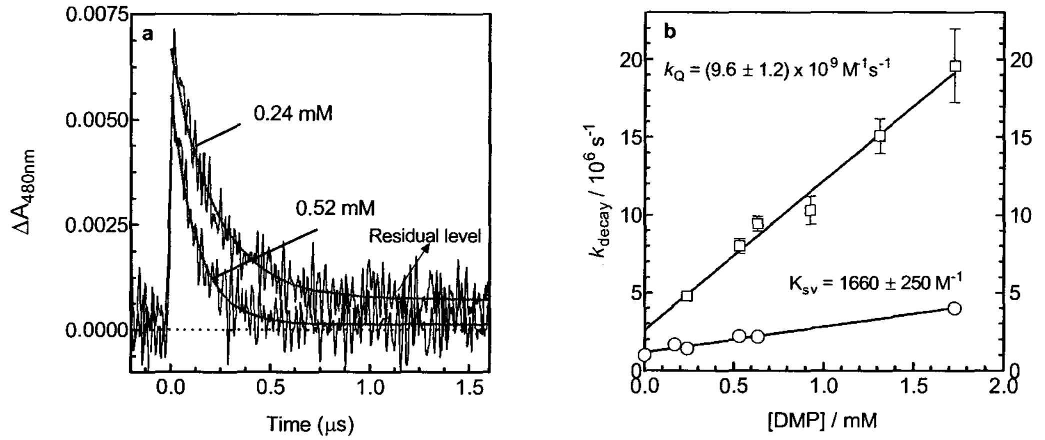

Figure 2.20. (a) Effects of added DMP on the transient decay profiles recorded at 480 nm by laser flash photolysis of **23**; (b) Plots of pseudo-first-order rate constant (k_{decay}) of $GeMe_2$, monitored at 480 nm (□) and $(\Delta A_{370})_{max,0}/(\Delta A_{370})_{max,Q}$ (○) versus [DMP], showing linear least-squares fits of data to eqs (2.17) and (2.16), respectively.

Leigh *et al.* reported that $GePh_2$ and GeMePh react with isoprene and DMP reversibly at close to the diffusion-controlled rate in hexanes.[2,25] Moreover, they reported the direct detection of new absorption bands assignable to the corresponding germacyclopropane or germacyclopropene derivatives.[2] The absorption maxima and lifetimes of the absorption bands assigned to these intermediates are given in Table 2.3. However, laser flash photolysis of **23** in the presence of 5 mM or 10 mM isoprene did not produce new transient absorption bands that could be attributed to the analogous primary products. This is most likely because they absorb at shorter wavelengths than can be monitored in our experiments (< 270 nm). In the presence of such isoprene concentrations neither $GeMe_2$ nor Ge_2Me_4 could be detected; however, the transient absorption band at 290 nm was still observed and exhibits a similar kinetic behavior as the 290 nm transient in the absence of the scavenger. These observations indicate that the same long-lived absorption at 290 nm is observed regardless of whether these scavengers are present or not.

Table 2.3. A comparison of the transient intermediates formed from the reactions of $GePh_2$[a] and GeMePh[b] with isoprene, DMP and TBE in hexanes

Reagent	Intermediate		R = Ph	R = Me, Ph
Isoprene	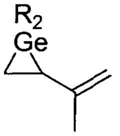	λ_{max} (nm)	285	285
		τ	500 ± 10 μs	0.67 ms
DMP	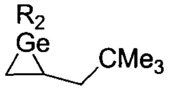	λ_{max} (nm)	~275	275
		τ	1.2 ± 0.1 ms	2.6 ms
TBE	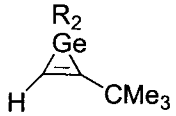	λ_{max} (nm)	~ 275	270
		τ	600 ms	> 2000 ms

From (a) Ref. 2; (b) Ref. 25.

The rate constants can be compared to those reported in earlier studies for the same reactions: the rate constants reported in cyclohexane for the reaction of "$GeMe_2$" with DMB at room temperature are in the range $k_Q = 1.7 - 2.4 \times 10^7$ $M^{-1}s^{-1}$,[30,43,44] while that with isoprene in cyclohexane is $k_Q = 1.63 \times 10^7$ $M^{-1}s^{-1}$.[30] None of these values are consistent with the ones determined in the present study. However, as we previously discussed, in these reports, different absorption bands were assigned to $GeMe_2$, indicating that these authors were not looking at the same transient species.

The value of $k_Q = (1.08 \pm 0.28) \times 10^{10}$ M^{-1}s^{-1}, determined for the reaction of the 470 nm species for **23** with isoprene is consistent with the rate constant of 1.1 x 10^{-11} cm^3 molecule^{-1}s^{-1} (6.6 x 10^9 M^{-1}s^{-1}) reported for the reaction of butadiene with $GeMe_2$ in the gas phase.[3] $GeMe_2$ was found to react with DMP with a rate constant of (9.6 ± 1.2) x 10^9 M^{-1}s^{-1} and this value is also comparable to that obtained by Becerra *et al.* for the reaction of $GeMe_2$ with 3,3-dimethylbut-1-ene in the gas phase, k_Q = 1.3 x 10^{-11} cm^3 molecule^{-1}s^{-1} (*ca.* 7.8 x 10^9 M^{-1}s^{-1}).[3]

In the presence of 3,3-dimethyl-1-butyne (TBE), it is observed that $GeMe_2$ decays with first-order kinetics to the pre-pulse level at all concentrations studied (up to 1.4 mM). This behavior is consistent with irreversible scavenging of $GeMe_2$. Figure 2.21a shows the transient decay profiles recorded in the presence of 0.06 mM and 0.13 mM. Moreover, the signals due to Ge_2Me_4 showed decreasing maximum intensities with increasing concentration of TBE and a lengthening in their growth time (Figure 2.21b). A plot of k_{decay} versus [TBE] is linear and affords a bimolecular rate constant, $k_{TBE} = (1.3 \pm 0.3) \times 10^{10}$ M^{-1} s^{-1} for the reaction (Figure 2.21c). This value is in good agreement with the rate constant reported in the gas phase for the reaction of $GeMe_2$ with acetylene, where k = 1.3 x 10^{-11} cm^3 molecule^{-1} s^{-1} (corresponding to k = 7.8 x 10^9 M^{-1} s^{-1} in solution).[3]

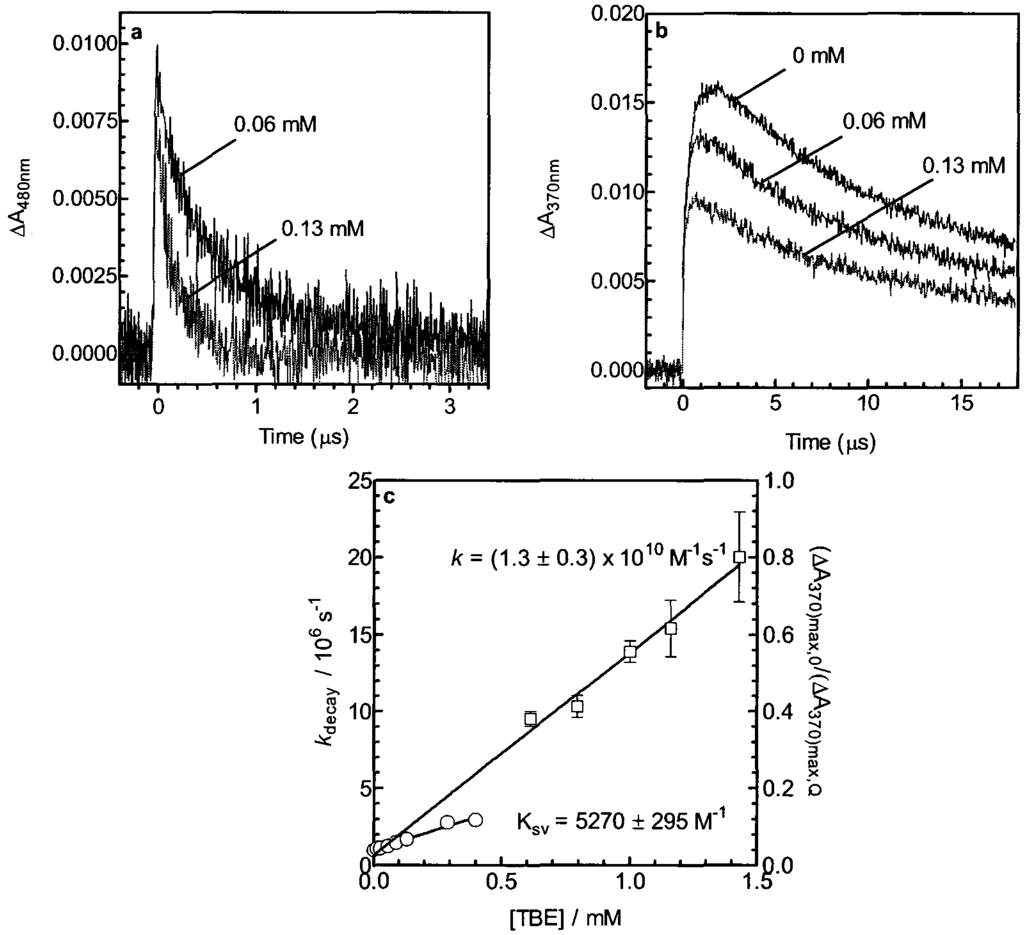

Figure 2.21. Effects of added TBE on the (a) transient decay profiles monitored at 480 nm and (b) transient growth/decay profiles monitored at 370 nm, and (c) plots of pseudo-first-order rate constant (k_{decay}) of $GeMe_2$, monitored at 480 nm (□) and $(\Delta A_{370})_{max,0}/(\Delta A_{370})_{max,Q}$ (○) versus [TBE], showing linear least-squares fits of data to eqs (2.17) and (2.16), respectively.

The rate and equilibrium constants determined for the reactions of $GeMe_2$ in this work, together with those determined for reaction of the same substrates for GeMePh,[25] $GePh_2$,[2] and $SiMe_2$[26] are given in Table 2.4. It can be observed that the rate constants for the reactions of the germylenes toward the alkene, alkyne and diene studied increase in the order $GePh_2$ < GeMePh < $GeMe_2$. The rate constants obtained for the reactions of $GeMe_2$ are roughly twice higher than those determined for $GePh_2$. Moreover, the estimated equilibrium constants for the reactions of $GeMe_2$ with DMP and isoprene ($K_{eq} \sim 20\ 000\ M^{-1}$) are markedly higher than those determined for $GePh_2$ (see Table 2.4). These results indicate that $GeMe_2$ forms thermodynamically more stable primary products than does $GePh_2$. The rate constants for the reactions of $SiMe_2$ are considerably larger than those of $GeMe_2$ under the same set of conditions. In addition, while the reactions of $GeMe_2$ are reversible with DMP, DMB and isoprene, those of $SiMe_2$ are irreversible. This is indicative of higher exothermicities of the reactions of $SiMe_2$ with these reagents as compared to $GeMe_2$, consistent with theoretical predictions.[45,46]

Table 2.4. Comparison of bimolecular rate constants, k_Q (10^9 $M^{-1}s^{-1}$) and equilibrium constants, K_{eq} (M^{-1}) for the reactions of $GeMe_2$, $GePh_2$ and $SiMe_2$ with alkene, diene and alkyne in hexanes at 23-25 °C

Reagent		**$GeMe_2$**[a]	**GeMePh**[b]	**$GePh_2$**[c]	**$SiMe_2$**[d]
			k_Q (10^9 $M^{-1}s^{-1}$)		
Isoprene	k_Q	10.8 ± 2.8	8.0 ± 0.9	5.5 ± 1.2	19.8 ± 0.7
	K_{eq}(M^{-1})	> 20 000	12000-15000	6000 ± 2500	Irreversible
DMB	k_Q	12.5 ± 5.8	4 ± 2	≥ 5 x 10^9	15.9 ± 0.7
	K_{eq}(M^{-1})	> 20 000	< 1000	< 1000	Irreversible
DMP	k_Q	9.6 ± 1.2	5.1 ± 0.7	4.2 ± 0.2	11.7 ± 0.5
	K_{eq}(M^{-1})	> 20 000	4000-8000	2 500 ± 600	Irreversible
TBE	k_Q	13 ± 3	5.9 ± 0.4	5.18 ± 0.47	17.8 ± 0.6
	K_{eq}(M^{-1})	Irreversible (K_{eq} > 100 000)	Irreversible	Irreversible	Irreversible

(a) This work; (b) Ref. 25; (c) Ref. 2; (d) Ref. 26.

2.8.4 Reaction with amines

Germylenes are known to react with amines to form Lewis acid-base complexes in low temperature matrixes and in solution.[1,2,25,47] Moreover, kinetic studies performed in our group revealed that $GePh_2$ and GePhMe react reversibly with n-$BuNH_2$ and Et_3N in hexanes.[2,25] In all cases, the corresponding equilibrium constants are too large to be measured by laser flash photolysis methods, i.e. their values are in excess of ca. 25 000 M^{-1} in hexanes at 25 °C. Product studies for the reaction of $GePh_2$ with n-$BuNH_2$ afforded mostly oligo-or polymeric material, and a small amount of nitrogen-containing product which was tentatively assigned to the N-H insertion product (Scheme 2.15).[1]

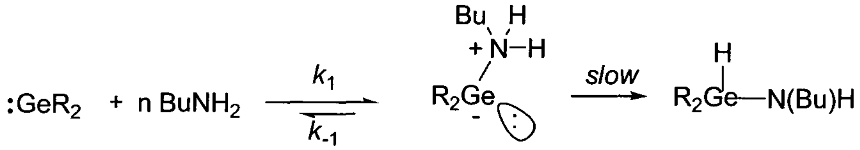

Scheme 2.15 Postulated mechanism for the reaction of GeR_2 with a primary or secondary amine; for e.g. n-$BuNH_2$.

We observed that increasing concentrations of n-$BuNH_2$ or Et_3N led to an increase in the decay rates of the $GeMe_2$ absorption. In both cases, the signal decays to baseline with first-order kinetics, and plots of k_{decay} versus [amine] are linear. A decrease in the maximum intensity of the signals due to Ge_2Me_4 was also observed, and in the case of n-$BuNH_2$, this was accompanied by a slight lengthening of the growth time of the signal. As mentioned earlier, the latter behavior is indicative of reversible scavenging and is comparable to that observed for $GePh_2$ and GeMePh in the presence of Et_3N.[2] Figure 2.22 shows transient growth/decay profiles recorded at 480 nm and 370 nm by laser flash photolysis of **23** in the presence of increasing concentrations of n-$BuNH_2$ in hexanes. No residual absorptions were observed in the $GeMe_2$ decay profiles, consistent with an equilibrium constant (K_{eq}) for the reaction that exceeds 25 000 M^{-1}, the approximate upper limit at which we can detect effects of reversibility on the germylene decay profiles.[2] The k_Q values obtained show that $GeMe_2$ reacts with both Et_3N and n-$BuNH_2$ at close to the diffusion-controlled rate in hexanes at 25 °C.

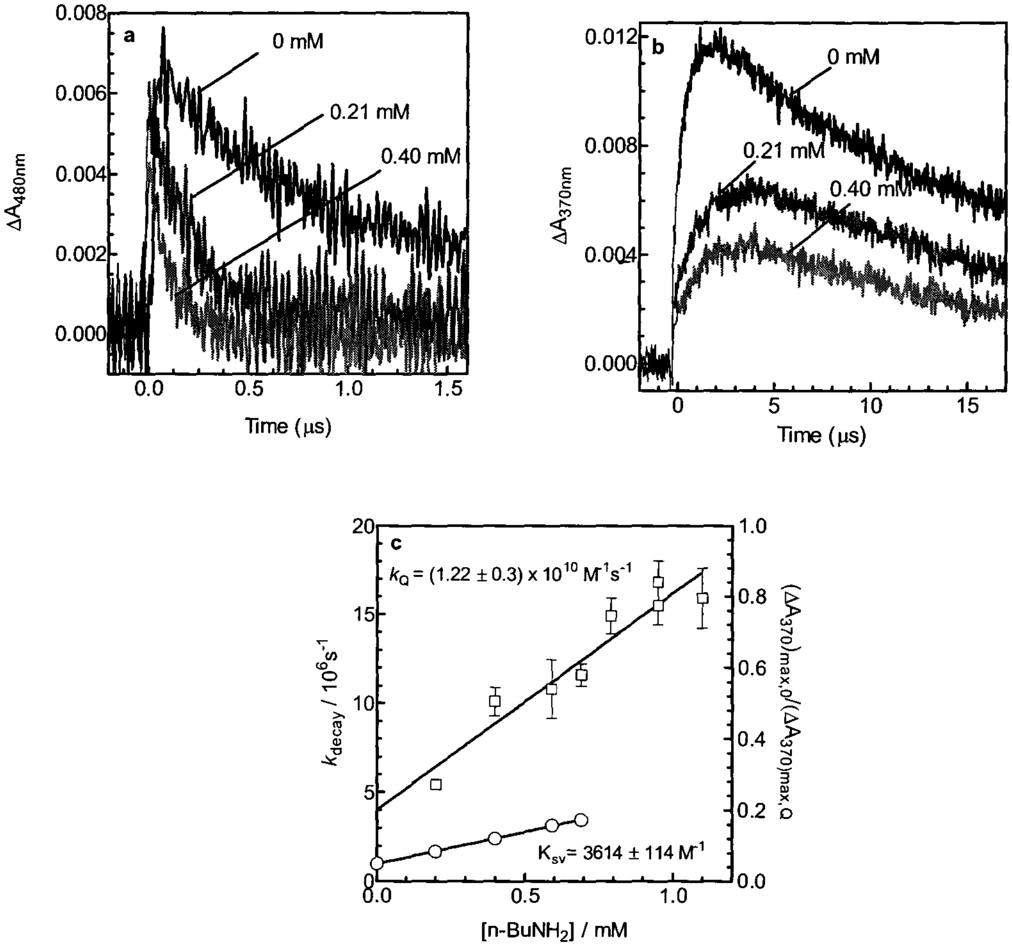

Figure 2.22. Effects of added n-BuNH$_2$ on the (a) transient decay profiles of GeMe$_2$ at 480 nm and (b) transient growth/decay profiles of Ge$_2$Me$_4$ at 370 nm, and (c) plots of the pseudo-first-order decay rate constant (k_{decay}) of GeMe$_2$, monitored at 480 nm (□) and $(\Delta A_{370})_{max,0}/(\Delta A_{370})_{max,Q}$ (○) versus [n-BuNH$_2$], showing linear least-squares fits of data to eqs (2.17) and (2.16), respectively.

A transient absorption spectrum recorded by laser flash photolysis of **23** in the presence of 2 mM of Et_3N showed no indication of new transient absorption bands assignable to the Me_2Ge-NEt_3 complex, most likely because the species exhibits an absorption maximum at shorter wavelengths than can be monitored in our experiments (< 270 nm). Indeed, Levin *et al.* reported that the Me_2Si-NEt_3 complex absorbs at ≤ 270 nm.[48] We did observe strong absorptions at ca. 290 nm which are formed with the laser pulse, and decayed with a lifetime $\tau \sim 2$ μs; however, these are due to the competing photolysis of the amine.[2]

2.8.5 Reaction with carbon tetrachloride

Quenching of $GeMe_2$ with CCl_4 in hexanes afforded a rate constant of $(8 \pm 2) \times 10^7$ $M^{-1}s^{-1}$ (Figure 2.23). Absolute rate constants assigned to the reaction of "$GeMe_2$" with CCl_4 have been reported by several authors in the literature. For example, Mochida *et al.* reported rate constants of 4.9×10^8 $M^{-1}s^{-1}$ and 7.3×10^8 $M^{-1}s^{-1}$ for the same reaction in cyclohexane using dodecamethylcyclohexagermane and decamethylcyclopentagermane as $GeMe_2$ precursors, respectively;[44,49] Bobbitt *et al.* reported a rate constant of 3.2×10^8 $M^{-1}s^{-1}$, using $PhMe_2GeSiMe_3$ as a precursor to $GeMe_2$ in cyclohexane.[30] The rate constant determined in the present work does not match any of the earlier reported values, again indicating that the species assigned to $GeMe_2$ in the early reports are different from that obtained from **23** and **24**.

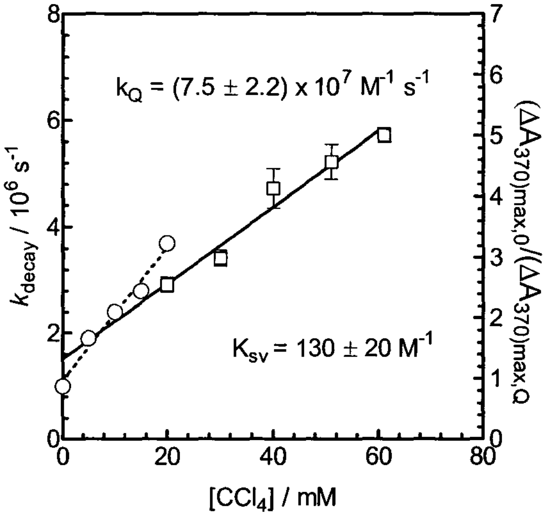

Figure 2.23. Effects of added CCl_4 on the pseudo-first-order decay rate constants of $GeMe_2$ (□), monitored at 480 nm, and on the maximum signal intensity (○) of Ge_2Me_4, monitored at 370 nm. The solid lines are the linear least-squares fits to eq (2.17) and eq (2.16), respectively.

It was reported that the generation of $GeMe_2$ in the presence of CCl_4 in hydrocarbon solvent yields Me_2GeCl_2 and C_2Cl_6 as the major products.[50,51] Based on these results and CIDNP experiments, a two-step radical abstraction-recombination mechanism has been proposed, as shown in Scheme 2.15.[50,52] Interestingly, several $GeMe_2$ or diarylgermylene complexes with chlorocyclohexane or chlorobenzene have been detected in matrixes at 77 K; these observations suggest that the mechanism of these reactions proceeds through initial Lewis acid-base complexation.[47] In the present study, no new transients attributable to $GeMe_2$-CCl_4 complexes could be detected, and to the best of our knowledge there are no reports of the detection of germylene-halocarbon complexes in solution at room temperature. The rate constant for the reaction of $GeMe_2$ with CCl_4 is roughly one order of magnitude higher than that exhibited by $GePh_2$ (k_{CCl4} = (1.09 ± 4) x 10^7 $M^{-1}s^{-1}$).[2]

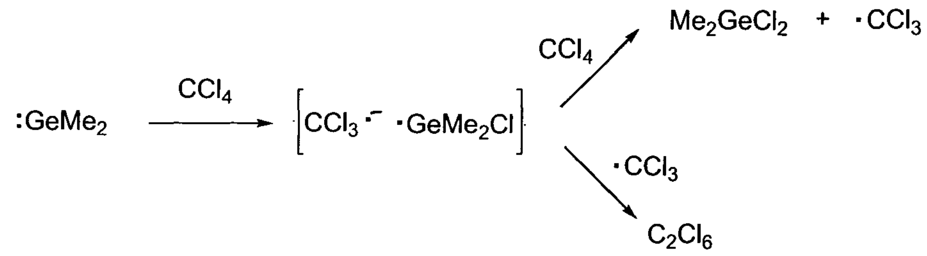

Scheme 2.16 Postulated mechanism for the reaction of $GeMe_2$ with CCl_4.

2.8.6 Reaction with oxygen

Laser flash photolysis of **23** was performed in air and oxygen-saturated hexanes. A bimolecular rate constant, k_{O2} = (9.0 ± 1.2) x 10^7 $M^{-1}s^{-1}$ was estimated from the difference between the pseudo-first-order decay rate constants of $GeMe_2$ in oxygen- and air-saturated hexanes ($[O_2]$ in oxygen-saturated hexanes is 0.0151 M at 25 °C[53]). The rate constant determined for $GeMe_2$ is roughly 50 times less than that reported for the reaction of $SiMe_2$ with O_2 (k = (4.7 ± 0.4) x 10^8 $M^{-1}s^{-1}$).[26] The reactions of germylenes with oxygen have not been studied mechanistically. However, based on product studies it is suggested that germylenes react with oxygen to form the corresponding germanones, which then further react to form dioxadigermetane rings (eq 2.19).[54] No direct evidence for the formation of germanones from these reactions has been reported so far.

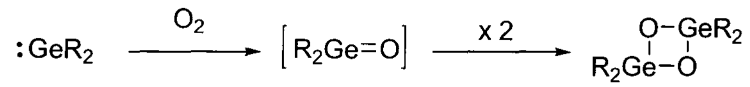

(2.19)

2.9 Summary and Conclusions

Steady state photolysis of 1,1-dimethyl-3-phenylgermacyclopent-3-ene (**23**) or 1,1,1-trimethyl-3-phenylgermacyclopent-3-ene (**24**) in cyclohexane in the presence of AcOH, DMB or methanol yields the expected $GeMe_2$-trapping products along with the extruded diene as the only products. The quantum yield for the extrusion of $GeMe_2$ from **23** was determined to be $\Phi = 0.55 \pm 0.09$. Transient absorption spectra recorded by laser flash photolysis of **23** and **24** in deoxygenated hexanes exhibit a UV/Vis absorption band centered at 470 nm, which has been assigned to $GeMe_2$. In the absence of added substrates, this species decays with second-order kinetics with concomitant formation of a second transient with absorption centered at 370 nm, which is assigned to Ge_2Me_4. The extinction coefficient of $GeMe_2$ at its maximum absorption was determined to be $\varepsilon = 730 \pm 300$ dm^3 mol^{-1} cm^{-1}.

Our kinetic studies show that most of the reactions of $GeMe_2$ that have been studied proceed at close to the diffusion-controlled rate in hexanes. The reactions of $GeMe_2$ with AcOH, 3,3-dimethyl-1-butyne, CCl_4, group 14 metal hydrides (Et_3SiH, Et_3GeH and nBu_3SnH) are irreversible, while those with amines (Et_3N and n-$BuNH_2$), 4,4-dimethyl-1-pentene, and dienes (isoprene and 2,3-dimethylbuta-1,3-diene) were found to be reversible, with equilibrium constants of $K_{eq} \sim 20\ 000$ M^{-1}. The rate constants determined in the present work are in agreement with the ones reported in the gas phase for the same or similar set of scavengers (Table 2.5).

Table 2.5. Rate constants for the reactions of $GeMe_2$ in deoxygenated hexanes and the gas phase at 298 K[a]

Scavenger	**$GeMe_2$ (solution)**	**$GeMe_2$ (gas phase)**
	$k_Q / 10^9\ M^{-1}s^{-1}$	
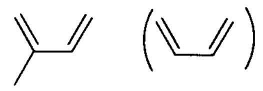	10.9	6.6
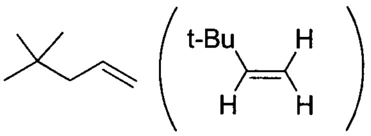	8.9	7.8
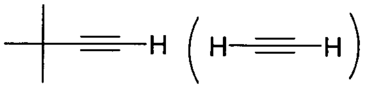	10.8	7.8
O_2	0.09	0.027
Et_3SiH (Me_3SiH)	0.00055	< 0.0036
Et_3GeH (Me_3GeH)	0.05	< 0.024

a- gas phase rate constants were reported in $cm^3 molecule^{-1}s^{-1}$ but have been converted to molar units to facilitate comparison.[3] These rate constants were determined at 100 Torr (SF_6). The scavengers studied in gas phase experiments are given in parentheses when different from that studied in solution.

The rate constants for the reactions of $GeMe_2$ follow the same trends as those of GeMePh and $GePh_2$ with the same scavengers. However, in all cases, they are found to be higher than those of the phenylated analogues. Overall, the reactivity of GeMePh lies between those of $GeMe_2$ and $GePh_2$, as might be expected. The K_{eq} for the reactions of $GeMe_2$ with 4,4-dimethyl-1-pentene, 2,3-dimethyl-1,3-butadiene and isoprene are higher than that of GeMePh and $GePh_2$. Therefore, we conclude that $GeMe_2$ generally forms more stable primary reaction products than the phenylated germylenes. It is interesting to note that in most cases the reactivity of $GeMe_2$ parallels that of $SiMe_2$, with those for the germylene being slightly lower. The same trend is evident in the equilibrium constants for the reactions of the two species with 4,4-dimethyl-1-pentene, 3,3-dimethyl-1-butyne and diene (isoprene and 2,3-dimethylbuta-1,3-diene), consistent with the indication from theory that germylenes are of greater thermodynamic stability than silylenes of otherwise identical structures.

References

1. Leigh, W. J.; Harrington, C. R.; Vargas-Baca, I. *J. Am. Chem. Soc.* **2004**, *126*, 16105.
2. Leigh, W. J. and Harrington, C. R. *J. Am. Chem. Soc.* **2005**, *127*, 5084.
3. Becerra, R.; Boganov, S. E.; Egorov, M. P.; Lee, V.; Nefedov, O. M.; Walsh, R. *Chem. Phys. Lett.* **1996**, *250*, 111.
4. Jiang, P. and Gaspar, P. P. *J. Am. Chem. Soc.* **2001**, *123*, 8622.
5. Mazerolles, P. and Manuel, G. *Bull. Soc. Chim. Fr.* **1965**, *56*, 327.
6. Brown, P. A.; Bonnert, R. V.; Jenkins, P. R.; Lawrence, N. J.; Selim, M. R. *J. Chem. Soc., Perkin Trans I.* **1991**, 1893.
7. Barker, G. K.; Drake, J. E.; Hemmings, R. T. *Can. J. Chem.* **1974**, 2622.
8. Klein, B.; Neumann, W. P.; Weisbeck, M. P.; Weinken, S. *J. Organomet. Chem.* **1993**, *446*, 149.
9. Toltl, N. P.; Stradiotto, M. J.; Morkin, T. L.; Leigh, W. J. *Organometallics* **1999**, *18*, 5643.
10. Becerra, R.; Egorov, M. P.; Krylova, I. V.; Nefedov, O. M.; Walsh, R. *Chem. Phys. Lett.* **2002**, *351*, 47.
11. Mochida, K.; Kayamori, T.; Wakasa, M.; Hayashi, H.; Egorov, M. P. *Organometallics* **2000**, *19*, 3379.
12. Carmichael I.; Hug, G. L. In *CRC handbook of organic photochemistry, Vol. I*; CRC Press: Boca Raton, 1989; Chapter 16, pp. 369-404.

13. Carmichael, I. and Hug, G. L. *J. Phys. Chem. Ref. Data* **1986**, *15*, 1.
14. Carmichael, I.; Helman, W. P.; Hug, G. L. *J. Phys. Chem. Ref. Data* **1987**, *16*, 239.
15. Debye, P. *Trans. Electrochem. Soc.* **1942**, 265.
16. Murov, S. L.; Carmichael, I.; Hug, G. L. In *Handbook of photochemistry*, 2 ed.; Dekker: New York, 1993.
17. Leigh, W. J. and Sluggett, G. W. *J. Am. Chem. Soc.* **1994**, *116*, 10458.
18. Leigh, W. J.; Toltl, N. P.; Apodaca, P.; Castruiti, M.; Pannell, K. H. *Organometallics* **2000**, *19*, 3232.
19. Morkin, T. L. and Leigh, W. J. *Acc. Chem. Res.* **2001**, *34*, 129.
20. Leigh, W. J. and Li, X. *Organometallics* **2002**, *21*, 1197.
21. Leigh, W. J. and Li, X. *J. Phys. Chem.* **2003**, *107*, 1517.
22. Harrington, C. R.; Leigh, W. J.; Chan, B. K.; Gaspar, P. P.; Zhou, D. *Can. J. Chem.* **2005**, *83*, 1324.
23. Fujii, Y.; Yamada, H.; Mizuta, M. *J. Phys. Chem.* **1988**, *92*, 6768.
24. Huck, L. A. and Leigh, W. J. *Organometallics* **2007**, *26*, 1339.
25. Leigh, W. J.; Dumbrava, I.; Lollmahomed F.B. *Can. J. Chem.* **2006**, *84*, 934.
26. Moiseev, A. G. and Leigh, W. J. *Organometallics* **2007**, *26*, 6277.
27. Kanabus-Kaminska, J. M.; Hawari, J. A.; Griller, D.; Chatgilialoglu, C. *J. Am. Chem. Soc.* **1987**, *109*, 5267.
28. Clark, K. B. and Griller, D. *Organometallics* **1991**, *10*, 746.

29. Burkey, T. J.; Majewski, M.; Griller, D. *J. Am. Chem. Soc.* **1986**, *108*, 2218.
30. Bobbitt, K. L.; Maloney, V. M.; Gaspar, P. P. *Organometallics* **1991**, *10*, 2772.
31. Sefcik, M. D. and Ring, M. A. *J. Am. Chem. Soc.* **1973**, 5168.
32. Sefcik, M. D. and Ring, M. A. *J. Organomet. Chem.* **1973**, *59*, 167.
33. Sakurai, H.; Kobayashi, Y.; Nakadaira, Y. *J. Organomet. Chem.* **1976**, *120*, C1-C5.
34. Baggott, J. E.; Blitz, M. A.; Frey, H. M.; Walsh, R. *J. Am. Chem. Soc.* **1990**, *112*, 8337.
35. Becerra, R.; Boganov, S. E.; Egorov, M. P.; Nefedov, O. M.; Walsh, R. *Mendeleev Commun.* **1997**, *7*, 87.
36. Becerra, R.; Carpenter, I. W.; Gordon, M. S.; Rostop, L.; Walsh, R. *J. Phys. Chem. Chem. Phys.* **2007**, 2121.
37. Becerra, R.; Boganov, S. E.; Egorov, M. G.; Faustov, V. I.; Nefedov, O. M.; Walsh, R. *J. Am. Chem. Soc.* **1998**, *120*, 12657.
38. Su, M.-D. and Chu, S. *J. Phys. Chem. A.* **1999**, *103*, 11011.
39. Becerra, R. and Walsh, R. *Res. Chem. Kinet.* **1995**, *3*, 263.
40. Becerra, R.; Boganov, S. E.; Egorov, M. P.; Faustov, V. I.; Krylova, I. V.; Nefedov, O. M.; Promyslov, V. M.; Walsh, R. *Phys. Chem. Chem. Phys.* **2007**, *9*, 4395.
41. Becerra, R.; Boganov, S. E.; Egorov, M. P.; Faustov, V. I.; Krylova, I. V.; Nefedov, O. M.; Promyslov, V. M.; Walsh, R. *J. Phys. Chem. A.* **2008**, *112*, 849.
42. Becerra, R. and Walsh, R. *Phys. Chem. Chem. Phys.* **2007**, *9*, 2817.

43. Mochida, K.; Yoneda, I.; Wakasa, M. *J. Organomet. Chem.* **1990**, *399*, 53.

44. Mochida, K.; Kanno, N.; Kato, R.; Kotani, M.; Yamauchi, S.; Wakasa, M.; Hayashi, H. *J. Organomet. Chem.* **1991**, *415*, 191.

45. Horner, D. A.; Grev, R. S.; Schaefer, H. F. *J. Am. Chem. Soc.* **1992**, *114*, 2093.

46. Su, M.-D. *Chem. Eur. J.* **2004**, *10*, 6073.

47. Ando, W.; Itoh, H.; Tsumuraya, T. *Organometallics* **1989**, *8*, 2759.

48. Levin, G.; Das, P. K.; Bilgrien, C.; Lee, C. L. *Organometallics* **1989**, *8*, 1206.

49. Mochida, K. and Tokura, S. *Bull. Chem. Soc. Jpn.* **1992**, *65*, 1642.

50. Köcher, J.; Lehnig, M.; Neumann, W. P. *Organometallics* **1988**, *7*, 1201.

51. Adachi, M.; Mochida, K.; Wakasa, M.; Hayashi, H. *Main Group Met. Chem.* **1999**, *22*, 227.

52. Köcher, J. and Lehnig, M. *Organometallics* **1984**, *3*, 937.

53. Battino, R.; Rettich, T. R.; Tominaga, T. J. *J. Phys. Chem. Ref. Data* **1983**, *12*, 163.

54. Tokitoh, N.; Kishikawa, K.; Okazaki, R.; Sasamori, T.; Nakata, N.; Takeda, N. *Polyhedron* **2002**, *21*, 563.

CHAPTER 3

Reinvestigation of some dimethylgermylene precursors in solution by laser flash photolysis

3.1 Introduction

Time-resolved UV-Vis absorption spectroscopy has been the most widely used method in the study of transient germylenes and a great deal of information about the kinetics of their reactions has been obtained using this method. However, one major disadvantage of this method is that the absorption bands are usually broad and featureless, and in any event the UV-Vis spectrum affords only an extremely limited amount of structural information on the transient molecule in question. This may become problematic especially in cases where two or more transients are formed in the photochemical reaction employed for the transient production. Often several transient species display absorption bands in similar spectral range and thus in these cases the identification of the transient species of interest can be ambiguous.

As mentioned in Chapter 1, "$GeMe_2$" (the quotation marks are used to refer to all the transient species assigned to $GeMe_2$ prior to the work performed by Leigh *et al.* in 2004[1]) is the most widely explored transient germylene in solution. Prior to our work, the absorption spectrum of $GeMe_2$ in solution was not established, as evident from the fact that its reported absorption maximum varies between 370-490 nm.[2] The assignments of "$GeMe_2$" in solution, in most of these cases, have been based on comparisons of the UV-

Vis absorption spectrum to that obtained in low temperature matrixes, the identities of trapping products obtained from the photochemical decomposition of the precursors in the absence and presence of germylene scavengers, and kinetic studies of some of its reactions. The latter also show marked inconsistencies from study to study.

Driven by the transient UV-Vis absorption spectroscopic and kinetic studies discussed in Chapter 2, we decided to reinvestigate the photochemistry of dodecamethylcyclohexagermane **14** and dimethylphenyl(trimethylsilyl)germane **18**. The reported product studies from photolysis of **14** showed evidence for $GeMe_2$ trapping products.[3] However, the transient UV-Vis spectrum and kinetic behavior of the species observed in laser flash photolysis of the compound, and assigned to $GeMe_2$ are in marked disagreement with our data. On the other hand, product studies from the photolysis of compound **18** showed that though $GeMe_2$ is formed as the major transient species, its formation is accompanied by the formation of a conjugated germene (*vide infra*). Details about the reported photochemical and UV-Vis spectroscopic studies of compounds **14** and **18** are given below.

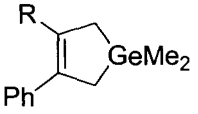

23 R = H
24 R = Me

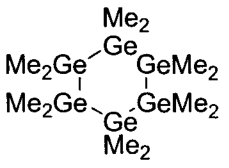

14

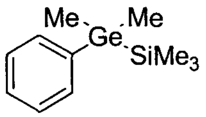

18

Mochida *et al.* reported that laser flash photolysis of dodecamethylcyclohexagermane (**14**) in deoxygenated cyclohexane resulted in the formation of a transient species with λ_{max} = 450 nm, which they assigned to $GeMe_2$.[3] They observed that the transient species decayed with second-order kinetics ($k/\varepsilon = 2.7 \times 10^7$ cm s^{-1}) to form a second transient species with λ_{max} = 370 nm, which in turn decays with second-order kinetics ($k/\varepsilon = 3.9 \times 10^6$ cm s^{-1}). The latter transient was assigned, probably correctly, to Ge_2Me_4. Photolysis of **14** in degassed cyclohexane containing 2,3-dimethylbuta-1,3-diene (DMB, 0.28 M) afforded 1,1,3,3-tetramethyl-1-germacyclopent-3-ene in 12 % yield, while in the presence of CCl_4 (0.28 M), dimethyldichlorogermane was formed in 41 % yield (see eq 3.1). However, they failed to detect methoxydimethylgermane as a product of photolysis of **14** in the presence of methanol in cyclohexane. We speculate that due to the high propensity of compounds of this type to decompose by α-elimination, the product most likely did not survive their analytical methods (GLC and GC-MS).[4]

In 1972, Carberry, Dombek and Cohen reported that irradiation of **14** in nitrogen-saturated cyclohexane with a low-pressure mercury lamp (254 nm) afforded decamethylcyclopentagermane **15** in 65 % yield along with a small amount of polydimethylgermane.[5] In another publication, Mochida *et al.* reported that photolysis of **15** under similar conditions also afforded $GeMe_2$.[6] However, steady state photolysis of **15** in the presence of DMB and CCl_4 yielded only a trace amount of 1,1,3,3-tetramethylgermacyclopent-3-ene (**7**) and 21 % of dimethyldichlorogermane, respectively (see eq 3.2). A completely different transient UV-Vis spectrum, with an absorption maximum (λ_{max}) of 490 nm, was assigned to $GeMe_2$. The authors did not comment on the discrepancies in their results for the two compounds. Figures 3.1a and 3.1b show the transient absorption spectra reported in the early laser flash photolysis studies of Ge_6Me_{12} and Ge_5Me_{10}, respectively in degassed cyclohexane.[3,6]

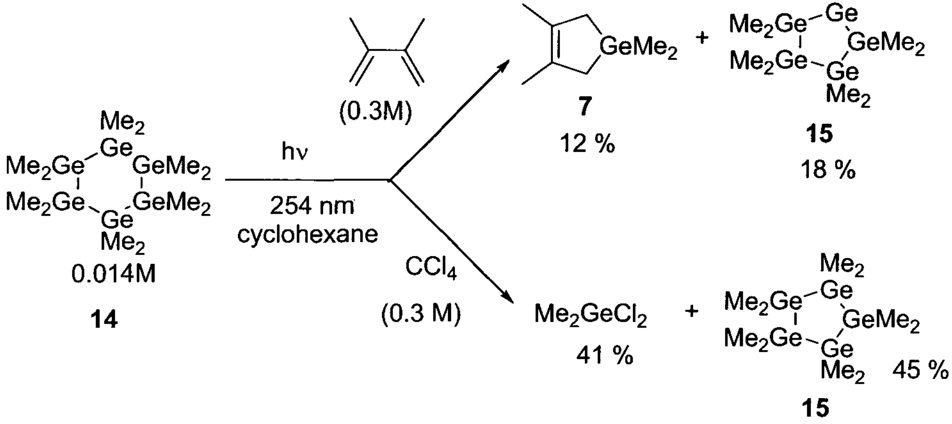

(3.1)

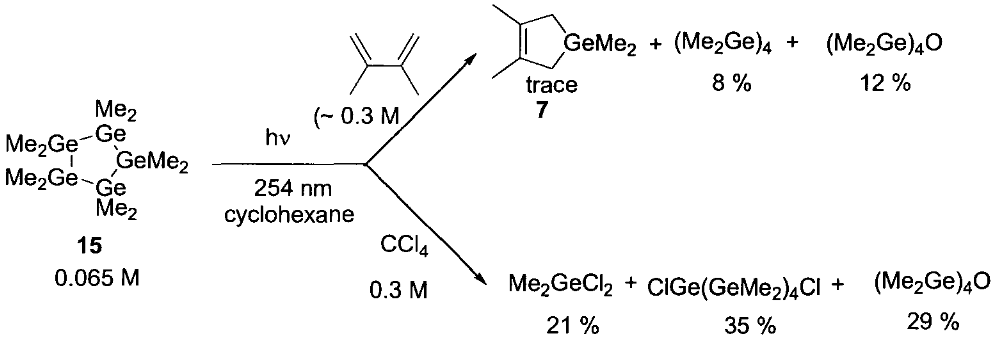

(3.2)

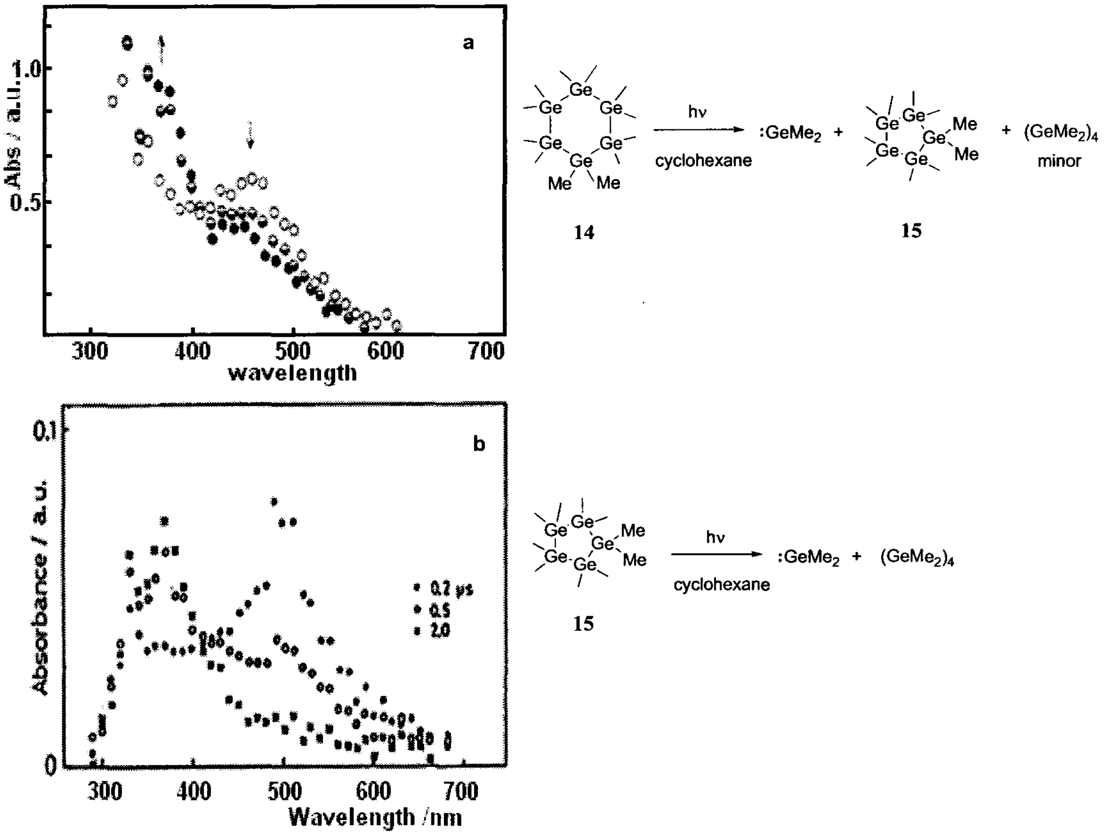

Figure 3.1. Transient absorption spectra recorded by laser flash photolysis of: (a) cyclo-Ge_6Me_{12} (**14**) in cyclohexane at 293 K, recorded (○) 0.2 μs, (◉) 1 μs and (•) 2 μs after the laser pulse. Reproduced with permission from Ref. 3. Copyright 1991, Elsevier Sequoia S.A. (b) cyclo-Ge_5Me_{10} (**15**) in cyclohexane at 293 K recorded (•) 0.2 μs, (□) 0.5 μs and (■) 2 μs after the laser pulse. Reproduced with permission from Ref. 6. Copyright 1992, The Chemical Society of Japan.

Bobbitt *et al.* reported that 254 nm photolysis of **18** in pentane containing 2,3-dimethylbuta-1,3-diene as scavenger afforded **7** (the $GeMe_2$ trapping product) in 55-78 % yield and ene adduct **39** (the 1,3,5-(1-germa)hexatriene **38** trapping product) in 20-28 % yield (Scheme 3.1).[7] The 1,3,5-(1-germa)hexatriene **38** is formed by formal 1,3-silyl migration to the aromatic ring. Laser flash photolysis of **18** (1.05×10^{-3} M) in degassed cyclohexane led to the formation of a transient exhibiting $\lambda_{max} = 425$ nm, which was assigned to $GeMe_2$ based on comparison of the rate constants for its reactions with various scavengers in cyclohexane at room temperature, and by comparison with previously reported spectral data for other $GeMe_2$ precursors in low temperature matrixes. The transient absorption spectrum reported is shown in Figure 3.2. No mention of the expected transient spectral characteristics of **38** was made. The alternate possible assignment of the 425 nm species to germahexatriene **38** was evidently not considered.

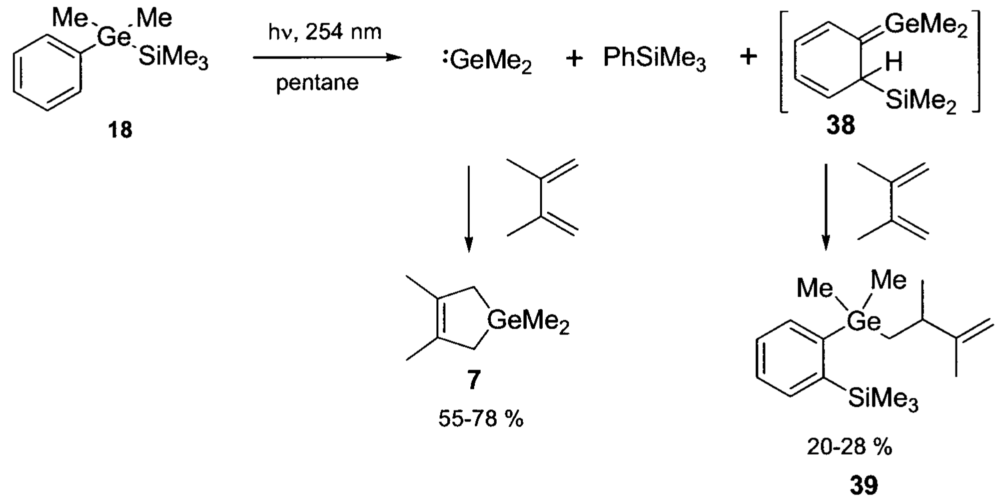

Scheme 3.1 Photolysis of **18** in the presence of DMB.[7]

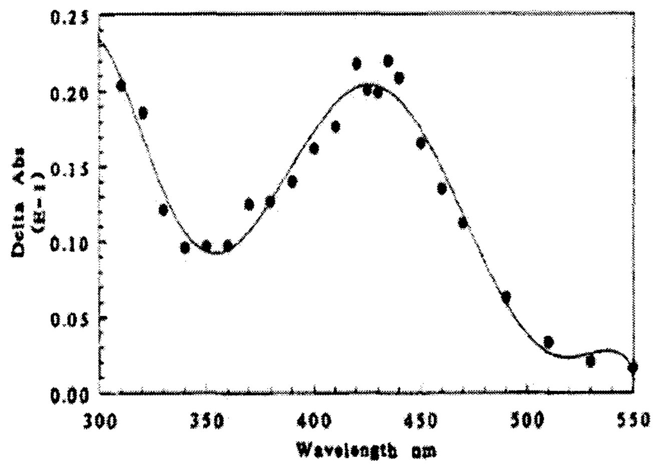

Figure 3.2. Transient absorption spectrum recorded by laser flash photolysis of **18** in degassed cyclohexane recorded 0-5 μs after the laser pulse. Reproduced with permission from Ref. 7. Copyright 1991, American Chemical Society.

In a similar study, Mochida *et al.* reported that irradiation of a solution of **18** (ca. 0.1 M) in cyclohexane containing CCl_4, methanol or DMB afforded products consistent with the formation of dimethylphenylgermyl radical, $GeMe_2$ and the 1,3,5-(1-germa)hexatriene derivative **38**.[8] The products were separated by preparative GLC. These results and product yields are summarized in Scheme 3.2. Laser flash photolysis of **18** in degassed cyclohexane was also performed. These authors reported the observation of two transients with absorption bands centered at 320 nm and 430 nm. The transient at 320 nm was assigned to the dimethylphenylgermyl radical based on the reported transient absorption spectra of other germanium-centered radicals,[9] while that at 430 nm was assigned to $GeMe_2$.[10]

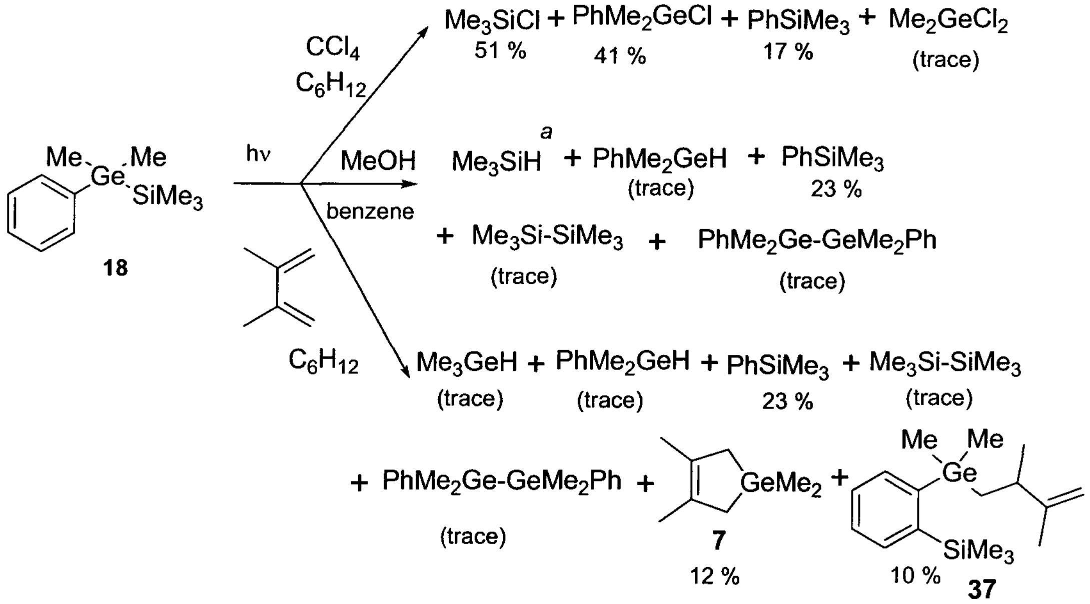

a - yield could not be determined

Scheme 3.2 Photolysis of **18** in the presence of CCl_4, MeOH and DMB.[8]

These assignments cannot be correct; $GeMe_2$ is claimed to be the major transient species formed from photolysis of **18**, and yet the transient absorption spectrum reported does not agree with the one reported by us in Chapter 2. Leigh *et al.* suggested that the transient species at 425-430 nm assigned to $GeMe_2$ by these authors is more reasonably assigned to the 1,3,5-(1-germa)hexatriene derivative **38** based on what they knew at the time of the behavior of the corresponding Si derivatives and of the differences in the reactivity of Ge=C and Si=C bonds.[11]

In this Chapter, we present a reinvestigation of the photochemistry of **14** and **18** using the same experimental conditions and setup used for the UV-Vis spectroscopic and kinetic studies of germacyclopent-3-ene precursors **23** and **24**. The aim was to understand the inconsistencies surrounding the photochemistry of these two compounds, using our acquired knowledge of $GeMe_2$, and to identify the transient species which are produced in the laser flash photolysis experiments.

3.2 Laser flash photolysis studies of dodecamethylcyclohexagermane (14)

3.2.1 Synthesis of 14

Compound **14** was synthesized by the method reported of Carberry *et al.*[5] Dichlorodimethylgermane was added dropwise to finely cut lithium wire in anhydrous THF at room temperature and the solution was stirred for a total of 4 hours. The crude product consisted of a mixture of **14**, **15** and other polygermanes, as determined by ^1H NMR spectroscopy. The desired product (**14**) was obtained in ≥ 96% purity, contaminated with ca. 4% of decamethylcyclopentagermane as determined by ^1H NMR spectroscopy and GC/MS, after purification by column chromatography followed by repeated recrystallizations from acetone. The overall yield of **14** varied between 6 and 18 %.

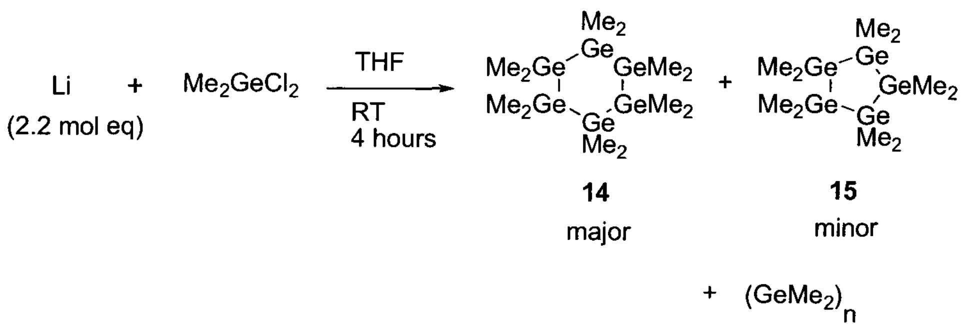

(3.3)

3.2.2 Laser flash photolysis of 14 in hexane solution

Transient absorption spectra recorded by 248 nm laser flash photolysis of **14** (4.23×10^{-3} M) in deoxygenated anhydrous hexane at 25 °C showed the formation of two overlapping transient absorption bands formed with the laser pulse; one that is much shorter-lived (λ_{max} = 490 nm) than the other (λ_{max} = 470 nm). The transient absorption spectra recorded ca. 0-16 ns and 80-112 ns after the laser pulse are shown in Figure 3.3a. In addition, an absorption band at ~ 290 nm is observed but we did not focus on its identification in this work. The short-lived transient, monitored at 490 nm (shown in Figure 3.3 b), exhibits a lifetime (τ) $\leq$ 10 ns ($k_{decay} \geq 9.5 \times 10^{7}$ s^{-1}), which was estimated by fitting a decay profile (recorded under conditions of maximum time resolution of our instrument) to first-order kinetics according to eq (2.8). The 470 nm transient decays with second-order kinetics ($k_{dim}/\varepsilon = (3.1 \pm 0.6) \times 10^{7}$ cm s^{-1}), according to eq (2.3) with concomitant formation of another transient species at 370 nm, consistent with the formation of Ge_2Me_4. Transient decay/growth profiles recorded at 470 nm and 370 nm are shown in the inset in Figure 3.3a. Note that a short-lived decay with the laser pulse, due to the 490 nm transient, is apparent in the decay profile recorded at 470 nm.

The present results, with the exception of the short-lived transient at 490 nm, are consistent with our results from laser flash photolysis of germacyclopent-3-enes derivatives **23** and **24**, but differ significantly from that reported by Mochida *et al.*, where a transient absorption band centered at 450 nm was assigned to $GeMe_2$.[3] Nevertheless, the authors observed a growth at 370 nm which they attributed to Ge_2Me_4. They did not mention anything about the very short-lived transient at 490 nm; therefore, it is hard to say whether they detected it or not.

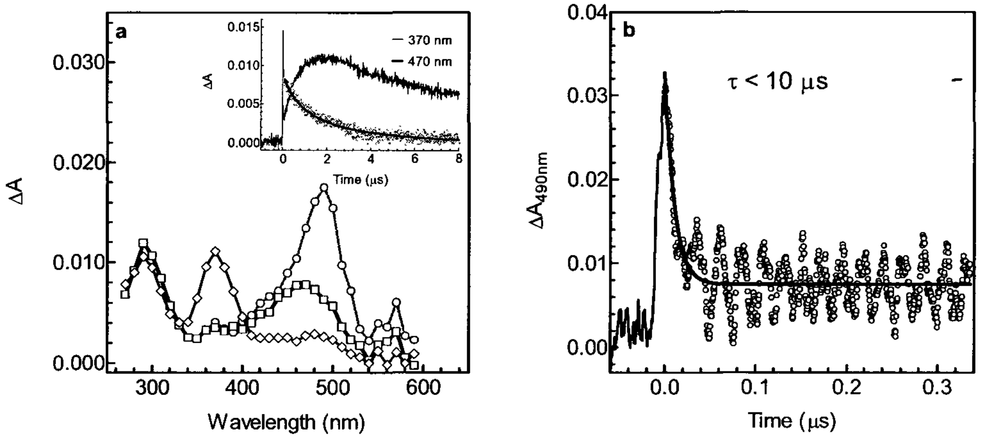

Figure 3.3. (a) Transient absorption spectra recorded by laser flash photolysis of deoxygenated solution of **14** (ca. 4 x 10^{-4} M) in hexane (○) 16 ns, 80-112 ns (□) and (◊) 2.08-2.13 μs after the laser pulse. The inset shows transient decay/growth profiles recorded at 470 nm and 370 nm. The solid line represents the non-linear least-squares fit to eq (2.3); (b) Transient decay profile recorded at 490 nm. The solid line represents the nonlinear least-squares fit of the data to eq (2.4).

3.2.3 Laser flash photolysis of 14 in the presence of THF

Transient absorption spectra in deoxygenated hexane containing THF (15 mM or 50 mM) showed the presence of a new, more intense transient absorption band centered at 310 nm that was formed with the laser pulse. Under these conditions, the short-lived species at 490 nm persisted with no decrease in its apparent maximum intensity, and the absorptions due to Ge_2Me_4 were observed to grow in on a much longer time scale than in hexane. A series of transient absorption spectra recorded in the presence of 15 mM THF are shown in Figure 3.4. It is observed that the initial portion of the 310 nm signal decays coincidently with the formation of the band at 370 nm (see inset in Figure 3.4).

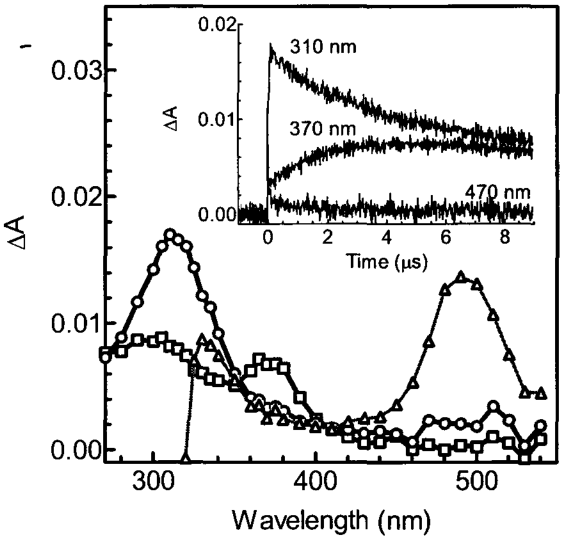

Figure 3.4. Transient absorption spectra recorded by laser flash photolysis of **14** in deoxygenated hexane containing 15 mM THF 16-32 ns (△), 48-80 ns (○) and 7.76-7.82 μs (□) after the laser pulse. The sharp drop in the ΔA signals at < 320 nm is due to fluorescence from the sample. The inset shows transient growth/decay profiles recorded at 310 nm, 370 nm and 470 nm from the same experiment.

The results obtained in the present study are in excellent agreement with those presented in Chapter 4 (*vide infra*): $GeMe_2$ reacts reversibly to form the Me_2Ge-THF complex which exhibits an absorption maximum at 310 nm. It was also observed that the complex decays with the formation of Ge_2Me_4, but significantly more slowly than the corresponding processes for $GeMe_2$ in hexane (see Chapter 2). Under these conditions the signals at 470 nm are very weak, and are most likely due to the $GeMe_2$ remaining at equilibrium with the Me_2Ge-THF complex. In Chapter 4, we also show that the reaction of $GeMe_2$ with THF is characterized by a bimolecular rate constant $k_{THF} = (1.05 \pm 0.22) \times 10^{10}\ M^{-1}\ s^{-1}$ and an equilibrium constant, $K_{eq} = 9800 \pm 3800\ M^{-1}$. The behavior observed here is consistent with these parameters. The present results thus further support our assignment of the transient at 470 nm in pure hexane solution to $GeMe_2$.

3.2.4 Further identification of the 470 nm transient

Addition of AcOH (0.05-1 mM), CCl_4 (10-65 mM) or DMB (0.1-1 mM) caused the decay of the 470 nm transient to accelerate. A decrease in the maximum signal intensity of the 370 nm transient was also observed with increasing concentrations of the scavenger. This behavior is closely analogous to that observed with the germacyclopentene precursors **23** and **24** (Chapter 2). In no case was an effect on the intensity of the 490 nm short-lived transient apparent. Figure 3.5a shows representative decay profiles recorded in the presence of increasing acetic acid concentrations. The data are reproduced on a magnified scale in Figure 3.5b to better illustrate the effect on the 470 nm signal. Figure 3.5c shows corresponding effects on the Ge_2Me_4 signal at 370 nm. Since the decay profiles recorded at 470 nm include the overlapping 490 nm transient, we fit the decays in the presence of the scavenger, to first-order kinetics excluding the data from the first ~ 50 ns after the pulse. Plots of k_{decay} vs. [Q] according to eq (2.17) were linear. This is illustrated in Figure 3.5d for quenching by AcOH and a value of $k_Q = (9.4 \pm 0.9) \times 10^9\ M^{-1}s^{-1}$ was obtained, in good agreement with the value determined using **23** as precursor ($k_Q = (7.5 \pm 0.9) \times 10^9\ M^{-1}s^{-1}$). Similar experiments with CCl_4 and DMB as scavengers afforded rate constants of $k_{CCl4} = (9 \pm 1) \times 10^7$ $M^{-1}s^{-1}$ and $k_{DMB} = (1.4 \pm 0.1) \times 10^{10}$ $M^{-1}s^{-1}$, which also agree well with the values obtained with **23** as precursor.

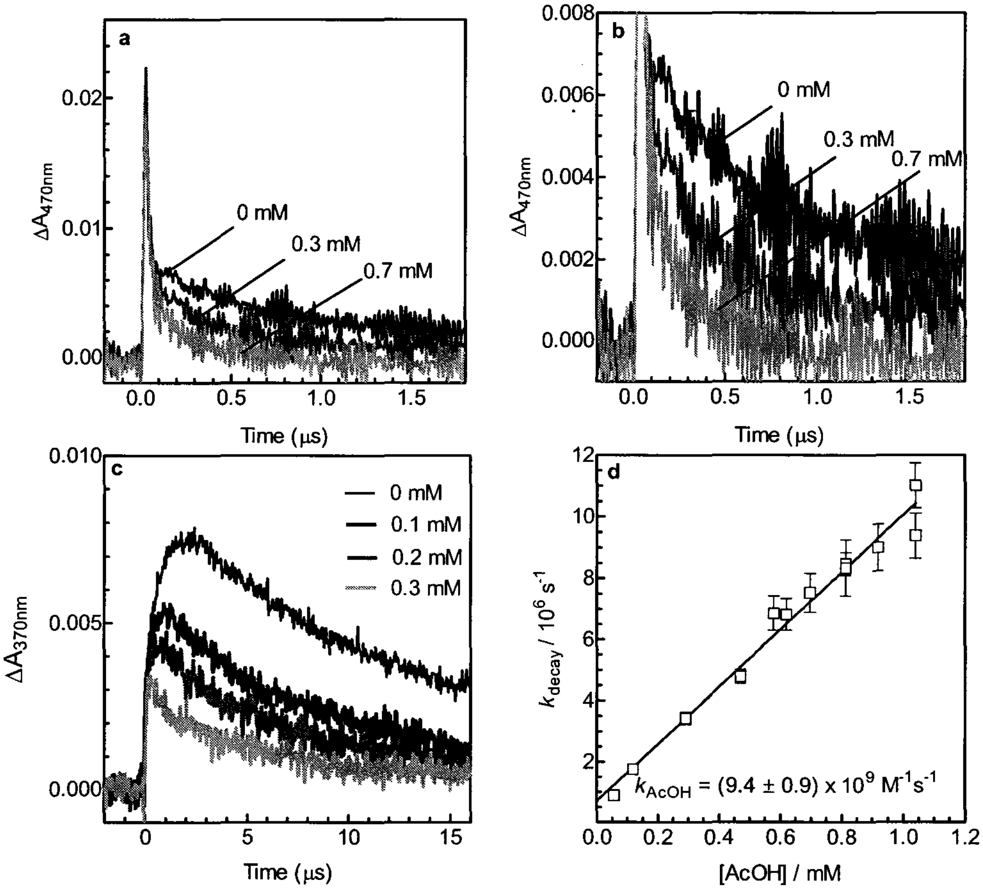

Figure 3.5. (a) Effects of added AcOH on the transient decay profiles recorded at 470 nm by laser flash photolysis of **14** in deoxygenated hexane at 25 °C; (b) Identical decay profiles as in (a) but on a magnified scale; (c) Effects of added AcOH on the transient growth/decay profiles recorded at 370 nm; (d) Plots of k_{decay} versus [AcOH].

3.2.5 Reaction with oxygen

Saturation of a hexane solution of **14** with oxygen also resulted in enhancement of the decay rates of the 470 nm transient and a decrease in the maximum signal intensities of the 370 nm transient. An estimated bimolecular rate constant $k_{O2} \sim 1.4 \times 10^8$ $M^{-1}s^{-1}$ was obtained for the reaction of the 470 nm transient with O_2, from its pseudo-first-order decay rate constant $k_{O2} = 2.1 \times 10^6$ s^{-1}. Again, the value is in good agreement with the rate constant determined in Chapter 2 for the reaction of $GeMe_2$ with oxygen ($k_{O2} = 9 \times 10^7$ M^{-1} s^{-1}) under the same conditions.

The intensity of the transient absorption at 490 nm appeared to be markedly reduced in oxygen-saturated hexane compared to argon-saturated hexane. Because this transient species decays with the laser pulse, it is not clear whether this occurs because of fast quenching of the transient, and/or quenching of a precursor to the species responsible for the absorption. Fast quenching of the transient species will result in a drop in the apparent initial intensity of its signals because of inadequate time resolution, while precursor quenching will cause a reduction in its yield. One possible assignment for this short-lived transient species is the 1,6-biradical resulting from homolysis of the Ge-Ge bond in **14** (eq 3.4). This assignment is broadly consistent with recent work by Wakasa *et al.* on octa(isopropyl)cyclotetragermane, $(Ge^iPr_2)_4$; laser flash photolysis of the latter compound in cyclohexane at 25 °C gave rise to a short-lived transient with $\lambda_{max} = 540$ nm and $\tau = 50 \pm 5$ ns, which was assigned to the 1,4-biradical $\bullet Ge^iPr_2(Ge^iPr_2)_2{}^iPr_2Ge\bullet$.[12] Another possible assignment is an excited state of the precursor.

The effect of oxygen on the initial signal intensities of the $GeMe_2$ signal (monitored at 470 nm) was investigated in order to determine whether the 490 nm could be a precursor to $GeMe_2$. However, only a slight reduction in the signal intensity was observed in the presence of air or oxygen and it was hard to make any conclusions based on the data obtained. We also considered the assignment of the species to the excited triplet state of $GeMe_2$, but tentatively ruled out the possibility based on comparison of the spectrum to that predicted by TD-DFT calculations (λ_{max} = 279, 324, 383, 417 nm).[13]

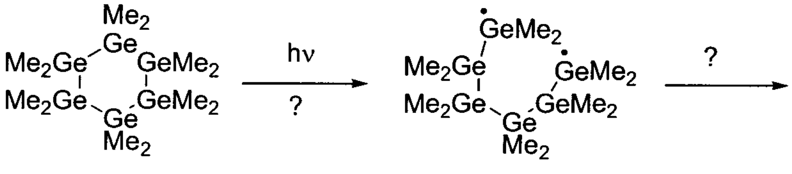

14

(3.4)

The effects of laser intensity on the yields of the 470 nm and 490 nm transients were also investigated in order to determine whether the two species resulted from mono- or biphotonic processes. Plots of the initial transient absorbance values at 470 nm and 490 nm versus laser dose were both linear (Figure 3.6), indicating that both species are formed from single-photon photochemical processes.

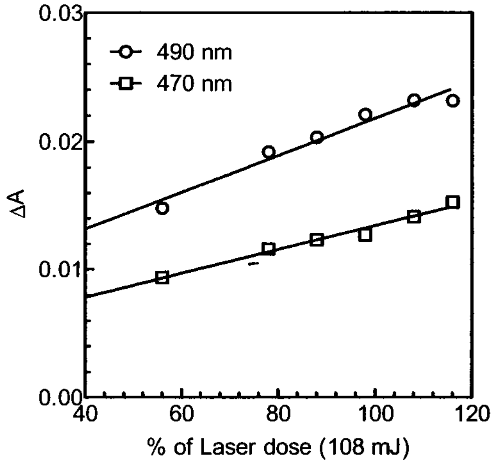

Figure 3.6. Effects of laser dose (% of 108 mJ) on the initial transient absorbance values of the 470 nm and 490 nm transient, from laser flash photolysis of **14** in anhydrous hexane.

In Table 3.1, the rate constants determined in this work are compared with those determined using **23** as precursor in Chapter 2, and with those reported by Mochida *et al.* for the transient they detected (λ_{max} = 450 nm) by laser flash photolysis of **14** in cyclohexane. For each of the scavengers studied, the agreement with the values using **23** as $GeMe_2$ precursor is excellent, which supports the assignment of the 470 nm transient to $GeMe_2$. In contrast, there is overall poor agreement with the rate constants reported by Mochida *et al.* in their study of **14**.[3] This indicates that the species detected in their study of **14** is *different* from the one obtained in our hands. The disparities in our results may have arisen because of differences in reaction conditions and experimental setup used. We emphasize that high purity precursors, anhydrous solvents and a flow system should be used in these experiments. Failing to use a flow system will result in the build-up of photochemical products that will obscure detection of $GeMe_2$.

Table 3.1. Comparison of absorption maximum and bimolecular rate constants (k_Q / 10^9 $M^{-1}s^{-1}$) for the reactions of the transients assigned to $GeMe_2$ in hexane.

λ_{max} (nm)	**470[a]**	**470[b]**	**450[c]**
Reagent			
Acetic acid	9.4 ± 0.9	7.5 ± 0.4	-
DMB	14 ± 1	13 ± 6	0.49
O_2	~ 0.14	0.09 ± 0.01	0.22
CCl_4	0.09 ± 0.01	0.08 ± 0.02	0.97

(a) This work; (b) From Chapter 2 of this thesis; (c) Ref. 3.

3.3 Laser flash photolysis studies of dimethylphenyl(trimethylsilyl)germane (18)

3.3.1 Synthesis of dimethylphenyl(trimethylsilyl)germane (18)

Dimethylphenyl(trimethylsilyl)germane **18** was synthesized by the procedure described by Bobbitt *et al.* (eq 3.5).[7] Dichlorodimethylgermane was treated with one equivalent of phenylmagnesium bromide in anhydrous THF to give chlorodimethylphenylgermane. The latter was treated with finely cut Li wire at room temperature to give dimethylphenylgermyllithium. Further reaction with chlorotrimethylsilane afforded the crude product, which was purified by column chromatography to afford **18** in 65 % overall yield, and in greater than 99 % purity as estimated by GC/MS. The material exhibited ^1H and ^{13}C NMR, and mass spectral data that were similar to those reported.[7]

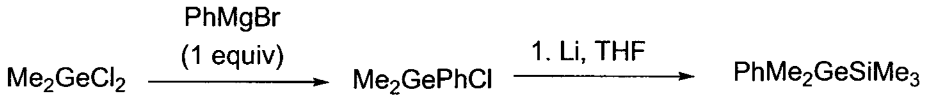

$$\mathrm{Me_2GeCl_2} \xrightarrow{\substack{\text{PhMgBr} \\ \text{(1 equiv)}}} \mathrm{Me_2GePhCl} \xrightarrow[\text{2. Me}_3\text{SiCl}]{\text{1. Li, THF}} \underset{\mathbf{18}}{\mathrm{PhMe_2GeSiMe_3}} \qquad \mathbf{(3.5)}$$

3.3.2 Laser flash photolysis of 18 in deoxygenated hexane

Laser flash photolysis of a continuously flowing, argon-saturated solution of **18** (ca. 6 x 10^{-4} M) in deoxygenated anhydrous hexane gave rise to two distinct transient absorption bands centered at ~ 300 nm and 430 nm, which decayed with mixed-order kinetics on the microsecond time scale (see Figure 3.7). Overall, the transient absorption spectrum is in good agreement with the ones reported by Mochida *et al.* and Bobbitt *et al.*[7,8] Mochida *et al.* reported two transient absorption bands at 320 nm and 430 nm; however, in their report, the two bands were almost of equal intensities at 200 ns after the laser pulse in cyclohexane. Bobbitt *et al.* reported a transient absorption spectrum containing a band centered at 425 nm and another at < 320 nm (see Figure 3.2); however, they only studied the transient species centered at 425 nm in detail.[8] In both cases, the transient species at 430 nm (or 425 nm) was assigned to $GeMe_2$. Mochida *et al.* assigned the transient absorption at ~ 300 nm to the dimethylphenylgermyl radical by analogy to the previously reported absorption spectra of phenyl-substituted germyl-centered radicals; in the present work, we did not focus on confirming or refuting this absorption, but concentrated instead on identifying the 425-430 nm transient.[9]

A transient profile recorded at 370 nm shows a hint of a growth (see inset in Figure 3.7), which is consistent with the formation of Ge_2Me_4 in the photolysis mixture, and provides indirect evidence that $GeMe_2$ is present as well. We conclude that its absorptions are simply too weak relative to those due to the other transient products for it to be detected under the conditions of our experiments.

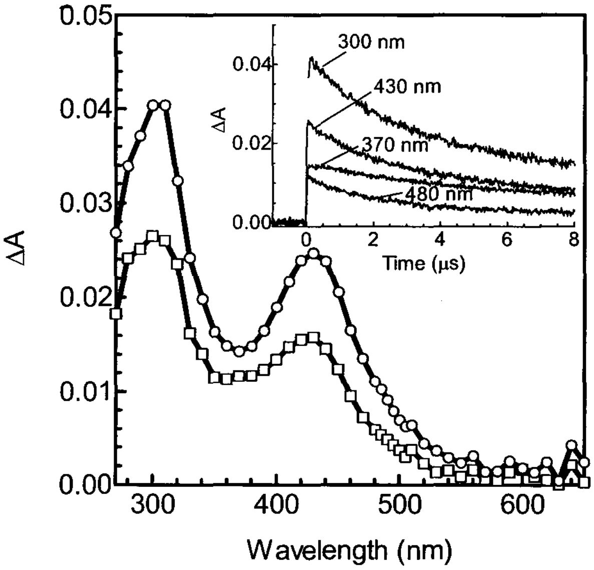

Figure 3.7. Transient absorption spectra recorded by laser flash photolysis of a deoxygenated solution of **18** (ca. 6 x 10^{-4} M) in hexane at 25 °C, 50-210 ns (○) and 2.14-2.26 μs (□) after the laser pulse. The inset shows transient profiles recorded at 300 nm, 370 nm, 430 nm and 480 nm during the same experiment.

3.3.3 Kinetic studies of precursor 18 in hexane

As mentioned above, a number of years ago, Leigh *et al.* speculated that the transient absorption band at 430 nm could be due to the 1,3,5-(1-germa)hexatriene derivative **38**, based on the comparisons of its spectral and kinetic characteristics to those determined for the closely related derivatives **40-42**.[14] While the 1,3,5-(1-germa)hexatriene derivative **42** reacts with acetic acid with rate constant, k_Q = 3.8 x 10^5

$M^{-1}s^{-1}$ in hexane,[14] $GeMe_2$ reacts at close to the diffusion-controlled limit with this substrate in hexane (k_{AcOH} = 7.5 x 10^9 $M^{-1}s^{-1}$; see Chapter 2). We anticipated that the addition of small amounts of acetic acid might allow the detection of the weak absorption expected for $GeMe_2$ from this precursor, as a weak short-lived decay centered at 470 nm, superimposed on the longer-lived decay due to the 430 nm species.

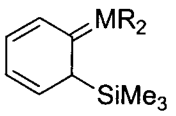

40 M = Si, R = Me
41 M = Si, R= Ph
42 M = Ge, R = Ph

Addition of 0.5 mM AcOH caused the slight growth of the signal at 370 nm to disappear, but resulted in no discernible change in the appearance of the signals at 480 nm. This provides further evidence that while $GeMe_2$ is formed upon photolysis of **18**, it is too weakly absorbing to be detected. Transient absorption spectra recorded by laser flash photolysis of **18** in deoxygenated hexane containing 3 mM acetic acid (see Figure 3.8) were similar to those recorded in the absence of the acid. Under these conditions, the lifetime of $GeMe_2$ is expected to be < 50 ns and thus it should not be detectable. The formation of Ge_2Me_4 is suppressed due to the irreversible scavenging of $GeMe_2$ with the acid (see Chapter 2). Hence, the transient absorption band at 430 nm belongs to another transient species. The inset in Figure 3.8 shows transient decay profiles recorded at 300 nm and 430 nm; the initial fast decay component that is observed in the transient decay profile at 300 nm is tentatively attributed to a higher energy absorption band of the transient species at 430 nm.

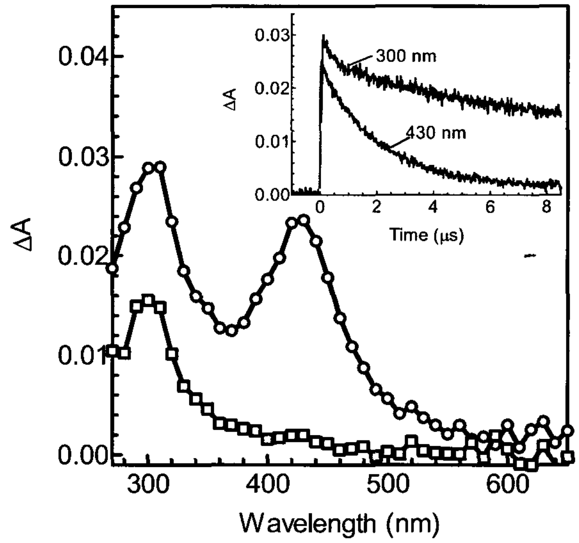

Figure 3.8. Transient absorption spectra recorded by laser flash photolysis of **18** in deoxygenated hexane containing 3 mM AcOH, recorded 96-128 ns (○) and 8.34-8.46 μs (□) after the laser pulse. The inset shows transient decay profiles recorded at 300 nm and 430 nm during the same experiment.

A first-order decay coefficient k_{decay} = (5 ± 1) x 10^5 s^{-1} was obtained by fitting decays recorded at 430 nm in the presence of 3 mM AcOH to first-order kinetics (according to eq 2.4), using neutral density filters to reduce contributions from second-order decay processes. This affords an upper limit of $k_{AcOH} \leq 10^8$ $M^{-1}s^{-1}$, for the rate constant for quenching of the 430 nm transient by AcOH.

3.3.3.1 Reactions with oxygen

Saturation of a solution of **18** in hexane with air or oxygen resulted in a slight decrease in the initial signal intensities of the transient at 430 nm, and a shortening of its lifetime. On the other hand, a more pronounced decrease in the initial signal intensities was observed for the 300 nm transient species. The transient absorption spectra recorded by photolysis of **18** in hexane are shown in Figure 3.9, and the decay profiles recorded at 300 nm and 430 nm are given in the inset.

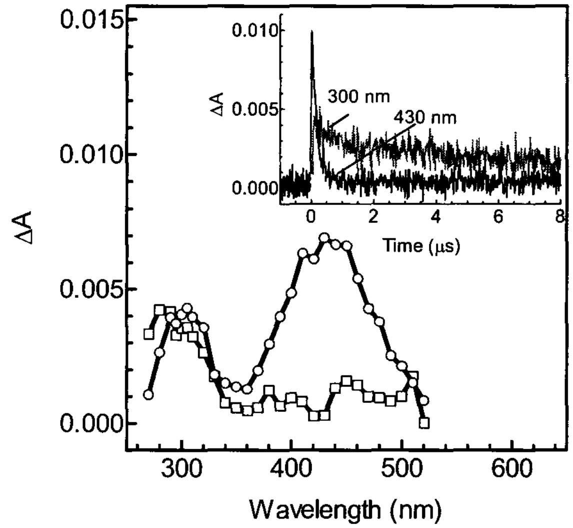

Figure 3.9. Transient absorption spectra recorded by laser flash photolysis of **18** in oxygen-saturated hexane at 25 °C, 0.07-0.10 μs (○) and 0.42-0.46 μs (□) after the laser pulse. The inset shows transient decay profiles recorded at 300 nm and 430 nm during the same experiment.

The transient decay profiles at 430 nm in air-saturated (3.1 mM O_2) and oxygen-saturated hexane (15.7 mM O_2)[15] fit to first-order kinetics, while that recorded in argon-saturated solution fit approximately to first-order kinetics. These transient decay profiles are shown in Figure 3.10a. The pseudo-first-order rate constants determined at each oxygen concentration are listed in Table 3.2.

Table 3.2. Pseudo-first-order decay rate constants for the reactions of oxygen with the 430 nm transient species produced by laser flash photolysis of **18** in hexane at 25 °C

$[O_2]$ /mM	k_{decay} / 10^6 s^{-1}
0	0.42 ± 0.01
3	1.60 ± 0.03
15	4.2 ± 0.2

A plot of the pseudo-first-order decay rate constants in argon-saturated, air-saturated and oxygen-saturated hexane versus $[O_2]$ (see Figure 3.10 b) afforded a bimolecular rate constant, $k_{O2} = (3.6 \pm 0.2) \times 10^8$ $M^{-1}s^{-1}$. This rate constant is markedly different than the values reported by Bobbitt *et al.* ($k_{O2} = 2 \times 10^9$ $M^{-1}s^{-1}$) and Mochida *et al.* ($k_{O2} = 2.1 \times 10^9$ $M^{-1}s^{-1}$) for the transient they detected at 425-430 nm for reasons we do not understand.[7,8] However, the value is comparable to the rate constants for quenching of the 1,3,5-(1-sila)hexatriene derivatives **40** ($k_Q = 6.9 \times 10^8$ $M^{-1}s^{-1}$) and **41** ($k_Q = 1.9 \times 10^8$ $M^{-1}s^{-1}$), and the 1,3,5-(1-germa)hexatriene derivative **42** ($k_Q = 1.0 \times 10^8$ $M^{-1}s^{-1}$) by oxygen.[14] This indicates that there is only a factor of ca. 2 difference in the reactivities of (1-sila)- and (1-germa)hexatrienes of otherwise identical structures toward oxygen. The results are clearly consistent with the assignment of the 430 nm transient to 1,3,5-(1-germa)hexatriene **38**.

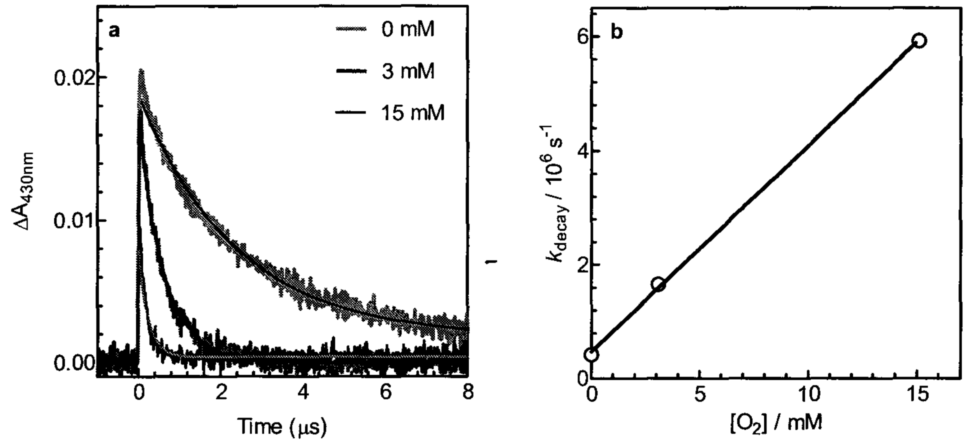

Figure 3.10. (a) Effects of oxygen concentration on transient decay profiles recorded at 430 nm by laser flash photolysis of a solution of **18** (6 x 10^{-4} M) in hexane. The solid lines represent the non-linear least-squares fit to first-order kinetics, according to eq (2.4); (b) Plots of k_{decay} versus [O_2] for the 430 nm transient. The solid line represents the linear least-squares fit to eq (2.17).

We are not able to obtain a rate constant for the reaction of the 300 nm transient with oxygen due to the decrease in the initial signal intensities. These results are inconsistent with those of Mochida *et al.*, from which they reported a rate constant of k_{O2} = 1.0 x 10^9 $M^{-1}s^{-1}$ for the same reaction in cyclohexane. They did not mention a decrease in signal intensity as we observed in our experiments. The decrease in signal intensity could be a consequence of much faster quenching of the transient than 1 x 10^9 $M^{-1}s^{-1}$. Leigh and Sluggett reported that the formation of silyl radicals from the photolysis of aryldisilanes occurs via the lowest triplet excited state of the precursor.[16] A similar process has not been explored for the analogous germylsilane derivative such as **18**; thus we cannot rule out the possibility of a decrease in the yield of the radical due to (triplet) precursor quenching.

3.3.3.2 Reactions with other reagents

The 430 nm transient species was further characterized by determining rate constants for its reactions with DMB, CCl_4, and acetone. In all cases, the decays follow pseudo-first-order kinetics in the presence of the scavenger. Plots of the pseudo-first-order rate constants versus [scavenger] were linear, as shown in Figure 3.11.

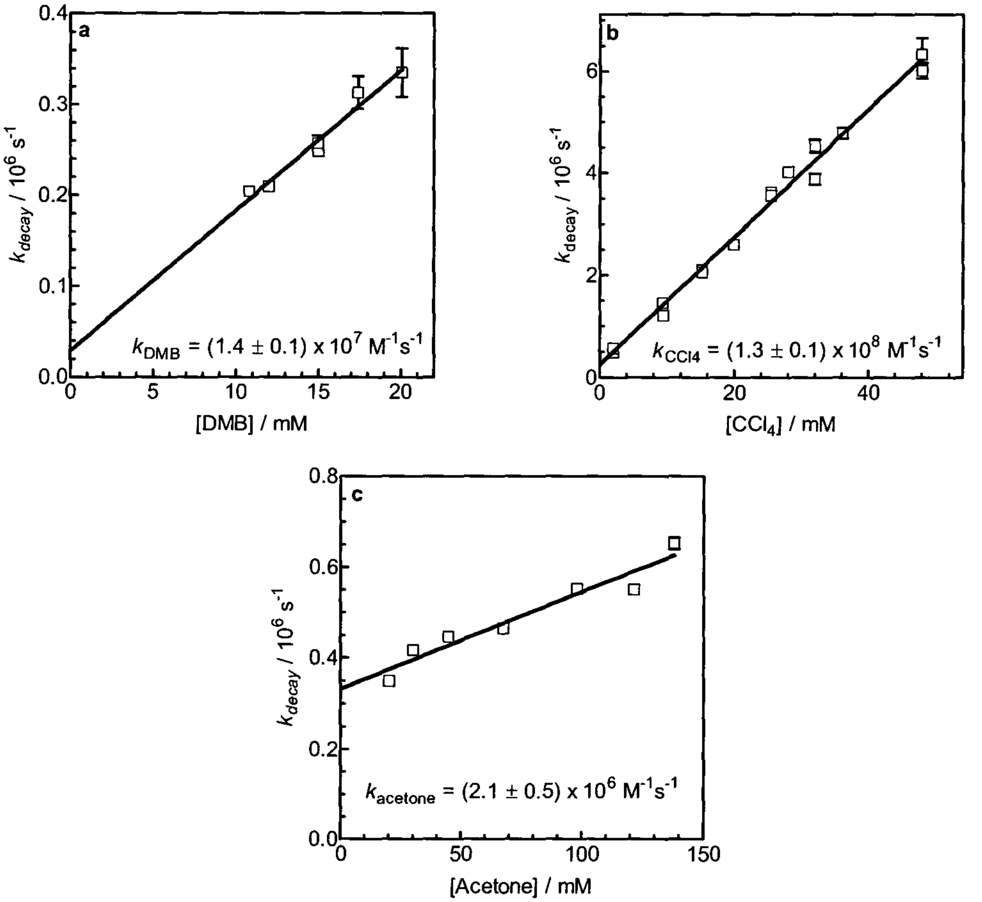

Figure 3.11. Dependence of the pseudo-first-order decay rate constant (k_{decay}) of the 430 nm transient on [Q] in anhydrous hexane for reactions with (a) DMB, (b) CCl_4 and (c) acetone. The solid lines are the linear least-squares fit to eq (2.17).

The bimolecular rate constants obtained for the reactions of the 430 nm transient are collected in Table 3.3, and are compared with the rate constants reported for "$GeMe_2$" from photolysis of **18** and with the related conjugated silenes (**40** and **41**) and germene (**42**). With the exception of the reaction with 2,3-dimethylbuta-1,3-diene (DMB), all the rate constants obtained for the 430 nm transient differ by 2-5 times compared to those reported by Mochida, Gaspar *et al.*[7,8] A comparison of the rate constants of the phenyl-substituted conjugated silene **41** with that of the phenyl-substituted germene **42** reveals that, in general, the silene is more reactive toward the scavengers listed. A marked difference in their rate constants is observed for their reactions with O-donors such as acetic acid (k_{41}/k_{42} ~ 950) and acetone (k_{41}/k_{42} ~ 2600), as compared to, for example, DMB (k_{41}/k_{42} ~ 10). A similar comparison of the rate constants determined for methyl-substituted conjugated silene **40** with that of **38** shows that the relative rate constants k_{40}/k_{38} parallels that of k_{41}/k_{42} for all reactions, with pronounced difference in reactivities with acetone and acetic acid. The reactions of silenes or germenes with O-donors have been postulated to occur by the initial formation of a Lewis acid-base complex. The reactions with silenes are thought to be faster than those with germenes owing to the higher polarity of the $^{\delta+}Si{=}C^{\delta-}$ bond as compared to the $^{\delta+}Ge{=}C^{\delta-}$ bond, silicon being more electropositive than Ge.[17,18] The rate constants for the reactions of the conjugated silenes and germenes with DMB are less dependent on whether M is Si or Ge. These reactions were postulated to proceed by an ene-addition mechanism (see eq 3.6); however, minor products consistent with the intermediacy of biradical intermediates have also been observed.[14] The reactions with oxygen and carbon tetrachloride are even less dependent on the group 14 element; these reactions are postulated to occur by mechanisms involving radical or biradical intermediates.[14,19]

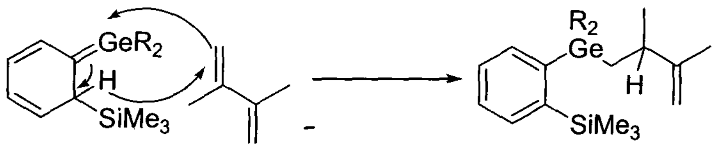

(3.6)

It is observed that the rate constants for the reactions of methyl-substituted conjugated silene **40** with all the scavengers are higher than for the phenyl-substituted homologue (**41**). The relative rate constants $k_{40/41}$ and $k_{38/42}$ for each scavenger are given in Table 3.3. A similar trend is observed in the relative rate constants for the reactions of the conjugated germene **42** and the 430 nm transient from **18**. The relative rate constants for the methyl- and phenyl substituted silenes ($k_{40/41}$) are similar to those of the analogous germenes ($k_{38/42}$) in all cases. The $k_{38/42}$ value for the reaction with AcOH is likely overestimated because only an upper limit is available for the reaction with **38**. All these findings strongly support the assignment of the 430 nm transient to conjugated germene **38**.

The course of the photolysis of **18** is depicted in Scheme 3.3; the conjugated germene **38** and dimethylphenylgermyl radical are the only prominent transient species that have been observed by laser flash photolysis in hexane.

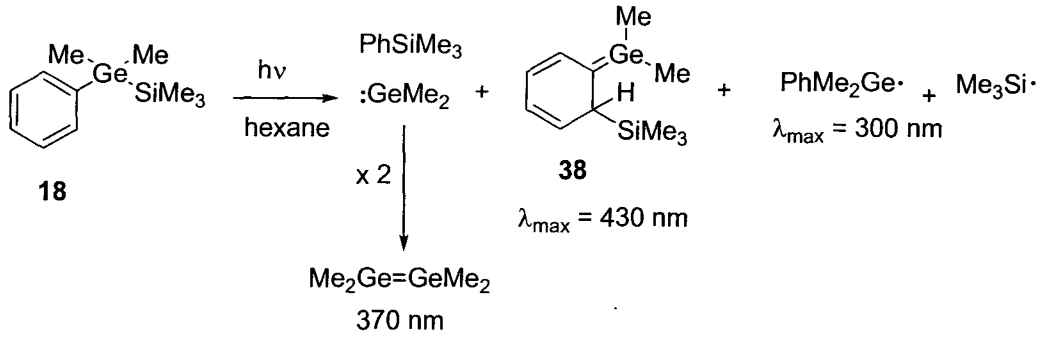

Scheme 3.3 Photolysis of **18** in hexane.

Table 3.3. A comparison of the rate constants (k_Q / 10^8 $M^{-1}s^{-1}$) for the reactions of 1,3,5-(1-metalla)hexatriene derivatives **40-42** in hydrocarbon solvents with the transient (λ_{max} = 425-430 nm) formed by laser flash photolysis of **18**.

Scavenger	"$GeMe_2$"		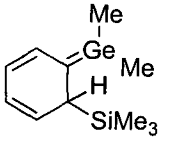 **38**[c]	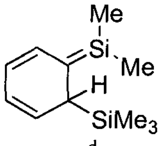 **40**[d]	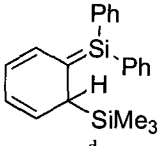 **41**[d]	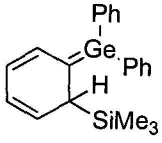 **42**[e]	k_{40}/k_{41}	k_{38}/k_{42}
λ_{max} (nm)	425[a]	430[b]	430	425	490	480		
DMB	0.17	0.41	0.14 ± 0.01	1.28 ± 0.03	0.30 ± 0.01	0.030 ± 0.003	~ 4	~ 5
Acetic acid	-	-	≤ 1	17 ± 2[a]	3.69 ± 0.48	0.0039 ± 0.0005	~ 5	~ 250
Oxygen	20	21	3.8 ± 0.2	6.9 ± 0.4	1.9 ± 0.2	0.961 ± 0.045	~ 4	~ 4
CCl_4	3.15	-	1.3 ± 0.1	4.4 ± 0.1	1.1 ± 0.1	0.29 ± 0.03	~ 4	~ 4
Acetone	-	-	0.021 ± 0.005	45.0 ± 0.6	5.42 ± 0.05	0.0021 ± 0.0005	~ 8	~ 10

(a) Ref. 7 in cyclohexane at 20 °C; (b) Ref. 8 in cyclohexane at 20 °C; (c) This work in hexane at 25 °C; (d) Ref. 20 in isooctane at 21 °C; (e) Ref. 14 in hexane at 23 °C.

3.3.4 Laser flash photolysis of 18 in THF

In another attempt to detect $GeMe_2$ from photolysis of **18**, this time as the Me_2Ge-THF complex, laser flash photolysis of **18** was performed in deoxygenated THF solution. In Chapter 5, we will show that the transient absorption spectra recorded by laser flash photolysis of 1,1-dimethyl-3-phenylgermacyclopent-3-ene **23** in deoxygenated THF show a new intense, relatively long-lived ($\tau \sim 45$ μs) transient absorption band centered at ~ 310 nm, that is assigned to the Me_2Ge-THF complex. The species decays over a much longer time scale compared to free $GeMe_2$ in hexane, with concomitant growth of absorptions due to Ge_2Me_4 (λ_{max} = 370 nm). Transient absorption spectra recorded by laser flash photolysis of **18** in deoxygenated THF showed two distinct transient absorption bands centered at ca. 300 nm and 430 nm, similar to that recorded in hexane (see Figure 3.12). There are no spectral shifts of the transient absorption bands compared to those observed in hexane, indicating that neither the dimethylphenylgermyl radical nor the conjugated germene **38** complexes strongly with the solvent. It is worth mentioning that the fact that the 430 nm transient is observed in both deoxygenated hexane and deoxygenated THF provides further proof that its assignment to $GeMe_2$ by Mochida, Gaspar *et al.* is incorrect, since the propensity of transient germylenes to complex with ethers is well-known.[21,22] We note that the transient absorption spectra recorded in THF show maximum initial intensities of the absorption bands at ~ 300 nm and 430 nm that are roughly equal, while in deoxygenated hexane it was observed that the absorption maximum corresponding to the 430 nm transient is lower than that at 310 nm. This might suggest an increase in the quantum yield of the transient at 430 nm in THF, but we did not investigate this further. Transient profiles recorded at 300 nm show that it decays with complex kinetics under these conditions. Unfortunately, from this experiment no conclusions could be made about the presence of the Me_2Ge-THF complex (λ_{max} = 310 nm) because of the (potential) overlapping transient band due to the dimethylphenylgermyl radical (λ_{max} ~ 300 nm). In addition, we discuss in Chapter 5 that in anhydrous THF, the Me_2Ge-THF complex dimerizes to form Ge_2Me_4, whose formation is evidenced by a growth in the signals at 370 nm; no such behavior is evident here.

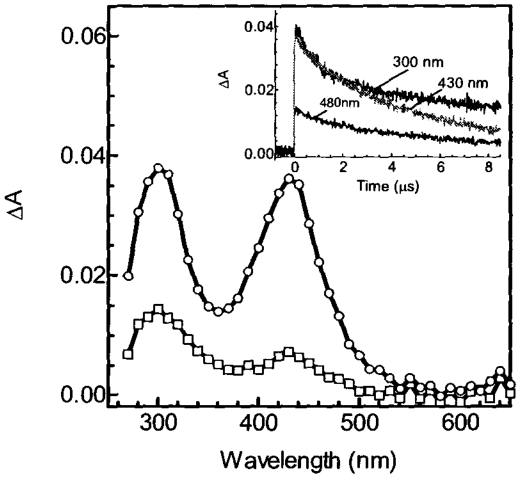

Figure 3.12. Transient absorption spectra recorded by laser flash photolysis of **18** in deoxygenated THF at 25 °C, 0.03-0.10 μs (○) and 7.87-7.94 μs (□) after the laser pulse. The inset shows transient decay profiles recorded at 300 nm, 430 nm and 480 nm during the same experiment.

Laser flash photolysis of **18** carried out in oxygen-saturated THF showed less complex spectra (see Figure 3.13); a ca. 3-fold decrease in the maximum signal intensities of both the 430 nm and 300 nm transient is observed. The loss in signal intensities is roughly equal for both transients in oxygen-saturated THF and is probably due to inadequate time resolution at both wavelengths. There may be a fast decay component at 300 nm which is not evident in our data. In contrast, in oxygen-saturated hexane, the loss in signal intensity was greater for the transient at 300 nm in THF. This suggests the presence of a new transient contributing to the transient absorption band at 300 nm. The transient absorption spectrum recorded 16-48 ns after the pulse, shown in Figure 3.13, is distorted in the spectral region < 360 nm due to interference from fluorescence.

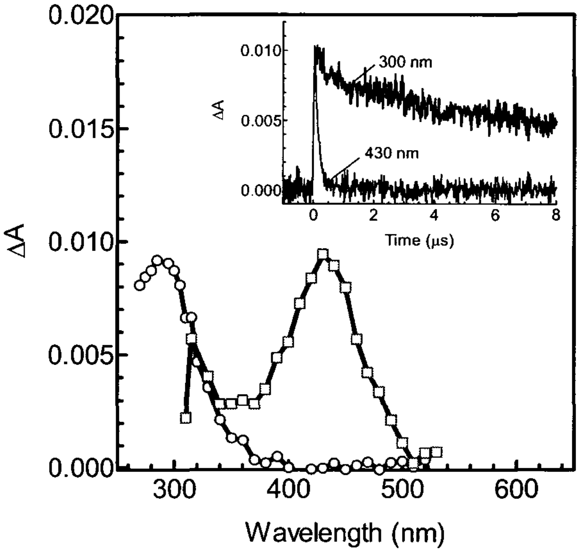

Figure 3.13. Transient absorption spectra recorded by laser flash photolysis of a solution of **18** (ca. 6 x 10^{-4} M) in oxygen-saturated THF solution 16-48 ns (□) and 0.88-0.94 μs (○) after the laser pulse. The inset shows transient decay profiles recorded at 300 nm and 430 nm during the same experiment.

Under these conditions, the transient profile recorded at 310 nm exhibits a two-phase exponential decay (see Figure 3.14a); analysis according to eq (3.7) afforded an initial fast decay with $\tau \sim 5$ μs and a much slower residual decay, $k_{slow} \sim (5.7 \pm 1.7)$ x

10^3 s^{-1}. We have observed that the Me_2Ge-THF complex exhibits a lifetime of $\tau \sim 6$ μs in oxygen-saturated solution (see Chapter 5). However, it is hard to prove that the species observed in these two independent experiments are the same. The results only allow us to conclude that the absorption at 310 nm in oxygen-saturated THF is due to the presence of at least two transient species: one reacting faster with oxygen than the other, one of them possibly being the Me_2Ge-THF complex.

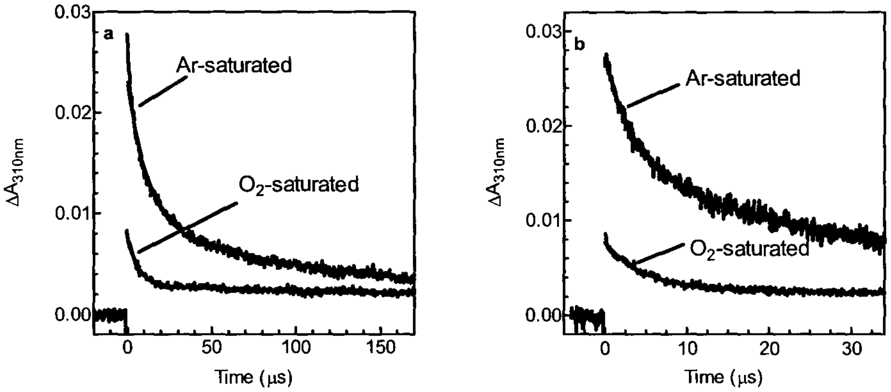

Figure 3.14. Transient decay profiles recorded by laser flash photolysis of **18** in argon-saturated THF and oxygen-saturated THF showing the bimodal decay at 310 nm on (a) long time scale and (b) initial decay component on shorter time scale. The solid lines represent the non-linear least-squares fit to two-phase exponential decay, according to eq (3.7).

The transient at 430 nm decays with first-order kinetics with a lifetime (τ) of ca. 150 ns in oxygen-saturated THF, which corresponds to an estimated bimolecular rate constant $k_{O2} \sim 6.5 \times 10^8$ $M^{-1}s^{-1}$ for its reaction with oxygen. Figures 3.15a-b show the transient decay profiles recorded at 430 nm in argon-saturated and oxygen-saturated THF.

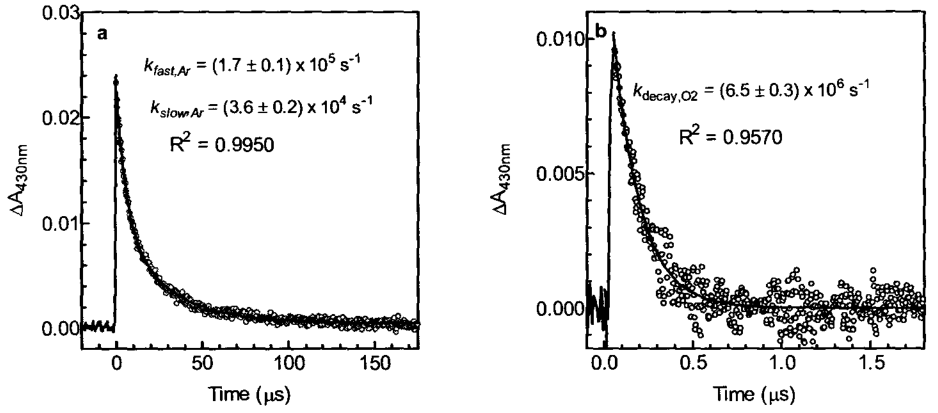

Figure 3.15. Transient decay profiles recorded at 430 nm by laser flash photolysis of **18** in (a) argon-saturated THF; the solid line represents the non-linear least-squares fit to eq (3.7), and (b) oxygen-saturated THF; the solid line represents the non-linear least-squares fit to eq (2.17).

$$\Delta A_t = (\Delta A_0)_1\, e^{-k_1 t} + (\Delta A_0)_2\, e^{-k_2 t} + \Delta A_\infty \qquad \textbf{(3.7)}$$

Overall, from this study we have been able to show that the transient species at 430 nm from laser photolysis of **18** is assignable to the 1,3,5-(1-germa)hexatriene derivative **38**, and that $GeMe_2$ could not be detected by laser photolysis of this precursor.

3.4 Summary and Conclusions

The transient absorption spectra obtained in laser flash photolysis experiments with dodecamethylcyclohexagermane (**14**) in deoxygenated hexane are in excellent agreement with the ones recorded by laser flash photolysis of germacyclopent-3-enes **23** and **24**, except for the presence of an additional, very short-lived transient ($\tau \sim 10$ ns) with λ_{max} = 490 nm that is formed with the laser pulse from **14**. A second, longer-lived transient species (λ_{max} = 470 nm) is formed with the laser pulse, and decays with concomitant formation of another transient species at 370 nm. The rate constants determined for the reactions of the 470 nm transient with acetic acid, DMB, carbon tetrachloride and oxygen are in very good agreement with the ones determined for $GeMe_2$ in Chapter 2. These results confirm our assignment of the transient species with λ_{max} = 470 nm to $GeMe_2$ and the one at 370 nm to its dimer Ge_2Me_4. Moreover, a transient absorption spectrum recorded in hexane containing THF showed the formation of a new transient absorption band at ~ 310 nm, consistent with the Me_2Ge-THF complex.

Transient absorption spectra recorded by laser photolysis of dimethylphenyl(trimethylsilyl)germane under our experimental conditions are in good agreement with the reported ones;[7,8] two distinct transient absorption bands at 300 nm and 430 nm were observed. Although the reported product studies suggested the formation of $GeMe_2$ in major yield, we were unable to detect it by time-resolved UV-Vis absorption spectroscopy in hexane. This is because the extinction coefficient of $GeMe_2$ is too low for the species to be detected in the presence of other more intensely absorbing transients with UV-Vis absorptions in a similar wavelength range. On the other hand, kinetic studies in the presence of DMB, oxygen, acetic acid, acetone and CCl_4 afforded rate constants that are consistent with the assignment of the 430 nm transient to 1,3,5-(1-germa)hexatriene derivative **38**. We conclude that given the low extinction coefficient of $GeMe_2$, it is difficult to detect its absorption when it is in the presence of a more strongly absorbing overlapping transient such as the 1,3,5-(1-germa)hexatriene derivative **38**.

This study clarified some of the ambiguities in the literature regarding the UV-Vis absorption spectrum of $GeMe_2$ reported from laser flash photolysis of compounds **14** and **18** in hydrocarbon solvents, and verifies our assignment of $GeMe_2$ from laser photolysis of 1-germacyclopent-3-ene derivatives **23** and **24**. We emphasize that the use of high purity precursors, scrupulously dry glassware, anhydrous solvents, and a flow system are essential in these spectroscopic and kinetic studies. As mentioned in Chapter 1, we recommend the use of a flow system not only to replenish the starting material but also to prevent accumulation of other absorbing or reactive products. The conditions used in the earlier flash photolysis experiments with **14** and **18** were simply inappropriate for the direct detection of $GeMe_2$.

References

1. Leigh, W. J.; Harrington, C. R.; Vargas-Baca, I. *J. Am. Chem. Soc.* **2004**, *126*, 16105.
2. Boganov S. E.; Egorov, M. P.; Faustov, V. I.; Nefedov, O. M. In *The chemistry of organic germanium, tin and lead compounds*; John Wiley & Sons Ltd: 2002; Chapter 12, pp. 749-841.
3. Mochida, K.; Kanno, N.; Kato, R.; Kotani, M.; Yamauchi, S.; Wakasa, M.; Hayashi, H. *J. Organomet. Chem.* **1991**, *415*, 191.
4. Satge, J.; Massol, M.; Riviere, P. *J. Organomet. Chem.* **1973**, *56*, 1.
5. Carberry, E.; Dombek, B. D.; Cohen, S. C. *J. Organomet. Chem.* **1972**, *36*, 61.
6. Mochida, K. and Tokura, S. *Bull. Chem. Soc. Jpn.* **1992**, *65*, 1642.
7. Bobbitt, K. L.; Maloney, V. M.; Gaspar, P. P. *Organometallics* **1991**, *10*, 2772.
8. Mochida, K.; Kikkawa, H.; Nakadaira, Y. *J. Organomet. Chem.* **1991**, *412*, 9.
9. Chatgilialoglu, C.; Ingold, K. U.; Lusztyk, J.; Nazran, A. S.; Scaiano, J. C. *Organometallics* **1983**, *2*, 1332.
10. Wakasa, M.; Yoneda, I.; Mochida, K. *J. Organomet. Chem.* **1989**, *366*, C1-C5.
11. Leigh, W. J. and Sluggett, G. W. *Organometallics* **1994**, *13*, 269.
12. Wakasa, M.; Takamori, Y.; Takayanagi, T.; Orihara, M.; Kugita, T. *J. Organomet. Chem.* **2007**, *692*, 2855.
13. Huck, L. A., Private Communication.
14. Leigh, W. J.; Toltl, N. P.; Apodaca, P.; Castruiti, M.; Pannell, K. H. *Organometallics* **2000**, *19*, 3232.
15. Battino, R.; Rettich, T. R.; Tominaga, T. J. *J. Phys. Chem. Ref. Data* **1983**, *12*, 163.

16. Leigh, W. J. and Sluggett, G. W. *J. Am. Chem. Soc.* **1993**, *115*, 7531.

17. Leigh, W. J. and Sluggett, G. W. *J. Am. Chem. Soc.* **1994**, *116*, 10458.

18. Leigh, W. J. *Pure. Appl. Chem.* **1999**, *71*, 453.

19. Leigh, W. J.; Moiseev, A. G.; Coulais, E.; Lollmahomed, F.; Askari, M. S. *Can. J. Chem.* **2008**, *86*, 1105.

20. Leigh, W. J. and Sluggett, G. W. *J. Am. Chem. Soc.* **1993**, *115*, 7531.

21. Ando, W.; Itoh, H.; Tsumuraya, T.; Yoshida, H. *Organometallics* **1988**, *7*, 1880.

22. Ando, W.; Itoh, H.; Tsumuraya, T. *Organometallics* **1989**, *8*, 2759.

CHAPTER 4

Reactions of $GeMe_2$ with THF and alcohols in hexane

4.1 Introduction

The reactions of transient silylenes and germylenes with electron pair donors such as amines, phosphines, alcohols and ethers are well recognized.[1-3] There are several experimental reports (UV-Vis spectroscopic or kinetic), in the gas phase or solution or low-temperature matrixes, supported by theoretical calculations that show that these reactions occur via the initial formation of a donor-acceptor complex.[2-7] However, prior to the work published in 2006-2009 by our group,[8-11] there were only a few kinetic studies regarding these reactions, most of which were concerned with transient silylenes in solution.

Silylenes and germylenes react with ethers, such as THF, in both soft matrixes at low temperatures and in cyclohexane solution, to form Lewis acid-base complexes, which exhibit absorption maxima that are blue-shifted with respect to the free species (see eq 4.1).[2,6,12] In the absence of a scavenger, it has been found that these R_2Si-THF complexes (for e.g. R = Me or (2,4,6)-trimethylphenyl) decay to form the corresponding disilene.[7,13]

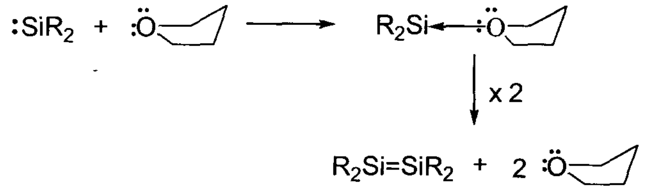

(4.1)

When alcohols are used as scavengers, hydridoalkoxysilanes or hydridoalkoxygermanes are obtained as the final products.[2,7,14,15] In early studies, Steele and Weber explored the reactions of $SiMe_2$ and SiMePh with alcohols by competition experiments, and concluded that these reactions occur by one of two possible pathways: a stepwise mechanism involving initial formation of a complex followed by rate-determining transfer of hydrogen from the alcohol oxygen to the Si atom, or concerted insertion into the O-H bond.[16] Although they favored the first mechanism, no conclusive argument could be made to support it. A few years later, the complexation mechanism was supported by the direct detection of several R_2M-alcohol complexes (M = Si or Ge) in low-temperature matrixes by UV-Vis spectroscopy, and by various theoretical calculations performed on the reactions of MR_2 with water and methanol.[1,2,6,12,17-20] Ando *et al.* reported that when $GePh_2$, $GeMes_2$, $GeAr_2$ are generated in 3-methylpentane/isopentane (3:1) matrixes doped with EtOH, BuOH, ^{i}PrOH and ^{t}BuOH, annealing of the matrix gave rise to new absorption bands at short-wavelengths, assignable to the GeR_2-alcohol complexes.[2] However, the direct detection of germylene-alcohol complexes in solution has not yet been reported.

The results described in Chapter 2 showed that $GeMe_2$ reacts with nucleophiles such as amines and acetic acid at close to the diffusion-controlled rate in hexane at 25 °C. Therefore, it is reasonable to expect that they should exhibit comparable reactivity toward alcohols. Shizuka *et al.* reported that $SiMe_2$ reacts with methanol with a rate constant of 9.1×10^9 $M^{-1}s^{-1}$ in methylcyclohexane at 293 K, while Baggott *et al.* reported a bimolecular rate constant, $k_Q = 1.18 \times 10^{-12}$ cm^3 molecule^{-1} s^{-1} (7.1×10^8 M^{-1}s^{-1}) for the same reaction in the gas phase.[4,21] However, several other authors have reported on the basis of fast kinetic studies that germylenes exhibit low or no reactivity toward alcohols.[22-25] Based on the UV-Vis spectroscopic studies of $GeMe_2$ and $GePh_2$ carried out in our group, it became clear to us that the reported kinetic studies of the reactions of $GeMe_2$ and $GePh_2$ with alcohols were based on wrong spectral assignments and can therefore be disregarded.

We were interested in exploring the kinetics and mechanism of the reactions of transient germylenes with alcohols in solution. Our main questions were: How fast are these reactions? Are the reactions reversible? Can we detect R_2Ge-alcohol complexes in solution? What is the mechanism for the decomposition of the complex to products? Pliego and De Almeida investigated the reactions of CCl_2 with water using ab initio molecular orbital theory.[26] Their results predicted that the reaction of CCl_2 with water proceeds more favorably by a catalytic mechanism involving a second water molecule rather than by a direct insertion mechanism. Based on these results, they suggested that similarly, carbenes can react with alcohols by a catalytic mechanism, in which the decomposition of the complex is aided by the assistance of a second alcohol molecule.[26] Given that theoretical calculations predict that the activation energy barrier for the rearrangement of the R_2M-alcohol complex (M = Si or Ge) via a three-centered transition state is high,[17,19,27] it can be anticipated that a similar mechanism might operate in the cases of silylenes and germylenes.

The kinetic studies of the reactions of $GeMe_2$ with THF, methanol (MeOH) and t-butanol (t-BuOH) in deoxygenated hexane at 25 °C are discussed in this chapter. The aim of the study is to probe the kinetics of the reactions of $GeMe_2$ with these substrates in order to get insight into the mechanisms of the reaction of dialkylgermylenes with alcohols and THF in solution. The results obtained for $GeMe_2$ are compared to those reported for $GePh_2$ and $GeMes_2$, and for the silicon homologue, $SiMe_2$, under similar conditions.

4.2 The reaction of $GeMe_2$ with THF

Laser flash photolysis of **23** (ca. 7 x 10^{-5} M) in deoxygenated anhydrous hexane containing THF (0.05 - 1.1 mM) caused the absorptions due to $GeMe_2$ (monitored at 480 nm) to decay with bimodal kinetics, consisting of a fast initial decay followed by a slower decaying component. Increasing concentrations of THF resulted in an acceleration of the decay rate of the initial component and a decrease in the intensity of the residual absorption. For example, Figure 4.1a shows the transient decay profiles for $GeMe_2$ recorded in the presence of THF in deoxygenated hexane; the behavior is consistent with *reversible* scavenging of $GeMe_2$ by the ether. We note that a systematic drop in the initial absorption intensity ($\Delta A_{0,480nm}$) of the decay profile was observed with increasing concentrations of THF due to inadequate time resolution of our instrument.

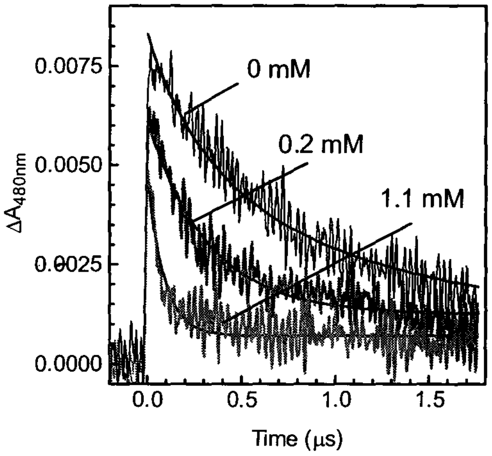

Figure 4.1. Effects of added THF on the transient decay profiles recorded at 480 nm by laser flash photolysis of **23** in deoxygenated hexane.

Addition of THF also causes a lengthening in the growth time of Ge_2Me_4 monitored at 370 nm. Interestingly, the maximum signal intensities of Ge_2Me_4 were found to increase at low [THF], and then fluctuate slightly over the range of THF concentration (0 - 45 mM) studied. Typical growth/decay profiles recorded at 370 nm in the presence of THF are shown in Figure 4.2 to illustrate these behaviors. We speculate that the apparent increase in the signal intensities is due to the suppression of one of the decay pathways of the digermene, most involving a reaction with free $GeMe_2$. This observation is supported with the report of Hurni *et al.*;[28] they irradiated hexamesitylcyclotrigermane in THF at -70 °C and obtained an increased yield of tetramesityldigermene as compared to irradiation of the same compound in toluene at -70 °C. The latter authors attributed the decreased yield of the digermene in toluene to the reaction of free dimesitylgermylene with tetramesityldigermene to form the corresponding cyclotrigermane.[28] The formation of

Ge_2Me_4 persists with no reduction in yield even at concentrations of THF at which $GeMe_2$ cannot be detected, suggesting that it is also formed by dimerization of the complex. Transient profiles recorded at 370 nm on longer time scales show that the decay rate of Ge_2Me_4 is roughly independent of [THF] over the range of 10^{-4} - 12.3 M, indicating that it is unreactive toward THF.

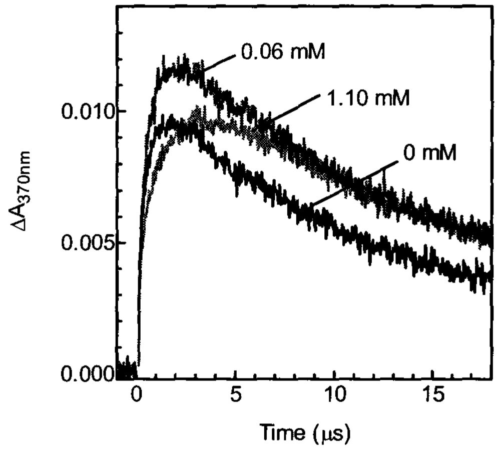

Figure 4.2. Effects of added THF on the transient decay/growth profiles monitored at 370 nm by laser flash photolysis of **23** in deoxygenated hexane.

Addition of THF also led to the formation of a new transient absorption band at 310 nm, and its absorption intensity increased with increasing THF concentration. A series of transient absorption spectra recorded by laser flash photolysis of **23** in hexane containing 0.015 M THF is shown in Figure 4.3. In the presence of 0.015 M THF the 310 nm transient decays over several hundred microseconds with complex kinetics, while the absorptions due to free $GeMe_2$ at 480 nm are very weak. Saturation of the solution with air has little effect on the decay kinetics of the 310 nm transient, indicating that the absorption is not due to a radical or triplet state. Ando *et al.* reported that diphenyl- and dimesitylgermylene-ether complexes (ether = 3-MeTHF) exhibit absorption bands centered at 325 nm and 360 nm, respectively, blue-shifted with respect to the free germylene (λ_{max}: $GePh_2$ = 463 nm and $GeMes_2$ = 550 nm) in 3-methylpentane/isopentane matrixes at 77 K, respectively.[1,2] Similarly, Levin *et al.* observed a new longer-lived absorption band at 310 nm, assignable to the Me_2Si-THF complex, when $SiMe_2$ was generated in the presence of THF in cyclohexane solution at 23 °C.[6,12] On the basis of these reports, we assign the transient absorption band at 310 nm to the Me_2Ge-THF complex.

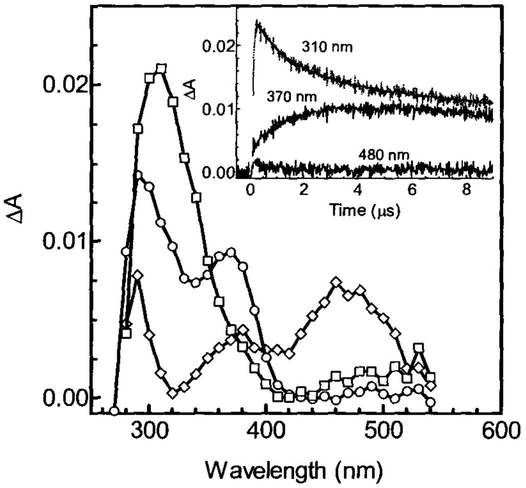

Figure 4.3. Transient absorption spectra from laser flash photolysis of **23** (ca. 7 x 10^{-5} M) in 0.015 M THF recorded 0.02 - 0.22 μs (□) and 7.90 - 9.62 μs (○) after the laser pulse. The transient absorption spectrum of **23** recorded in deoxygenated hexane at 0.13 - 0.18 μs (◊) after the laser pulse is also shown for comparison. The inset shows the transient growth/decay profiles recorded at 310 nm, 370 nm and 480 nm.

As mentioned above, the overall transient behavior exhibited by $GeMe_2$ and Ge_2Me_4 in the presence of THF is characteristic of reversible scavenging of $GeMe_2$ by the ether. In the presence of 0.5-1.0 mM THF, the following was observed: (i) an initial fast decay of $GeMe_2$, followed by a much slower residual decay, and (ii) lengthening of the formation of Ge_2Me_4. The initial fast decay is interpreted as a rapid approach to equilibrium between free $GeMe_2$ and the primary product of its reaction with THF, while the residual slowly-decaying absorptions are attributed to free $GeMe_2$ undergoing dimerization after equilibrium has been established. The $GeMe_2$ decay profiles were analyzed as a single-exponential decay to a non-zero non-decaying residual absorption, according to eq (4.2); the quality of the fits improved above 0.2 mM THF. A plot of k_{decay} versus [THF] according to eq (4.3) is linear (see Figure 4.3 a); k_{decay} is the pseudo-first-order decay constant for the approach to equilibrium, k_Q is the forward bimolecular rate constant for the reaction of $GeMe_2$ with THF, while k_{-Q} is the unimolecular rate constant for the decomposition of the complex to re-form $GeMe_2$ and THF. A bimolecular rate constant of $(1.05 \pm 0.24) \times 10^{10}$ $M^{-1}s^{-1}$ was obtained for the reaction of $GeMe_2$ with THF indicating that the reaction occurs at close to the diffusion-controlled rate.

$$\Delta A_t = (\Delta A_t - \Delta A_{res})\, e^{-k_{decay}t} + \Delta A_{res} \qquad \textbf{(4.2)}$$

$$k_{decay} = k_Q [Q] + k_{-Q} \qquad \textbf{(4.3)}$$

The equilibrium constant (K_{eq}) for the reaction could be determined using eq (4.4), where the span of the decay profile ($\Delta A_{0,480nm} - \Delta A_{res,480nm}$) is proportional to the concentration of the complex at equilibrium and $\Delta A_{res,480nm}$ is proportional to the concentration of $GeMe_2$ at equilibrium. The value of $\Delta A_{0,480nm}$ used in our calculations represents the maximum intensity of the $GeMe_2$ decay profile in the absence of THF, while $\Delta A_{res,480nm}$ is the intensity at the *start* of the slowly decaying residual component in the presence of a given concentration of THF. According to eq (4.5), the slope of the plot of ($\Delta A_{0,480nm}$ / $\Delta A_{res,480nm}$) versus [THF] afford K_{eq}. An estimated value of K_{eq} = 9800 ± 820 M^{-1} was obtained from the slope of the plot (Figure 4.4b).

$$\frac{[\text{Complex}]}{[\text{GeMe}_2]_{eq}[\text{Q}]} \approx \frac{\Delta A_{0,480nm} - \Delta A_{res,480nm}}{\Delta A_{res,480nm}[\text{Q}]} = K_{eq} \qquad \textbf{(4.4)}$$

$$\Delta A_{0,480nm} / \Delta A_{res,480nm} = 1 + K_{eq}[\text{Q}] \qquad \textbf{(4.5)}$$

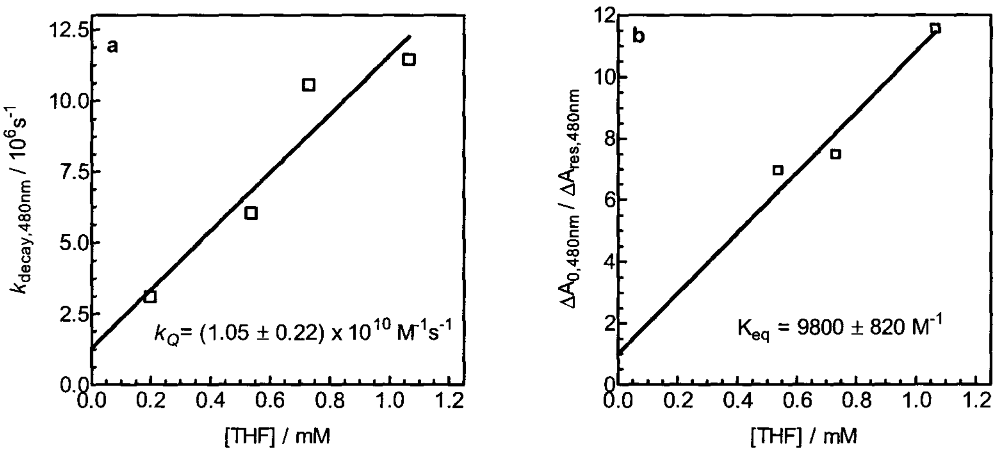

Figure 4.4. (a) Determination of K_{eq} for the reaction of $GeMe_2$ with THF in hexane at 25 °C. Plots of $\Delta A_{0,480nm}$ / $\Delta A_{res,480nm}$ for $GeMe_2$, monitored at 480 nm versus [THF]; (b) Plot of k_{decay} at 480 nm versus [THF].

The reaction of $GeMe_2$ with THF can be compared to that of $SiMe_2$ under similar conditions. Both $GeMe_2$ and $SiMe_2$ react with THF to form Lewis acid-base complexes with absorption maximum, λ_{max} = 310 nm.[11] The rate constant determined for the reaction of $GeMe_2$ with THF is similar to that reported for the reaction of $SiMe_2$ with THF in hexane ($k_{THF} = (1.73 \pm 0.15) \times 10^{10}\ M^{-1}s^{-1}$).[11] In addition, the rate constant for the reaction of $GeMe_2$ is only slightly higher than that of $GePh_2$ ($k_Q = (6.3 \pm 0.6) \times 10^{9}\ M^{-1}s^{-1}$), indicating close similarities in the reactivities of $GeMe_2$ and $GePh_2$ toward THF. The equilibrium constant for the formation of Me_2Ge-THF complex is roughly 2 times smaller than that for the formation of Ph_2Ge-THF complex.[8] This indicates greater Lewis acidity of $GePh_2$ as compared to $GeMe_2$.

It can be seen that the decay of the Me_2Ge-THF complex proceeds with concomitant formation of Ge_2Me_4 (see inset in Figure 4.3). On the basis of these observations, we postulate that Ge_2Me_4 is formed by three reaction pathways, as depicted in Scheme 4.1: (i) dimerization of free $GeMe_2$ at equilibrium, (ii) reaction of free $GeMe_2$ with the Me_2Ge-THF complex, and (iii) dimerization of the Me_2Ge-THF complex. These pathways were also suggested by Gillette *et al.* from their low temperature matrix studies of the reactions of a series of silylenes with ethers, sulfides and tertiary amines.[7] However, pathway (iii) is expected to be minor in dilute THF solution in hexane.

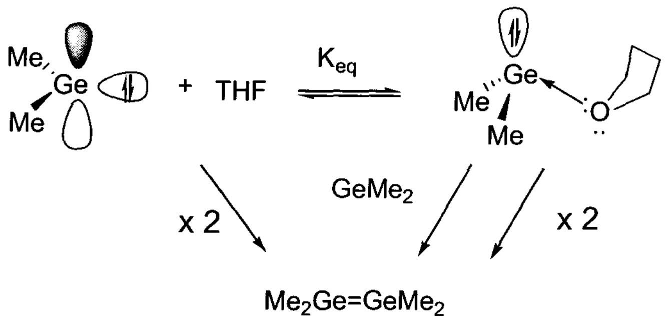

Scheme 4.1 Reactions of $GeMe_2$ in deoxygenated hexane containing THF.

4.3 The reaction of $GeMe_2$ with methanol

Laser flash photolysis of a solution of **23** (ca. 7 x 10^{-5} M) in deoxygenated anhydrous hexane in the presence of methanol showed different transient behavior as compared to that in the presence of THF. Addition of MeOH (1 mM – 4.3 mM MeOH) caused the transient decay profiles to decay with bimodal kinetics but this behavior was less obvious as compared to those recorded in the presence of THF. The decay of $GeMe_2$ at all concentrations consists of a fast initial decay followed by a slower residual decay of the signal to baseline. This contrasts the observation with THF where non-decaying residual absorptions were observed at higher concentrations (Figure 4.2). Moreover, a loss in the initial signal intensities is observed with increasing additions of methanol. This is interpreted as being due to a fast decay component that cannot be resolved from the pulse. Figure 4.5 shows decay profiles recorded in the presence of 0 mM, 1.90 mM and 4.30 mM MeOH. Our interpretation of the kinetics of this reaction is mostly based on the reaction of $GePh_2$ with methanol and THF, where the decay profile of the germylene exhibits more obvious bimodal kinetics because dimerization is much slower.

This initial fast decay is attributed to the fast reversible reaction of the germylene with methanol (approach to equilibrium). The remaining decaying absorptions that are observed are interpreted as due to the dimerization of free $GeMe_2$ at equilibrium. The initial fast component could no longer be discerned at higher MeOH concentrations ([MeOH] > 6 mM). Overall, these observations are consistent with what we would expect to see if the equilibrium constant for the reaction of the germylene with the scavenger is low ($K_{eq} < 1000\ M^{-1}$). We thus interpreted the data based on this model.

Due to the loss in signal intensities of the $GeMe_2$ signals, it was not possible to determine the forward rate constant for its reactions with MeOH. However, in general, kinetic experiments using other nucleophiles, such as Et_3N or n-$BuNH_2$, as reagents showed that $GeMe_2$ reacts faster with the nucleophiles than $GePh_2$. The forward rate constant for the reaction of $GePh_2$ with methanol in hexane is determined to be $k_{MeOH} = (6.1 \pm 1.1) \times 10^9\ M^{-1}s^{-1}$, therefore we can expect that $GeMe_2$ most likely reacts with a rate constant that is faster than this.

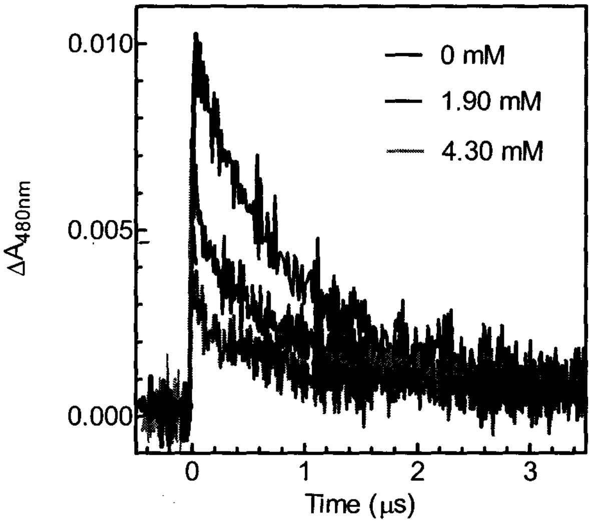

Figure 4.5. Effects of added methanol on the transient decay profiles of $GeMe_2$ recorded at 480 nm by laser flash photolysis of **23** in deoxygenated anhydrous hexane at 25 °C.

We were able to estimate the equilibrium constant, K_{eq}, for the reaction by using eq (4.5). The initial maximum absorption intensity of the decay profile recorded at 0 mM MeOH was used as $\Delta A_{0,480nm}$ in each calculation. The residual absorption due to $GeMe_2$, $\Delta A_{res,480nm}$, at each concentration (3 - 6 mM) was assumed to be at the start of the slower decaying component and was estimated by eye-ball extrapolation, as illustrated in Figure 4.6a. It is emphasized that this method only provides a crude estimate of the K_{eq} because dimerization of $GeMe_2$ remains fast under these conditions, coupled with the fact that the $GeMe_2$ signals are characteristically weak and noisy. The resulting plot of $\Delta A_{0,480nm}$ / $\Delta A_{res,480nm}$ versus [MeOH] is linear over the concentration range studied, and the slope afforded an equilibrium constant, $K_{eq} = 900 \pm 60\ M^{-1}$. This equilibrium constant is substantially lower than those obtained for the reactions of $GeMe_2$ with nucleophiles such as $BuNH_2$ ($K_{eq} > 25\ 000\ M^{-1}$; $k_Q = 1.34 \times 10^{10}\ M^{-1}s^{-1}$) and Et_3N ($K_{eq} > 25\ 000\ M^{-1}$; $k_Q = 8.7 \times 10^{9}\ M^{-1}s^{-1}$), presumably because of the much lower basicity of the alcohol. Similarly, we observed that the K_{eq} for the formation of the Me_2Ge-THF complex is ca. 10 times higher than that for the Me_2Ge-MeOH complex because of higher basicity of the ether. The K_{eq} for the reaction of $GePh_2$ with MeOH to form the Ph_2Ge-MeOH complex ($K_{eq} = (3300 \pm 800)\ M^{-1}$) is roughly 4 times higher than that of $GeMe_2$, again indicating higher thermodynamic stability of the complex with $GePh_2$.

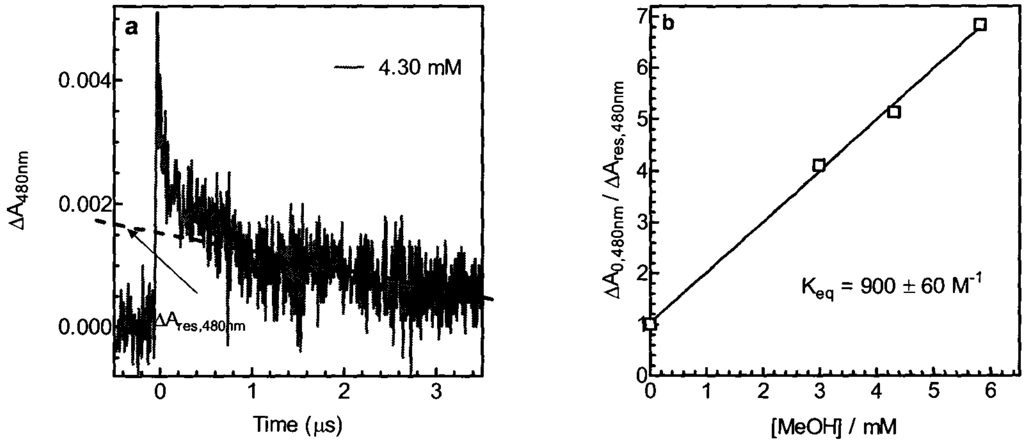

Figure 4.6. (a) Transient decay profile of $GeMe_2$, monitored at 480 nm in deoxygenated hexane containing 4.30 mM methanol. The broken line illustrates the extrapolation used to estimate the residual absorption intensity ($\Delta A_{res,480nm}$) at 480 mM; (b) Plot of ($\Delta A_{0,480nm}$ / $\Delta A_{res,480nm}$) versus [MeOH].

Analogous to the behavior observed in the presence of THF, small additions of methanol (< ca. 1.5 mM) resulted in a slight but noticeable increase in the maximum signal intensity of Ge_2Me_4 at 370 nm; however, at higher concentrations (> 1.5 mM) a decrease in the signal intensities was observed. The small increase in the intensity of Ge_2Me_4 signals at low [MeOH] is again attributed to the suppression of one of the decay pathways of Ge_2Me_4, presumably its reaction with $GeMe_2$. A Stern-Volmer plot for the reduction in the yield of Ge_2Me_4 according to eq (2.16) is shown in Figure 4.7. The K_{sv} value, which reflects the efficiency of the scavenging reaction relative to dimerization, was determined over the 0 – 6 mM concentration range in MeOH. A K_{sv} value of 105 ± 16 M^{-1} was obtained, assuming a diffusion-controlled forward rate constant ($k_Q \sim 10^{10}$ M^{-1} s^{-1}), a small K_{sv}/k_Q ratio (1.1 x 10^{-8} s) is obtained, consistent with a reversible scavenging of the germylene.

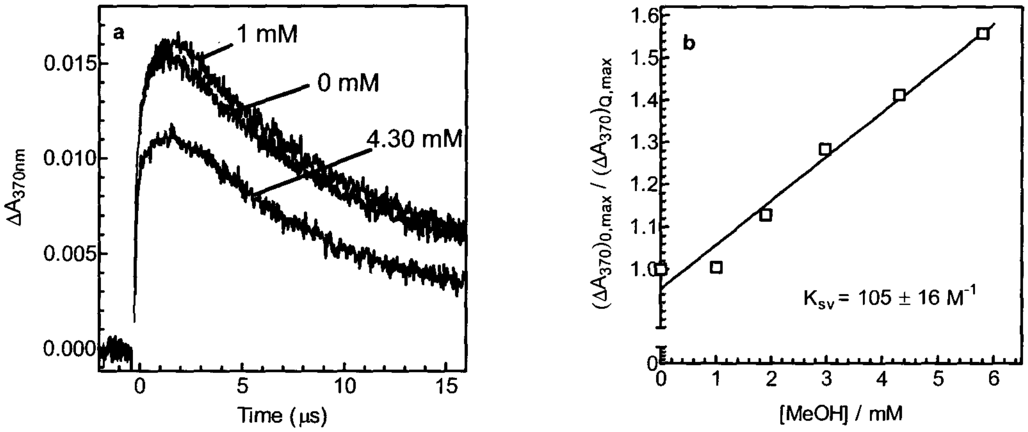

Figure 4.7. (a) Effects of added MeOH on the transient decay profiles recorded at 370 nm by laser flash photolysis of **23** in deoxygenated hexane; (b) Plot of ratio of the absorption maximum [$(\Delta A_{370})_{0,max}$ / $\Delta A_{370})_{Q,max}$] versus [MeOH].

Addition of methanol resulted in the formation of a new transient absorption band at ~ 295 nm, which is assigned to the Me_2Ge-MeOH complex. The intensity of this band increases with increasing concentrations of methanol up to 0.054 M, which was the maximum concentration examined in our experiments. Transient absorption spectra recorded by laser flash photolysis of **23** in deoxygenated hexane containing 0.054 M MeOH are shown in Figure 4.8. Under these conditions, the 295 nm transient decays over several hundred microseconds with complex kinetics. The initial fast decay component is assigned to the Me_2Ge-MeOH complex (see 295 nm transient profile in the inset of Figure 4.8a). We have not identified the second decay component that is observed on a much longer time-scale (see Figure 4.8b). The formation of Ge_2Me_4 is still evident at concentrations of methanol high enough that free $GeMe_2$ can no longer be detected. These observations suggest that under those conditions, Ge_2Me_4 is formed from three pathways: dimerization of free $GeMe_2$, the reaction of $GeMe_2$ with the complex or dimerization of the complex.

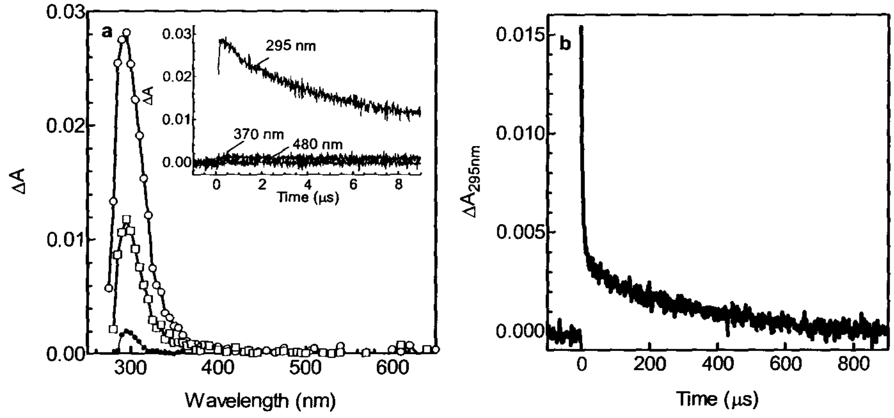

Figure 4.8. Transient absorption spectra recorded by laser photolysis of **23** (7 x 10^{-5} M) at 25 °C in deoxygenated hexane containing 54 mM MeOH (a) 0.14-0.21 μs (O), 9.46-9.97 μs (△) and 136-142 μs (•) after the laser pulse. The inset shows the transient decay profiles recorded at 295 nm, 370 nm and 430 nm in the presence of 0.054 M MeOH; (b) The transient decay profile recorded at 295 nm.

4.4 The reaction of GeMe$_2$ with t-butanol

In contrast to the decay profiles recorded for GeMe$_2$ in the presence of MeOH, there was no evidence of bimodal decay of the GeMe$_2$ signal in the presence of t-BuOH. Addition of t-BuOH to hexane solutions of **23** caused reductions in the apparent ΔA_0 of the 480 nm signal with increasing [t-BuOH], but the decays appeared to maintain clean second-order kinetics at all concentrations. This behavior of the GeMe$_2$ signals is consistent with a fast forward rate constant and a small K_{eq} for the reaction with t-BuOH. The equilibrium constant for the reaction was estimated using a small modification of eq (4.5). Here $\Delta A_{res,480\,nm}$ is assumed to be equal to the initial signal intensity of the profiles at 480 nm (i.e $\Delta A_{res,480nm} = \Delta A_{Q,max}$). The plot of the ratio $\Delta A_{0,max}$ / $\Delta A_{Q,max}$ versus [t-BuOH] over the 1 - 5 mM concentration range in t-BuOH according to eq (4.6) afforded an equilibrium constant, $K_{eq} = 335 \pm 50\ M^{-1}$ (see Figure 4.9c). This value is about half of that determined for the reaction with methanol, indicating that the Me_2Ge-t-BuOH complex is less thermodynamically stable than the Me_2Ge-MeOH complex, presumably due to difference in steric effects. A Stern-Volmer plot over the concentration range 0 - 4 mM afforded a $K_{sv} = (82 \pm 26)\ M^{-1}$ (Figure 4.9d); this value is similar to that obtained for scavenging with methanol.

$$\Delta A_{0,max} / \Delta A_{Q,max} = 1 + K_{eq}[Q] \qquad \textbf{(4.6)}$$

where $\Delta A_{Q,max} = \Delta A_{res,480nm}$

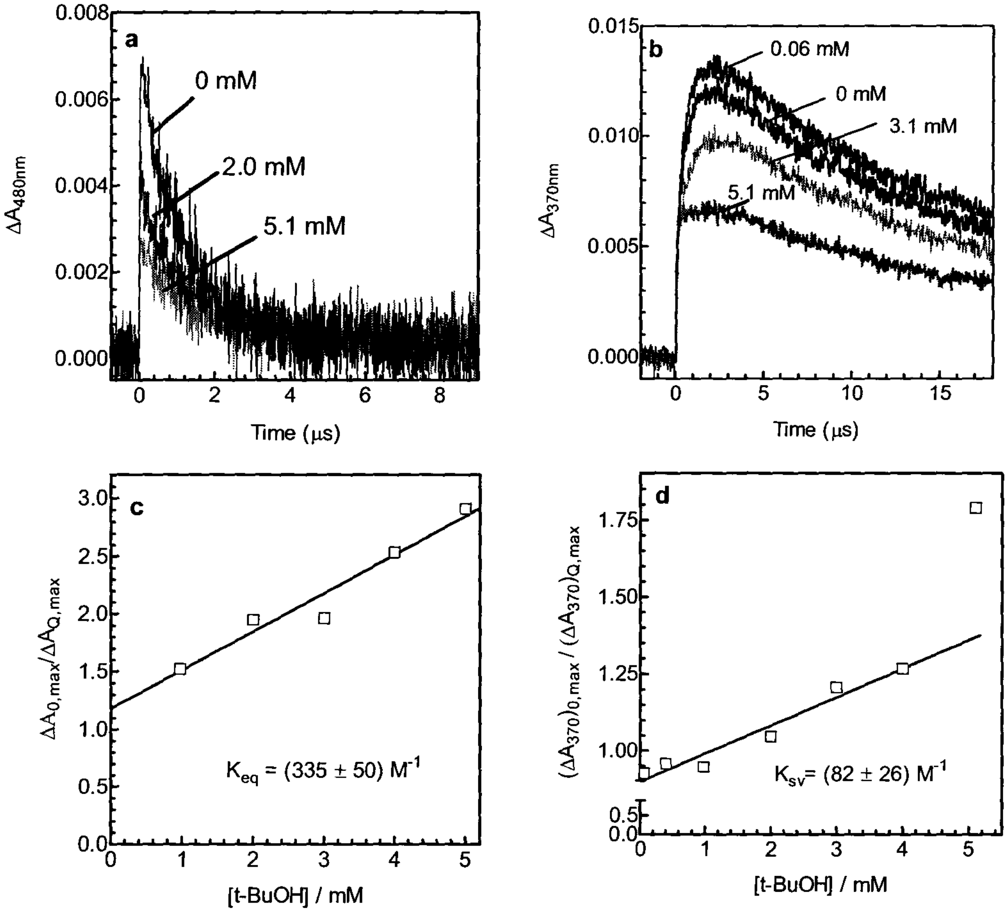

Figure 4.9. Effects of added t-BuOH on the: (a) transient decay profiles recorded at 480 nm; (b) Transient growth profiles recorded at 370 nm; (c) Ratio $\Delta A_{0,max}/\Delta A_{Q,max}$ of the transient profiles recorded at 480 nm; (d) Ratio of the maximum absorption, $(\Delta A_{370})_{0,max}/(\Delta A_{370})_{Q,max}$, at 370 nm recorded in the absence and presence of t-BuOH.

Addition of t-BuOH led to the formation of a new transient absorption band with λ_{max} ~ 300 nm. The initial signal intensity of the transient at 300 nm increases with increasing t-BuOH concentration. Transient absorption spectra of **23** recorded in hexane containing 8.2 mM t-butanol are shown in Figure 4.10. The transient absorption band centered at 300 nm is assigned to the Me_2Ge-tBuOH complex. We observe that the complex decays with the concomitant formation of Ge_2Me_4 (see inset in Figure 4.10).

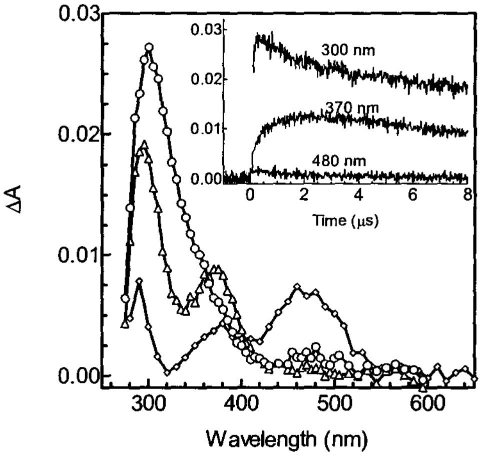

Figure 4.10. Transient absorption spectra recorded by laser flash photolysis of **23** in 8.2 mM t-BuOH in deoxygenated hexane at 0.14-0.21 μs (o) and 8.42-8.53 μs (△) after the laser pulse. Also shown the transient absorption spectrum of **23** recorded in deoxygenated hexane at 0.13-0.18 μs (◊) after the laser pulse. The inset shows growth/decay transient profiles monitored at 300 nm, 370 nm and 480 nm.

4.5 A comparison of the reactivities of GeR_2 with alcohols and THF in hexane

Parallel studies with $GePh_2$ and $GeMes_2$ were carried out in our group in order to investigate the effects of substituents on the reactivities of diorganogermylenes with MeOH, t-BuOH and THF in solution.[8] It was observed that similarly to $GeMe_2$, generation of $GePh_2$ and $GeMes_2$ by laser flash photolysis of suitable precursors in hexane containing MeOH, t-BuOH and THF led to the formation of new intense long-lived absorption bands that are blue-shifted relative to the absorption spectra of the free germylenes. These new transient absorption bands were assigned to the corresponding R_2Ge-alcohol or R_2Ge-THF complexes (R = Ph or Mes). The spectroscopic and kinetic data characterizing the reactions of $GeMe_2$, $GePh_2$ and $GeMes_2$ with MeOH, t-BuOH and THF are summarized in Table 4.1.

For a specific reagent shown in Table 4.1, the magnitude of K_{eq} increases as follows: $GeMes_2 << GeMe_2 < GePh_2$. This indicates that $GePh_2$ forms more thermodynamically stable complexes with oxygen-containing electron pair donors than $GeMe_2$ and $GeMes_2$. The K_{eq} for the reaction with each reagent dramatically decreases in the case of $GeMes_2$, indicating that the presence of bulky substituents on the Ge atom destabilizes the corresponding alcohol and ether complexes significantly.

A very similar reactivity pattern is observed for $GeMe_2$ and $GePh_2$: the equilibrium constants measured are in each case largest for their reactions with THF, and higher with methanol than with t-BuOH. The equilibrium constant is highest for THF indicating that the stability of the complexes increases with an increase in the Lewis base strength of the electron pair donor. There is a clear decrease in the equilibrium constant from methanol to t-butanol, independent of the nature of substituents on the germylene. Since the gas-phase basicity of t-BuOH is higher than that of MeOH,[29] we would expect the K_{eq} to be higher for t-BuOH. Therefore, the lower K_{eq} values compared to that of MeOH can be attributed to the steric destabilization of the complex by the bulkier t-BuOH group. It was suggested that the extent of the blue shift in the UV-Vis absorption band of the complexes relative to the free germylene reflects the strength of the Lewis acid-base interaction in the complexes: the greater the blue shift the more stable are the complexes.[2,7] However, the present results contradict this statement, for example, the absorption maximum for the Me_2Ge-THF complex is at 310 nm, while that of Me_2Ge-MeOH complex is at $\lambda_{max} < 295$ nm; yet the equilibrium constant for the formation of Me_2Ge-THF complex ($K_{eq} = 9\ 800\ M^{-1}$) is the largest among the three determined for $GeMe_2$.

Table 4.1. A comparison of the absolute rate constants (k_Q) and equilibrium constants (K_{eq}) for the reactions of $GeMe_2$, $GePh_2$ and $GeMes_2$ with methanol, t-butanol and THF in hexanes at 25 °C.

Scavenger	**Complex (λ_{max})** (hexane)	k_Q **/ 10^9 $M^{-1}s^{-1}$**	K_{eq} **/ M^{-1}**
		$GeMe_2$	
MeOH	~ 295	A	900 ± 60
t-BuOH	300	A	335 ± 50
THF	310	10.5 ± 2.2	9800 ± 3800
		$GePh_2$	
MeOH	350	6.1 ± 1.1	3300 ± 800
t-BuOH	340	4.8 ± 1.6	1000 ± 250
THF	355	6.3 ± 0.6	23 000 ± 5000
		$GeMes_2$	
MeOH	285, ~ 330	A	13.1 ± 2.5
t-BuOH	290, ~ 330	A	3.7 ± 0.2
THF	285, ~ 360	A	1.2 ± 0.2

A = cannot be determined. Values for $GePh_2$ and $GeMes_2$ were obtained from Ref. 8

On the basis of the results, the postulated reaction pathways for GeR_2 in the presence of alcohols in hexane are shown in Scheme 4.2. We observed that GeR_2 reacts with alcohols reversibly to form relatively long-lived transient species assignable to R_2Ge-alcohol complexes. These complexes react with free germylenes at equilibrium to form the corresponding digermenes or react to form alkoxygermane: The results do not allow us to determine the mechanism by which the alkoxygermane is formed. However, we can conclude that this process is the rate-determining step, and occurs with a first-order rate constant, $k_2 < 10^4$ s^{-1}. It thus becomes interesting to know whether the decay of the complex can be catalyzed by the neutral alcohols or by even stronger acids or bases.

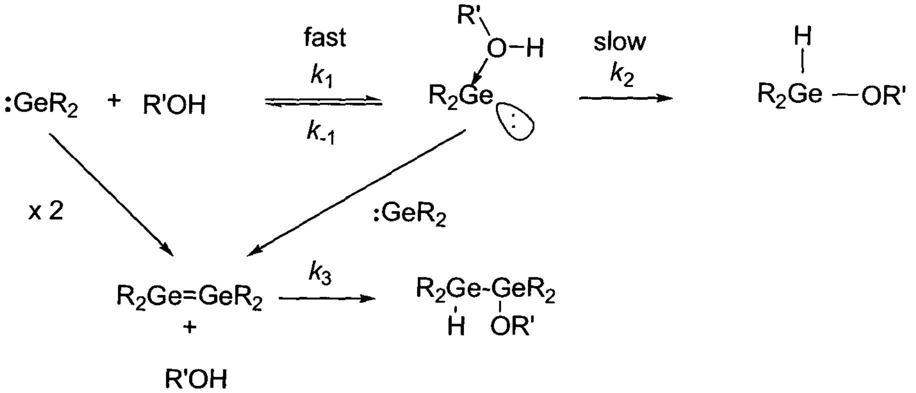

Scheme 4.2 Postulated reaction pathways for the reactions of GeR_2 in the presence of alcohols.

One of the major impurities in hexane is water and alcohols formed by autoxidation processes. We can anticipate that these species react in the same fashion as methanol with the germylene. That is, the reaction is reversible with a small equilibrium constant ($K_{eq} < 50$ M^{-1}), and is characterized by a diffusion-controlled forward rate constant ($k_Q >$

10^9). Indeed, we observe a low initial maximum signal intensity of the transient decay profile of the germylene at the start of our experiments in the absence of a scavenger, and this led us to conclude that this is due to the presence of adventitious water in the solution containing the precursor. Based on the kinetic studies discussed in this Chapter, we can now understand why it is crucial to work under anhydrous conditions for the successful detection and kinetic studies of $GeMe_2$ in solution.

4.6 Conclusions

In this Chapter, we showed that $GeMe_2$ reacts reversibly with Lewis bases, namely MeOH, t-BuOH and THF, to form new longer-lived transients which exhibit distinct absorption bands in the UV range 295-310 nm. These were assigned to the corresponding Me_2Ge-alcohol or -THF complexes. These reactions occur at close to the diffusion-controlled rate in hexane and proceed by nucleophilic attack of the Lewis base on the vacant p-orbital on the germylene. This type of initial electrophilic attack is typical of germylene reactions; in most reactions germylenes react by an initial interaction of their vacant p-orbital with the scavenger, followed by a nucleophilic stage involving attack of the complexed scavenger by the non-bonding pair of electrons of Ge (see Chapter 2).

Based on the magnitude of the equilibrium constants, we can conclude that for $GeMe_2$, the thermodynamic stability of the complexes increases in the order: t-BuOH < MeOH << THF. The stability of the complexes increases with an increase in the Lewis basicity of the scavenger and decreases with an increase in the steric bulk of the scavenger. The same trends in thermodynamic stabilities of the complexes were observed for $GePh_2$ under similar experimental conditions. In the case of $GeMes_2$, it was observed that K_{eq} is considerably reduced due to the bulky mesityl substituents on the germanium atom. Overall, the results show that the stability of germylene-Lewis base complexes depends on the steric bulk of the substituents on the germylene and in the scavenger; moreover, the more basic the Lewis base the more stable is the complex.

The Me_2Ge-THF complex and the Me_2Ge-alcohol complexes were all found to be relatively long-lived in hexane solution at 25 °C. An upper limit of the decay rate constant for the unimolecular rearrangement of the complex via intramolecular H-transfer in hexane was estimated to be $k_H < 10^4$ s^{-1}. This indicates that intramolecular proton transfer within the complex is quite slow, and suggests that the decay of the complex might be susceptible to catalytic assistance. The present data do not allow us to address the mechanism by which the proton transfer occurs, whether intramolecular or via a catalytic pathway involving a second molecule of alcohol. This mechanistic concern will be addressed in Chapter 5, in which the effects of Brønsted acids and bases on the decomposition of Me_2Ge-MeOH and Me_2Ge-THF complexes will be discussed.

References

1. Ando, W.; Itoh, H.; Tsumuraya, T.; Yoshida, H. *Organometallics* **1988**, *7*, 1880.
2. Ando, W.; Itoh, H.; Tsumuraya, T. *Organometallics* **1989**, *8*, 2759.
3. Becerra, R.; Carpenter, I. W.; Gutsche, G. J.; King, K. D.; Lawrance, W. D.; Staker, W. S.; Walsh, R. *Chem. Phys. Lett.* **2001**, *333*, 83.
4. Baggott, J. E.; Blitz, M. A.; Frey, H. M.; Lightfoot, P. D.; Walsh, R. *Int. J. Chem. Kinet.* **1992**, *24*, 127.
5. Baggott, J. E.; Blitz, M. A.; Lightfoot, P. D. *Chem. Phys. Lett.* **1989**, *154*, 330.
6. Levin, G.; Das, P. K.; Bilgrien, C.; Lee, C. L. *Organometallics* **1989**, *8*, 1206.
7. Gillette, G. R.; Noren, G. H.; West, R. *Organometallics* **1989**, *8*, 487.
8. Leigh, W. J.; Lollmahomed, F.; Harrington, C. R.; McDonald, J. M. *Organometallics* **2006**, *25*, 5424.
9. Lollmahomed, F.; Huck, L. A.; Harrington, C. R.; Chitnis, S. S.; Leigh, W. J. *Organometallics* **2009**, *28*, 1484.
10. Moiseev, A. G. and Leigh, W. J. *Organometallics* **2007**, *26*, 6268.
11. Moiseev, A. G. and Leigh, W. J. *Organometallics* **2007**, *26*, 6277.
12. Levin, G.; Das, P. K.; Lee, C. L. *Organometallics* **1988**, *7*, 1231.
13. Yamaji, M.; Hamanishi, K.; Takahashi, T.; Shizuka, H. *J. Photochem. Photobiol. A: Chem.* **1994**, *81*, 1.
14. Gu, T. Y. and Weber, W. P. *J. Organomet. Chem.* **1980**, *184*, 7.

15. Klein, B.; Neumann, W. P.; Weisbeck, M. P.; Weinken, S. *J. Organomet. Chem.* **1993**, *446*, 149.
16. Steele, K. P. and Weber, W. P. *Inorg. Chem.* **1981**, *20*, 1302.
17. Raghavachari, K.; Chandrasekhar, J.; Frisch, M. J. *J. Am. Chem. Soc.* **1982**, *104*, 3779.
18. Raghavachari, K.; Chandrasekhar, J.; Gordon, M. S.; Dykema, K. J. *J. Am. Chem. Soc.* **1984**, *106*, 5853.
19. Su, M.-D. and Chu, S. *J. Phys. Chem. A* **1999**, *103*, 11011.
20. Raghavachari, K.; Chandrasekhar, J.; Gordon, M. S.; Dykema, K. *J. Am. Chem. Soc.* **2002**, *106*, 5853.
21. Shizuka, H.; Tanaka, H.; Tonokura, K.; Murata, K.; Hiratsuka, H.; Ohshita, J.; Ishikawa, M. *Chem. Phys. Lett.* **1988**, *143*, 225.
22. Konieczny, S.; Jacobs, S. J.; Braddock-Wilking, J. K.; Gaspar, P. P. *J. Organomet. Chem.* **1988**, *341*, C17-C22.
23. Mochida, K.; Kanno, N.; Kato, R.; Kotani, M.; Yamauchi, S.; Wakasa, M.; Hayashi, H. *J. Organomet. Chem.* **1991**, *415*, 191.
24. Mochida, K. and Tokura, S. *Bull. Chem. Soc. Jpn.* **1992**, *65*, 1642.
25. Toltl, N. P.; Leigh, W. J.; Kollegger, G. M.; Stibbs, W. G.; Baines, K. M. *Organometallics* **1996**, *15*, 3732.
26. Pliego, J. R. J. and De Almeida, W. B. *J. Phys. Chem.* **1999**, *103*, 3904.
27. Su, M.-D. *Chem. Eur. J.* **2004**, *10*, 6073.

28. Hurni, K. L.; Rupar, P. A.; Payne, N. C.; Baines, K. M. *Organometallics* **2007**, *26*, 5569.
29. Anslyn E. V.; Dougherty, D. A. *Modern Physical Organic Chemistry*; University Science Books, California: 2006; Chapter 5, pp. 259-296.

CHAPTER 5

The reactivities of the Me_2Ge-MeOH and Me_2Ge-THF complexes in the neat O-donors as solvents

5.1 Introduction

In Chapter 4, we showed that $GeMe_2$ reacts with methanol, t-butanol and THF in deoxygenated hexane to form relatively long-lived Lewis acid-base complexes exhibiting UV-Vis absorption maxima of $\lambda_{max} \sim$ 290-310 nm. In the case of the alcohols, the results indicate that the final (O-H insertion) product must be formed in a second, rate-determining proton transfer step. On the basis of the relatively small upper limit of the unimolecular rate constant that could be estimated from the decay of the complexes, it was suggested that the proton-transfer step should be prone to catalysis by a second molecule of methanol or by stronger acids or bases (eq 5.1). Several questions arise: Can we still detect these complexes in neat methanol? To what extent are these complexes susceptible to protonation or deprotonation? What are the effects of the substituents on the Ge atom on the rates of these reactions, and what are the mechanisms for product formation from the complexes?

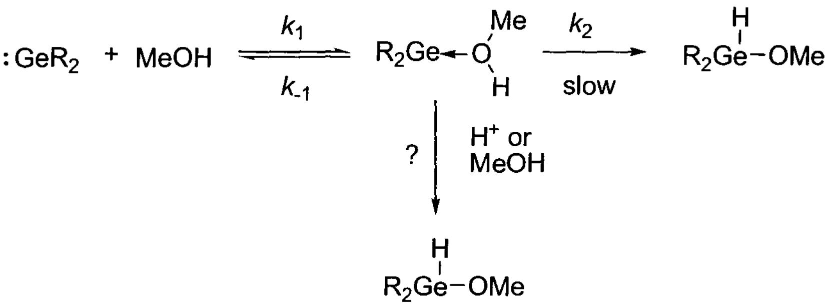

(5.1)

Generally, simple alkyl-substituted or aryl-substituted germylenes, as well as silylenes, are highly electrophilic species. They react with several classes of scavengers such as carboxylic acids, terminal alkynes, and amines in hydrocarbon solutions at close to the diffusion-controlled rate. It would be interesting to explore how their reactivity is affected when they are complexed with a Lewis base such as an ether or a tertiary amine. These types of Lewis bases can only coordinate with germylenes and do not form addition products. Ando *et al.* observed that when a series of alkyl or aryl-substituted germylenes are generated in 3-methylpentane/isopentane (3:7) matrixes doped with 2-methyltetrahydrofuran or ethanol at 77 K, new absorption bands assignable to the germylene Lewis acid-base complexes were formed.[1] Annealing of the matrix gave rise to the corresponding digermenes in the case of the ether, while the hydridoethoxygermane derivative was obtained with ethanol. Similar observations have been reported for silylenes.[2] *Gillette et al.* studied the reactions of a series of diorganosilylenes in 3-methylpentane matrixes doped with THF or diethyl ether at 77 K, and upon slight warming of the matrix observed new transient absorption bands at short wavelengths assignable to Lewis acid-base complexes of the silylenes.[2] Further warming of the matrix led to the formation of the corresponding disilenes.

In 1980, Steele and Weber compared the product ratios from competition studies of the reactions of free $SiMe_2$ with mixtures of alcohols (methanol, ethanol, isopropyl alcohol, *tert*-butyl alcohol or neopentyl alcohol) in cyclohexane, THF and diethyl ether, and found that the Me_2Si-ether complexes react preferentially with less hindered alcohols.[3] On the basis of these results, they concluded that Me_2Si-ether complexes are "more selective" than the free silylene. In 1987, Gillette *et al.* further supported these results by conducting a series of competition experiments for the reactions of $SiMes_2$ with alcohol mixtures (ethanol, propanol or 2-propanol) in pentane, diethyl ether, and 2-methyltetrahydrofuran, and found that the selectivity of $SiMes_2$ toward less hindered alcohols is also increased in ethereal solvents.[4] Levin *et al.* investigated the kinetics of the reactions of the Me_2Si-THF complex with ethanol, tri-n-propylsilane, 2-methyl-2-propanol, 1-hexene and trimethylvinylsilane in cyclohexane at 296 K, and found that the rate constants for these reactions are significantly lower than those of the free $SiMe_2$.[5] On the basis of these results, they concluded that the availability of the vacant p-orbital on the Si atom is necessary for these reactions to be facile.

The kinetics of the reactions of germylene-alcohol or germylene-ether complexes has not yet been explored. However, Klein *et al.* reported that Me_2Ge-water or Me_2Ge-phenol complexes react with alkynes and alkenes (such as acrylonitrile and acrylic esters) to form addition products.[6] On the basis of these results, they concluded that germylene complexes can be considered as real intermediates that can undergo further reaction to give products.

It is interesting to investigate how coordination of the germylene to a Lewis base such as THF will affect the rates of those reactions that demand an initial electrophilic interaction of the germylene with the substrate. For example, theoretical calculations suggest that the reactions of germylene with carbon-carbon multiple bonds proceed through the formation of π-type complexes between the germylene and the substrate;[7,8] the reaction of a germylene with AcOH is also postulated to occur by an initial electrophilic interaction. Thus, the question remains as to whether the complex is reactive toward those scavengers. We also wanted to investigate whether the reactions of the Me_2Ge-THF complex with certain scavengers (e.g. diene and AcOH) afford the same final products as from reactions of the free $GeMe_2$. Furthermore, we were eager to know whether germyl cations or germyl anions are formed when these complexes are reacted with Brønsted acids or bases.

The reaction pathways for the free germylene and the complexed-germylene in the presence of an added scavenger (Q) in neat THF are shown in Scheme 5.1. If the complexation reaction is fast relative to k_Q and k'_Q, the overall observed rate constant for the reaction can be expressed by eq (5.2). In a situation when the reaction occurs only via the free germylene, k'_Q will be negligible, and the overall rate constant will be reduced to the first term (eq 5.3). In other words, the bimolecular rate constant (k_Q) determined in hexane will be reduced by a factor of ca. $1/K_{eq}[\mathrm{THF}]$. On the other hand, if the reaction proceeds only via the complex, the overall rate constant will be reduced to eq (5.4). It should be noted that under conditions where eq (5.2) holds, the observed rate constant is independent of which species is being monitored (either the free germylene or the complexed germylene). Given that the K_{eq} determined in hexane for the reaction of $GeMe_2$ with THF is 9800 ± 3800 M^{-1}, if the reaction proceeds only through free $GeMe_2$, we would expect a bimolecular rate constant of ca. 120,000 times slower in THF as compared to that in hexane, assuming there is no bulk solvent polarity effect on the rate constant (k_Q).

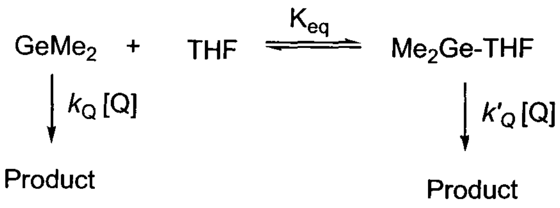

Scheme 5.1 Reaction pathways of $GeMe_2$ and Me_2Ge-THF complex in the presence of Q in neat THF.

$$k_{decay} = \left\{ \frac{1}{1+K_{eq}[\mathrm{THF}]} k_Q + \frac{K_{eq}[\mathrm{THF}]}{1+K_{eq}[\mathrm{THF}]} k'_Q \right\} [\mathrm{Q}] \qquad \mathbf{(5.2)}$$

If $k_Q >> k'_Q$, *then*

$$k_{decay} \sim \frac{k_Q}{K_{eq}[\mathrm{THF}]_Q} \qquad \mathbf{(5.3)}$$

Or if $k'_Q >> k_Q$

then $k_{decay} \sim k'_Q$ **(5.4)**

In this Chapter, we discuss the results of a study of the reactions of the Me_2Ge-MeOH complex with methanesulfonic acid ($MeSO_3H$), AcOH, and sodium methoxide (MeONa) in methanol solution. The reaction of the Me_2Ge-THF complex with AcOH, CCl_4, isoprene, 4,4-dimethyl-1-pentene, methanol, $MeSO_3H$ and MeONa in THF at 25 °C were also studied, and the rate constants obtained are compared to the corresponding ones for free $GeMe_2$ in hexane.

5.2 Direct detection and kinetic studies of the Me_2Ge-MeOH complex in methanol

5.2.1 Direct detection of the Me_2Ge-MeOH complex in methanol

Laser flash photolysis of **23** (ca. 7×10^{-5} M) in deoxygenated methanol afforded a single transient which exhibited $\lambda_{max} < 295$ nm. The absorption spectrum of the transient is essentially identical to the one recorded by laser photolysis of **23** in hexane containing methanol, and is thus assigned to the Me_2Ge-MeOH complex. The spectrum is shown in Figure 5.1, along with the transient absorption spectrum recorded in deoxygenated hexane containing 54 mM methanol. It is interesting to note that the absorption maximum recorded for the Ph_2Ge-MeOH complex is blue-shifted by ca. 30 nm in neat MeOH relative to its position in hexane solution containing small amounts of the alcohol.[9] This shift in the absorption maximum could be attributed to the effects of hydrogen-bonding with the solvent, or possibly to the formation of higher-order complexes (e.g. $Ph_2Ge-(ROH)_2$) in the neat alcohol. We are not able to make similar comparisons for the Me_2Ge-MeOH complex because its absorption band appears at very short wavelengths, on the edge of our lower detection limit. We believe that we are detecting only the long wavelength edge of the absorption spectrum of the species. It appears as a distinct band because of distortion of the true absorption due to ground state bleaching of the precursor (i.e **23**).

In methanol, the 300 nm transient decays with first-order kinetics (τ = 4 μs), and exhibits a much shorter lifetime and different kinetic behavior as compared to what was observed in dilute methanol solution in hexane. The change to first-order kinetics in methanol is consistent with solvent-catalyzed decomposition of the complex, presumably involving proton transfer to give hydridomethoxydimethylgermane. This suggestion is supported by theoretical studies, reported by Pliego and De Almeida for the reaction of dichlorocarbene with water.[10] A mechanism that involves a cyclic five-atom transition structure was proposed; the interaction occurs between the vacant p-orbital on the C atom and the lone pair of electrons on the oxygen of the water, and through H-bonding with the hydrogen from a second water molecule. Moreover, the two water molecules exist as dimers through H-bonding. The same mechanism is suggested here for $GeMe_2$ with methanol in neat methanol (as shown in Scheme 5.2). Our group also determined a kinetic isotope effect, k_H/k_D of 2.5 ± 0.8, for the first-order decay of the Ph_2Ge-MeOH and Ph_2Ge-MeOD complexes in MeOH and MeOD, respectively.[9] This result verifies that proton transfer must be responsible for the decay of the Ph_2Ge-MeOH complex and occurs in the rate-determining step of the reaction.

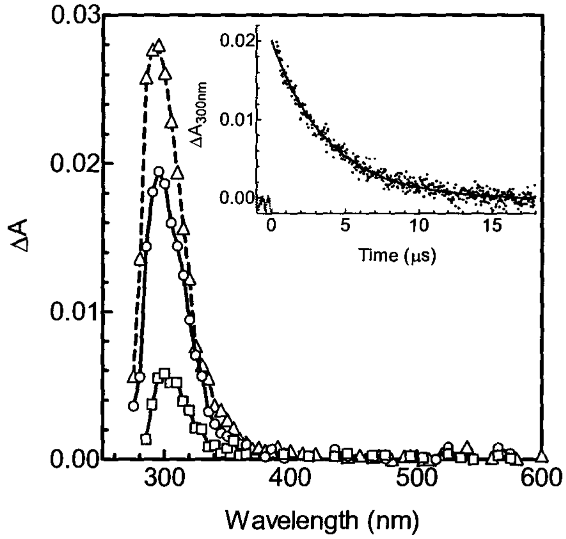

Figure 5.1. Transient absorption spectra recorded by laser flash photolysis of **23** in deoxygenated methanol, 0.19-0.32 μs (○) and 4.51-5.44 μs (□) after the laser pulse. The transient absorption spectrum recorded for **23** in deoxygenated hexane containing 0.054 M MeOH (0.16-0.22 μs (△) after the laser pulse) is also shown for comparison. The inset shows a transient decay profile recorded at 300 nm. The solid line represents the non-linear least-squares fit of the data to a single-exponential decay, according to eq (2.4) (k_{decay} = (2.60 ± 0.08) x 10^6 s^{-1}; R^2 = 0.9781).

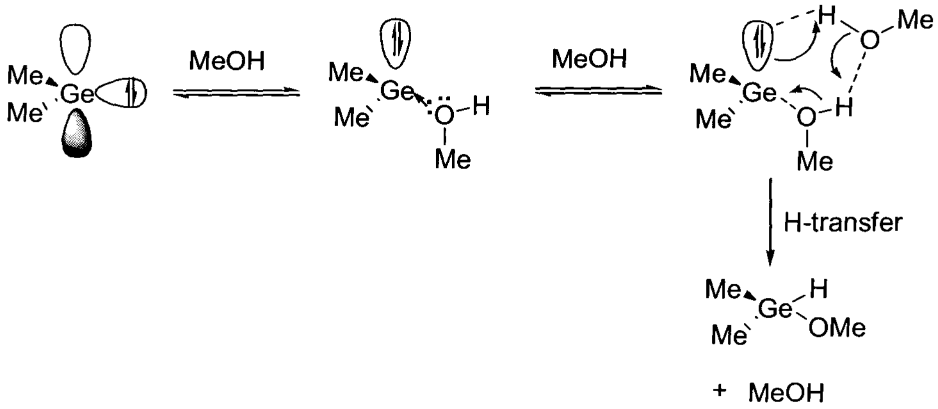

Scheme 5.2 Proposed mechanism for the solvent-catalyzed decay of the Me_2Ge-methanol complex in methanol.

5.2.2 Reactions of the Me_2Ge-MeOH complex with acids in MeOH solution

Addition of $MeSO_3H$ (0-0.6 mM) or AcOH (0-75 mM) to a solution of **23** (ca. 7 x 10^{-5} M) in methanol resulted in a shortening of the lifetime of the Me_2Ge-MeOH complex in proportion to concentration added. The decay profiles fit well to pseudo-first-order kinetics (eq 2.8), and the decay rates increase linearly with the nominal acid concentration, consistent with eq (2.17) (see Figure 5.2). The intercept of the plot (k_0) corresponds to the pseudo-first-order decay rate constant of the Me_2Ge-MeOH complex in the absence of the acid. The slope (k_Q) represents the bimolecular rate constant for the reaction of the Me_2Ge-methanol complex with the scavenger ($MeSO_3H$ or AcOH). The absolute rate constants for the reactions of the complex and the pK_a of the acid in methanol are given in Table 5.1.

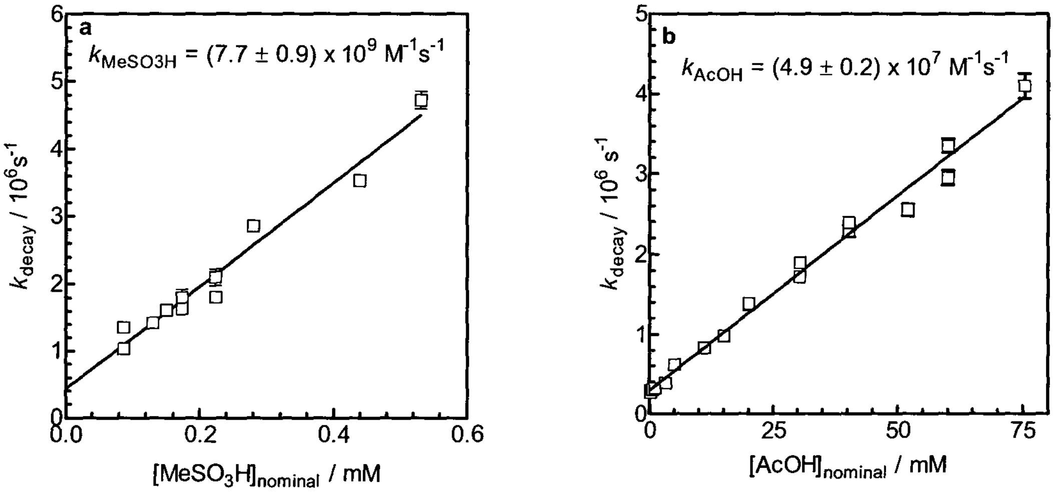

Figure 5.2. Effects of added (a) $MeSO_3H$ and (b) AcOH on the pseudo-first-order decay rate constants of the Me_2Ge-MeOH complex, monitored at 295 nm, in deoxygenated methanol at 25 °C. The solid lines are the best linear least-squares fit of the data to eq (2.17).

Table 5.1. Absolute rate constants for the reactions of the Me_2Ge-MeOH complex with Brønsted acids in deoxygenated methanol at 25 °C, and the pK_a values of the acids in methanol.

Scavenger	k_Q ($M^{-1}s^{-1}$)	pK_a
MeOH	$(2.57 \pm 0.07) \times 10^5$	16.71[a]
AcOH	$(4.9 \pm 0.2) \times 10^7$	9.63[b]
$MeSO_3H$	$(7.7 \pm 0.9) \times 10^9$	~ 3[c]

(a) Ref. 11; (b) Ref. 12; (c) pK_a of $MeSO_3H$ in MeOH was estimated based on the reported pK_a of $MeSO_3H$ in water (pK_a = -1.86 at 25 °C), and on comparisons of the pK_a of a series of carboxylic acids in methanol.[12,13] Errors are reported as ± 2σ from the linear least-squares analyses.

The pK_a of $MeSO_3H$ in methanol is not known; thus an estimate was made based on the observation that the pK_a values of a series of carboxylic acids in methanol differ from the aqueous pK_a's by a value of ca. +5.[12] The aqueous pK_a of $MeSO_3H$ is reported to be -1.86 at 25 °C;[13] if we assume that the same increment is valid for $MeSO_3H$, this affords an estimate of $pK_a = 3$ in methanol. The pK_a of AcOH is reported to be 9.63 in methanol at 25 °C.[12] Given that they are both weak acids in methanol, their percent dissociation decreases with increasing nominal concentration. The fact that the plots of k_{decay} versus $[Q]_{nominal}$ are linear in both cases indicates that the Me_2Ge-MeOH complex reacts unselectively toward both $Me_2Ge\text{-}MeOH_2^+$ and the undissociated acid. This observation is consistent with a mechanism that involves a general acid catalysis.

The rate constant for reaction of the Me_2Ge-MeOH complex with $MeSO_3H$ is approximately 200 times faster than that for AcOH, and suggests that the reaction involves a mechanism with a rate-determining protonation at Ge. However, further mechanistic study is needed to be able to postulate a mechanism for this reaction; parallel work has been performed in our group in order to get mechanistic details about these reactions, and these are discussed in section 5.2.4.

5.2.3 Reaction of the Me_2Ge-MeOH complex with MeONa

Addition of a solution of MeONa in methanol caused accelerations in the decay rates of the Me_2Ge-MeOH complex monitored at 295 nm (see Figure 5.3a). The decay profiles fit well to first-order kinetics, and a plot of k_{decay} versus [MeONa] is linear (Figure 5.3b), affording a bimolecular rate constant of $k_{MeO-} = (1.8 \pm 0.2) \times 10^9\ M^{-1}s^{-1}$. It is to be noted that in a control experiment we found that the addition of 5 M MeOH had no discernible effect on the decay rate of the Me_2Ge-THF complex, leading to estimate of 10^6 $M^{-1}s^{-1}$ for the upper limit of the rate constant for the reaction of the complex with methanol.

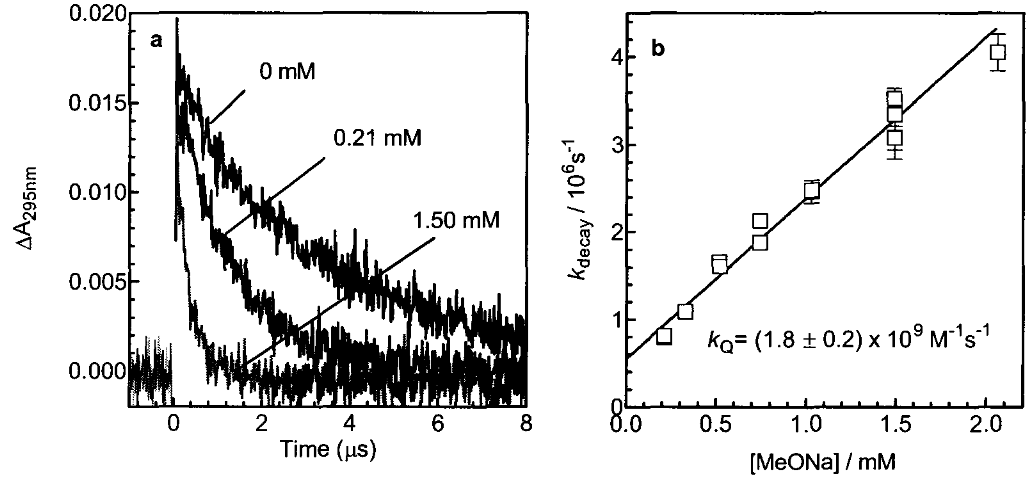

Figure 5.3. (a) Effects of added MeONa on the transient decay profiles of Me_2Ge-MeOH monitored at 295 nm by laser flash photolysis of **23** in deoxygenated methanol at 25 °C; (b) Plots of k_{decay} versus [MeONa] for the Me_2Ge-MeOH complex monitored at 295 nm. The solid line represents the linear least-squares fit to eq (2.17).

5.2.4 Mechanistic study of acid- or base-catalyzed decomposition of R_2Ge-MeOH complexes in neat MeOH

A similar study was carried out in our group for the reactions of Ar_2Ge-MeOH complexes (**43b**-**43e**) with $MeSO_3H$ in neat methanol.[14] A kinetic isotope effect of k_H/k_D = 2.2 ± 0.2 was determined for the reactions of the $(4-(CF_3)C_6H_4)_2Ge$-MeOL complex

(**43e**; L = H or D) with $MeSO_3L$ in MeOL. This result supports a mechanism that involves a proton transfer in the rate-determining step. In addition, a Hammett plot of the rate constants for the reaction of Ar_2Ge-MeOH complexes (**43b**-**43e**) with $MeSO_3H$ afforded a reaction constant of $\rho = -0.56 \pm 0.08$. This result indicates that positive charge is developed at the germanium center in the transition state for the rate-determining step in the reaction. On the basis of these results, it is postulated that the reaction of the R_2Ge-MeOH complex in the presence of the added acid occurs by an initial rate-determining protonation of the germylene-methanol complex by the lyonium ions to form a solvated germyl cation, followed by a rapid loss of a proton to the solvent to give the corresponding alkoxygermane (Scheme 5.3).

We did not obtain any UV-Vis spectroscopic evidence for the formation of a germyl cation intermediate in our experiments because they are most likely too short-lived in neat MeOH to be observed by our technique. However, in the case of **43b**, an indication for the formation of a new transient species exhibiting transient absorption band in the neighborhood of the complex was observed. However, the data did not allow any further conclusive study due to fluorescence and the fact that the transient species was short-lived.[14]

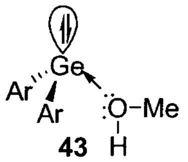

43

a Ar = Ph
b Ar = 4-MeC_6H_4
c Ar = 3,4-$Me_2C_6H_3$
d Ar = 4-FC_6H_4
e Ar = 4-$(CF_3)C_6H_4$

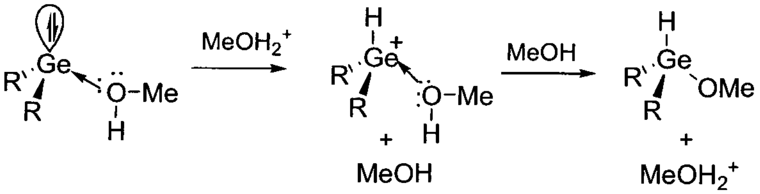

Scheme 5.3 Reactions of R_2Ge-MeOH complex in the presence of a Brønsted acid in neat MeOH.

Another study, carried out in our group, for the reactions of the Ar_2Ge-MeOH complexes (**43a**-**43e**) with MeONa in MeOH showed that the rates of these reactions increase with increasing electron-withdrawing power of the substituents on the aromatic rings.[14] A Hammett reaction constant of $\rho = +0.16 \pm 0.08$ was obtained from a plot of $\log(k_{MeONa})$ versus $\Sigma\sigma$. In any case, the positive ρ value is consistent with negative charge development at Ge in the transition state of the rate-determining step of the reaction. No new transients were observed from the reactions of Me_2Ge-MeOH and Ar_2Ge-MeOH complexes with MeONa with the exception of **43e**, in which case the formation of a new transient species that absorbs in the same spectral region of the absorptions due to the complex was observed. The new transient species was assigned to the corresponding $Ar_2(OMe)Ge^-$ anion.[14] It is thus clear that the reaction of R_2Ge-MeOH complex with

MeO^- in MeOH affords the corresponding R_2GeOMe^- anion, which undergoes rapid protonation by the solvent.

A kinetic isotope effect, $k_H/k_D = 1.40 \pm 0.07$, was obtained from the reactions of Ph_2Ge-MeOL (L = H or D) complex with MeONa in MeOL. The results did not enable us to distinguish whether this should be interpreted as a primary isotope effect due to rate-determining proton transfer or a secondary kinetic isotope effect due to nucleophilic displacement of the coordinated MeOH molecule by the more nucleophilic methoxide ion.

Two possible reaction mechanisms can be proposed for the reaction of the R_2Ge-MeOH complex with MeONa, as shown in Scheme 5.4. The first is a stepwise mechanism that proceeds by deprotonation of the coordinated MeOH in the complex by the methoxide ion in the rate-determining step to form a germyl anion. This is followed by protonation by solvent in a subsequent fast step to give the product. The second possible mechanism involves nucleophilic displacement of the coordinated MeOH by methoxide ion to form the germyl anion intermediate, followed by protonation by the solvent.

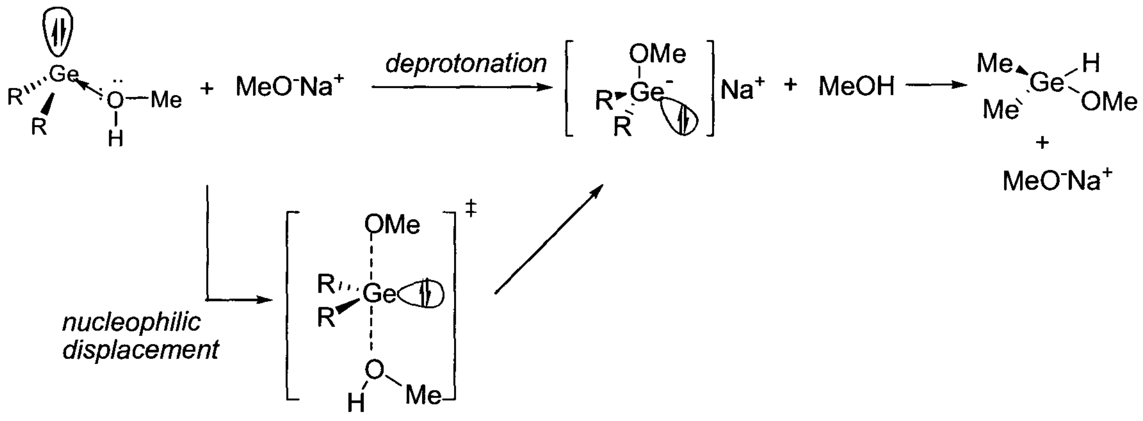

Scheme 5.4 Proposed mechanisms for the reactions of germylene-MeOH complexes with MeONa in MeOH.

It is noteworthy that Satgé *et al.* reported that $Me_2Ge(H)OMe$ is unstable in MeOH, and decomposes by α-elimination to generate the germylene.[15] This process is known to be catalyzed by the presence of methoxide ions. Therefore, the studies in the presence of MeONa, discussed above define the kinetics of certain aspects of the reverse process associated with the base-catalysed α-elimination of alkoxygermanes.

5.3 Reactivity of the Me_2Ge-THF complex in THF

5.3.1 Steady state photolysis of 1,1-dimethyl-3-phenylgermacyclopent-3-ene in THF-d_8 in the presence of AcOH and $MeSO_3H$

An argon-saturated solution of **23** (0.025 M) in THF-d_8 containing AcOH (0.04 M) and hexamethyldisilane (0.005 M; integration standard) at 25°C was irradiated (254 nm, 6 low-pressure mercury lamps) on a merry-go-round apparatus and the photolysis mixture was monitored periodically by ^1H NMR spectroscopy. Figure 5.4 shows the ^1H NMR spectra recorded before and after 40 % conversion of **23**. The ^{1}H NMR spectra showed peaks consistent with the formation of acetoxydimethylgermane **34** (δ 5.60 (sept, 1H, ^3J = 2.4 Hz), 1.92 (s, 3H), 0.58 (d, 6H, ^3J = 2.4 Hz) ppm), and diene **28** (δ 7.26-7.33 (m, 6H), 6.63 (dd, 1H; ^3J = 10.8, 17.4 Hz), 5.13-5.18 (m, 4H) ppm). The concentrations of the reactants and products were determined from the integrals relative to that of the integration standard, and plotted versus time in the usual way. The yields of **28** and **34** were determined from the slopes of the concentration versus time plots relative to consumed **23** over the range of 0-40 % conversion of **23**, and were found to be 86 % and 97 %, respectively (Figure 5.5). The result shows that generation of $GeMe_2$ in THF containing AcOH leads to the same Ge-derived product as in hexane under otherwise similar conditions, and that the photochemistry of **23** is the same in THF as in hexane (eq 5.5).

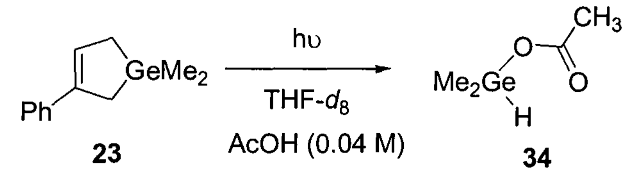

(5.5)

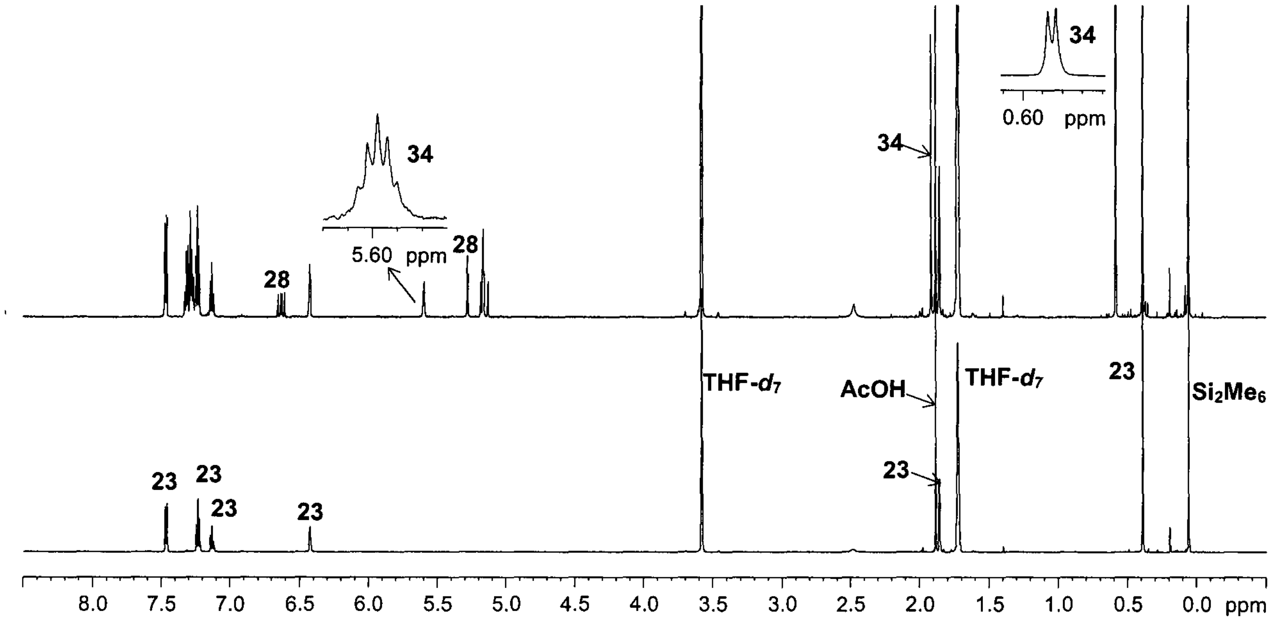

Figure 5.4. ^{1}H NMR spectra (600 MHz) of the crude photolysis mixture of **23** (0.025 M) and AcOH (0.04 M) in deoxygenated THF-d_8: (a) before photolysis, and (b) after 40 % conversion of **23**. The insets are expansions of the Ge-$\underline{H}$ and Ge(C$\underline{H}_3$)$_2$ peaks due to the major product **34**.

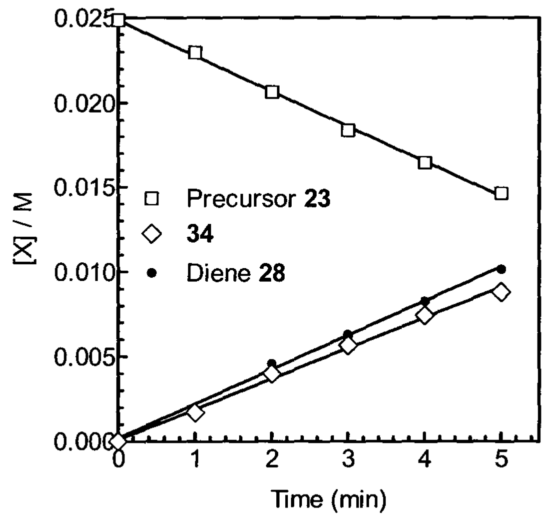

Figure 5.5. Concentration versus time plots for $GeMe_2$ precursor **23**, diene **28** and insertion product **34** as a function of photolysis time, from irradiation of a mixture of **23** (0.025 M) and AcOH (0.04 M) in THF-d_8. Hexamethyldisilane was used as integration standard. The slopes are: **23**, $(-2.08 \pm 0.04) \times 10^{-3}$; **34**, $(1.83 \pm 0.03) \times 10^{-3}$ and **28**, $(2.07 \pm 0.03) \times 10^{-3}$.

An argon-saturated solution of **23** (0.035 M) in the presence of $MeSO_3H$ (0.09 M) and hexamethyldisilane (0.006 M) in THF-d_8 was irradiated using 6 low-pressure mercury lamps (254 nm) and the course of the reaction was monitored periodically by ^1H NMR spectroscopy (600 MHz) up to 60 % conversion of **23**. The ^1H NMR spectra recorded before and after 60 % conversion of **23** are shown in Figure 5.6. The ^1H NMR spectra show the presence of three doublets: δ 0.42 ppm, 0.52 ppm and 0.76 ppm, and a septet at δ 5.9 ppm, whose intensities increase with photolysis times (these are shown more clearly in Figure 5.7). Figure 5.8 shows the concentration versus time plots for the precursor **23**, the diene **28**, and peaks at δ 0.76 ppm (doublet) and δ 5.90 ppm (septet). The concentrations at each time interval were calculated using the peak for hexamethyldisilane as integration standard. The ratio of the slope of the plot for precursor **23** to that for the diene **28** shows that the latter is formed quantitatively. The slope of the plot for the peak at 0.76 ppm (d, $^3J = 2.0$ Hz, 6H assumed) closely matches that for the septet at 5.9 ppm (sept, ^3J = 2.0 Hz, 1H) strongly suggesting they belong to the same product. By comparison with the chemical shift for the acetoxygermane **34**, we assign these peaks to the insertion product **44** (see eq 5.6), which in this case is formed in ca. 43 % yield (calculated from the ratio of the slopes over t = 3 min). We note that the plot was not linear after 3 mins, indicating that the product is not stable. We were not able to identify the other peaks in the spectrum. An attempt to isolate products from the reaction mixture was made by neutralizing the acid with aqueous sodium carbonate, extracting the organic layer with diethyl ether, and then subjecting to micro-column chromatography on silica gel. The ^{1}H NMR spectrum of the various evaporated residue of the fractions isolated from the column revealed substantial decomposition, so we did not pursue a more rigorous identification of the products.

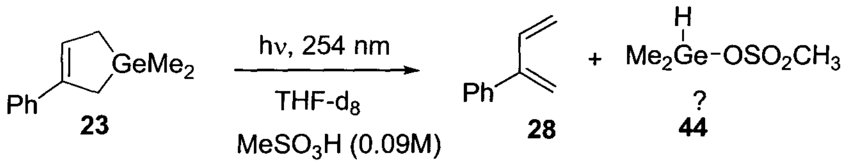

(5.6)

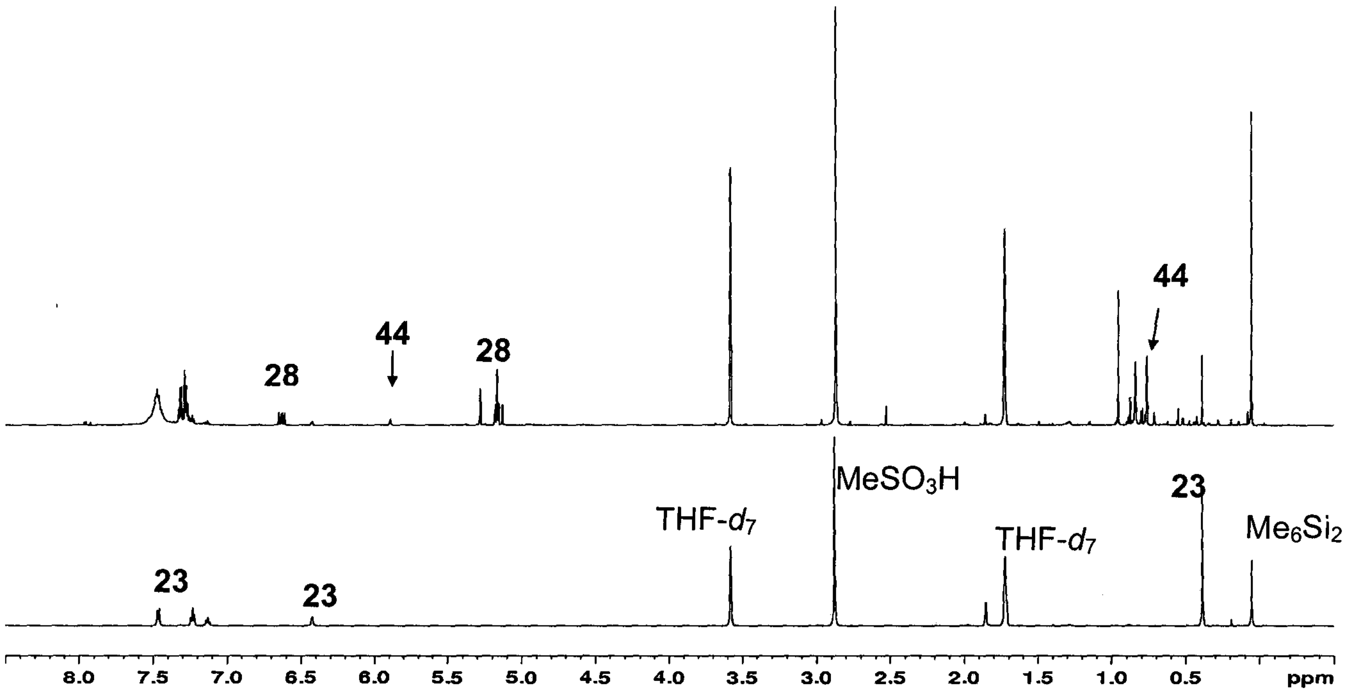

Figure 5.6. (a) ^{1}H NMR (600 MHz) spectrum of crude photolysis mixture recorded after 60 % conversion of irradiation of **23** in the presence of $MeSO_3H$, and (b) ^{1}H NMR (600 MHz) spectrum of starting mixture (0.035 M of **23**, and 0.09 M $MeSO_3H$ in THF-d_8) at t = 0 min. Hexamethyldisilane was used as an integration standard.

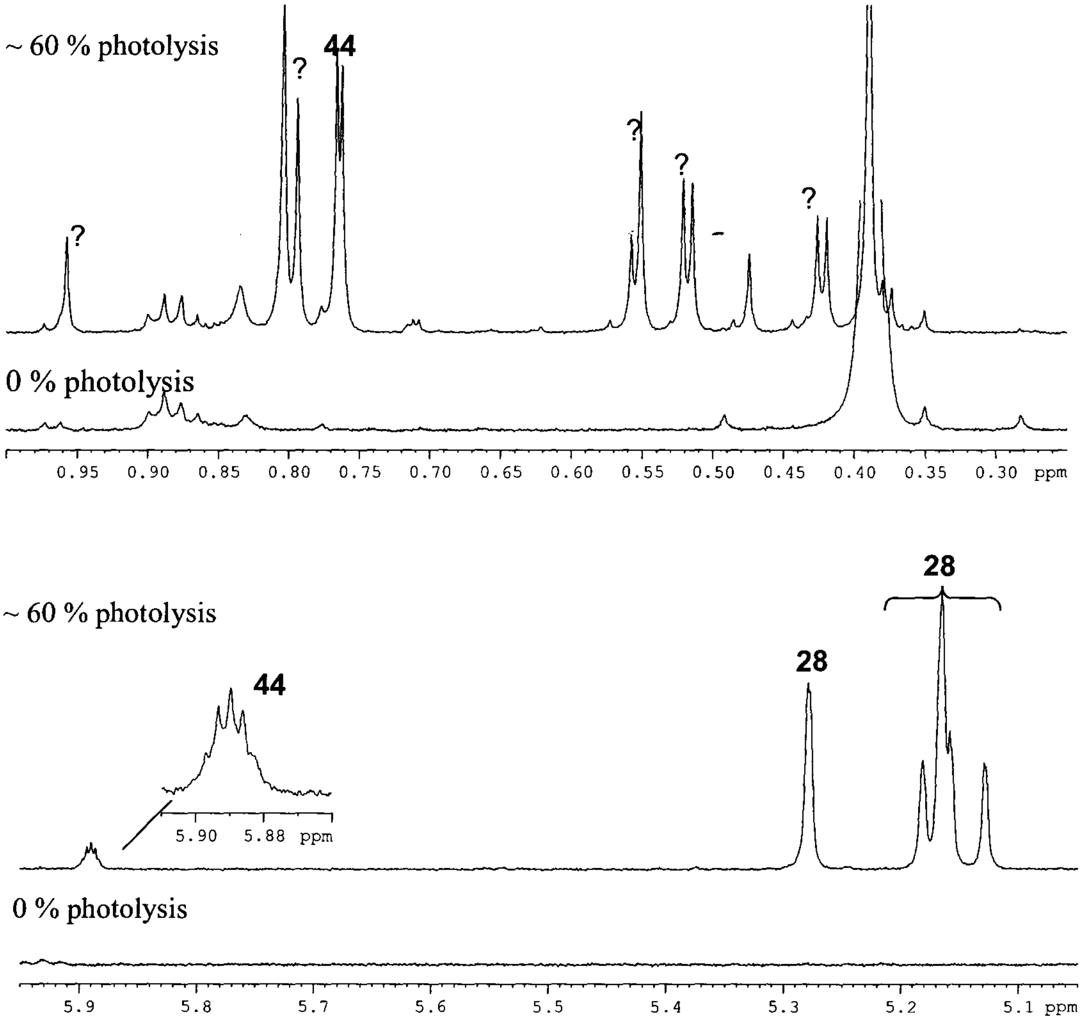

Figure 5.7. Expanded ^{1}H NMR spectra (600 MHz) of photolysis mixture of **23** (0.035 M) and MeSO3H (0.09 M) in THF-d_8 before irradiation and after 60 % conversion.

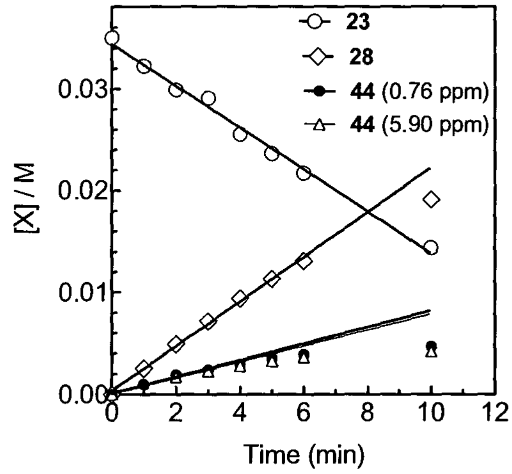

Figure 5.8. Plot of concentration for $GeMe_2$ precursor **23** (○), diene **28** (◇) and insertion product **44** (•, △) as a function of photolysis time of a mixture of **23** (0.035 M) and $MeSO_3H$ (0.09 M) in deoxygenated THF-d_8. Slopes are: **23**, (-2.20 ± 0.01) x 10^{-3}; **28**, (+2.27 ± 0.05) x 10^{-3}; **44**, (+0.96 ± 0.03) x 10^{-3}.

5.3.2 Direct detection and kinetic studies of the Me_2Ge-THF complex in THF

Laser flash photolysis of **23** in deoxygenated THF led to the formation of a species exhibiting λ_{max} ~ 310 nm, which is formed with the laser pulse (Figure 5.9). Under these conditions, the absorption band at 470 nm corresponding to free $GeMe_2$ is not observed; however, the characteristic absorption band due to Ge_2Me_4 (λ_{max} = 370 nm) is observed to grow in over the first ca. 2 μs after the pulse. Given the K_{eq} measured for the reaction of $GeMe_2$ with THF in hexane (K_{eq} = 9800 ± 3800 M^{-1}), and the fact that $GeMe_2$ is not detectable in neat THF, the formation of Ge_2Me_4 in THF under these conditions indicates that it must be formed by dimerization of the complex.

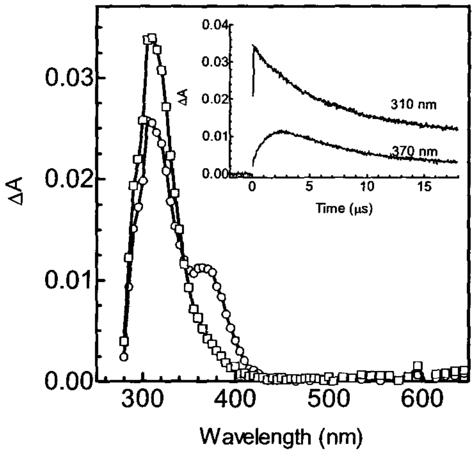

Figure 5.9. Transient absorption spectra recorded by laser flash photolysis of **23** (ca. 70 μM) in THF at 0.16 – 0.29 μs (□) and 2.75 – 2.98 μs (○) after the laser pulse. The inset shows transient decay/growth profiles at monitoring wavelengths 310 nm and 370 nm.

Interestingly, there is a blue-shift in the absorption band of the Ph_2Ge-THF complex in THF (λ_{max} = 340 nm) as compared to that observed in hexane containing small amounts of THF (λ_{max} = 355 nm).[14] This blue shift in the absorption band with increasing THF concentration may be due to greater stabilization of the ground state of the complex due to greater electrostatic dipole-dipole interaction in THF.[16] In the case of the Me_2Ge-THF complex, it was not possible to discern such a blue-shift in the absorption maximum because the absorption is found near that of the precursor.

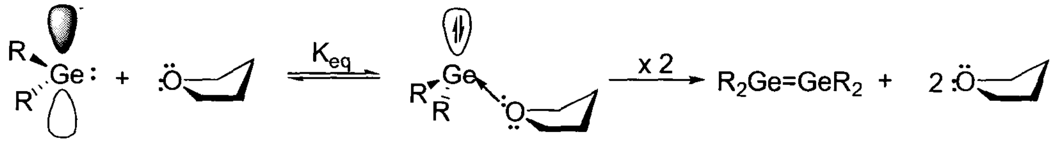

Scheme 5.5 Reactions of GeR_2 and the R_2Ge-THF complex in THF.

5.3.3 Reactions of the Me_2Ge-THF complex with acids in THF

The Brønsted basicity of the Me_2Ge-THF complex in THF was investigated by probing its reactions with $MeSO_3H$ and AcOH. The pK_a of AcOH in THF is reported to be 24.4,[17] and the pK_a of $MeSO_3H$ was estimated to be ~ 15 from its aqueous pK_a, based on the reported pK_a's of CF_3SO_3H in THF (pK_a ~ 7.8[18]) and water (pK_a ~ -5.9[19]). Addition of increasing concentrations of $MeSO_3H$ or AcOH led to enhancements in the decay rates of the Me_2Ge-THF complex and caused it to decay with first-order kinetics. Representative plots of the decay profiles recorded at 310 nm for $MeSO_3H$ are shown in Figure 5.10a. Plots of k_{decay} versus [Q] were linear (Figure 5.10b), and were analyzed according to eq (2.17).

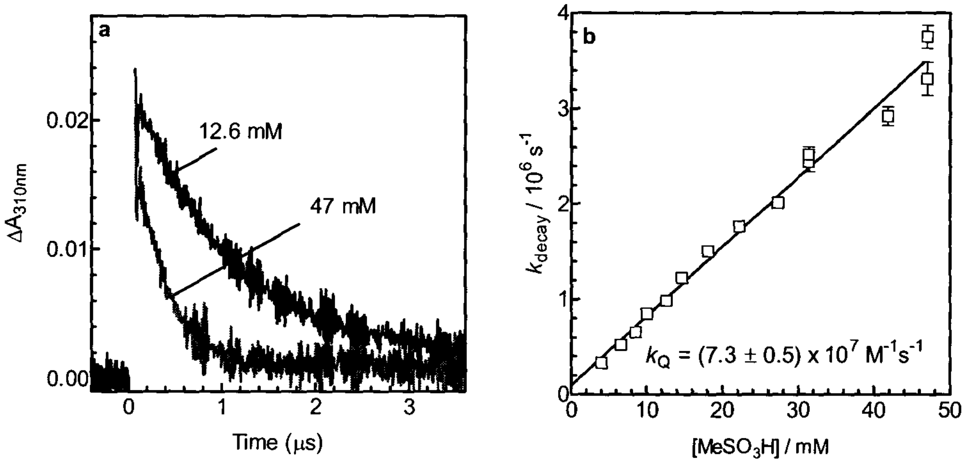

Figure 5.10. (a) Effects of added $MeSO_3H$ on the transient decay profiles recorded at 310 nm by laser flash photolysis of **23** in deoxygenated THF; (b) Plots of k_{decay} versus [$MeSO_3H$]. The solid line represents the linear least-squares fit of the data to eq (2.17).

Similar results were obtained when AcOH (k_{AcOH} = (1.3 ± 0.1) x 10^7 $M^{-1}s^{-1}$) was used as the scavenger. The rate constant determined for the reaction of the Me_2Ge-THF complex with AcOH is only ca. 500 times slower than that of free $GeMe_2$ with the same scavenger in hexane, thus indicating that the reaction in THF involves the complex and not the free germylene. The reaction of germylenes with AcOH in hexane is also postulated to occur by initial complexation.[20] A primary kinetic isotope effect (k_H/k_D) of 2.8 ± 0.4 was obtained from the ratio of the rate constants for quenching by AcOH and AcOD, indicating that proton transfer occurs in the rate-determining step of the reaction. Figure 5.11 shows the plots of k_{decay} versus [AcOL] for the reactions of Me_2Ge-THF complex with AcOL (L= H or D) in THF. The fact that k_{AcOH} is only ~ 5 times smaller than k_{MeSO3H} in THF, as compared to 200 times smaller in MeOH suggests a different mechanism for these reactions in methanol and THF.

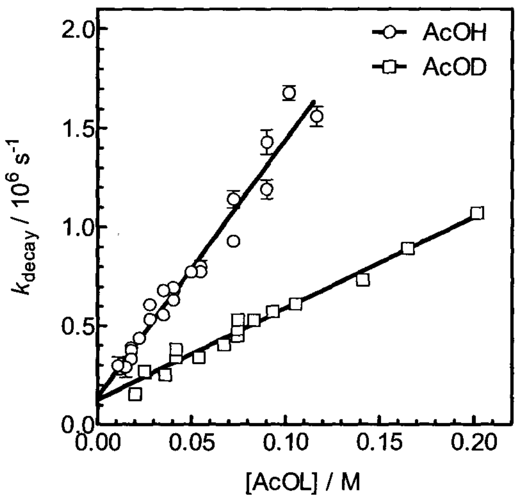

Figure 5.11. Plots of k_{decay} versus [AcOL] for quenching of the Me_2Ge-THF complex by AcOH (○) and AcOD (□) in THF at 25 °C. The solid lines are the linear least squares fits of the data to eq (2.17). The slopes are: $k_{AcOH} = (1.3 \pm 0.1) \times 10^7$ $M^{-1}s^{-1}$ and $k_{AcOD} = (4.6 \pm 0.4) \times 10^6$ $M^{-1}s^{-1}$.

A similar study in our group for the reactions of a series aryl-substituted germylene-THF complexes **45a-e** with $MeSO_3H$ in THF was performed. A Hammett plot for the reactions of **45a-e** afforded a reaction constant, $\rho = -0.17 \pm 0.01$, consistent with positive charge development at the Ge in the rate-determining step of the reaction.[9] The magnitude of this ρ-value is significantly smaller than the one determined from the reactions of Ar_2Ge-MeOH complexes **43a-e** with $MeSO_3H$ in MeOH. This suggests that there is relatively less positive charge development at the germanium center in the transition state of the rate-determining step in THF. The results favor a mechanism involving a concerted proton transfer from the acid to the germanium center, accompanied by displacement of the solvent molecule in the complex, as depicted in Scheme 5.6.

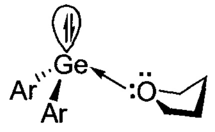

45

a Ar = Ph
b Ar = 4-MeC_6H_4
c Ar = 3,4-$Me_2C_6H_3$
d Ar = 4-FC_6H_4
e Ar = 4-$(CF_3)C_6H_4$

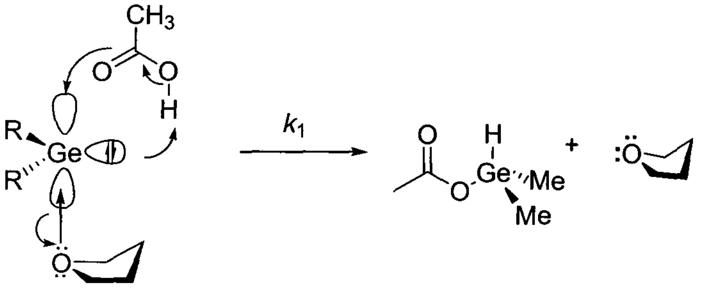

Scheme 5.6 Postulated mechanism for the reaction of the Me_2Ge-THF complex with AcOH in THF.

5.3.4 Reaction of the Me_2Ge-THF complex with MeONa

Addition of MeONa (added as a 0.1 M solution in MeOH) to a deoxygenated solution of **23** in THF also caused accelerations in the decay rates of the Me_2Ge-THF complex. The plot of k_{decay} versus [MeONa] was linear according to eq (2.17), see Figure 5.12. Interestingly, the bimolecular rate constant obtained for the reaction of the Me_2Ge-THF complex with MeONa, $k_{MeO^-} = (1.14 \pm 0.08) \times 10^9$ $M^{-1}s^{-1}$ is only slightly lower than that for the reaction of the Me_2Ge-MeOH complex with MeONa in MeOH ($k_{MeO^-} = (1.8 \pm$

0.2) x 10^9 $M^{-1}s^{-1}$). This observation suggests a similar type of reaction mechanism in both cases. Similar research work in our group showed that quenching of Ar_2Ge-THF complexes (**45a**-**e**, with the exception of **c** which was not studied) with MeONa (added as a 0.5 M solution in MeOH) revealed the formation of new transient species in each case. These were assigned to the corresponding $Ar_2(OMe)Ge^-$ anions.[9] A Hammett reaction constant of $\rho = +0.7 \pm 0.3$ was obtained, indicating substantial negative charge development at Ge in the transition state for the rate-determining step. The results are consistent with nucleophilic displacement of the coordinated THF in the complex by methoxide ion (Scheme 5.7). Mochida *et al.* previously reported an absorption maximum of 310 nm for $Ph_2MeGe^-Li^+$ anions in THF.[21] No spectral evidence for the formation of $Me_2(OMe)Ge^-$ anions could be obtained from our experiments, perhaps because the absorption spectrum is outside (i.e. to the blue) of the spectral range that can be monitored.

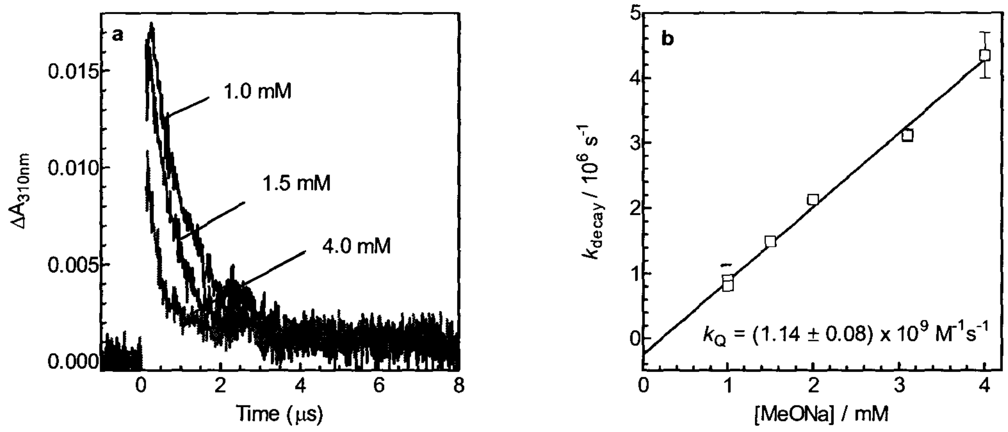

Figure 5.12. (a) Effects of added MeONa (as a 0.1 M solution in MeOH) on the transient decay profiles recorded at 310 nm, from laser flash photolysis of **23** in deoxygenated THF at 310 nm; (b) Plots of k_{decay} versus [MeONa]; the solid line represents the linear least-squares fit of the data to eq (2.17).

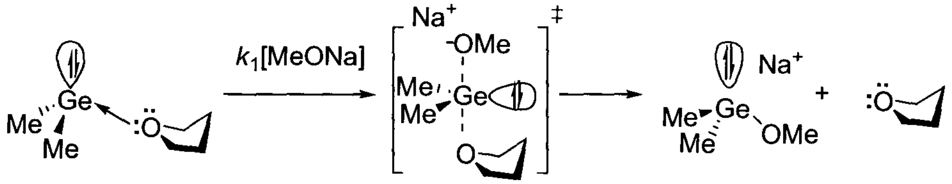

Scheme 5.7 Postulated mechanism for the reaction of the Me_2Ge-THF complex with MeONa in THF.

5.3.5 Reactions of the Me_2Ge-THF complex with other scavengers

The reactivity of the Me_2Ge-THF complex was also examined with oxygen, carbon tetrachloride (CCl_4), 4,4-dimethyl-1-pentene (DMP) and isoprene. In the presence of CCl_4, the decay profiles of the complex fit to first-order kinetics, and the plots of k_{decay} versus [scavenger] were linear. Figure 5.13 shows typical transient decay profiles recorded at 310 nm in the presence of a scavenger (for e.g. CCl_4), and the plot of k_{decay} vs. $[CCl_4]$.

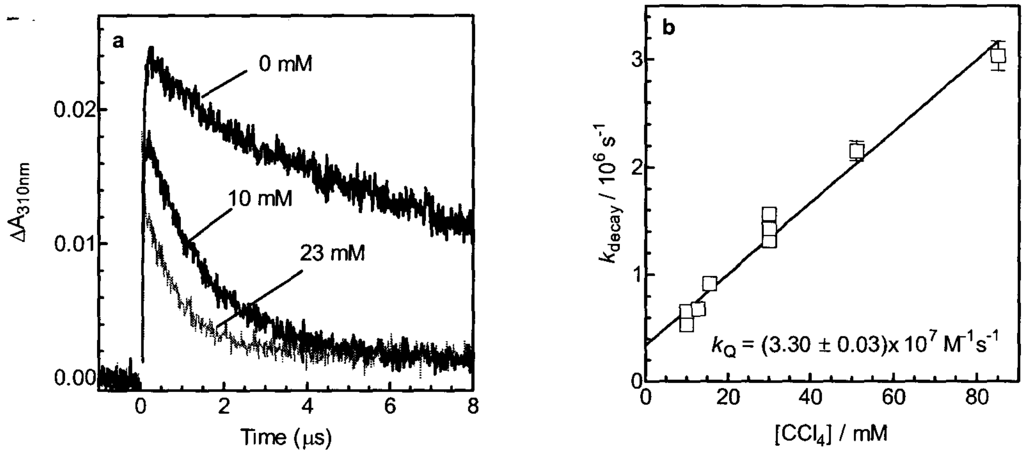

Figure 5.13. (a) Effects of added CCl_4 on the transient decay profiles recorded at 310 nm; (b) Plots of k_{decay} versus $[CCl_4]$ for the reactions of the Me_2Ge-THF complex with CCl_4 in THF.

Saturation of the solution with air or oxygen led to a slight increase in the decay rate of the complex, as shown in Figure 5.14. The decay profile in air-saturated THF did not fit to first-order kinetics. However, the decay profile in oxygen-saturated THF fit reasonably to first-order kinetics, affording a lifetime $\tau \sim 6$ μs. This corresponds to a bimolecular rate constant of $k_Q \sim 1.5 \times 10^7$ $M^{-1}s^{-1}$ for the reaction of the Me_2Ge-THF complex with oxygen.

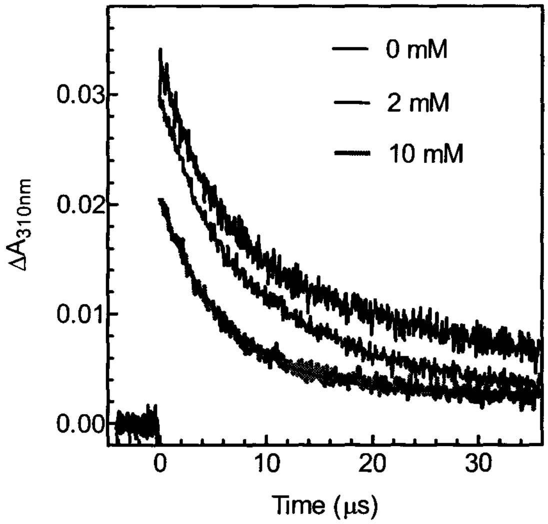

Figure 5.14. Effects of oxygen on the transient decay profiles recorded at 310 nm by laser flash photolysis of **23** in THF. The solid line represents the non-linear best fit line to eq (2.4), affording $k_{\text{decay}} = (1.56 \pm 0.04) \times 10^5\ s^{-1}$ ($R^2 = 0.9857$).

Addition of DMP or isoprene had only small effects on the decay rates of the Me_2Ge-THF complex. In these cases, the decay profiles fit approximately to first-order kinetics and upper limits of the rate constants were estimated at the highest concentration of the scavenger used, by dividing the decay rate constant obtained by that concentration. The rate constants for the reactions of Me_2Ge-THF complex determined in this work are listed and compared to the values determined for free $GeMe_2$ with the same reagents in Table 5.2.

Table 5.2. Rate constants for the reactions of the Me_2Ge-THF complex in deoxgenated THF and free $GeMe_2$ in deoxygenated hexane at 25 °C[a].

	Me_2Ge-THF complex (in THF)	$GeMe_2$[b] (in hexane)	k_{hex}/k_{THF}
λ_{max} (nm)	≤ 310	470	
Scavenger	k_Q / 10^7 M^{-1} s^{-1}		
$MeSO_3H$	7.3 ± 0.5	-	-
MeONa/MeOH	114 ± 8	-	-
AcOH	1.4 ± 0.1	750 ± 40	536
CCl_4	3.3 ± 0.3	8 ± 2	~ 3
DMP	< 0.23 (100 mM)[c]	890 ± 80	~ 3900
Isoprene	< 0.4 (8 mM)[c]	1080 ± 280	~ 2700
O_2	1.6 ± 0.5[d]	9 ± 1	5

(a) Errors are reported as ± 2σ; (b) From ref 22; (c) Upper limits were estimated at the concentrations indicated in parentheses; (d) Calculated from the first-order lifetime in O_2-saturated THF (10.7 mM O_2).

Reactions with DMP and isoprene are markedly impeded in THF, for e.g., the rate for the reaction of Me_2Ge-THF complex with isoprene is at least 2700 times slower than that of $GeMe_2$. The substantial retardation in the rates of these reactions in THF indicates that the availability of the vacant p orbital on the germanium center is important for these reactions to be facile. Indeed, this is consistent with theoretical predictions that the mechanism involves the initial formation of a π complex with the alkene, alkyne or diene, in which GeR_2 behaves as an electrophile.[7,23,24] It is also consistent with recent experimental kinetic studies on the reactions of diarylgermylenes with dienes, which demonstrate a strong dependence of the rate constants for reaction on germylene electrophilicity for both the (1+2)- and (1+4)-cycloaddition pathways.[25,26]

Interestingly, the rate constant obtained for the reaction of the Me_2Ge-THF complex with CCl_4 ($k_Q = (3.30 \pm 0.03) \times 10^7$ $M^{-1}s^{-1}$) is only ca. three times slower than that determined for the reaction of free $GeMe_2$ with CCl_4 in hexane ($k_Q = (8 \pm 2) \times 10^7$ $M^{-1}s^{-1}$). This small difference in the reactivity of the Me_2Ge-THF complex and free $GeMe_2$ suggests that another mechanism, other than an initial complexation of CCl_4, is important for the reaction of the complex. One possibility is an electron transfer mechanism, which has previously been proposed for the reactions of some germylenes with halocarbons.[27] The rates of electron transfer reactions are accelerated in polar solvents, thus we might speculate that if there is a contribution from this type of mechanism, this could compensate for the rate retardation caused by complexation of $GeMe_2$ with THF. Further study is required to address these mechanistic concerns.

5.4 Summary and Conclusions

Laser flash photolysis of **23** in deoxygenated MeOH or THF affords transient absorptions at short wavelengths assignable to the Me_2Ge-MeOH (λ_{max} < 295 nm) and Me_2Ge-THF (λ_{max} < 310 nm) complexes. In MeOH, the Me_2Ge-MeOH complex decomposes mainly by a solvent-catalyzed pathway. The decay of the complex is enhanced considerably in the presence of added acid or base ($MeSO_3H$ and MeONa; $k_Q > 10^9$ M^{-1} s^{-1}). The results suggest that the reactions with acids proceed by initial rate-determining protonation at Ge, followed by fast deprotonation from oxygen. On the other hand, the reaction of the Me_2Ge-MeOH complex with MeONa in MeOH is proposed to occur either by deprotonation or by nucleophilic displacement to form the $Me_2(MeO)Ge^-$ anion in the rate determination step, the latter undergoes rapid protonation by the solvent to yield $Me_2Ge(OMe)H$.

The Me_2Ge-THF complex reacts with MeONa at close to the diffusion-controlled rate in THF. We suggest that the reaction occurs by nucleophilic displacement of the complexed THF to form the methoxydimethylgermyl anion as the primary transient product. The Me_2Ge-THF complex is also reactive toward $MeSO_3H$ and AcOH, and the rate constant decreases with decreasing acid strength. A primary kinetic isotope effect (k_H/k_D) of ca. 2.8 ± 0.2 was obtained for scavenging of the Me_2Ge-THF complex with AcOH and AcOD, consistent with a mechanism that involves proton transfer in the rate-determining step. The Me_2Ge-THF complex is less reactive toward $MeSO_3H$ and AcOH compared to the Me_2Ge-MeOH complex in MeOH, because these acids are not appreciably dissociated in THF. A mechanism involving concerted nucleophilic displacement of the coordinated solvent and proton transfer to germanium is consistent with the data.

The relative rate constant of the reactions of free $GeMe_2$ to that of the Me_2Ge-THF complex ($k_{GeMe2}/k_{Me2Ge\text{-}THF}$) with CCl_4 ($k_{GeMe2}/k_{Me2Ge\text{-}THF} \sim 3$), O_2 ($k_{GeMe2}/k_{Me2Ge\text{-}THF} \sim 6$) and AcOH ($k_{GeMe2}/k_{Me2Ge\text{-}THF} \sim 500$) suggest that these reactions occur through the Me_2Ge-THF complex, through different mechanistic pathways than those involving the free germylene. On the other hand, we have observed that the Me_2Ge-THF complex reacts very slowly ($k_Q < 10^6$ $M^{-1}s^{-1}$) with 4,4-dimethyl-1-pentene and isoprene as compared to the free germylene ($k_Q > 10^9$) in hexane. These results indicate that the vacant p-orbital on the germanium atom plays a critical role in the mechanism of these reactions, with the germylene acting as an electrophile and the alkene or diene as a nucleophile.

References

1. Ando, W.; Itoh, H.; Tsumuraya, T. *Organometallics* **1989**, *8*, 2759.
2. Gillette, G. R.; Noren, G. H.; West, R. *Organometallics* **1989**, *8*, 487.
3. Steele, K. P. and Weber, W. P. *J. Am. Chem. Soc.* **1980**, *102*, 6095.
4. Gillette, G. R.; Noren, G. H.; West, R. *Organometallics* **1987**, *6*, 2617.
5. Levin, G.; Das, P. K.; Lee, C. L. *Organometallics* **1988**, *7*, 1231.
6. Klein, B.; Neumann, W. P.; Weisbeck, M. P.; Weinken, S. *J. Organomet. Chem.* **1993**, *446*, 149.
7. Becerra, R.; Boganov, S. E.; Egorov, M. G.; Faustov, V. I.; Promyslov, V. M.; Nefedov, O. M.; Walsh, R. *Phys. Chem. Chem. Phys.* **2002**, *4*, 5079.
8. Su, M.-D. *Chem. Eur. J.* **2004**, *10*, 6073.
9. Lollmahomed, F.; Huck, L. A.; Harrington, C. R.; Chitnis, S. S.; Leigh, W. J. *Organometallics* **2009**, *28*, 1484.
10. Pliego, J. R. J. and De Almeida, W. B. *J. Phys. Chem.* **1999**, *103*, 3904.
11. Leung, C. S. and Grunwald, E. *J. Phys. Chem.* **1970**, *74*, 696.
12. Rived, F.; Rosés, M.; Bosch.E. *Analyt. Chim. Acta* **1998**, *374*, 309.
13. Serjeant, E. P.; Dempsey, B. *Ionisation of Organic Acids in Aqueous Solution*, Pergamon Press, New York: 1979; 989.
14. Lollmahomed, F.; Huck, L. A.; Harrington, C. R.; Chitnis, S. S.; Leigh, W. J. *Organometallics* **2009**, *28*, 1484.

15. Satge, J.; Massol, M.; Riviere, P. *J. Organomet. Chem.* **1973**, *56*, 1.
16. Reichardt, C. *Solvents and solvent effects in organic chemistry*, Wiley-VCH: Weinheim, 2003; 329.
17. Barron, D.; Buti, S.; Ruiz, M.; Barbosa, J. *Phys. Chem. Chem. Phys.* **1999**, *1*, 295.
18. Deshmukh, B. K.; Siddiqui, S.; Coetzee, J. F. *J. Electrochem. Soc.* **1991**, *138*, 124.
19. Guthrie, J. P. *Can. J. Chem.* **1978**, *56*, 2342.
20. Huck, L. A. and Leigh, W. J. *Organometallics* **2007**, *26*, 1339.
21. Mochida, K.; Wakasa, M.; Sakaguchi, Y.; Hayashi, H. *J. Am. Chem. Soc.* **1987**, *109*, 7942.
22. Leigh, W. J.; Lollmahomed, F.; Harrington, C. R. *Organometallics* **2006**, *25*, 2055.
23. Sakai, S. *Int. J. Quantum Chem.* **1998**, *70*, 291.
24. Su, M.-D. and Chu, S.-Y. *J. Am. Chem. Soc.* **1999**, *121*, 4229.
25. Nag, M. and Gaspar, P. P. *Organometallics* **2009**, *28*, 5612.
26. Huck, L. A. and Leigh, W. J. *in press* **2009**.
27. Egorov, M. P.; Gal'minas, A. M.; Basova, A. A.; Nefedov, O. M. *Dokl. Akad. Nauk. SSR (Engl. Transl.)* **1993**, *329*, 102.

CHAPTER 6

Kinetic studies of some reactions of tetramethyldigermene in hexane

6.1 Introduction

The chemistry of digermenes has attracted considerable attention in the past years. These compounds exhibit a rich and unique reactivity owing to their relatively weak Ge=Ge double bonds. While the chemistry of stable digermenes has been well documented, the study of transient digermenes is still under-explored.[1-4] Spectroscopic and kinetic data for a few transient digermenes, including Ge_2Me_4, have been reported in solution; however, there is yet to be a systematic study of the effects of substituents on their reactivities.[5-11]

Ge_2Me_4 exhibits an absorption maximum (λ_{max}) of 370 nm, and in the absence of added scavengers it decays with mixed-order kinetics over ca. 100 μs. In this chapter, we discuss the results of a kinetic study of the reactions of Ge_2Me_4 in hexane at 25 °C. The results are compared with analogous data for Ge_2Ph_4[12] and $Ge_2Ph_2Me_2$[8] under similar conditions. The rate constants determined in this work are also compared with those reported in the literature for Ge_2Me_4.

The dimerization of germylenes is one of the most common sources of digermenes in solution.[1,2] In our experiments, Ge_2Me_4 is formed as a secondary photolysis product from dimerization of $GeMe_2$, and we note that this method of preparation of the species is not ideal for the purpose of kinetic studies. It is completely unsuitable for product studies. This is more or less because our ability to detect and monitor the kinetics of its reactions is dependent on the rate constants for the reactions of $GeMe_2$ with the scavenger of interest. In general, we had two scenarios: (a) $GeMe_2$ reacts irreversibly with the added scavenger (Q), and (b) $GeMe_2$ reacts reversibly with Q (See Scheme 6.1). In the first case, as discussed in Chapter 2, increasing additions of Q *irreversibly* quenches $GeMe_2$, which results in a concomitant decrease in the yield of Ge_2Me_4. Thus, in this scenario, experiments were limited to low concentration ranges of the added scavenger. When Ge_2Me_4 did not decay with perfect first-order kinetics (e.g. with DMP; *vide infra*) only upper limits for the rate constants were obtained. When the reaction of the scavenger Ge_2Me_4 was fast enough such that it followed first-order kinetics, the absolute rate constant for the reaction could be determined (e.g. AcOH; *vide infra*). On the other hand, in cases where $GeMe_2$ reacts *reversibly* with Q, Ge_2Me_4 could still be detected at concentrations at which $GeMe_2$ was no longer observable (e.g. MeOH). This is explained by the formation of Ge_2Me_4 from the dimerization of free $GeMe_2$ present at equilibrium, and from the reaction of $GeMe_2$ with the primary product (in the case of methanol, the Me_2Ge-MeOH complex; as discussed in Chapter 4). In this scenario, a wider range of concentrations of the scavenger can be employed in kinetic experiments, and absolute rate constants for the reactions of Ge_2Me_4 can be determined.

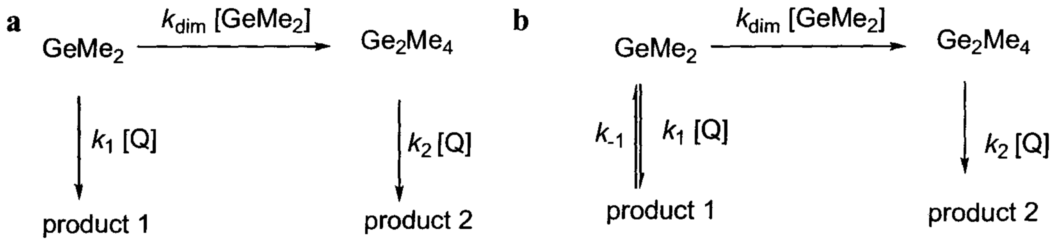

Scheme 6.1 Reaction pathways of $GeMe_2$ and Ge_2Me_4 in the presence of a scavenger (Q) when (a) the reaction of $GeMe_2$ with Q is *irreversible*, and (b) the reaction of $GeMe_2$ with Q is *reversible*.

Successful product studies typically require high concentrations of scavenger in order to ensure quantitative trapping of the reactive intermediate of interest. Under the conditions of our experiments, this leads to quantitative trapping of $GeMe_2$, and thus Ge_2Me_4 is never formed. In order to trap the digermene high concentration of the germylene is required. This can be achieved by using preparative laser photolysis, such as the laser-drop technique.[13] Leigh *et al.* reported that high laser intensity and sufficiently low concentration of a scavenger are required in order to produce high concentrations of the germylene, and allow dimerization to compete with the reaction of the germylene with the scavenger. They carried out laser flash photolysis (using focused pulses from a KrF excimer) of $GePh_2$ precursor **6** (0.003 M) in the presence of MeOH (0.003 M) in a laser-drop apparatus and a mixture of hydridomethoxydiphenylgermane (**46**; $GePh_2$ trapping product), 1-methoxy-1,1,2,2-tetraphenyldigermane (**47**; Ge_2Ph_4 trapping product) and 2,3-dimethyl-1,3-butadiene were obtained (Scheme 6.2).[9] The relative yields of the $GePh_2$ or Ge_2Ph_4 trapping products were reported to depend on the laser intensity and on the concentration of methanol; the yield of **47** increases with higher laser intensity but decreases with increasing methanol concentration. Similar experiments were not performed for $GeMe_2$, since the product of Ge_2Me_4 with methanol has been characterized to be 1-methoxy-1,1,2,2-tetramethyldigermane by Mochida *et al.*[7]

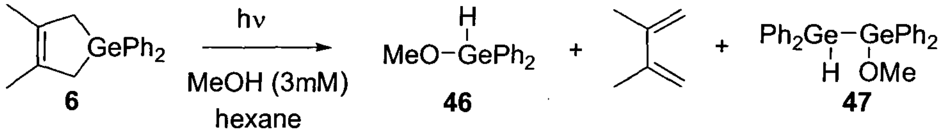

Scheme 6.2 Trapping of $GePh_2$ and Ge_2Ph_4 by methanol in a laser-drop experiment.

Addition of acetic acid (AcOH), methanol (MeOH), t-butanol (t-BuOH), oxygen, carbon tetrachloride (CCl_4), n-butylamine (n-$BuNH_2$) and tri-*n*-butylstannane (Bu_3SnH) resulted in enhancements in the decay rates of Ge_2Me_4, monitored at 370 nm. In all of these cases, the decay profiles fit to first-order kinetics (according to eq 2.4), and plots of k_{decay} versus [Q] according to eq (2.17) are linear. The intercept from these plots represents the hypothetical pseudo-first-order rate constant for the decay of Ge_2Me_4 in the absence of the scavenger.

The addition of other reagents such as 2,3-dimethylbuta-1,3-diene (DMB), t-butyl acetylene (TBE) or 4,4-dimethyl-1-pentene (DMP) caused little change in the decay kinetics of the Ge_2Me_4 signal over the range in which it could be monitored. In these cases, upper limits for the rate constants were estimated by fitting the 370 nm decay profile, recorded at the highest concentration of the scavenger used, to first-order kinetics, and then dividing the resulting decay constant by the concentration eq (6.1).

$$k_Q < k_{decay}/[Q] \qquad \textbf{(6.1)}$$

6.2 Reaction with acetic acid

Addition of acetic acid resulted in accelerations in the decay rates of Ge_2Me_4, and a plot of k_{decay} versus [AcOH] afford a bimolecular rate constant, $k_{AcOH} = (1.2 \pm 0.2) \times 10^7$ $M^{-1}s^{-1}$ from analysis according to eq (2.17) (Figure 6.1). Huck and Leigh reported that tetramesityldigermene reacts with AcOH to form the corresponding 1,2-addition product.[10] A Hammett reaction constant of $\rho = +0.33 \pm 0.01$, was obtained from a study of the reactivities of several ring-substituted tetraaryldigermenes with AcOH in hexane, indicating there to be negative charge development at the Ge=Ge bond in the rate determining step.[10] No deuterium kinetic isotope effect was observed on these reactions. Therefore, they ruled out the possibility of a concerted mechanism or a mechanism that involves proton transfer in the rate-determining step. The results are consistent with a mechanism that involves an initial nucleophilic attack by the acid at the Ge=Ge bond in the rate determining step to form a zwitterionic intermediate, followed by a fast proton-migration step to form the product, analogous to the reaction of digermenes with other carbonyl compounds[14] (Scheme 6.3).

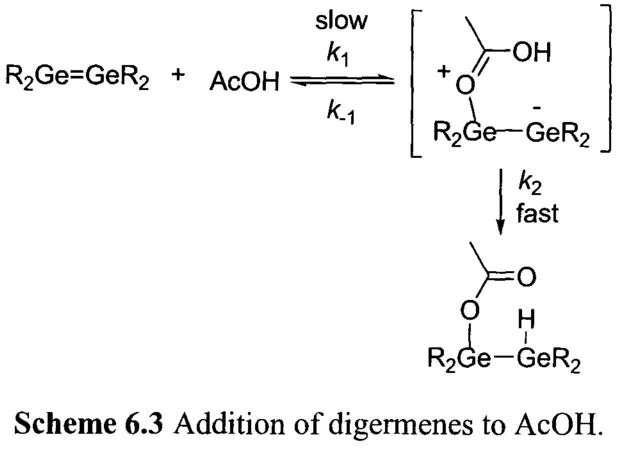

Scheme 6.3 Addition of digermenes to AcOH.

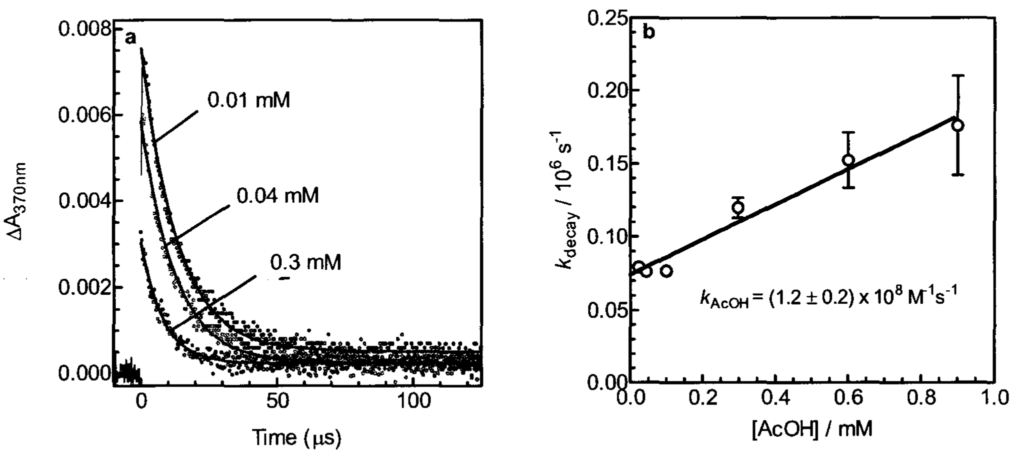

Figure 6.1. (a) Effects of added AcOH on the decay profiles of Ge_2Me_4, monitored at 370 nm. The solid lines represent the non-linear least-squares fits of the data to a single-phase exponential decay, according to eq (2.4). $k_{decay} = k_0 + k_Q[Ge_2Me_4]$; (b) Plot of k_{decay} versus [AcOH]. The solid line is the linear least-squares fit to eq (2.17).

6.3 Reactions with n-BuNH$_2$ and alcohols

Addition of increasing concentrations of MeOH, t-BuOH and n-BuNH$_2$ caused a linear decrease in the lifetime of Ge_2Me_4. Representative decay profiles and plots of k_{decay} versus [Q] are given in Figure 6.2 for n-BuNH$_2$. The rate constants for these reactions are shown in Table 6.1 together with those reported for Ge_2Ph_4.[12] Digermenes react with alcohols to form the corresponding hydridoalkoxydigermane derivatives (eq 6.2).[7,9,15] Although, it has been suggested that the reactions with amines should proceed similarly,[10] products have not been isolated yet.

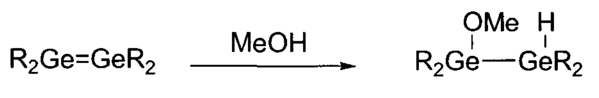

$$R_2Ge{=}GeR_2 \xrightarrow{MeOH} R_2\overset{OMe}{\overset{|}{Ge}}{-}\overset{H}{\overset{|}{Ge}}R_2$$

R = Me [a]
R = Ph [b]
R = 2,6-diethylphenyl [c]

(6.2)

(a) Ref. 7; (b) Ref. 9; (c) Ref. 16.

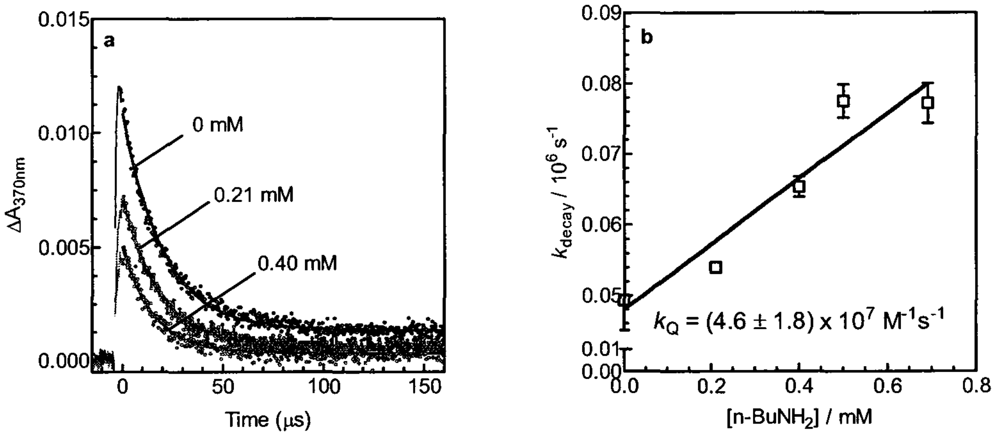

Figure 6.2. (a) Effects of added n-$BuNH_2$ on transient decay profiles recorded at 370 nm, by laser flash photolysis of **23** in deoxygenated anhydrous hexane. The solid lines represent the non-linear least-squares fits of the data to single-phase exponential decays, according to eq (2.4); (b) Plot of k_{decay} versus [n-$BuNH_2$], according to eq (2.17).

Huck and Leigh proposed that the reactions of digermenes with alcohols and amines proceed by initial nucleophilic attack at the Ge=Ge bond to form a zwitterionic intermediate, followed by proton transfer.[10] A small positive Hammett reaction constant, $\rho = +0.11 \pm 0.07$, was obtained for the reactions of the series of arylated digermenes with diethylamine in hexane at 25 °C, consistent with nucleophilic attack by the amine in the rate-determining step of the reaction.[10]

The rate constant determined for the reaction of Ge_2Me_4 with n-$BuNH_2$ ($k_{n\text{-}BuNH2}$ = (4.6 ± 1.8) x 10^7 $M^{-1}s^{-1}$) is at least an order of magnitude larger than those for the reactions with MeOH (k_{MeOH} = (2.7 ± 0.8) x 10^6 $M^{-1}s^{-1}$) and t-BuOH ($k_{t\text{-}BuOH}$ = (5 ± 1) x

10^5 $M^{-1}s^{-1}$), consistent with the higher nucleophilicity of the amine. The rate constant for the reaction of Ge_2Me_4 with methanol is ca. 5 times faster than that for t-butanol, most likely due to the lower steric bulk in the alcohol. We note that the measured rate constant for the reaction with t-butanol is one order of magnitude lower than that reported by Mochida *et al.* for the same reaction ($k_Q = 2.4 \times 10^6$ $M^{-1}s^{-1}$).[7] -

Ge_2Ph_4 is more reactive than Ge_2Me_4 toward the alcohols and n-$BuNH_2$, suggesting that it is more electrophilic in nature. Theoretical studies performed by Leigh *et al.* predicted that the HOMO of Ge_2Me_4 is higher in energy than in Ge_2Ph_4 by 0.2 eV.[9] We can conclude that the LUMO of Ge_2Ph_4 is lower than that of Ge_2Me_4 based on their respective absorption maxima ($\lambda_{max,Ge2Ph4}$ = 440 nm and $\lambda_{max,Ge2Me4}$ = 370 nm). Thus, the higher rate constants obtained for Ge_2Ph_4 are consistent with its LUMO being lower in energy than that of Ge_2Me_4.

Table 6.1. Bimolecular rate constants (k_Q / 10^6 $M^{-1}s^{-1}$) for the reactions of Ge_2R_4 in hexane at 25 °C.

Reagent	Ge_2Me_4[a]	Ge_2Ph_4[b]
MeOH	2.7 ± 0.8	19 ± 4
t-BuOH	0.5 ± 0.1	2.1 ± 0.5
$BuNH_2$	46 ± 18	3640 ± 380
AcOH	121 ± 21	≤ 20

(a) This work; (b) Ref. 12. Errors are quoted as ± 2σ.

6.4 Reactions with group 14 metal hydrides

The rate constants for the reactions of Ge_2Me_4 with group 14 metal hydrides follow a similar trend as that observed for $GeMe_2$, increasing in order Et_3SiH < Et_3GeH < Bu_3SnH. The rate constants determined for the reactions of Ge_2Me_4 with Et_3SiH, Et_3GeH and Bu_3SnH are similar to those found for Ge_2Ph_4 (see Table 6.2). The rate constants correlate with the BDE of the M-H bonds; the smaller the BDE the faster the rate of the reaction.

Products from the reactions of digermenes with group 14 metal hydrides have not been isolated yet. Mochida *et al.* found no products formed from Ge_2Me_4 in the presence of various concentrations of Et_3SiH.[7] However, DeYoung *et al.* reported that tetramesityldisilene reacts with n-Bu_3SnH to give 1,2-addition product (see eq 6.3).[17]

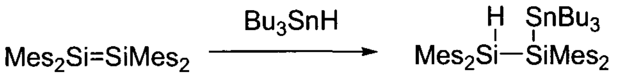

$$Mes_2Si{=}SiMes_2 \xrightarrow{Bu_3SnH} Mes_2\overset{H}{Si}{-}\overset{SnBu_3}{Si}Mes_2 \qquad (6.3)$$

Table 6.2. Absolute rate constants (k_Q / 10^6 M^{-1} s^{-1}) for the reactions of Ge_2Me_4 and Ge_2Ph_4 with group 14 metal hydrides in hexane at 23-25 °C

Reagent	**BDE (kcalmol^{-1})**	$Me_2Ge{=}GeMe_2$[a]	$Ph_2Ge{=}GePh_2$[b]
Et_3SiH	90.1[c]	≤ 0.1	-
Et_3GeH	82.3[d]	5 ± 1	5.6 ± 1.6
Bu_3SnH	73.7[e]	300 ± 40	410 ± 200

(a) This work; (b) Ref. 12; (c) Ref. 18; (d) Ref. 19; (e) Ref. 20.

6.5 Reaction with carbon tetrachloride

A rate constant, $k_{CCl4} = 2.3 \times 10^7$ $M^{-1}s^{-1}$, was obtained for the reaction of Ge_2Me_4 with CCl_4 in deoxygenated hexane. Figure 6.3 shows the growth/decay profiles monitored at 370 nm in the absence and presence of 10 and 30 mM CCl_4, and the plot of k_{decay} versus [CCl_4]. This value is roughly two times greater than those reported by Mochida *et al.* in their various studies of Ge_2Me_4 in the presence of this substrate, which is not a serious discrepancy (see Table 6.3).[5-7] Both digermenes and disilenes react with halocarbons to give products that are consistent with an initial chlorine abstraction, followed by a competition between coupling of the initially formed radical pair or cage escape reactions.[7,21,22] Product studies by Mochida *et al.* showed that Ge_2Me_4 reacts with CCl_4 in benzene at room temperature to form 1,2-dichloro-1,1,2,2-tetramethyldigermane, consistent with initial chlorine atom abstraction to afford the corresponding 2-(chlorogermyl)germyl radical, followed by abstraction of chlorine atom from a second molecule of CCl_4 (Scheme 6.4).[7] Similarly, Samuel *et al.* reported that Ge_2Mes_4 reacts with chloroform in toluene at -70 °C to form the corresponding chloro(dichloromethyl)digermane derivative, consistent with the net addition of the digermene into the C-Cl bond of $HCCl_3$.[21]

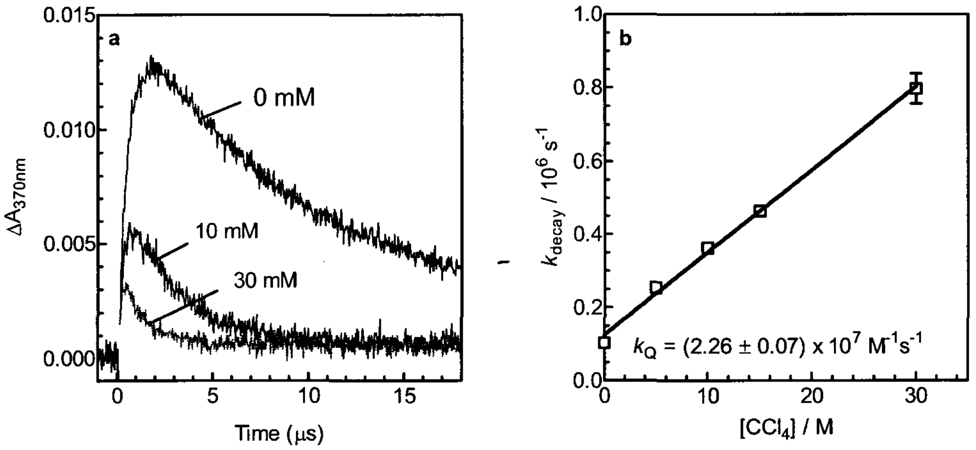

Figure 6.3. (a) Effects of added CCl_4 on the growth/decay profiles recorded at 370 nm; (b) Plots of k_{decay} versus [CCl_4], monitored at 370 nm. The solid line represents the linear least-squares fit of the data to eq (2.17).

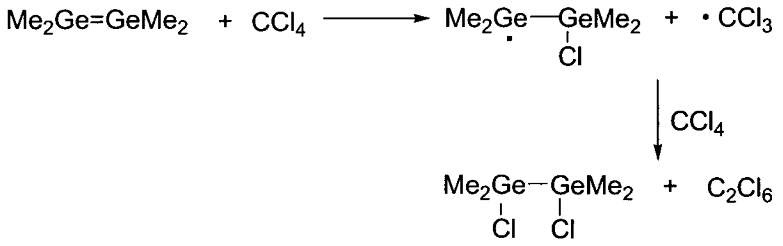

Scheme 6.4 Postulated reaction mechanism of Ge_2Me_4 with carbon tetrachloride.

Table 6.3. Bimolecular rate constants for the reactions of digermenes and Si_2Me_4 with CCl_4 in hexane at 25 °C.

Dimetallene	k_Q / 10^6 $M^{-1}s^{-1}$	Dimetallene	k_Q / 10^6 $M^{-1}s^{-1}$
$Me_2Ge{=}GeMe_2$	23 ± 2[a]	MePhGe=GePhMe	6 ± 1[e]
$Me_2Ge{=}GeMe_2$	< 10^{b}	$Ph_2Ge{=}GePh_2$	2.0 ± 0.2[f]
$Me_2Ge{=}GeMe_2$	14[c]	$Me_2Si{=}SiMe_2$	2300 ± 200
$Me_2Ge{=}GeMe_2$	12[d]		

(a) This work; (b) Ref. 5; (c) Ref. 23; (d) Ref. 7; (e) Ref. 8; (f) Ref. 12.

A decrease in the reactivity of the digermene is observed with increasing phenyl substitution on the germanium, i.e. Ge_2Me_4 > $Ge_2Me_2Ph_2$ > Ge_2Ph_4. Kira *et al.* reported a mechanistic study of the reactions of a series of stable tetrakis(trialkylsilyl)- and tetraaryldisilenes with haloalkanes, and their results were in favor of a radical mechanism for these reactions.[22] Moreover, their kinetic studies showed that the rate constants of the disilenes studied correlate with their π-bond energies.[22] In addition, theoretical calculations by Chen *et al.* led to the suggestions that the reactivities of digermenes toward halocarbons increase with a decrease in their π-bond energies, which in turn correlate with the relative singlet-triplet energy gap of the corresponding germylenes.[24] Huck *et al.* have determined a negative reaction constant, $\rho = -0.31 \pm 0.03$ for the reactions of a series of tetraarylated digermenes with CCl_4, suggestive of an electron-transfer mechanism with the digermene playing the role of an electron donor.[25] The fact that Ge_2Me_4 is ca. ten times more reactive than Ge_2Ph_4 toward CCl_4 is consistent with its HOMO being higher in energy.[26]

6.6 Reaction with oxygen

The oxidation of digermenes by molecular oxygen is well known and has been particularly well studied for stable digermenes.[1-3,27] The course of the reaction is shown in Scheme 6.5. Digermenes react with oxygen to form the corresponding 1,2-digermadioxetane **48** and 1,2-digermaoxirane **49**.[28,29] Usually, under the conditions of the reaction 1,2-digermaoxirane derivative **49** further reacts with oxygen to give the final product, 1,3-digermadioxetane **50**. The initially formed 1,2-digermadioxetane **48** is also unstable and undergoes photochemical or thermal rearrangement to give **50** as well.

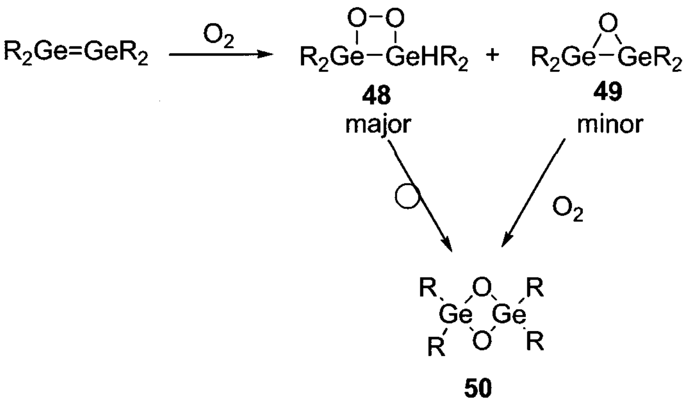

Scheme 6.5 Reaction of digermenes with oxygen.

A rate constant of ca. 1.8 x 10^7 $M^{-1}s^{-1}$ was obtained for the reaction of Ge_2Me_4 with oxygen under our experimental conditions (see Figure 6.4). This value is at least 10 times smaller than those reported by Mochida *et al.* (see Table 6.4).[5-7] In an earlier study, Toltl *et al.* reported a much lower reactivity for tetramesityldigermene toward oxygen, (k_{O2} = 2.3 ± 0.4) x 10^5 $M^{-1}s^{-1}$),[11] indicating that the reaction is impeded by steric effects of the substituents on the Ge=Ge bond. The trend in the reactivities of methyl- and phenyl-substituted digermenes is given in Table 6.4. It is observed that Ge_2Me_4 reacts faster than Ge_2Ph_4. There has not been any systematic study of the substituent effect on the reactivity of digermene with oxygen to help understand this trend. In addition, it is observed that Si_2Me_4 reacts ca. 4 times faster than Ge_2Me_4.

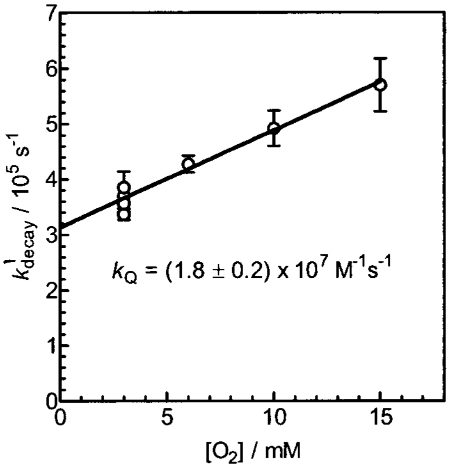

Figure 6.4. Plots of k_{decay} versus [O_2], monitored at 370 nm. The solid line represents the linear least-squares fit to eq (2.17).

Table 6.4. Absolute rate constants for the reaction of digermenes with oxygen in hexane at 25 °C.

Digermene	k_Q / 10^6 $M^{-1}s^{-1}$
$Me_2Ge=GeMe_2$	18 ± 2[a]
$Me_2Ge=GeMe_2$	280,[b] 180,[c] 400[d]
PhMeGe=GeMePh	24 ± 3[e]
$Ph_2Ge=GePh_2$	4.8 ± 0.8[f]
$Mes_2Ge=GeMes_2$	2.3 ± 0.4[g]
$Me_2Si=SiMe_2$	200 ± 40[h]

Errors are quoted as twice the standard deviation (± 2σ); (a) This work; (b) Ref. 5; (c) Ref. 6; (d) Ref. 7; (e) Ref. 8; (f) Ref. 12; (g) Ref. 11; (h) Ref. 30.

6.7 Reactions with alkenes, alkynes and dienes

Addition of TBE (0-0.50 mM), DMB (0-0.52 mM), DMP (0-1.73 mM) and isoprene (0-1.30 mM), led to very slight enhancements in the decay rates of Ge_2Me_4. These reactions were too slow to be monitored, given that Ge_2Me_4 is formed as a secondary product and its precursor (i.e. $GeMe_2$) is more reactive toward the added scavenger. Nevertheless, we estimated upper limits ($k_Q < k_{decay}/[Q]$) from the decay rates measured at the highest concentration of the scavenger used, by fitting the data to a single-exponential decay, according to eq (2.4). Figure 6.5 shows the transient decay profiles recorded at 370 nm in the presence of the highest concentration used for quenching of Ge_2Me_4 by TBE, DMB, DMP and isoprene. It is to be noted that these are crude upper limits because the decay of the digermene at these concentrations most likely contains a contribution from oligomerization of the digermene.

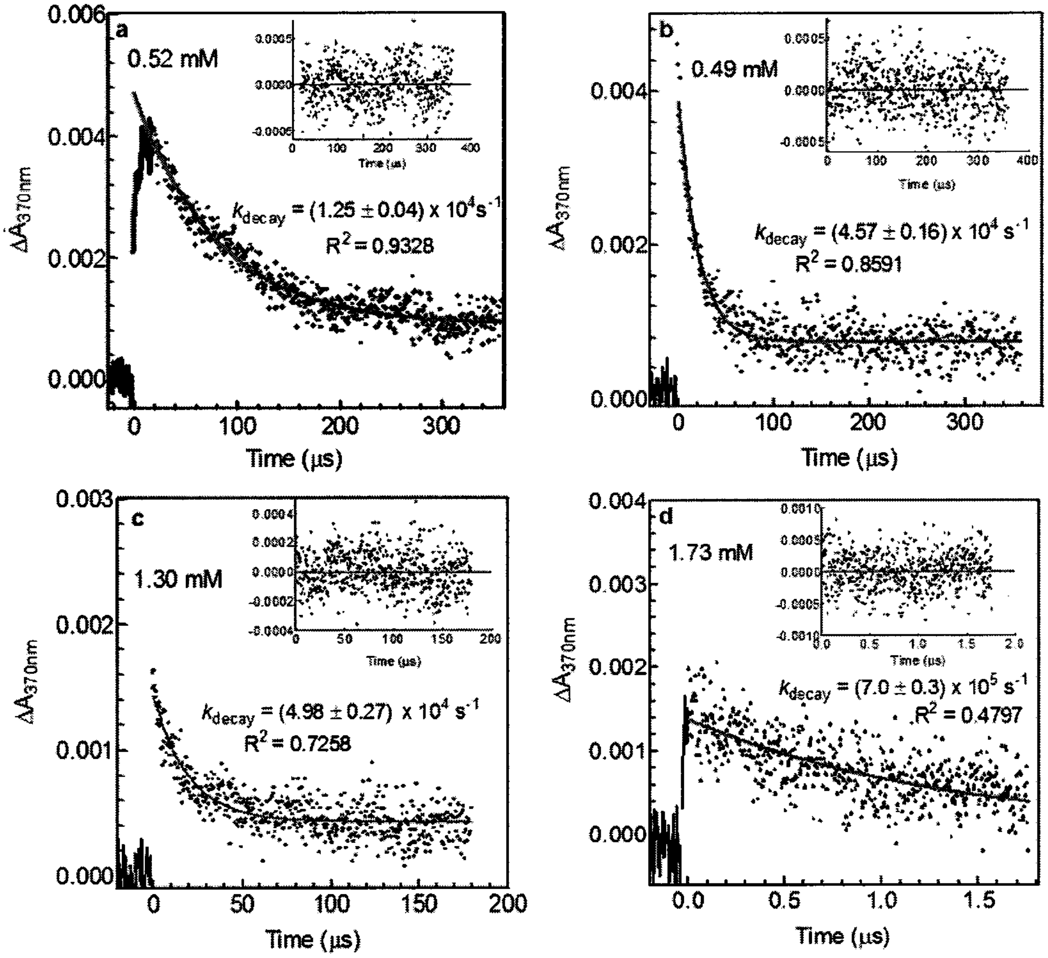

Figure 6.5. Transient decay profiles recorded at 370 nm by laser flash photolysis of **23** in deoxygenated hexane containing (a) 0.52 mM DMB; (b) 0.49 mM TBE; (c) 1.30 mM isoprene and (d) 1.73 mM DMP. The solid lines represent the non-linear least-squares fits of the data to a single-phase exponential decay, according to eq (2.4). The inserts shows the residuals obtained after fitting the data.

Digermenes undergo [2+2]- or [2+4]-cycloaddition reactions with a variety of unsaturated compounds such as alkynes, alkenes, dienes, aldehydes and ketones, to give the corresponding cycloadducts (some reported examples are given in Scheme 6.6).[31-36] However, it has been reported that stable and relatively stable digermenes are unreactive toward dienes.[37] Ge_2Me_4 reacts with DMB to form the corresponding 1,2-digermacyclohex-4-enes (**51** and **52**).[7]

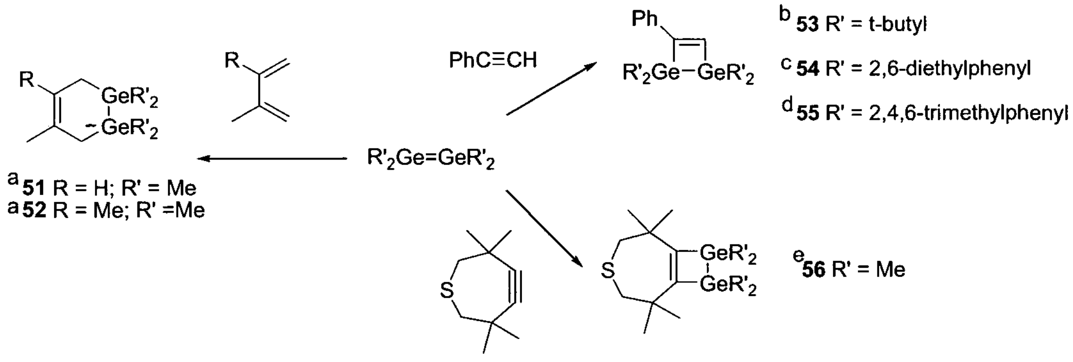

(a) Ref. 7; (b) Ref. 38; (c) Ref. 36; (d) Ref. 39; (e) Ref. 31.

Scheme 6.6 Reactions of digermene with diene and alkyne.

The upper limit for the rate constant obtained in this work ($k_Q < 4 \times 10^7$ $M^{-1}s^{-1}$) for the reaction of Ge_2Me_4 with DMB is ca. two orders of magnitude higher than the rate constant determined by Mochida *et al.* (5.3×10^5 $M^{-1}s^{-1}$) in cyclohexane.[7] Our upper limit is most likely overestimated due to other reactions of Ge_2Me_4 at the concentration used. Nevertheless, the upper limits of the rate constants for the reactions of Ge_2Me_4 are compared with those estimated for Ge_2Ph_4 and with the absolute rate constants for Si_2Me_4 in Table 6.5. The rate constants determined for the reactions of Si_2Me_4 is found to be at least one order of magnitude higher than those estimated for Ge_2Me_4.

Table 6.5. Rate constants (k_Q / 10^6 $M^{-1}s^{-1}$) for the reaction of Ge_2Me_4, Ge_2Ph_4 and Si_2Me_4 with alkene, alkyne and diene in deoxygenated hexane.

Reagents	**Ge_2Me_4[a]**	**Ge_2Ph_4[b]**	**Si_2Me_4[c]**
Isoprene	≤ 80	≤ 0.3	400 ± 200
DMB	≤ 40	nd	nd
DMP	≤ 40	≤ 5.1	500 ± 200
TBE	≤ 90	≤ 20	810 ± 40

(a) This work; (b) Ref. 12; (c) Ref. 30. nd –not determined.

6.8 Summary and Conclusions

Absolute rate constants for the reactions of Ge_2Me_4 with n-$BuNH_2$, AcOH, MeOH, O_2, Et_3GeH, Et_3SiH and Bu_3SnH have been determined. Since the reactivity of $GeMe_2$ is much higher than that of Ge_2Me_4 toward the scavengers of interest, we were very limited in our ability to study the reactivity of the digermene in our experiments. Thus, in many cases, particularly in the case of isoprene, tert-butyl acetylene, 4,4-dimethyl-1-pentene and 2,3-dimethylbuta-1,3-diene, we were able to obtain upper limits of the rate constants only.

Ge_2Me_4 exhibits similar reactivities as Ge_2Ph_4 and $Ge_2Me_2Ph_2$. The higher rate constants observed for the phenylated digermenes with amines and alcohols, indicate that they are more electrophilic than Ge_2Me_4. No substituent effects were observed in reactions involving a germanium centered radical intermediate (e.g. reaction with group 14 metal hydrides) suggesting no extra stabilization from the phenyl substituents.

Although details of some reactions remain to be elucidated, estimates of rate constants are provided in this work. Clearly, more work remains to be done with a better digermene precursor, such as 7,8-digermabicylo[2.2.2]octadiene derivative **22** employed by Mochida *et al.*,[7] to further study the mechanisms of these reactions.

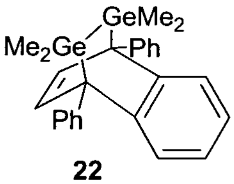

22

References

1. Barrau, J.; Escudié, J.; Satgé, J. *Chem. Rev.* **1990**, *90*, 283.
2. Baines, K. M. and Stibbs, W. G. *Adv. Organomet. Chem.* **1996**, *39*, 275.
3. Tsumuraya, T.; Batcheller, S. A.; Masamune, S. *Angew. Chem. Int. Ed.* **1991**, *30*, 902.
4. Escudie, J.; Couret, C.; Ranaivonjatovo, H.; Satge, J. *Coord. Chem. Rev.* **1994**, *130*, 427.
5. Mochida, K.; Kanno, N.; Kato, R.; Kotani, M.; Yamauchi, S.; Wakasa, M.; Hayashi, H. *J. Organomet. Chem.* **1991**, *415*, 191.
6. Mochida, K. and Tokura, S. *Bull. Chem. Soc. Jpn.* **1992**, *65*, 1642.
7. Mochida, K.; Kayamori, T.; Wakasa, M.; Hayashi, H.; Egorov, M. P. *Organometallics* **2000**, *19*, 3379.
8. Leigh, W. J.; Dumbrava, I.; Lollmahomed F.B. *Can. J. Chem.* **2006**, *84*, 934.
9. Leigh, W. J.; Harrington, C. R.; Vargas-Baca, I. *J. Am. Chem. Soc.* **2004**, *126*, 16105.
10. Huck, L. A. and Leigh, W. J. *Organometallics* **2007**, *26*, 1339.

11. Toltl, N. P.; Leigh, W. J.; Kollegger, G. M.; Stibbs, W. G.; Baines, K. M. *Organometallics* **1996**, *15*, 3732.
12. Leigh, W. J. and Harrington, C. R. *J. Am. Chem. Soc.* **2005**, *127*, 5084.
13. Banks, J. T. and Scaiano, J. C. *J. Am. Chem. Soc.* **2002**, *115*, 6409.
14. Samuel, M. S. and Baines, K. M. *J. Am. Chem. Soc.* **2003**, *125*, 12702.
15. Snow, J. T.; Murakami, S.; Masamune, S.; Williams, D. J. *Tetrahedron Lett.* **1984**, *25*, 4191.
16. Snow, J. T.; Murakami, S.; Masamune, S.; Williams, D. J. *Tetrahedron Lett.* **1984**, *25*, 4191.
17. De Young, D. J.; Fink, M. J.; West, R.; Michl, J. *Main Group Met. Chem.* **1987**, *10*, 19.
18. Kanabus-Kaminska, J. M.; Hawari, J. A.; Griller, D.; Chatgilialoglu, C. *J. Am. Chem. Soc.* **1987**, *109*, 5267.
19. Clark, K. B. and Griller, D. *Organometallics* **1991**, *10*, 746.
20. Burkey, T. J.; Majewski, M.; Griller, D. *J. Am. Chem. Soc.* **1986**, *108*, 2218.
21. Samuel, M. S.; Jennings, M. C.; Baines, K. M. *Organometallics* **2001**, *20*, 590.

22. Kira, M.; Ishima, T.; Iwamoto, T.; Ichinohe, M. *J. Am. Chem. Soc.* **2001**, *123*, 1676.
23. Mochida, K. and Tokura, S. *Bull. Chem. Soc. Jpn.* **1992**, *65*, 1642.
24. Chen, W. C.; Su, M. D.; Chu, S. Y. *Organometallics* **2001**, *20*, 564.
25. Huck, L. A., Private Communication.
26. Becerra, R.; Gaspar, P. P.; Harrington, C. R.; Leigh, W. J.; Vargas-Baca, I.; Walsh, R.; Zhou, D. *J. Am. Chem. Soc.* **2005**, *127*, 17469.
27. Escudie, J. and Ranaivonjatovo, H. *Adv. Organomet. Chem.* **1999**, *44*, 113.
28. Masamune, S.; Batcheller, S. A.; Park, J.; Davis, W. M.; Yamashita, O.; Ohta, Y.; Kabe, Y. *J. Am. Chem. Soc.* **1989**, *111*, 1888.
29. Samuel, M. S.; Jennings, M. C.; Baines, K. M. *J. Organomet. Chem.* **2001**, *636*, 130.
30. Moiseev, A. G. and Leigh, W. J. *Organometallics* **2007**, *26*, 6277.
31. Nefedov, O. M.; Egorov, M. P.; Gal'minas, A. M.; Kolesnikov, S. P. *J. Organomet. Chem.* **1986**, *301*, C21-C22.
32. Batcheller, S. A. and Masamune, S. *Tetrahedron Lett.* **1988**, *29*, 3383.
33. Dixon, C. E.; Cooke, J. A.; Baines, K. M. *Organometallics* **1997**, *16*, 5437.

34. Apeloig, Y.; Bravo-Zhivotovskii, D.; Zharov, I.; Panov, V.; Leigh, W. J.; Sluggett, G. W. *J. Am. Chem. Soc.* **1998**, *120*, 1398.

35. Weidenbruch, M.; Hagedorn, A.; Peters, K.; Schnering, H. G. v. *Angew. Chem. Int. Ed. Engl.* **1995**, *34*, 1085.

36. Ando, W. and Tsumuraya, T. *J. Chem. Soc., Chem. Commun.* **1989**, 770.

37. Baines, K. M.; Cooke, J. A.; Dixon, C. E.; Liu, H. W.; Netherton, M. R. *Organometallics* **1994**, *13*, 631.

38. Manfred, W.; Annette, H.; Karl, P.; Hans Georg, v. S. *Angew. Chem. Int. Ed. Engl.* **1995**, *34*, 1085.

39. Batcheller, S. A. and Masamune, S. *Tetrahedron Lett.* **1988**, *29*, 3383.

CHAPTER 7

Summary and Future Work

7.1 Summary

Transient germylenes are important reactive intermediates that are formed in a wide variety of reactions of organogermanium compounds. The interest in their chemistry has considerably increased through the years, mainly due to the development of a number of stable germylenes. However, mechanistic and kinetic studies of reactions of transient germylenes are still under-developed.[1] The kinetic behavior and spectral characteristics of dimethylgermylene ($GeMe_2$), which is one of the most studied germylenes in the literature, have been subject to a lot of controversies through the years. We speculated that the main source of these controversies stemmed from the use of photochemical precursors that generate other transient species in addition to $GeMe_2$, as well as inappropriate reaction conditions. One of the major contributions of this thesis has been to establish the absorption spectrum of $GeMe_2$ in solution, for which we assign an absorption maximum at 470 nm. The spectrum was derived from laser flash photolysis of 1,1-dimethyl-3-phenylgermacyclopent-3-ene (**23**) and 1,1,3-trimethyl-4-phenylgermacyclopent-3-ene (**24**), both of which were synthesized for the first time in my studies, and dodecamethylcyclohexagermane (**14**), one of the $GeMe_2$ precursors employed in earlier studies. The photochemical precursors **23** and **24** yield $GeMe_2$ as the only reactive intermediate, with high quantum yield ($\Phi \sim 0.55$).

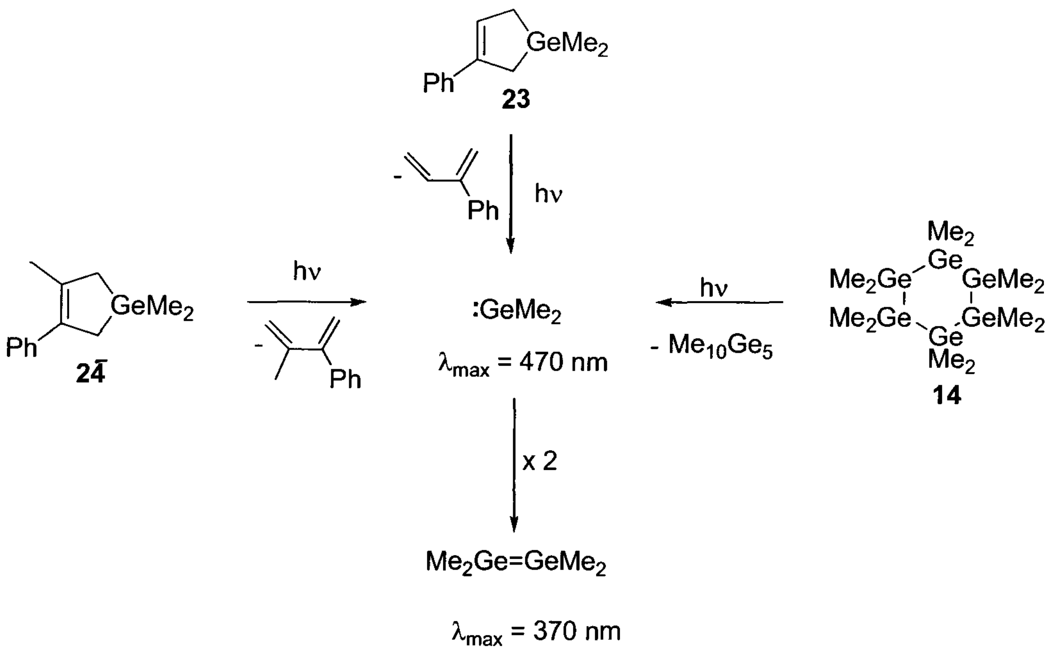

Scheme 7.1 Photochemical generation of $GeMe_2$

We have carried out a comprehensive kinetic study of the reactions of $GeMe_2$ with typical germylene scavengers in hexanes. The rate constants for the reactions of $GeMe_2$ with acetic acid, 4,4-dimethyl-1-pentene, 2,3-dimethylbuta-1,3-diene, isoprene, 3,3-dimethyl-1-butyne, triethylamine, n-butylamine, tributylstannane, triethylsilane, triethylgermane, carbon tetrachloride and oxygen have been determined in hexanes. Most of these reactions occur at close to the diffusion-controlled rates in hexanes. For the first time, the rate constants determined in hydrocarbon solution are in very good agreement with those the gas phase for the same or closely related substrates. Our study also showed that the reactivity of $GeMe_2$ parallels that of $SiMe_2$; but with the rate constants determined for the reactions of $GeMe_2$ being slightly lower. In general, the equilibrium constants for the reactions of $GeMe_2$ are considerably smaller than those for the corresponding reactions of $SiMe_2$.

Our studies showed that the reactions of $GeMe_2$ with the alkene, dienes and amines are *reversible* and all the reactions studied with other scavengers are *irreversible.* $GeMe_2$ is a highly electrophilic species, with reactivity greater than that of the phenylated analogue, $GePh_2$, under similar conditions. The equilibrium constants for the reactions of $GeMe_2$ with isoprene and 4,4-dimethyl-1-pentene are significantly higher than that of $GePh_2$, indicating that the primary products are thermodynamically more stable in the case of $GeMe_2$.

Although, the reactions of germylenes with alcohols are known, prior to the work performed in our group the kinetics of these reactions have not been studied in solution. Our studies have shown that the reactions of $GeMe_2$ with Lewis bases such as THF, methanol and t-butanol are reversible and proceed through the initial formation of Lewis acid-base complexes, which exhibit absorption maxima at ca. 290-310 nm. In the case of the alcohols, the second step of the reaction, which involves a unimolecular H-migration to form the corresponding alkoxygermane, is slow in hexane and is catalysed by a second molecule of alcohol in neat alcohol. In addition, our studies have shown that this process is dramatically accelerated in the presence of acid (methanesulfonic acid) or base (sodium methoxide) catalysts.

The work performed in this thesis also represents the first kinetic study of the reactivity of germylenes in complexing solvents. $GeMe_2$ reacts with THF to form the corresponding Me_2Ge-THF complex which, in the absence of an added scavenger, decays to form Ge_2Me_4. Kinetic studies performed in neat THF showed that the Me_2Ge-THF complex exhibits reactivity distinct from that of free $GeMe_2$ toward scavengers such as CCl_4, AcOH, and O_2.

On the other hand, the complex exhibits orders of magnitude lower reactivity toward 4,4-dimethyl-1-pentene, 2,3-dimethyl-1,3-butadiene and methanol, indicating that reactions with these scavengers require the availability of the vacant p-orbital on the germylene in order for the reactions to proceed at measurable rates.

A number of the reactions of germylenes have been studied theoretically, many of which are based on $GeMe_2$. Hence, the work performed in this thesis allows a direct comparison of experimental measurements in solution with theory. The solution phase avoids many of the problems that are often encountered in gas phase kinetic studies, where incomplete collisional relaxation of primary reaction products can lead to difficulties in comparing experimental and theoretical results.

7.2 Future Work

The present study provides kinetic information about the reactions of the simplest dialkyl-substituted germylene in solution with alkene (4,4-dimethyl-1-pentene) and diene (isoprene and 2,3-dimethyl-1-butadiene). The mechanisms of the reactions of germylenes toward alkenes are still not completely understood, and the electronic and steric factors that control the rate of these reactions need to be elucidated. In this thesis, we have found that $GeMe_2$ reacts with isoprene and 2,3-dimethyl-1-butadiene reversibly and estimated the equilibrium constants to be $K_{eq} > 20\ 000\ M^{-1}$, at least 5 times larger than those determined for $GePh_2$. Currently, our group is exploring the reactivity of diarylgermylenes with electron-poor and electron-rich alkenes, namely acrylonitrile and the hexene isomers. It is found that the equilibrium constants for the reactions of $GePh_2$ with the above-mentioned alkenes decrease with an increase in substitution on the alkenes. It may be possible to measure equilibrium constants for reaction of $GeMe_2$ with some of these alkenes, thus enabling the first direct experimental comparison of equilibrium constants for $GeMe_2$ and $GePh_2$.

The work presented in this thesis shows that the reaction of $GeMe_2$ with alcohol occurs via the initial formation of a Lewis acid-base complex followed by proton transfer which is aided by another alcohol molecule. The unimolecular H-proton transfer from the complex is found to be slow with rate constant, $k_H < 10^4$ s^{-1}. To date all the theoretical calculations performed on the reactions of germylenes or silylenes with alcohols have predicted an initial formation of a complex followed by a unimolecular H-migration via a three-centered transition state. In the future, it will be insightful if theoretical calculations could be used to investigate the mechanism which involves an initial complexation reaction followed by catalysis by a second alcohol molecule. The base-catalysed decomposition of the complex is another mechanism of interest. From our study, we postulated that the reactions occur either by an initial deprotonation of the methanol in the complex or by a nucleophilic displacement of the methanol molecule in the complex by the methoxide ions. It would be valuable to investigate the lowest energy reaction pathways predicted by high level theoretical methods for the base-catalysed decomposition of the Me_2Ge-MeOH complex by MeONa.

The steric and the electronic nature of the substituents on the Ge are controlling factors that affect the thermodynamic and kinetic stabilities of germylenes.[2] Transient dialkylgermylenes or diarylgermylenes are potentially ambiphilic but most of the reactions studied so far have shown their strong tendency to act as electrophiles. The ambiphilic nature of transient germylenes and silylenes has been significantly less explored as compared to that of carbenes. Three main types of electronic stabilization have been used to describe the electronic effects of substituents on carbenes, namely, push-pull, push-spectator and push-push effects.[3] The possibility of altering the reactivity of germylenes by modification of the electronic nature of the substituents on the Ge needs to be investigated. Germylenes can have promising use in synthesis if their reactivities are tailored. The presence of n- or π-type donors on the germanium reduces the electron deficiency on the germanium atom by the transfer of electron density into its empty p-orbital, thus providing thermodynamic stability to the germylene.[4] On the other hand, bulky substituents make the reactive site less easily accessible to substrates. For example, π-donor substituents such as methoxy or amino groups can enhance the nucleophilicity of the germylene by donating the lone pair of electrons on the oxygen or nitrogen to the formally vacant p-orbital on the Ge. Halogen substituents can act as π-donors as well as σ-withdrawers. Thus, replacing one of the methyl groups on $GeMe_2$ or phenyl group on $GePh_2$ by OMe, halogen (F or Cl) or NMe_2 or CF_3 or phosphino (PR_2) groups could lead to some interesting variation in the rates and mechanisms of the reactions of germylenes. It would be interesting to explore how these substituents will influence the kinetic and mechanisms of the reactions of germylenes, especially toward alkenes, alkynes, dienes or Lewis bases (e.g. ether or alcohols), where the electrophilic nature of the germylene plays a major role in the mechanism of the reaction. The kinetics of the reactions of transient germylenes with Lewis acids have not been explored yet. Thus, further research effort could be directed toward exploring the nucleophilic capabilities of transient germylenes.

References

1. Leigh, W. J. and Harrington, C. R. *J. Am. Chem. Soc.* **2005**, *127*, 5084.

2. Tokitoh, N. and Okazaki, R. *Coord. Chem. Rev.* **2000**, *210*, 251.

3. Bourissou, D.; Guerret, O.; Gabbaï, F. P.; Bertrand, G. *Chem. Rev.* **2000**, *100*, 39.

4. Barrau, J. and Rima, G. *Coord. Chem. Rev.* **1998**, *178-180*, 593.

CHAPTER 8

Experimental

8.1 General

^{1}H NMR spectra (200 MHz or 600 MHz or 700 MHz) and ^{13}C NMR (50 MHz or 150 MHz) spectra were recorded on Bruker AV200 or AV600 or AV700 spectrometer in chloroform-*d* or THF-d_8 or cyclohexane-d_{12} or C_6D_6 and are referenced to the residual solvent proton and ^{13}C signals, respectively. Gas chromatographic (GC) separations employed a Hewlett-Packard 5090 Series II gas chromatograph equipped with a HP3396A integrator, a flame ionization detector and a DB-5 column (30m, 0.25 μm; Chromatographic Specialties, Inc.). GC/MS analyses were carried out on a Varian Saturn 2200 GC/MS/MS system equipped with a VF-5ms capillary column (30 m × 0.25 mm; 0.25 μm; Varian, Inc.), or a Micromass/Waters GCT GC/MS equipped with a DB-XLB column (30 m, 0.25 mm; Chromatographic Specialties, Inc.), using (70 eV) electron impact ionization; *m/z* values marked with an asterisk indicate ions containing ^{74}Ge. High resolution exact masses were determined on the latter instrument using a mass of 12.000000 for carbon-12. Melting points were determined using a Mettler FP82 hot stage mounted on a microscope and controlled by a Mettler FP80 central processor. Separations by column chromatography were performed using columns packed with silica gel (230-400 mesh, Silicycle) in a ratio of 1 g of mixture to 100 g of the silica gel. Steady-state photolysis experiments were carried out in a Rayonet photochemical reactor

(Southern New England Ultraviolet Co.) equipped with a merry-go-round and six RPR-2537 (254 nm) low-pressure Hg lamps.

Hexanes (EMD, OmniSolv), ether (Caledon Reagent) and THF (Caledon HPLC grade) were dried by passage through activated alumina (250 mesh, neutral) under nitrogen using a Solv-Tec solvent purification system (Solv-Tec, Inc.). Also, THF was refluxed under sodium and distilled under argon. Isoprene, 2,3-dimethyl-1,3-butadiene (DMB), 4,4-dimethyl-1-pentene (DMP) were purified by passage of the neat liquid through a small column of silica. 3,3-dimethyl-1-butyne (TBE) was distilled. Triethylsilane (Sigma-Aldrich Chemical Co.), triethylgermane (Gelest Inc.) and tri-n-butylstannane (Sigma-Aldrich Chemical Co.) were stirred for 12 hours over lithium aluminium hydride and were distilled at atmospheric pressure or under mild vacuum. Triethylamine and n-butylamine were refluxed over solid KOH for 12 hours and distilled. CCl_4 was refluxed over phosphorus pentoxide and distilled. Methanol and *tert*-butanol spectrophotometric grade) were used as received from Sigma-Aldrich Chemical Co. Methanesulfonic acid (Sigma-Aldrich Chemical Co.) was distilled. Sodium methoxide solutions were prepared by dissolving a weighed mass of sodium in methanol in a volumetric flask. Germanium tetrachloride (Gelest, Inc. or Teck-Cominco Metals, Ltd.), glacial acetic acid (Caledon Laboratories) and acetic acid-*d* (Aldrich) were used as received from suppliers. Glassware were flame-dried under a stream of dry argon or nitrogen prior to use. α-Bromostyrene was synthesized in a similar fashion as reported by Soderquist and Hassner.[1]

8.2 Laser Flash Photolysis

Laser flash photolysis experiments employed the pulses from a Lambda Physik Compex 120 excimer laser, filled with F_2/Kr/Ne (248 nm; ~25 ns; 100 ± 5 mJ) mixtures and a Luzchem Research mLFP-111 laser flash photolysis system.[2] Solutions were prepared at concentrations such that the absorbance at the excitation wavelength (248 nm) was between *ca.* 0.7 and 0.9. The solutions were pumped continuously through a vacuum oven-dried thermostatted 7 x 7 mm Suprasil flow cell connected to a calibrated 100 mL or 250 mL reservoir using a Masterflex™ 77390 peristaltic pump fitted with Teflon tubing (Cole-Parmer Instrument Co.). The calibrated reservoir was fitted with a glass frit to allow bubbling of argon gas through the solution for at least 30 minutes prior to and then throughout the duration of each experiment. The glassware, sample cells and transfer lines used for these experiments were stored in a vacuum oven kept at 85 °C under dry nitrogen. The temperatures of the solutions were measured with a Teflon-coated copper/constantan thermocouple inserted directly into the flow cell. Transient decay and growth rate constants were calculated by non-linear least squares analysis of the absorbance-time profiles using the Prism 5.0 software package (GraphPad Software, Inc.) and the appropriate user-defined fitting equations, after importing the raw data from the Luzchem mLFP software. Reagents were added directly to the reservoir by microliter syringe as aliquots of standard solutions. Rate constants were calculated by linear least-squares analysis of decay rate-concentration data (5-7 points) that spanned as large a range in transient decay rate as possible. Errors are quoted as twice the standard deviation obtained from the least-squares analyses.

8.3 Synthesis and Characterization of compounds

Germanium dichloride-dioxane. This procedure was adopted from that published by Leigh *et al.*[2] Germanium tetrachloride (25.0 g, 0.117 mol), 1.4-dioxane (18.0 g, 0.205 mol) and 1,1,3,3-tetramethyldisiloxane (17.3 g, 0.129 mol) were placed into a flame-dried 1-neck 250 mL round-bottom flask equipped with a reflux condenser and nitrogen inlet. The mixture was heated to 85 °C for 8 hours during which time white crystals were formed. The solution was decanted, the crystals were washed several times with pentane and were dried under vacuum to give the desired dichlorogermylene-dioxane complex as colorless needle-like crystals (22.9 g, 99 mmol, 85 %)

Synthesis of 2-phenyl-1,3-butadiene (28) The procedure is an adaptation of that of Brown et al for the synthesis of 2-phenyl-1,3-butadiene.[3] Magnesium filings (5.87 g, 0.24 g-atom) and anhydrous diethyl ether (30 mL) were placed in a flame-dried apparatus consisting of a 250 mL 2-neck round-bottom flask, magnetic stir-bar, reflux condenser, nitrogen inlet and addition funnel. A solution of (chloromethyl)trimethylsilane (15 g, 0.12 mol) in diethyl ether (30 mL) was added dropwise from the addition funnel over a period of 30 min and the reaction mixture was stirred at room temperature under nitrogen for 6 hours to give trimethylsilylmethylmagnesium chloride.

Benzoyl chloride (8.59 g, 0.06 mol), cuprous iodide (23 g, 0.12 mol) and anhydrous diethyl ether (60 mL) were placed in a flame-dried 250 mL 2-neck round-bottom flask equipped with a reflux condenser, magnetic stir bar, addition funnel, and dry ice-isopropanol bath. The solution of Grignard reagent from above was placed in the addition funnel and then added dropwise over ca. 60 minutes with stirring at -78°C. The cooling bath was removed and the reaction mixture was further stirred for 2 hrs. It was then quenched by dropwise addition of aqueous ammonium chloride (3.2 g, 0.06 mol, 1 equiv), the resulting aqueous phase was extracted with diethyl ether (3 x 15 mL) and the combined ether extracts were dried over anhydrous magnesium sulphate. The solvent was removed on a rotary evaporator to afford a colorless oil (10.91 g) which was identified as 1-phenyl-2-(trimethylsilyl)ethanone (**28**) (purity ca. 80%, yield ~ 93%) on the basis of its ^{1}H and ^{13}C NMR spectra:[4] ^{1}H NMR (200 MHz, $CDCl_3$): δ = 0.04 (s, 9H), 2.72 (s, 2H), 7.45 (m, 3H), 7.86 (m, 2 H) ppm; ^{13}C NMR (50 MHz, $CDCl_3$): δ = -0.9, 33.8, 128.4, 128.5, 132.7, 199.6 ppm.

1-Phenyl-2-(trimethylsilyl)ethanone (11.60 g, 0.06 mol) and THF (30 mL) were placed in a flame-dried 250 mL 2-neck round-bottom flask equipped with a reflux condenser, addition funnel, magnetic stir bar, nitrogen inlet, and ice bath. A solution of vinyl magnesium bromide (1M in THF, 9.58g, 73 mL, 0.07 mol) was then added dropwise with stirring over ca. 60 minutes at 0°C. The ice bath was removed, and the mixture was allowed to warm to room temperature and then stirred for 10 hours. The reaction mixture was quenched by dropwise addition of aqueous ammonium chloride (5 mL) and the resulting aqueous phase was extracted with ether (4 x 15 mL). The combined organic extracts were dried over anhydrous magnesium sulphate, filtered and the solvent was removed on a rotary evaporator to afford a colorless oil (11.30 g) which was identified as 2-phenyl-1-(trimethylsilyl)but-3-en-2-ol (**29**) (purity *ca.* 87%, yield ~ 85%) on the basis of its ^{1}H and ^{13}C NMR spectra:[3] ^{1}H NMR (200 MHz, $CDCl_3$): δ = -0.05 (s, 9H), 1.58 (m, 2H), 1.93 (s, 1H), 5.21 (dd, J = 10.5 and 17.2 Hz, 2H), 6.35 (dd, J = 10.5 and 17.2 Hz; 1H), 7.39 (m, 5H) ppm; ^{13}C NMR (50 MHz, $CDCl_3$): δ = 0.2, 32.5, 111.1, 125.3, 126.8, 128.2, 128.4, 146.8, 147.2 ppm.

The crude alcohol (12.5 g, 0.06 mol) was placed in a 2-neck 100 mL round-bottom flask equipped with a reflux condenser, magnetic stir bar and nitrogen inlet. A saturated solution of sodium acetate in glacial acetic acid (40 mL) was added and the resulting mixture was stirred for 18 hours at 60 °C under nitrogen. The reaction mixture was then neutralized with aqueous sodium carbonate and extracted with diethyl ether (3 x 15 mL). The combined ether extracts were dried over anhydrous magnesium sulphate, filtered, and the solvent was removed on a rotary evaporator to afford colorless oil (7.18 g, 0.055 mol, 98 %). The oil was purified by column chromatography, eluting with hexane, and was identified as 2-phenyl-1,3-butadiene (**28**) on the basis of its ^{1}H and ^{13}C NMR spectra:[3] ^{1}H NMR (200 MHz, $CDCl_3$), δ = 5.14-5.30 (m, 4H) , 6.62 (dd, J = 11.1, 17.2 Hz; 1H), 7.26 (br s, 5H) ppm; ^{13}C NMR (50 MHz, $CDCl_3$), δ = 117.1, 117.3, 127.6, 128.3, 128.4, 138.3 ppm. The quaternary carbons could not be detected in the latter spectrum.

Synthesis of 2-methyl-3-phenyl-1,3-butadiene (31). The procedure is a modification of that of Brown et al for the synthesis of 2-phenyl-1,3-butadiene.[3] 1-trimethylsilyl-2-propanone was synthesized by the method described by Hosomi *et al.*[5] Acetyl chloride (5.3 g, 0.068 mol), cuprous iodide (14.3 g, 0.075 mol) and anhydrous diethyl ether (75 mL) were placed in a flame-dried 250 mL 2-neck round-bottom flask equipped with an addition funnel and the resulting white suspension was cooled to -78°C (isopropanol/CO_2 bath). A solution of trimethylsilylmethylmagnesium chloride in ether (30 mL), prepared from (chloromethyl)trimethylsilane (10 g, 0.082 mol) as described above, was added to the suspension dropwise with continuous stirring over a period of 1 hr from an addition funnel. The reaction mixture was then stirred at room temperature for one hour, and after this time, it was hydrolysed with aqueous ammonium chloride (0.085 mol, 4.5 g in 30 mL distilled water), extracted with diethyl ether (2 x 20 mL) and pentane (2 x 20 mL). The combined organic extracts were washed with water, dried over anhydrous magnesium sulphate, filtered and the solvent was then removed on a rotary evaporator to give a blue-tinged oil (8.6 g) that was identified as 1-trimethylsilyl-2-propanone (purity ca. 60% , yield ~ 60%) on the basis of its ^{1}H and ^{13}C NMR spectra. The crude ketone was used in the next step without further purification. ^{1}H NMR (200 MHz, $CDCl_3$), δ = 0.09 (s, 9H), 2.05 (s 3H), 2.21 (s, 2H) ppm; ^{13}C NMR (50 MHz, $CDCl_3$), δ = -1.1, 14.1, 31.8, 207.49 ppm.

A solution of α-bromostyrene (0.05 mol, 9.15g) in anhydrous diethyl ether (30 mL) was added dropwise, from an addition funnel, to a flame-dried 250 mL 2-neck round-bottom containing magnesium filings (0.055 mol, 1.35 g) and anhydrous diethyl ether (20 mL) under nitrogen and gentle reflux. A brown solution was obtained. This was transferred to an addition funnel and was added dropwise under nitrogen to a 250 mL 2-neck round-bottom flask containing a solution of 1-methyl-2-(trimethylsilyl)ethanone (8.6 g) in anhydrous diethyl ether at 0°C. The reaction mixture was stirred at room temperature for 2 hrs and the resulting brownish solution was quenched with aqueous ammonium chloride (0.055 mol, 2.65 g in 20 mL distilled water), extracted with diethyl ether (1 x 50 mL) and pentane (1 x 30mL). The combined organic phase was then washed with (2 x 25 mL) water, dried over anhydrous magnesium bromide and solvent was removed on a rotary evaporator to give a viscous yellow oil (7.5 g) which was identified as 2-methyl-3-phenyl-1-(trimethylsilyl)-1-buten-3-ol on the basis of its ^{1}H and ^{13}C NMR spectra (purity ca.75 %; yield ~ 65 %). The alcohol was used without further purification in the next step. ^{1}H NMR (200 MHz, $CDCl_3$), $\delta = 0.09$ (s, 11H), 1.22 (s, 3H), 1.47 (s, 1H), 4.95 (d, $J = 1.4$ Hz; 1H), 5.41(d, $J = 1.4$ Hz; 1H), 7.33(m, 5H); ^{13}C NMR (50 MHz, $CDCl_3$), $\delta = 0.6$, 30.7, 31.6, 75.7, 112.3, 127.1, 128.6, 127.8, 129.1, 141.7 ppm. EI/MS, m/z (I) = 235 (19), 234 (32), 233 (55), 232 (40), 231 (100), 131 (63), 115 (92), 75(100), 73 (95). HRMS: Exact mass: calc. for $C_{14}H_{22}O^{29}Si$, 234.1440, found 234.1437.

The crude alcohol from above was added over a period of 30 min to a 100 mL 1-neck round-bottom flask containing glacial acetic acid (20 mL) saturated with sodium acetate at 60°C. The mixture was allowed to stir for further 30 min, after that time it was poured into a beaker containing cold water (100 mL), neutralized with sodium carbonate and extracted with diethyl ether (1 x 25 mL). The combined organic phase was dried over anhydrous magnesium sulphate, filtered and the solvent was removed on a rotary evaporator to yield yellow oil. This was distilled under vacuum to afford a colorless oil (3.5 g, 0.024 mol, 48 %; b.p. = 47-49 °C, 0.2 mmHg), which was identified as 2-methyl-3-phenyl-1,3-butadiene on the basis of its ^{1}H and ^{13}C NMR spectra. ^{1}H NMR (200 MHz, $CDCl_3$), δ = 2.0 (s, 3H), 4.86 (s, 1H), 5.11 (m, 2H), 5.31 (s, 1H), 7.29 (m, 5H) ppm. ^{13}C NMR (50 MHz, $CDCl_3$), δ = 21.3, 114.1, 117.1, 127.2, 128.0, 128.8, 144.2, 154.1 ppm.

Synthesis of 1,1-dimethyl-3-phenylgermacyclopent-3-ene (23). The compound was prepared by a modification of the procedure of Mazerolles and Manuel.[6] $GeCl_2$.dioxane (0.0123 mol, 2.85 g) in dry THF (25 mL) was placed into a flame-dried 100 mL 2-neck round-bottom flask equipped with a magnetic stir bar, reflux condenser, addition funnel and nitrogen inlet. The solution was heated to 70-75 °C while a solution of 2-phenyl-1,3-butadiene (0.016 mol, 2.08 g,) in THF (10 mL) was added dropwise with stirring. Heating was continued for one hour, then the solution was cooled and the solvent was removed by distillation. The resulting product was distilled under vacuum to afford a colorless oil identified as 1,1-dichloro-3-phenylgermacyclopent-3-ene (**32**: 0.007 mol, 2.0 g, 80 %; 99-100 °C , 0.01 mmHg) on the basis of its ^{1}H and ^{13}C NMR and mass spectra (Ge isotopomeric clusters are indicated with an asterisk). ^{1}H NMR ($CDCl_3$), δ = 2.48 (d, 2 H), 2.56 (d, 2 H), 6.52 (m, 1 H), 7.35 (m, 5H) ppm; ^{13}C NMR ($CDCl_3$), δ = 27.0, 28.3, 124.0, 125.8, 128.6 ppm; MS (EI), m/z (I) = 274* (2), 205 (10), 179* (14), 131* (98), 91 (100), 77 (48), 51(18); HRMS: Exact mass: cal. for $C_{10}H_{10}Cl_2{}^{74}Ge$, 273.9371; found 273.9371.

The product from above (0.00695 mol, 1.89 g,) in anhydrous diethyl ether (15 mL) was placed in a 100 mL 1-neck round-bottom flask equipped with a magnetic stirrer, reflux condenser, addition funnel and a nitrogen inlet. The solution was cooled with an ice bath and methylmagnesium bromide (0.017 mol, 15.8 mL (3M in diethyl ether) was added to it dropwise with stirring over 15 min. The reaction mixture was allowed to warm to room temperature and was further stirred for 5 hrs. After that time it was transferred to a separatory funnel and quenched with saturated aqueous ammonium chloride (15 mL). The aqueous fraction was extracted with diethyl ether (3 x 15 mL) and the combined ether extracts were dried over anhydrous magnesium sulfate. The solvent was removed under vacuum to give a light yellow oil, which was purified by vacuum distillation to give a colorless oil (68-70 °C (0.05 mmHg), 1.43 g, 89 %) or by column chromatography using a mixture of hexane and dichloromethane (2:1) as eluant. The product was identified as **23** on the basis its ^1H and ^{13}C NMR, IR, and mass spectra (Ge isotopomeric clusters are indicated with an asterisk). Limited spectroscopic data have been reported previously for this compound by Neumann *et al.*[7] IR (neat): 2972 (w), 2906 (m), 1606 (m), 1492 (m), 1444 (w), 1235 (m), 1031 (m), 828 (s) cm^{-1}; ^1H NMR (700 MHz, C_6D_6), $\delta = 0.24$ (s, 6H), 1.65 (m, 2 H), 1.78 (m, 2 H), 7.12 (m, 1 H), 7.23(m, 3H), 7.54 (m, 2H) ppm; ^{13}C NMR (700 MHz, C_6D_6), $\delta = -2.2$, 20.83, 20.9, 126.4, 127.0, 128.4, 128.6, 141.8, 143.0 ppm; EI-MS, m/z (I) = 234* (30), 219* (100), 129* (5), 119* (12), 89* (24), 69 (20). HRMS: Exact mass: calc. for $C_{12}H_{16}{}^{74}Ge$, 234.0464; found 234.0442.

Synthesis of 1,1,3-trimethyl-4-phenylgermacyclopent-3-ene (24). $GeCl_2$.dioxane (5.10 g, 0.0218 mol) in anhydrous THF (35 mL) was placed in a flame-dried 100 mL, 2-neck round-bottom flask equipped with a reflux condenser, addition funnel, magnetic stir bar and a nitrogen inlet. The solution was gently refluxed and 2-methyl-3-phenyl-1,3-butadiene (0.024 mol, 3.4 g) in THF (25 mL) was added dropwise over a period of 1 hr. The reaction mixture was further stirred for 10 min and then the THF was removed by distillation. The residue was distilled under vacuum to afford a colorless oil identified as 1,1-dichloro-3-methyl-4-phenylgermacyclopent-3-ene (**33**) by ^1H and ^{13}C NMR spectroscopy (0.0194 mol, 89 %; 100-101°C, 0.05 mmHg).

^1H NMR (200 MHz, $CDCl_3$), δ = 1.95 (s, 3H), 2.51 (d, 2H), 2.73 (d, 2H), 7.40 (m, 5H) ppm; ^{13}C NMR (50 MHz, $CDCl_3$), δ = 20.1, 25.6, 33.3, 67.0, 67.9, 127.0, 128.2, 132.5, 134.2, 140.3 ppm.

A solution of the 1,1-dichlorogermacyclopent-3-ene derivative from above (1.10 g, 0.0038 mol) in anhydrous diethyl ether (100 mL) was placed into a flame-dried 100 mL two-neck round-bottom flask equipped with a magnetic stirrer and nitrogen inlet and was cooled to 5°C with an ice-bath. Methylmagnesium bromide (3.20 mL (3M in ether), 0.0096 mol) was added via a syringe through a septum to the reaction mixture over a period of 10 min. The reaction mixture was allowed to stir at room temperature for 3 hrs and was then hydrolysed with saturated aqueous ammonium chloride (10 mL). The aqueous phase was separated and extracted with diethyl ether (1 x 10 mL). The combined organic extracts were washed with distilled water (1 x 20 mL) and dried over anhydrous magnesium sulfate. Removal of the solvent on a rotary evaporator yielded a yellow oil, from which **24** was obtained as a colorless oil by vacuum distillation (0.71 g, 0.0029 mol, 76 %; 85-86 °C, 0.1 mmHg). IR (neat) 2974.5 (m), 2907.9 (s), 2887 (s), 1599 (s), 1492 (s), 1135 (s), 829 (m), 790 (s) cm^{-1}; ^1H NMR (600 MHz, C_6D_6), δ = 0.28 (s, 6H), 1.67 (s, 2H), 1.80 (s, 3H), 1.97 (s, 2H), 7.09 (m, 4H), 7.24 (m, 1H); ^{13}C NMR (151 MHz, C_6D_6), δ = -2.4, 21.1, 27.4, 27.6, 126.2, 127.8, 128.2, 128.3, 128.6, 134.7, 137.0, 144.3; EI-MS, (m/z) (I) = 248* (58), 233* (48), 183 (24), 182 (12), 143 (28), 128 (42), 115 (38), 104* (50), 89* (100), 77 (28); HRMS: Exact mass: calc. for $C_{13}H_{18}{}^{79}Ge$, 248.0620; found, 248.0613.

Synthesis of dodecamethylcyclohexagermane (14). The compound was synthesized according to the procedure of Carberry *et al.*[8] Li (2.45 g, 0.11 mol, 30 % dispersion in mineral oil but washed with anhydrous hexane) in anhydrous THF (ca. 150 mL) was placed in a 250 mL round bottom flask. Dichlorodimethylgermane (7.58 g, 0.046 mol) was added very rapidly by means of a syringe to the flask. The reaction was vigorously stirred and became increasingly exothermic. After stirring at room temperature for 4 hours, the reaction mixture turned green. At that time, the liquid part was syringed out and the residual Li was quenched with dropwise with methanol. Diethylether (ca. 20 mL) was added to the reaction mixture followed by aqueous solution of NaCl (10 mL). The organic component was extracted with 2 x 15 mL diethyl ether.

Then, the combined organic phase was dried over anhydrous magnesium sulfate and filtered. The solvent was then removed on a rotary evaporator. Column chromatography using hexane as eluant, followed by repeated crystallization with acetone afforded a mixture (0.26 g, 6 %, mpt 206-210 °C) containing 96 % of dodecamethylcyclohexagermane and 4 % of decamethylcyclopentagermane (determined by GC/MS). ^{1}H NMR (200 MHz, $CDCl_3$) of **14**: δ 0.34 (s, 36 H) ppm. The MS (EI) of **15** and decamethylcyclopentagermane are in agreement with those reported by Carberry *et al.*[8]

Dimethylphenyl(trimethylsilyl)germane (18). The compound was synthesized according to the procedure described by Bobbitt *et al.* Li wire (0.19 g, 0.028 mols) in anhydrous THF (50 mL) was placed into a flame dried 100 mL 2-neck round-bottom flash equipped with a magnetic stir bar and an argon inlet. Chlorodimethylphenylgermane (1.5 g, 0.0069 mols) was added to the mixture and was allowed to stir at room temperature for 3 hours. Then chlorotrimethylsilane (3.02 g, 0.028 mols) was added dropwise to the flask. The reaction mixture was allowed to stir at room temperature for a further 3 hours.[9] After this time, the unreacted lithium was removed and the reaction mixture was quenched with water. The organic part was extracted with diethyl ether (4 x 15 mL). The solvent was evaporated on a rotary evaporator to afford the crude product as pale yellow oil. Column chromatography on silica gel with hexanes as eluant afforded the product as a colorless oil (0.6 g, 34 %; ^{1}H NMR (200 MHz, $CDCl_3$) δ 0.18 (s, 9H), 0.44 (s, 6H), 7.31-7.35 (m, 3H), 7.43-7.46 (m, 2H) ppm; ^{13}C NMR (50.32 MHz, $CDCl_3$) -4.5 ($GeMe_2$),

-1.54 ($SiMe_3$), 127.58 (para), 127.83 (ortho or meta), 133.55 (ortho or meta), 142.36 ppm; GC/MS, (m/z) (I), 254 (14), 252 (12), 250 (6), 239 (52), 237 (39), 235 (23), 181 (19), 179 (14), 177 (11), 136 (16), 135 (100), 75 (13), 73 (34), 45 (22), 44(7), 43 (19). The spectra are in good agreement with the one reported by Bobbitt *et al.*, except for some minor differences in the ^{13}C NMR spectrum.[9]

8.4 Steady state photolysis experiments

Photolysis of 1,1-dimethyl-3-phenylgermacyclopent-3-ene (23) in the presence of acetic acid in cyclohexane-d_{12}

An argon-saturated solution of **23** (0.05M) and glacial acetic acid (0.25 M) in cyclohexane–d_{12} was placed in a quartz NMR tube sealed with a septa. The solution was placed in a merry-go-round apparatus and was irradiated at 254 nm using 6 RPR-2537 lamps. The reaction mixture was photolysed for a period of 16 minutes (ca. 60 % conversion) during which the course of the reaction was monitored periodically by ^{1}H NMR spectroscopy. Acetoxydimethylgermane (**34**) was identified as the main product by comparison to the reported ^{1}H NMR spectrum.[10] The chemical yields of **34** and **28** after 60 % conversion were estimated as 91 % and 99 %, respectively. ^{1}H NMR (200 MHz, C_6D_{12}) of **34**: $\delta = 0.56$ (d, 6 H, $^3J = 2.4$ Hz), 5.63 (sept, 1H, $^3J = 2.4$ Hz) ppm. The acetyl methyl protons overlap with the acetyl methyl protons of acetic acid and cannot be distinguished.

Photolysis of 1,1-dimethyl-3-phenylgermacyclopent-3-ene (23) in the presence of 2,3-dimethyl-1,3-butadiene in cyclohexane-d_{12}

A solution of **23** (0.03 M), 2,3-dimethylbutadiene (0.05 M) and n-dodecane (0.003 M) in dry hexane was placed in a quartz photolysis tube, sealed with a rubber septum, and was deoxygenated with a stream of dry argon. The solution was placed in a merry-go-round apparatus and was irradiated at 254 nm using 6 RPR-2537 lamps. The reaction mixture was photolysed for a period of 12 minutes (ca. 80 % conversion), with periodic monitoring by GC-FID and GC-MS. The gas chromatogram indicated the presence of two major products with retention times of 4.32 and 5.12 minutes (n-dodecane, 6.65 min; **23**, 9.97 min), in roughly equal yields. The two peaks were identified as **28** and **7** by GC-MS, and confirmed by spiking the mixture with small amounts of authentic samples of the two compounds.[2] Two additional products (with retention times of 6.52 and 6.62 minutes) were also formed in yields of 3-5% each, but were not identified.

Photolysis of 1,1-dimethyl-3-phenylgermacyclopent-3-ene (23) in the presence of methanol in cyclohexane-d_{12}

A solution of **23** (0.0409 M), MeOH (0.2390 M) and hexamethyldisilane (0.0017 M) in cyclohexane-d_{12} was placed in an argon-filled quartz NMR tube and was sealed with a rubber septum. The solution was placed in a merry-go-round apparatus and was irradiated at 254 nm using 6 RPR-2537 lamps in a Rayonet photochemical reactor. The reaction mixture was photolysed for a period of 5 min (ca. 20 % conversion) and the course of the reaction was monitored at time intervals by ^{1}H NMR spectroscopy. The ^{1}H NMR spectra showed new peaks consistent with methoxydimethylgermane (**35**) in addition to those of **28**.[11] ^{1}H NMR (600 MHz, C_6D_{12}) of **35**: δ = 0.4 (d, 6 H, ^3J = 2.5 Hz), 3.5 (s, 3H) and 5.2 (sept, 1H, ^3J = 2.5 Hz) ppm.

Photolysis of 1,1-dimethyl-3-phenylgermacyclopent-3-ene (23) in THF-d_8 containing AcOH

A solution of **23** (0.025 M) in THF-d_8 containing AcOH (0.04 M) and hexamethyldisilane (0.005 M) as internal integration standard was placed in a quartz NMR tube, deoxygenated with a stream of dry argon, sealed with a rubber septum, and irradiated with 6 RPR-2537 lamps in a Rayonet photochemical reactor. The course of the photolysis was monitored as a function of time by ^{1}H NMR spectroscopy (600 MHz) up to ca. 40% conversion of **23**. Only two products were formed, which were identified as 2-phenyl-1,3-butadiene (**28**: δ 7.26-7.33 (m, 6H), 6.63 (dd, 1H; J = 10.8, 2.4 Hz), 5.13-5.18 (m, 4H)) and acetoxydimethylgermane (**34**: δ 5.60 (sept, 1H, J = 2.4 Hz), 1.92 (s, 3H), 0.58 (d, 6H, ^3J = 2.4 Hz) ppm). Product yields were determined relative to consumed **23** from the slopes of concentration versus time plots for **23**, **28**, and **34** constructed by integration of the spectra.

Photolysis of 1,1-dimethyl-3-phenylgermacyclopent-3-ene (23) in THF-d_8 containing $MeSO_3H$.

A solution of **23** (0.034 M) in THF-d_8 containing $MeSO_3H$ (0.09 M) and hexamethyldisilane (0.005 M) as internal integration standard was placed in a quartz NMR tube, deoxygenated with a stream of dry argon, sealed with a rubber septum, and irradiated with 6 RPR-2537 lamps in a Rayonet photochemical reactor. The course of the photolysis was monitored as a function of time by ^{1}H NMR spectroscopy up to ca. 60% conversion of **23**. The product exhibiting multiplets at δ 5.90 (sept, 1H) and δ 0.76 (d, 6H, J = 2.1 Hz) is tentatively identified as $Me_2Ge(H)OSO_2H$ (**44**). Product yields were determined relative to consumed **23** from the slopes of concentration vs. time plots for **23**, **28**, and **47** constructed by integration of the spectra.

Photolysis of 1,1,3-trimethyl-4-phenylgermacyclopent-3-ene (24) in cyclohexane-d_{12} containing AcOH

A solution of **24** (0.05 M), glacial acetic acid (0.26 M), and hexamethyldisilane (0.02 M) in cyclohexane–d_{12} was placed in a quartz NMR tube, sealed with a rubber septum, and deoxygenated with a stream of dry argon. The solution was placed in a merry-go-round apparatus and was irradiated at 254 nm using 6 RPR-2537 lamps. The reaction mixture was photolyzed for a period of 16 minutes (ca. 30 % conversion), monitoring periodically by ^{1}H NMR spectroscopy. The chemical yields of **31** and **34** after 30 % conversion were estimated as 99 % and 98 %, respectively.

References

1. Soderquist, J. A. and Hassner, A. *J. Org. Chem.* **1983**, *48*, 1801.
2. Leigh, W. J.; Harrington, C. R.; Vargas-Baca, I. *J. Am. Chem. Soc.* **2004**, *126*, 16105.
3. Brown, P. A.; Bonnert, R. V.; Jenkins, P. R.; Lawrence, N. J.; Selim, M. R. *J. Chem. Soc., Perkin Trans I.* **1991**, 1893.
4. Yamamoto, Y.; Ohdoi, K.; Nakatani, M.; Akiba, K. *Chem. Lett.* **1984**, *1984*, 1967.
5. Hosomi, A.; Hayashida, H.; Tominaga, Y. *J. Org. Chem.* **1989**, *54*, 3254.
6. Mazerolles, P. and Manuel, G. *Bull. Soc. Chim. Fr.* **1965**, *56*, 327.
7. Neumann, W. P.; Michels, E.; Köcher; J. *Tetrahedron Lett.* **1987**, *28*, 3783.
8. Carberry, E.; Dombek, B. D.; Cohen, S. C. *J. Organomet. Chem.* **1972**, *36*, 61.
9. Bobbitt, K. L.; Maloney, V. M.; Gaspar, P. P. *Organometallics* **1991**, *10*, 2772.
10. Barker, G. K.; Drake, J. E.; Hemmings, R. T. *Can. J. Chem.* **1974**, 2622.
11. Klein, B.; Neumann, W. P.; Weisbeck, M. P.; Weinken, S. *J. Organomet. Chem.* **1993**, *446*, 149.